Carbene-platinum conjugated : novel anticancer complexes

Mathilde Bouché

UNIVERSITÉ DE STRASBOURG

Ecole Doctorale de Physique et Chimie-Physique

Institut de Physique et Chimie des Matériaux de Strasbourg

THÈSE présentée par :

Mathilde BOUCHÉ

soutenue le : **26 Septembre 2017**

pour obtenir le grade de : **Docteur de l'Université de Strasbourg**

Discipline : Chimie

Carbène-Platine conjugués : de nouveaux outils thérapeutiques dans la lutte antitumorale

THÈSE dirigée par :

Dr BELLEMIN-LAPONNAZ Stéphane Directeur de Recherche, Université de Strasbourg

RAPPORTEURS :

Pr POYATOS Macarena Professeur, Universitat Jaume I

Pr GASSER Gilles Professeur, Chimie Paris Tech

AUTRES MEMBRES DU JURY :

Pr FOURNEL Sylvie Professeur, Université de Strasbourg

Dr NEWMAN Paul Research Officer, Cardiff University

Acknowledgement

J'aimerai ici remercier les gens qui m'ont aidée et soutenue au cours de ces trois années à Strasbourg et ont rendu cette expérience enrichissante aussi bien scientifiquement qu'humainement.

Avant tout, je tiens à remercier chaleureusement le Dr Stéphane Bellemin-Laponnaz pour ses conseils, sa disponibilité et pour m'avoir offert autant d'opportunités qui m'ont permis d'évoluer.

I would like to thank all the members of my jury, Pr Macarena Poyatos, Pr Sylvie Fournel, Dr Gilles Gasser and Dr Paul Newman, for making me the honour to evaluate this work and providing precious advices.

L'implication de mes collaborateurs a été décisive pour l'avancée de ces travaux, c'est pourquoi j'aimerai remercier à nouveau le Pr Sylvie Fournel et May Wantz. Merci au Dr Antoine Bonnefont pour m'avoir initiée à la cyclovoltammétrie. Un grand merci au Dr Jean-Louis Gallani ainsi que Dr Selvi Selvam pour m'avoir permis de découvrir le monde des nanoparticules et pour leur soutien moral en toute circonstance. Merci également au Dr Antoine Kichler pour les études de transfection, au Dr Sébastien Richeter pour avoir fourni les sels d'imidazolium porphyrinique, au Dr Gilles Guichard pour avoir fourni le peptide HB-19, au Pr Claire Billotey et Elsa Charignon pour les études de biodistribution et au Dr Sébastien Harlepp pour les études d'interaction avec l'ADN.

Je souhaite également remercier les services communs d'analyses : Dr Lydia Brelot, Corinne Bailly, Dr Jean-Marc Strub, Dr Emeric Wasielewski, Dr Martine Heinrich. Merci également au Dr Corinne Ulhaq pour les analyses TEM. J'aimerai particulièrement remercier le Dr Bruno Vincent et Maurice Coppe pour leur aide et leur bonne humeur constante.

Cette expérience restera inoubliable grâce à la sympathie de l'ensemble des collègues que j'ai pu côtoyer à l'IPCMS. Merci particulièrement à Thierry, Aline, Marco, Maya, Yannick, Julien, Damien et Michel pour leur présence au labo. Merci également à Melania/Carotte, Matthieu & Sonia & Heather, Anis, Catalina, Mimi V. & Christophe, Dédé, Senthil, Sébastien P., Janah, Sébastien K. pour les bons moments passés ensemble. Je tiens également à remercier l'ensemble des membres du DMO pour leur bonne humeur permanente. Merci particulièrement à Nico qui a toujours été là pour aider à résoudre n'importe quel problème technique. Mention spéciale pour Bertrand qui m'a prodigué de nombreux conseils pour mon envol vers Philly. Merci à l'équipe des TPs inorga et particulièrement à Vincent pour ses conseils avisés. Je veux également remercier Woody ainsi que Dominique qui m'ont soutenue et m'ont donné gout à la recherche.

Finalement, un énorme merci à mes Grands-Parents, Monique et Alain, pour leur appui et particulièrement à ma Mère, Christine, pour son soutien en toute circonstance et grâce à qui cet objectif a pu devenir une réalité. Je tiens également à remercier ma belle-famille pour leur aide et leur gentillesse constante. Enfin, merci à Niels qui a toujours été présent pour m'encourager et me tirer vers l'avant.

Abstract

Cisplatin and other platinum-based drugs are well established in the fight against cancer thanks to their great cytotoxic activity. However, numerous shortcomings remain to be tackled, namely their low stability, lack of selectivity and resistance of several cancer cell lines to platinum-based treatment. Therefore, improved anticancer drugs are strongly awaited to substitute agents currently used in clinics. N-Heterocyclic Carbene (NHC) appeared as a powerful class of ligands for drug development and their coordination to platinum centre has recently demonstrated very promising results as anticancer agents.

In the aim to access drugs displaying novel mode of action, both electronic and steric environment of the platinum centre have been finely tuned by variation of either its coordination sphere by simple ligand exchange, or the metal oxidation degree to access NHC-Pt(IV) prodrug candidates. Their stability has been explored and their potential at promoting cancer cell death prompted us to conduct a thorough mechanistical investigation on the most promising derivatives. This highlighted the efficiency of NHC-Pt(IV) complexes toward cisplatin-resistant cancer cell lines thanks to a mitochondria-mediated apoptosis pathway

Furthermore, NHC-Pt complex combination to nanodelivery devices has been investigated in order to improve both their biocompatibility and selectivity toward cancer cells. While NHC-Pt association to biocompatible protein proved convenient, drug encapsulation into liposomes appeared as a more promising strategy to promote safe and efficient drug delivery. Moreover, NHC-Pt grafting on polyethylenimine chains afforded polycationic macromolecules which proved highly efficient at promoting cancer cell death both *in vitro* and *in vivo*. Functionalization of the polymeric chain has been explored by combination to targeting peptide or conjugation of chromophores to unravel drug biodistribution and mechanism of action. Finally, we developed biocompatible gold nanoparticles for further conjugation of the cytotoxic NHC-Pt moieties with the aim to ultimately access theranostic devices for combined therapy and tumour imaging.

Table of Contents

Publications

1) M. Bouché, G. Dahm, A. Maisse-François, T. Achard, S. Bellemin-Laponnaz « Selective Formation of *cis*-N-Heterocyclic Carbene-Pt^{II}-Pnictogen Complexes and *in vitro* Evalutaion of Their Cytotoxic Activities toward Cancer Cell s» *Eur. J. Inorg.* **2016**, 2828-2836

2) M. Bouché, G. Dahm, M. Wantz, S. Fournel, T. Achard, S. Bellemin-Laponnaz « Platinum(IV) N-heterocyclic carbene complexes: their synthesis, characterization and cytotoxic activity » *Dalton Trans.* **2016**, *45*, 11362-11368

Abbreviations

Acac	**Ac**etyl**ac**etonate
A2780	Human ovarian carcinoma
A2780R	Cisplatin-resistant human ovarian carcinoma
BER	**B**ase **E**xcision **R**epair
BSA	**B**ovine **S**erum **A**lbumin
Cryo-EM	Cryo **E**lectron **M**icroscopy
CV	**C**yclic **V**oltammetry
Da	**Da**lton
DCA	**D**i**c**hloro**a**cetate
trans-DDP	*trans*-**d**iammine**d**ichloro**p**latinum(II)
DFF	**D**NA **F**ragmentation **F**actor
DFT	**D**ensity **F**unctional **T**heory
DLS	**D**ynamic **L**ight **S**cattering
DMF	**D**i**m**ethyl**f**ormamide
DMSO	**D**i**m**ethyl**s**ulf**o**xide
DNA	**D**esoxyribo**n**ucleic **A**cid
Dvtms	**D**i**v**inyl**t**etra**m**ethyl**s**iloxane
EDCI	N-(3-dimethylaminopropyl)-N’-ethylcarbodiimide
EtOH	Ethanol
EPR	**E**nhanced **P**ermeability **R**etention
FDA	**F**ood and **D**rug **A**dministration
GSH	Glutathione
HCT116	Colon cancer cell
HCT116p53KO	Colon cancer cell p53 KO
HOMO	**H**ighest **O**ccupied **M**olecular **O**rbital

HSA	**H**uman **S**erum **A**lbumin
HPLC	**H**igh **P**ressure **L**iquid **C**hromatography
Hz	Hertz
IC_{50}	Half inhibitory concentration
ICP-MS	**I**nductive **C**oupled **P**lasma-**M**ass **S**pectrometry
M	**M**olar
MAL	**M**ethyl-**a**mino**l**evulinate
MCF7	Breast carcinoma
MitoSox	Red Mitochondrial Superoxide Indicator
MLCT	**M**etal-**L**igand **C**harge **T**ransfer
MMR	**M**is**m**atch **R**epair
MRC5	Human foetus cell lung
NER	**N**ucleotide **E**xcision **R**epair
NHC	**N**-**H**eterocyclic **C**arbene
NHS	**N**-**H**ydroxy**s**uccinimide
NMR	**N**uclear **M**agnetic **R**esonance
NP	**N**ano**p**article
OCT	**O**rganic **C**ation **T**ransporter
OXONE	Potassium Peroxymonosulfate
P	**P**artition coefficient between water and an organic solvent
PBS	**P**hosphate-**B**uffered **S**aline
PC3	Prostate adenocarcinoma
PDT	**P**hoto**d**ynamic **T**herapy
PEG	**P**oly**e**thylene **g**lycol
PEI	**P**oly**e**thylen**i**mine
pH	**H**ydrogen **P**otential
R	**R**esistance Factor
RNA	**R**ibo**n**ucleic **A**cid
ROS	**R**eactive **O**xygen **S**pecies

SAR	**S**tructure **A**ctivity **R**elationship
SPDP	**S**uccinimidyl 3-[2-**p**yridil**d**ithio)**p**ropionate]
SRIXE	**S**ynchrotron **R**adiation-**I**nduced **X**-Ray
TBAB	Borane tert-butylamine complex
TEMPO	(2,2,6,6-Tetramethylpiperidin-1-yl)oxyl
THF	**T**etra**h**ydro**f**uran
TLC	**T**hin **L**ayer **C**hromatography
UV-vis	**U**ltra **V**iolet-**Vis**ible
XANES	**X**-Ray **A**bsorption **N**ear **E**dge **S**tructure
XPS	**X**-ray **P**hotoelectron **S**pectroscopy

Résumé étendu

Au cours des dernières décennies, la chimie inorganique médicinale a largement contribué au développement des sciences médicales par le biais des agents de chimiothérapie à base de métaux, des interactions métal-médicament ou encore de l'implication des ions métalliques dans les maladies. La diversité de propriétés des métaux de transition offre de nombreuses possibilités pour la découverte de nouveaux médicaments. Pourtant, bien que des dérivés tels que le NAMI-A, l'auranofin ou le budotitane aient montré des activités anticancéreuses *in vitro* intéressantes, à ce jour seuls quelques dérivés de platine sont utilisés mondialement en clinique. Le cisplatine reste donc encore aujourd'hui une référence pour le traitement du cancer grâce à sa forte cytotoxicité qui permet un taux de rémission allant jusqu'à 90% dans le cas du cancer de la prostate. Néanmoins, la faible stabilité du cisplatine provoque souvent de nombreux effets secondaires tels qu'une forte nephrotoxicité, ototoxicité ou encore une myélosuppression. De plus, ces effets indésirables sont parfois observés des années après le traitement dû à une mauvaise excrétion du platine. Finalement, les mécanismes de résistance cellulaire -intrinsèque ou acquis- au traitement basé sur le cisplatine restent des limitations de taille pour le traitement des cancers résistants. C'est pourquoi la recherche de nouveaux dérivés de platine anticancéreux a été un champ d'investigation particulièrement actif aussi bien dans la recherche académique qu'industrielle depuis plusieurs décennies. Etonnamment, parmi ces milliers de composés testés, seulement deux nouveaux dérivés de platine sont utilisés mondialement en clinique comme alternative au cisplatine. En conséquence, il est d'une importance capitale de trouver de nouveaux agents anticancéreux innovants.

Les ligands de type carbène N-hétérocycliques (NHC) sont maintenant bien établis dans le cadre du développement de métallo-médicaments grâce à leur facilité de fonctionnalisation. La stabilité chimique et thermique de la liaison carbène-platine donnent lieu à la formation de complexes particulièrement résistants. Considérant les conditions difficiles rencontrées par les

médicaments *in vivo*, la stabilité de la liaison carbène-platine est également essentielle afin d'éviter les interférences dues aux protéines et l'inactivation prématurée de la molécule active. Les premières études autour de dérivés NHC-Pt(II) anticancéreux ont confirmé le potentiel de cette famille de métallo-médicaments dont les cytotoxicités sont de l'ordre du micro-molaire sur de nombreuses lignées cellulaires cancéreuses. De plus, les récentes études mécanistiques sur les dérivés de NHC-platine ont suggéré un mécanisme d'action anticancéreux différent du cisplatine. Finalement, au vu des propriétés anticancéreuses prometteuses de ces complexes innovants, le développement d'une bibliothèque de dérivés NHC-platine et l'étude de la variation de leurs paramètres physico-chimiques est essentiel dans la recherche de la nouvelle génération d'agents anticancéreux.

La thèse présentée dans ce document se concentre sur les développements effectués autour de la fonctionnalisation de la brique moléculaire NHC-platine pour développer des médicaments innovants agissants selon un mode d'action différent des agents anticancéreux utilisés à ce jour. Le premier chapitre présente les propriétés et effets secondaires des complexes de platine anticancéreux ainsi que les développements proposés pour résoudre ces problèmes. Par la suite, plusieurs chapitres sont dédiés aux nombreuses fonctionnalisations étudiées, notamment la variation des ligands portés par le platine ou encore la modification du degré d'oxydation du centre métallique. Finalement, la combinaison des entités NHC-Pt à divers dispositifs permettant une libération contrôlée de dérivés cytotoxiques de platine a été l'objet de plusieurs développements dans le but de limiter les effets secondaires et augmenter leur sélectivité envers les cellules cancéreuses.

Le second chapitre de ce manuscrit détaille la synthèse sélective des complexes *trans* ou *cis* de formule générale [(NHC)PtX_2(pnictogène)] en fonction de la nature du fragment introduit par échange de ligand ainsi que l'évaluation de leurs propriétés anticancéreuses. Ainsi, plusieurs précurseurs de type *trans* [(NHC)PtX_2(pyridine)] ont été synthétisés par déprotonation d'un sel d'imidazolium en présence d'une base, d'un sel d'halogène et de la pyridine. Cette procédure a permis le développement d'une large gamme de dérivés NHC-Pt-pyridine où la variation des

ligands halogénés portés par le platine (chlore, brome ou iode) ou bien des motifs présents sur le NHC est effectuée avec de bons rendements. Les complexes ont été obtenus avec de bons rendements et caractérisés par RMN et spectroscopie de masse. La librairie de molécules a été étendue par une méthode d'échange de ligand sur ces précurseurs. En effet, le fort effet trans du NHC affaiblit la liaison platine-pyridine en *trans* et favorise l'échange de la pyridine par d'autres ligands. Une large gamme d'amines a ainsi été introduite avec succès et les dérivés *trans* [(NHC)PtX_2L] ont ainsi été obtenus avec de bons rendements. Ces post-fonctionnalisations ont permis la variation des propriétés physico-chimiques des dérivés correspondants. En particulier, l'influence de ces fonctionnalisations sur la lipophilicité a été étudiée par la méthode du flacon sous agitation. L'ensemble des dérivés étudiés s'est montrée bien plus lipophile que le cisplatine, suggérant une meilleure absorption de ces dérivés par les cellules cancéreuses.

La procédure basée sur l'échange de ligands a également été étendue au reste de la famille des pnictogènes avec succès. Alors que les ligands dérivés de phosphine sont bien établis dans le domaine de la catalyse, leur utilisation en combinaison avec les complexes NHC-platine reste mineure dans le cadre des applications biologiques. Il en va de même pour les ligands à base d'arsenic ou d'antimoine en raison de leur mauvaise réputation. Pourtant, l'utilisation en clinique de l'oxyde d'arsenic dans le traitement des leucémies a démontré le potentiel de ces dérivés dans la lutte antitumorale. Ainsi, plusieurs ligands dérivés de phosphine, arsine ou stibine ont été introduits par échange de ligand sur les complexes de NHC-platine dans le but d'accéder à de nouveaux dérivés à double action. La caractérisation de ces composés par RMN et diffraction aux rayons X sur monocristaux a révélé une configuration *cis* vis-à-vis du NHC des ligands à base de phosphore, arsenic et d'antimoine. Cette configuration est remarquable puisqu'elle a systématiquement été observée contrairement aux dérivés de type [(NHC)PtX_2(amine)] qui adoptent systématiquement une configuration *trans*.

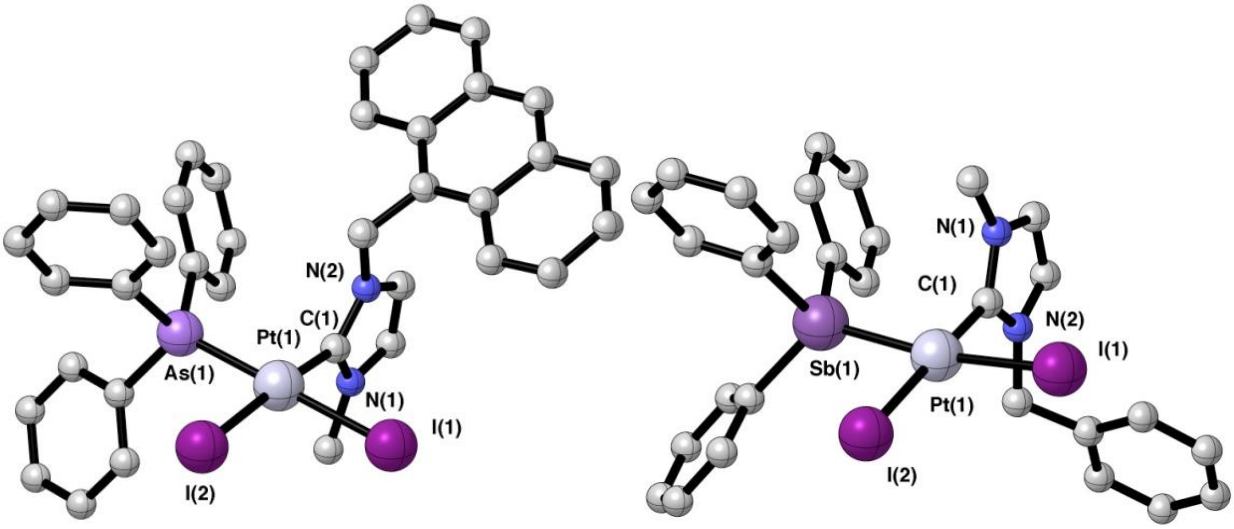

Figure 1: Structure moléculaire d'un complexe neutre d'arsenic **52b** (*gauche*) et d'un complexe d'antimoine **51c** (*droite*).

La librairie de complexes NHC-Pt-pnictogène a également pu être adaptée pour accéder à de nouveaux complexes cationiques de formule générale $[(NHC)PtX(PnPh_3)_2]I$ où Pn représente P, As ou Sb. La RMN du ^{31}P ainsi que la structure moléculaire d'un exemple représentatif $[(NHC)PtX(PPh_3)_2]I$ ont confirmé l'orientation *cis,cis* du complexe ainsi formé malgré les contraintes stériques induites par les deux ligands triphenylphosphine. Finalement, plusieurs dérivés représentatifs ont été évalués *in vitro* pour leurs propriétés anticancéreuses sur trois lignées cancéreuses et comparées à une lignée cellulaire saine pour étudier leur sélectivité. Alors que l'ensemble des dérivés NHC-platine testés ont montré une cytotoxicité supérieure au cisplatine sur les cellules cancéreuses, ils se sont également avérés être modérément toxiques envers la lignée cellulaire saine. Ainsi, bien que ces composés n'aient pas démontré d'activité synergique entre le platine et les pnictogènes et malgré leur manque de sélectivité *in vitro*, ces études ont confirmé le potentiel de la combinaison des briques moléculaires NHC-platine avec les ligands dérivés de pnictogène pour des applications biomédicales.

Le troisième chapitre se concentre sur la modification du degré d'oxydation du platine et son influence aussi bien sur la stabilité que la cytotoxicité de ces dérivés. En effet, l'oxydation du platine au degré d'oxydation +IV qui conduit à la formation de complexes de géométrie

octaédrique a été proposée afin d'augmenter l'inertie du centre métallique vis-à-vis des échanges de ligands. Cette stabilité accrue envers les protéines et autres biomolécules devrait permettre l'absorption d'une plus grande quantité d'agent anticancéreux par les cellules tumorales et limiter les interactions indésirables. De plus, les complexes de platine(IV) sont considérés comme des « pro-médicaments » qui sont métabolisés à l'intérieur des cellules par bioréduction sous leur forme active platine(II). En conséquence, leur stabilité vis-à-vis du milieu biologique ainsi que leur cinétique et potentiel de réduction sont des paramètres critiques à contrôler pour permettre une libération optimale du principe actif sans inactivation préalable.

Ainsi, une famille de complexes NHC-platine(IV) a été synthétisée par oxydation directe de précurseurs de platine(II) fonctionnalisés avec un faible excès de dibrome pour donner des complexes de formule [(NHC)$PtBr_4$L] (L = ligand azoté). Cette réaction a permis l'oxydation sélective d'une large gamme de précurseurs avec d'excellents rendements. Bien que l'oxydation directe de précurseurs de platine(II) soit hautement modulable, une seconde méthode de synthèse par post-fonctionnalisation de dérivés [(NHC)$PtBr_4$(pyridine)] a été développée afin d'introduire davantage de diversité chimique dans la famille des NHC-platine(IV). Celle-ci repose sur le fort effet trans du carbène situé en position *trans* par rapport au ligand pyridine qui est rendu labile et peut ainsi être échangé par d'autres ligands d'intérêt. Ainsi, plusieurs ligands comme la cyclohexylamine ont pu être introduits de façon quantitative sur les complexes de platine(IV), augmentant ainsi la lipophilicité et la diversité des dérivés [(NHC)$PtBr_4$L]. Finalement, la famille de complexes de type NHC-platine(IV) peut également être étendue en utilisant l'iode hypervalent $PhICl_2$ comme oxydant. En effet, cet oxydant a permis la synthèse d'une famille de composés de formule générale [(NHC)$PtCl_4$L] avec de bons rendements. Finalement, d'autres oxydants ont été envisagés dans le but d'accéder à des dérivés de platine(IV) fonctionnalisés par des ligands hydroxo, néanmoins tous les essais effectués se sont conclus par des échecs.

La caractérisation par RMN ^{1}H des dérivés de platine(IV) a confirmé l'oxydation sélective du centre métallique puisqu'un déplacement général des signaux vers les champs bas a été observé pour l'ensemble des complexes isolés et s'est montré typique des dérivés [(NHC)PtX_4L] avec X = chlore ou brome et L = amine. De même, le déblindage des signaux correspondants à la

résonnance des carbones en RMN ^{13}C est caractéristique de l'oxydation du platine au degré d'oxydation +IV. A noter, contrairement aux autre carbones, le carbone carbènique est systématiquement observé blindé à δ 109–120 ppm dans le cas des complexes NHC-Pt(IV). En outre, plusieurs cristaux uniques ont été obtenus par diffusion de vapeur et ont confirmé la structure octaédrique des complexes de type [(NHC)PtX_4L] où le NHC est situé en *trans* du ligand L alors que les quatre bromes font partie du même plan perpendiculaire. De plus, aucune différence significative de longueur de liaison n'est observée en fonction de la nature de l'halogène coordiné.

A) B)

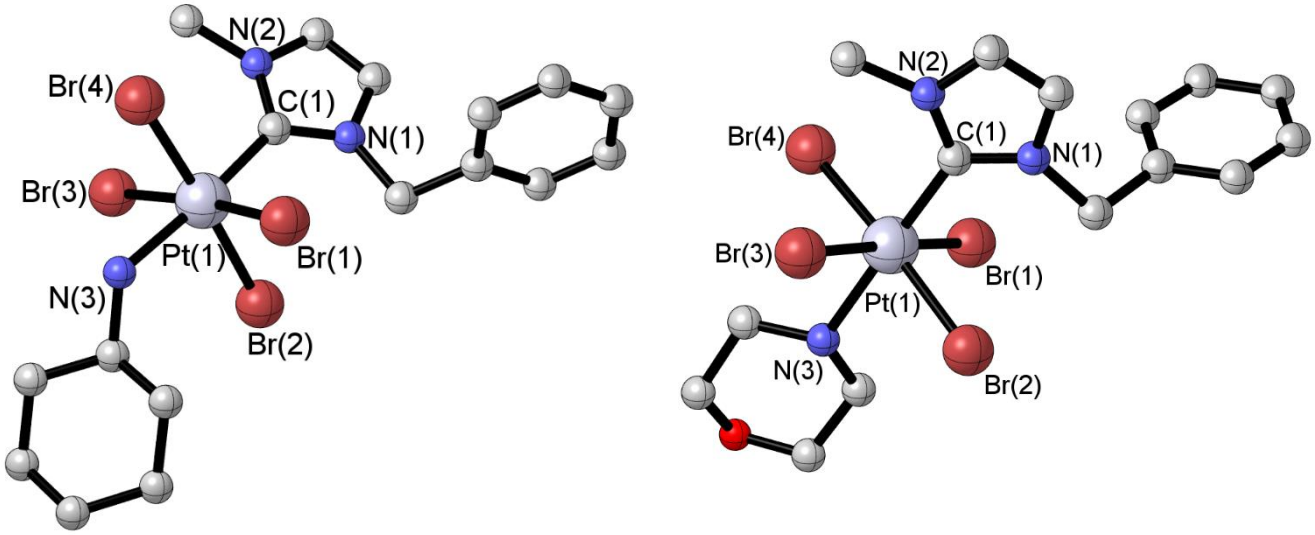

Figure 2: Structures moléculaires de deux complexes de type [(NHC)$PtBr_4$(pyridine)] **77** (A) et **81** (B).

Finalement, plusieurs exemples représentatifs des dérivés de type NHC-platine(IV) ont été analysés par RMN ^{195}Pt qui est apparu comme un outil de choix dans la chimie du platine puisqu'il a récemment été suggéré que ce déplacement soit dépendant de la densité électronique du centre métallique. Il est à noter qu'une grande différence de déplacement chimique du platine a été observé en fonction du degré d'oxydation du centre métallique entre les complexes NHC-Pt(IV) et NHC-Pt(II). En effet, les signaux correspondants aux complexes des familles [(NHC)$PtBr_4$L] et [(NHC)$PtCl_4$L] se trouvent à un déplacement chimique de δ 2000-2200

ppm et δ 800-900 ppm respectivement, alors que le platine résonne en dessous de δ 3000 ppm pour les complexes de type NHC-platine(II).

La stabilité d'une molécule est un paramètre important dans le développement de nouveaux médicaments puisqu'elle influence non seulement sa biodistribution dans le corps, mais également les effets secondaires liés à une mauvaise excrétion comme c'est le cas du cisplatine. Ainsi, une étude de stabilité a été conduite sur plusieurs exemples représentatifs de complexes NHC-platine(IV) vis-à-vis du DMSO qui est couramment utilisé pour solubiliser des dérivés lipophiles pour des applications *in vitro*. La réaction de l'ensemble des dérivés NHC-platine(IV) en présence de DMSO/H_2O a été observée par spectroscopie UV-vis et RMN ^1H, confirmant ainsi la formation d'une nouvelle espèce où le centre métallique est réduit au degré d'oxydation +II et la pyridine a été substituée par une molécule de DMSO. Pourtant, il est apparu que la cinétique de cette réaction est dépendante du potentiel redox des complexes puisque les dérivés [(NHC)$PtBr_4$L] réagissent en moins de 24h alors que la famille [(NHC)$PtCl_4$L] a montré une bonne stabilité sur plusieurs mois, montrant clairement leur plus grand intérêt pour des études biologiques. Ceci a pu être confirmé par voltamétrie cyclique et a souligné l'importance de la quantité d'eau présente dans la solution de DMSO sur la cinétique de cette réaction.

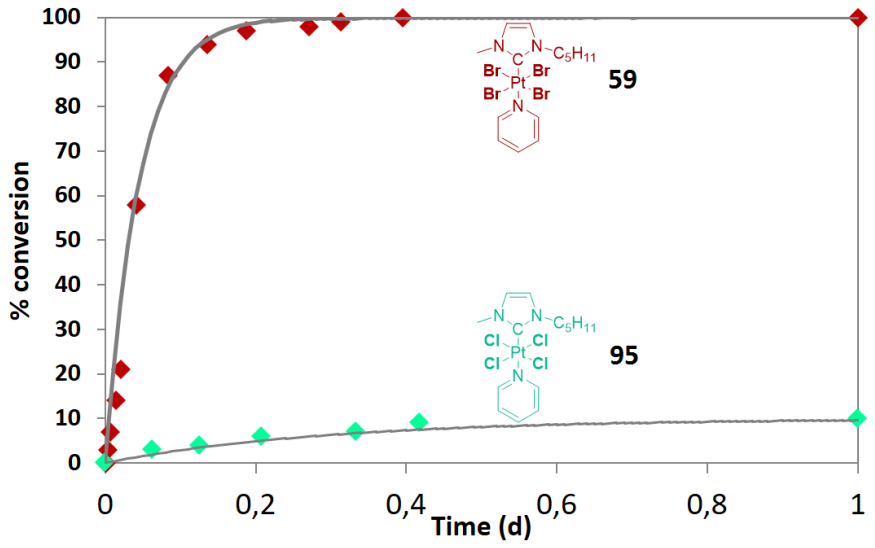

Figure 3: Tendances générales observées pour la conversion des complexes NHC-Pt(IV)-amine en une nouvelle espèce NHC-Pt(II)-DMSO en fonction du temps dans un mélange DMSO/H_2O

Afin de simuler au mieux le milieu biologique, une seconde étude de stabilité des NHC-platine(IV) a été menée dans du sérum de souris. Par spectroscopie UV-visible, il est apparu que le complexe était consommé en 30 minutes, ce qui semble raisonnable au vu de la demi-vie du cisplatine (21,6 min) et du satraplatin (6,3 min) dans le sang.

Il est bien établi que les complexes de type platine(IV) agissent comme des pro-médicaments et donc que leur bioréduction est une étape nécessaire pour permettre la délivrance du principe actif et une activité anticancéreuse efficace. De nombreuses protéines et molécules soufrées présentes dans le sérum et les tumeurs hypoxiques peuvent promouvoir le processus de réduction Pt(IV)/Pt(II). La glutathione est un bioréducteur largement présent dans le sang et a donc été utilisé comme un modèle pour étudier la réduction d'un complexe NHC-platine(IV) par voltammètrie cyclique. Une étude complémentaire par RMN ^{1}H a confirmé que l'espèce issue de cette bioréduction est effectivement le complexe NHC-platine(II) cytotoxique correspondant ce qui soutient la possibilité de réduction des NHC-platine(IV) *in vitro* et *in vivo*.

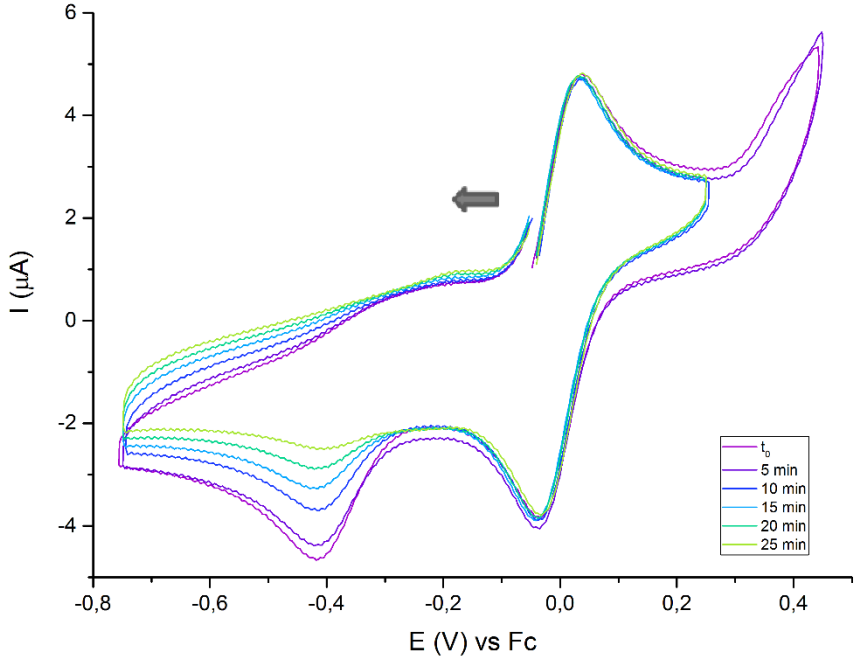

Figure 4: Evolution par voltammétrie cyclique à 100 $mV.s^{-1}$ d'un complexe $[(NHC)PtCl_4(pyridine)]$ dans une solution de DMSO et 0,1 M de $TBAPF_6$ en présence d'un équivalent de GSH

La cytotoxicité de plusieurs pro-médicaments NHC-platine(IV) a été analysée sur trois lignées cellulaires cancéreuses et comparée aux complexes de platine(II) correspondants ainsi qu'au cisplatine servant de référence. La majorité des complexes étudiés ont démontré des activités anticancéreuses prometteuses de l'ordre de la micromole. De plus, certains dérivés du type [(NHC)$PtCl_4$L] ont montré une cytotoxicité plus importante que leur équivalents platine(II), suggérant un mécanisme d'action supplémentaire à la délivrance du NHC-platine(II).

La résistance de certains types de cancer au traitement basé sur le cisplatine restant à ce jour une limitation de taille à surmonter, la modification du mécanisme d'action anticancéreuse des complexes NHC-platine(IV) par rapport au cisplatine a été envisagé comme une alternative prometteuse dans le traitement des cancers résistants. Ainsi, la cytotoxicité d'un pro-médicament NHC-platine(IV) a été évaluée *in vitro* sur une lignée cancéreuse standard et son équivalent mutée et résistante à l'action anticancéreuse du cisplatine. Il est apparu que le complexe NHC-platine(IV) est capable de contourner ce mécanisme de résistance et de promouvoir une cytotoxicité similaire sur les deux lignées cellulaires. Ces résultats ont été confirmés sur une autre lignée cellulaire cancéreuse où le gène p53 est inactivé. Afin de comprendre plus en détail les mécanismes mis en jeu par cette nouvelle classe d'agents anticancéreux et d'identifier la voie métabolique impliquée, plusieurs études mécanistiques ont été menées. Alors que les études préliminaires ne semblent pas indiquer d'interaction entre le platine et les nucléobases, les mitochondries sont apparues comme des cibles plus probables pour les pro-médicaments NHC-platine(IV). En effet, ces complexes favorisent l'apparition de fort stress oxydant dans les mitochondries et promeuvent la perte de viabilité de la respiration mitochondriale des cellules cancéreuses traitées de façon dose-dépendante.

Finalement, ces multiples études confirment le potentiel des pro-médicaments de type NHC-platine(IV) dans la lutte contre le cancer, particulièrement dans le cas des cancers réfractaires, grâce à leur activité anticancéreuse impliquant un mécanisme de mort mitochondriale par génération de stress oxydant.

Le quatrième chapitre de cette thèse introduit la délivrance contrôlée de médicaments par combinaison de motifs NHC-platine anticancéreux à différents systèmes nano-transporteurs. En effet, une partie des effets secondaires associés au traitement à base de cisplatine sont dus à la formation d'adduits entre le platine et les protéines qui interrompt certains processus biologiques. En conséquence, les systèmes transporteurs ont récemment connu un intérêt croissant dans l'espoir de limiter les réactions secondaires et accéder à de nouveaux médicaments sélectifs des cellules cancéreuses pour le traitement personnalisé.

Dans un premier temps, plusieurs dérivés NHC-platine(II)/(IV) ont été emprisonnés dans une protéine biocompatible, l'albumine bovine, qui est l'une des principales protéines dans le sang et qui est bien établie comme agent délivrant pour de nombreux médicaments. Ceci a pu être effectué avec succès selon une procédure simple et a permis une variation de la charge de platine attachée au transporteur par adaptation des quantités de précurseurs mises à réagir. L'analyse par spectroscopie UV-vis de la bande à λ = 280 nm correspondant aux transitions $\pi \rightarrow \pi^*$ des résidus aromatiques de l'albumine, a confirmé l'interaction avec l'albumine de l'ensemble des complexes NHC-platine utilisés. A noter, l'interaction semble plus forte dans le cas des complexes portant des ligands bromés que pour les complexes fonctionnalisés par des ligands chlorés. Finalement, le bon relargage des médicaments a pu être observé par RMN ^{1}H, et leurs activités anticancéreuses ont été étudiées *in vitro*, confirmant ainsi la différence de cytotoxicité marquée en fonction de la nature de l'halogène porté par le métal.

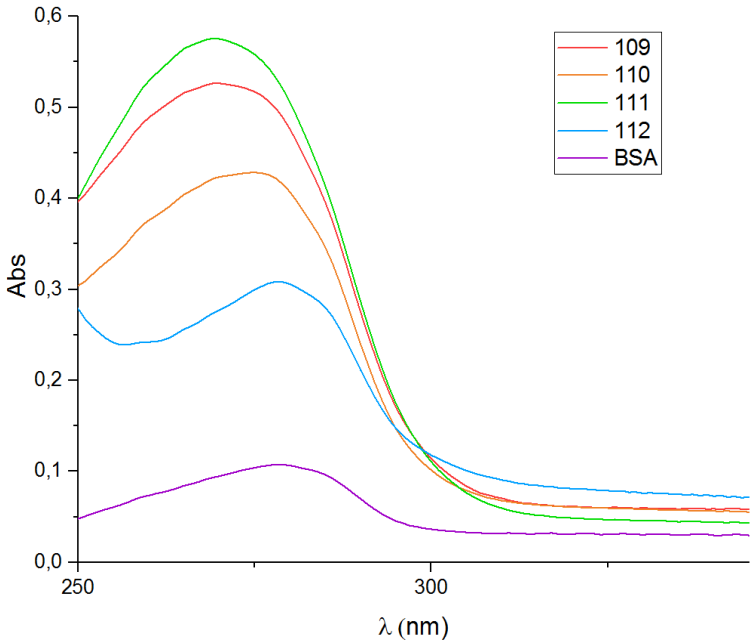

Figure 5: Evaluation de l'interaction des complexes NHC-Pt(II) **2**, **4** ainsi que des complexes NHC-Pt(IV) **59**, **95** avec l'albumine par spectroscopie UV-vis (ratio de 1Pt/1BSA)

Parallèlement, nous avons étudié l'encapsulation d'un dérivé NHC-platine(II) dans un liposome anionique formé d'une bicouche de phospholipides qui a été possible grâce à la fonctionnalisation du complexe de platine par deux longues chaines alkyles. Une étude préliminaire a suggéré des propriétés antiprolifératives *in vitro* modérées dans le cas de cellules cancéreuses traitées avec les liposomes chargés en NHC-platine.

Dans un autre développement, la combinaison des motifs NHC-platine cytotoxiques à un polymère biocompatible et hydrophile, le polyéthylènimine aussi appelé PEI, a été étudiée dans le but d'améliorer leurs propriétés physiologiques et permettre à terme une translation vers les études cliniques. En effet, les études préliminaires conduites dans notre groupe sur cette famille avaient souligné le fort potentiel de cette classe de médicaments et la nécessité d'augmenter la diversité chimique disponible pour améliorer les propriétés de ces métallo-polymères. L'adaptation de la synthèse précédemment développée dans notre groupe a permis la variation de la charge en platine le long du polymère. Les meilleures activités antiprolifératives ayant été observées *in vitro* pour un ratio d'un platine pour trente monomères. Autrement, plusieurs

méthodes de synthèse ont été développées pour permettre la pré- ou post-fonctionnalisation de ces macromolécules par des fragments d'intérêt tels qu'un sucre, des chaines PEG hydrophiles, des chromophores permettant des études mécanistiques *in vitro*, ou encore un agent de ciblage. L'ensemble des méthodes développées sont simples et ont permis l'accès à une large gamme de macromolécules de façon quantitative comme confirmé par RMN ^{1}H sur l'ensemble des dérivés. Plusieurs de ces macromolécules fonctionnalisées par des chromophores ont permis des études de biodistribution *in vitro* par épifluorescence et suggèrent une bonne absorption du métallo-polymère.

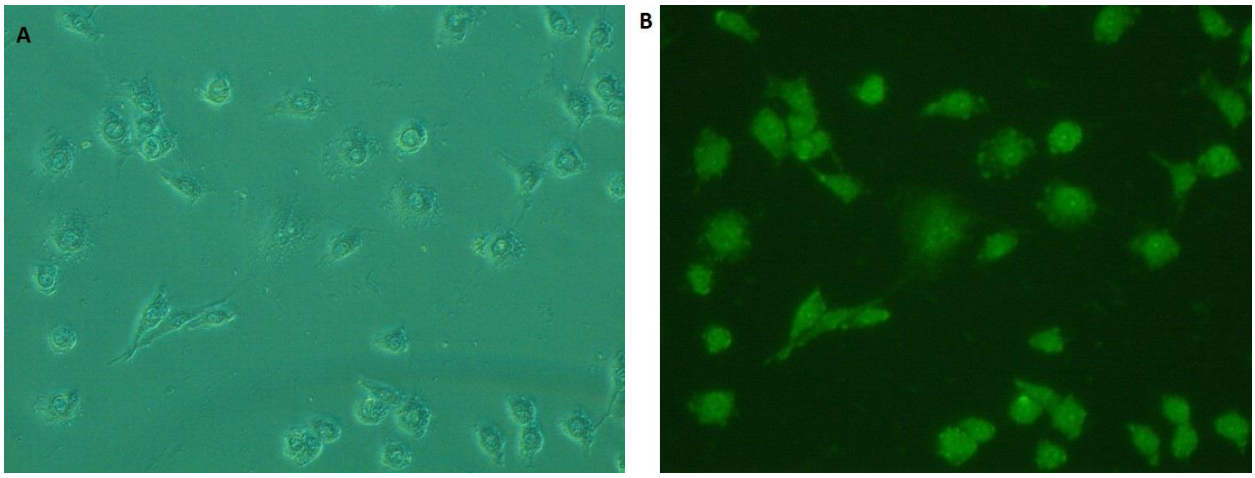

Figure 6: Vue de cellules cancéreuses traitées avec le complexe **133** par épifluorescence sous A) lumière blanche, B) lumière UV à λ = 365 nm

La fin de ce chapitre se concentre sur le développement de deux tailles de nanoparticules d'or stabilisées par du PEI dans le but d'attacher des fragments cytotoxiques de NHC-platine à leur surface et permettre une délivrance sélective vers les cellules cancéreuses par voie passive. Une méthode simple a permis l'obtention de deux tailles de nanoparticules de façon reproductible comme confirmé par la présence d'un signal intense et fin en UV-vis à λ = 520 nm correspondant à la résonnance plasmonique de surface des nanoparticules, ainsi que par microscopie électronique en transmission. Il est intéressant de noter que ces nanoparticules ont démontré une stabilité accrue aussi bien en solution aqueuse qu'en présence de sérum de souris. Il est apparu que la toxicité de ces nanoparticules était hautement dépendante de leur taille, les petites nanoparticules de 10 nm ne montrant pas d'activité cytotoxique *in vitro*, même

à haute concentration. Plusieurs méthodes ont ensuite été étudiées afin d'attacher les complexes NHC-platine à la surface de ces nano-transporteurs biocompatibles. Finalement, les propriétés en transfection de ces nanoparticules de PEI biocompatibles ont montré des résultats préliminaires prometteurs et ouvrent l'accès à la délivrance de matériel génétique et autres médicaments.

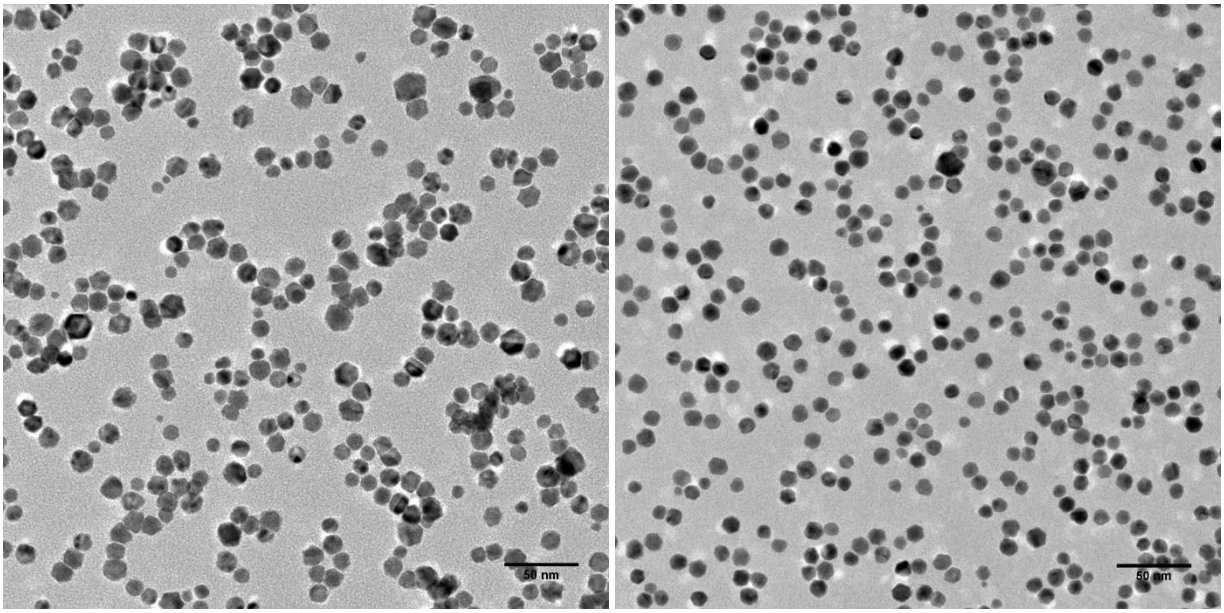

Figure 7: Images typiques obtenues par microscopie électronique en transmission sur un échantillon de PEI-AuNPs avec un diamètre moyen de 10 nm

Chapter 1: Introduction

For the past decades, large contribution to medicinal sciences originated from the field of inorganic medicinal chemistry whether it deals with metal-based chemotherapeutic drugs, metal-drug interactions, metal ions in disease and so forth.[1] The large range of properties available for transition metals offers high opportunities for drug discovery.[2,3] However, in the fight against cancer although NAMI-A,[4] auranofin[5] or budotitane[6] depicted high *in vitro* potencies, to date no non-platinum drug has been approved for worldwide commercialization and cisplatin remains nowadays the reference for chemotherapy.[7]

I. Cisplatin

Breakthrough in the fight against cancer arises from the fortunate discovery of cisplatin's potency by Rosenberg[8] and subsequent FDA approval for its use in clinics. Its high potency allows nowadays a cure rate of over 90% in testicular cancer[9] and appeared as a strong alternative in the treatment of ovarian, testicular, lung and bladder cancers. However, limitations due to major side effects and resistance to cisplatin-based treatment are common. Therefore, research in academy or pharmaceutical industry on platinum-based chemotherapy remains a very active field of investigation.[1]

1) Mechanism of cytotoxicity

a. Drug uptake

Cisplatin is usually intravenously injected as a saline solution[10] and progressively enters cancer cell following numerous pathways proceeding in parallel,[11] predominantly either passive

diffusion through gated channels or active protein-mediated transport.[12,13,14] In particular, various sulphur containing copper transporters[15,16,17] and other proteins such as organic cation transporters (OCTs)[18,19] have been suggested to favourably support platinum cellular accumulation.[20,21,22,23] The pathway for drug internalization in cancer cells impacts its biodistribution and accordingly both electronic and steric parameters at the platinum centre play a critical role in the efficient drug uptake.

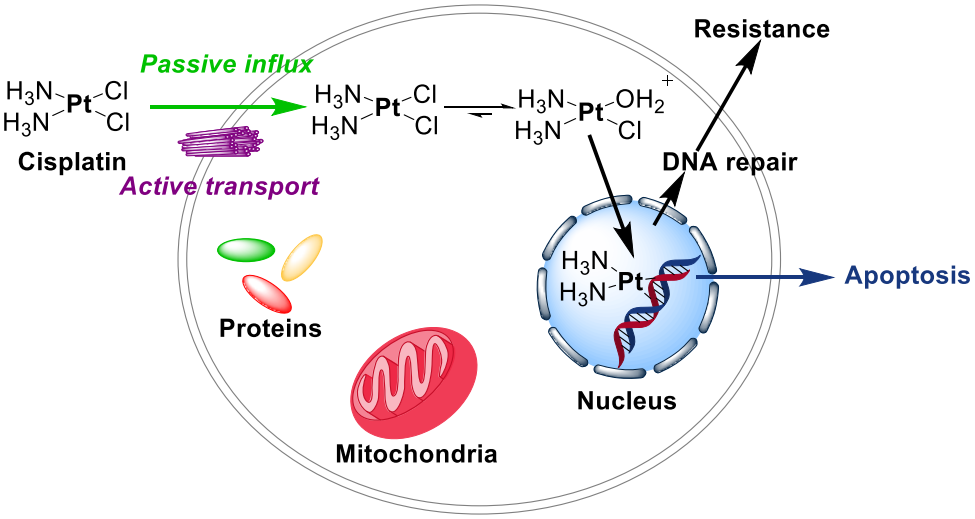

Scheme 1: Mechanism for cisplatin passive diffusion

The complex biological environment promotes cisplatin hydrolysis and metabolites formation[24] though analytic techniques as HPLC analysis, ^{195}Pt NMR[25] or radiolabelled platinum derivatives[26,27] failed to determine their nature due to sublethal platinum concentrations thus preventing *in vivo* mechanistic studies. Therefore, reactions in aqueous media mimicking the *in vivo* environment provided most knowledge concerning platinum fate (Scheme 1). While extracellular pH is 7.4 ± 0.1,[28] intracellular pH drops to 6.8 and chloride concentration dramatically decreases down to 4 mM in cells (*vs.* 100 mM in extracellular medium) thus promoting the formation of the mono-aquated by-product *cis*-$[(NH_3)_2PtCl(H_2O)]^+$. Subsequent metabolization proved to favour the formation of diaqua species, hydroxo derivatives, hydroxo-bridged multimers and so forth[29,30] which are capable to enter nucleus and further interact with DNA.[31]

b. DNA as the main target for platinum derivatives

DNA has been recognized as the main target for platinum derivatives due to the discovery of filamentous growth in *E. Coli* which is characteristic of cell division disruption and DNA synthesis inhibition though cell growth remained intact.[8] The accepted mechanism involves platinum coordination through ligand exchange at the nitrogen atom of nucleobases, especially the N7 atom of guanine (G) and adenine (A).[32,33] Several adducts have been evidenced and quantified, including 1,2-intrastrand d(GpG) cross linking (Figure 1A) and eventually 1,3-intrastrand d(GpTpG) cross linking (Figure 1B).[34]

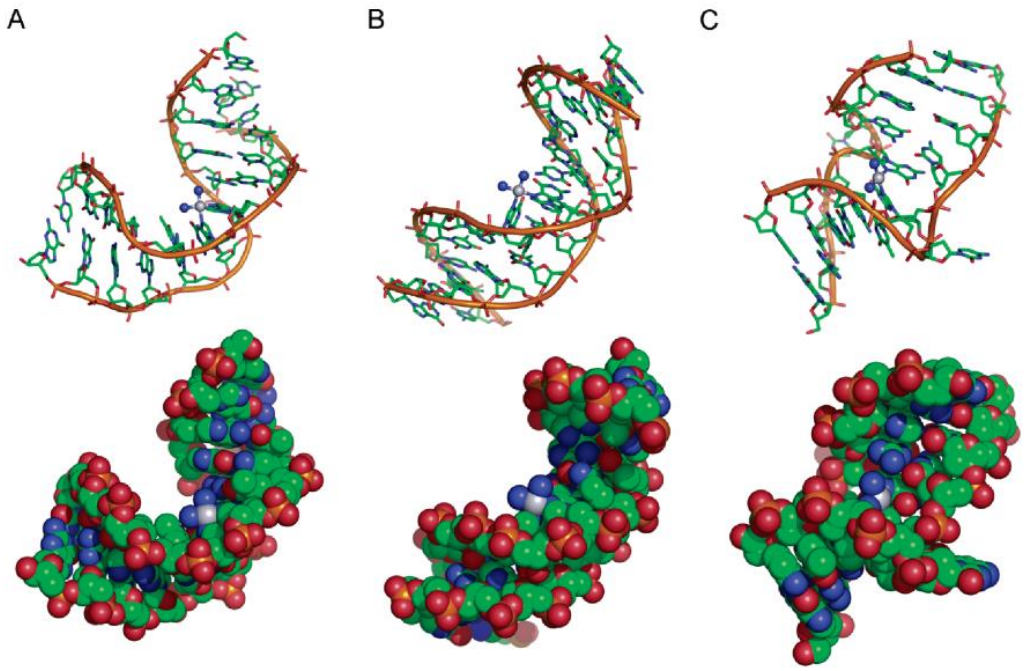

Figure 8: Platinum-DNA adduct structures. Duplex DNA containing (A) cisplatin 1,2-d(GpG), (B) 1,3-d(GpTpG) intrastrand, and (C) cross-links, generated by PyMol.[21]

On the other hand, *trans*-diamminedichloroplatinum(II) (*trans*-DDP) failed at promoting cancer cell cytotoxicity. It has been attributed to the slow closure rate for the formation of bi-functional Pt-DNA adducts ($t_{1/2}$ > 24h for *trans*-DDP while $t_{1/2}$ ~ 8h for cisplatin[35]) and may explain the formation of easily repaired 1,3-intrastrand and interstrand cross-links[36,37,38,39] rather than 1,2-

intrastrand cross-links.[40] This observation highlights the great influence of the platinum environment toward both involved its mechanism and subsequent cytotoxicity.

c. Cisplatin adducts with DNA: influence toward cell cycle, repair system and cell resistance

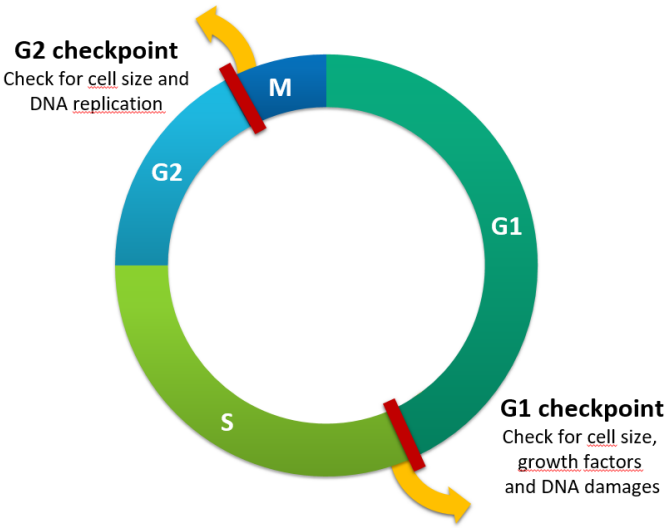

Figure 9: General cell cycle graph

The cell cycle in mammalians is divided into 4 phases (Figure 2): a) cell size increase in G1 due to gene transcription and proteins synthesis, b) DNA is replicated at S phase, c) G2 phase corresponds to cell growing and synthesis of RNA and proteins, d) during mitosis cell division and replication occur. Two checkpoints after G1 and G2 phases ensure the genome integrity by controlling DNA lesions, excising damaged areas on DNA strands or proceeding to cell death. It occurs following either a necrotic pathway, meaning loss of membrane cell integrity, or an apoptotic pathway corresponding to a programmed cell death going through damage recognition by proteins inducing further cycle arrest signal (Figure 3). Cisplatin is well known to induce caspase dependent apoptosis in cancer cells.[41] Indeed, while it appears to be inefficient at inducing cell death at the G1 checkpoint, cell cycle arrest at the G2 checkpoint has been evidenced and supports replication blocking during the S phase.[42,43] Moreover, the formation of DNA-platinum adducts promotes the deregulation of polymerases which act as a damage

recognition factor thus initiating a nucleotide excision repair[44] and subsequent inhibition of the RNA transcription process.[45] Finally, caspases 3 and 7 enzymes which are responsible for polypeptidic chains cleavage have been largely accepted as being involved in the cisplatin induced apoptosis thus supporting DNA fragmentation.[46]

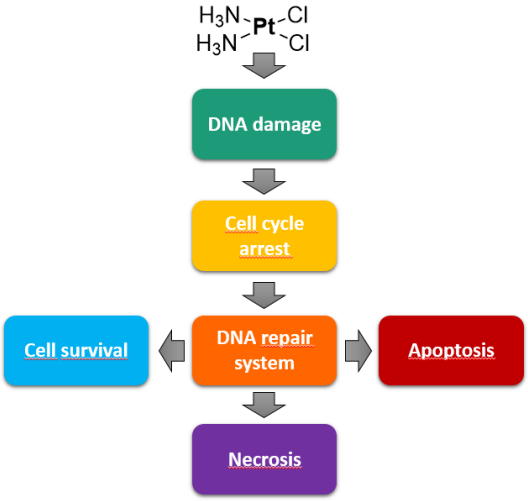

Figure 10: Pathways for cisplatin-induced apoptosis and necrosis

Although cisplatin induces high cytotoxicity toward cancer cells, either intrinsic or acquired resistance are often associated with the treatment thus degenerated tissues, which initially responded favourably to the treatment acquire drug resistance over exposure. Resistance mechanisms can be related to four major events: 1) a decrease in drug uptake and/or increased efflux; 2) a local increase in thiols concentration; 3) a failure in the cell death signalling pathway; 4) either an increase in the repair process efficiency or an improved tolerance to damages. DNA repair processes, namely nucleotide excision repair process (NER), base excision repair process (BER) and DNA mismatch repair process (MMS), are capable to identify and correct damages during DNA replication. DNA-Pt adducts mainly 1,2-intrastrand cross-links have been suggested to be primarily removed by the NER.[47] DNA lesions recognition involves the binding of several proteins (namely XPA, RPA and XPC)[48] which promote the excision of damaged DNA and replacement by a short complementary oligonucleotide sequence freshly synthesized by DNA

polymerase (Figure 4).[49] This is evidenced by up to 10-fold increased sensitivity to cisplatin on NER deficient cell line compared to regular cell line.[50,51]

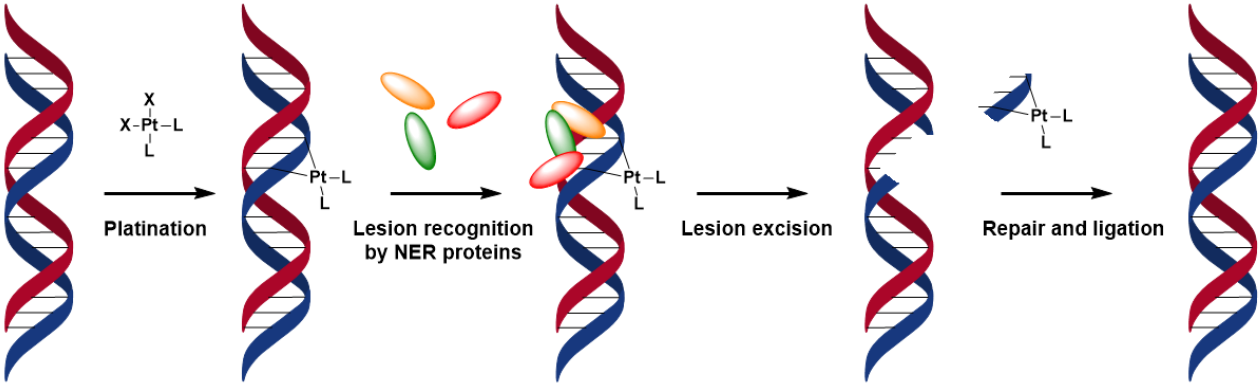

Figure 11: Nucleotide excision repair after Pt-DNA adduct recognition by NER proteins

To note, several studies suggested a correlation between cancer cell lines resistance and their inability to efficiently undergo mismatch repair process.[52,53] Yet, it is noteworthy to mention that contradictory results were obtained *in vitro* and *in vivo*[54] thus suggesting the occurrence of a more complex mechanism of resistance.[55,56,57,58,59] Furthermore, the cellular tumour antigen p53 has a crucial influence in the recognition of DNA damages and can induce transitory stop in the cell cycle before DNA replication[60] thus preventing mutation replication and ensuring conservation of the genome integrity. Remarkably, numerous cancer cells depict a mutation inactivating the p53 gene and resistance phenomena observed with cisplatin are often associated to the disability of p53 mutated gene to promote cell cycle stop.[61]

2) Stability and side effects

Despite the impressive results obtained with cisplatin for cancer treatment in clinics, its poor stability causing severe side effects remains a major issue.[62] Moreover, additional adverse effects sometimes appear several years after cisplatin administration due to uncomplete

platinum excretion.[63] Hepatotoxicity which corresponds to liver tissues necrosis due to disruption of the redox homeostasis[64] and cardiotoxicity which is usually due to both necrosis and degeneration of the cardiac muscle[65,66] are among the most common side effects. Moreover, nephrotoxicity is related to a large accumulation of platinum in the kidney during excretion and irreversibly damages surrounding tissues.[67] Finally, ototoxicity is a common side effect and not dose-limiting thus causing immediate and permanent deafness or tinnitus. Remarkably, it is now widely accepted that only 1% of the initially injected platinum drug reaches the nucleus,[68,69] the remaining platinum being bound to thiols such as cysteine, glutathione (GSH), methionine and so forth.[70,71,72,73,74] While such interactions can improve the sensitivity of several cancer cells to DNA damages,[75] development of chemotherapy resistance can also be promoted.[76] Finally, cisplatin is not selective for cancerous cells thus proving highly toxic toward the whole human body and inducing severe side effects. Accordingly, numerous drug combinations with cisplatin are currently under clinical trial and better analogs are awaited with great interest in order to limit or even suppress such unfortunate events.[77]

3) *Other platinum(II) drugs*

Over 4000 platinum derivatives with good leaving groups *trans* to aminated ligands have been investigated to lower side effects, increase cytotoxicity and selectivity or even facilitate drug administration, yet only a few reached clinical trials.[78,79]

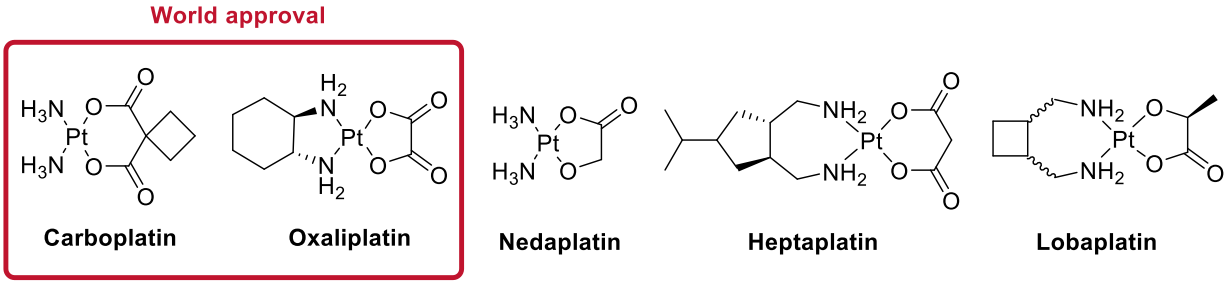

Scheme 2: Platinum(II) drugs approved in clinics

a. Carboplatin

Carboplatin was developed by Johnson Matthey and further approved in 1989 for worldwide use. While its overall stability is increased thanks to chelate effect of novel oxygen ligand, slower aquation decrease nucleus osmosis. Yet its binding modes proved identical as cisplatin. Moreover, increased protein binding and drug deactivation appeared linked to the fact that nephro- and neurotoxicity[80] and cell resistance similar as cisplatin were observed, thus limiting its use against several cancers.

b. Oxaliplatin

Second generation drug, oxaliplatin, was available on the market starting from 2002. It appeared as a strong alternative to cisplatin thanks to its improved design promoting both slower aquation rate and improved stability. Moreover, oxaliplatin depicted somewhat lower affinity for deactivation through protein binding. Potency through DNA binding and NER resistance account for its efficiency at overcoming resistance even in cisplatin-resistant cell lines. Finally, clinical tests confirmed its high efficiency in the treatment of colon cancer where no cross-resistance was observed.[81] However, strong neurological symptoms are still deplored after prolonged treatment.

c. Other Pt(II) drugs with promising clinical responses

Nedaplatin is commercialized by Shionogi Pharmaceutical Company in Japan for the treatment of head, neck and testicular cancers. While fewer side effects have been observed, its mechanism of action proved similar and no overall toxicity improvement was perceived.[82] Heptaplatin is used in clinics in South Korea to cure gastrointestinal diseases. It depicted lower side effects than cisplatin in addition to high activity toward cisplatin resistant cancer cells.[83]

Lobaplatin, which was developed by ASTA Pharma in Germany, has been approved in China for the treatment of various cancers such as myelogenous leukemia, breast cancer and so forth.[84,85] Finally, the variety of Pt(II) drugs tested for anticancer applications highlighted the importance of the nature of ligands surrounding the platinum centre. Therefore, the coordination of a stabilizing ligand is expected to overcome restrictions related to low stability and major side effects observed with drugs following the structure-activity relationship (SAR).[86]

II. *N*-Heterocyclic Carbenes

As previously underlined, the ligands electronic and steric parameters have a strong influence toward complexes pharmacological properties, namely solubility, stability and so forth. Moreover, platinum (II) anticancer drugs translation to clinics remains confronted to cell resistance mechanism. Consequently, the replacement of amine ligands by more strongly bound ligands has been proposed to go beyond the well-established structure-activity and modify the *in vivo* platinum fate. N-heterocyclic carbenes (NHCs) recently appeared as a powerful class of ligand for metal coordination in numerous fields ranging from catalysis,[87,88,89] photophysic[90] and bioinorganic drug.[91] Indeed, in addition to being easily fine-tuned and available at low cost in large quantity,[92] NHCs unique properties allow them to perfectly adjust reactivity, oxidation state and geometry of transition metals.

1) Electronic and steric properties of N-heterocyclic carbenes

In the late sixties, Wanzlick[93] and Öfele[94] independently reported the successful synthesis of NHC-metal complexes by imidazolium deprotonation and *in situ* coordination to transition metal. However, the development of NHC ligands remained restricted for years due to failed attempts of free-carbene isolation. A major advance in the field was achieved by Bertrand who isolated the first free phosphino-carbene in 1988.[95,96] Subsequent isolation of the highly

stabilized free bis-mesityl carbene by Arduengo in 1991[97] paved the way for the NHCs which are nowadays well-established ligands in numerous fields of investigation.

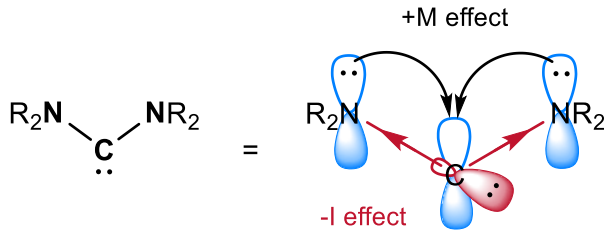

Scheme 3: Mesomeric and inductive effects in N-heterocyclic carbenes

Two different electronic states exist for N-heterocyclic carbenes, namely triplet and singlet state which is more common. Several factors affecting the singlet–triplet gap have been established, namely the geometry at the carbene and the presence of neighbouring π systems. For singlet NHCs, -I inductive effect of both nitrogens stabilizes the σ orbital at the carbene. In parallel, the empty carbon 2p orbital is stabilized by +M mesomeric electrons withdraw from the two adjacent non-bonding nitrogen orbitals[98] as shown in Scheme 3. Accordingly, the ligand's $HOMO_{NHC}$ is found higher in energy, thus enlarging the energy gap between the σ occupied and p empty orbitals. Accordingly, the high $HOMO_{NHC}$ accounts for the great σ-donor character of NHC ligands. Moreover, NHCs can act as π acceptors for electron-rich metals in a classical d-π* back-donation where electronic density is withdrawn from d orbitals to empty low-energy π orbitals of the NHC. Thus NHC-metal bond is mostly a σ covalent bond, π acceptance depending on several aspects such as the nature of N-substituents, of the metal or the other ligands.

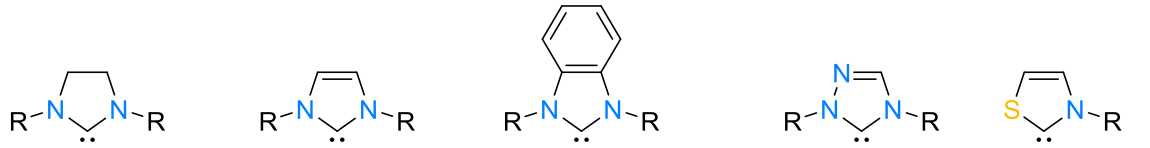

Scheme 4: Most common backbones of free NHCs

Both steric and electronic properties can be ascertained with the combined use of characterization and calculation methods.[99,100] This has been highlighted using different techniques ranging from measurements of the free carbene pKa, IR spectra of the

corresponding Ir-carbonyl complex, calculated Tolman parameter and percentage of buried volume, electrochemical determination of the LEP parameter, in addition to carbenic carbon ^{13}C NMR characterization as an indicator of the electronic density in the corresponding bis-NHC moiety.[101,102]

Remarkably, the replacement of one N-R function by an electronegative sulphur atom in the heterocycle usually gives rise to weaker donor ligand according to the HEP parameter. Likewise, in the case of triazole derivatives, the third nitrogen atom within the aromatic ring appears to decrease donor properties compared to classical NHCs.[103]

2) *Metal complexes of NHCs*

The biological properties of NHC-metal complexes were initially investigated by the group of Cetinkaya in 1996 and highlighted the potential of NHC-Ru(I) and Ru(II) complexes as antibacterial agents.[104,105] This breakthrough paved the way for NHC-metal complexes expansion in the field of bioinorganic drugs.[106,107,108] Accordingly, while NHC-gold complexes have been widely investigated as novel anticancer drug candidates,[109,110] combination of NHC with silver,[111,112] copper,[113] ruthenium,[114] palladium,[115,116] platinum,[117,118,119] and other transition metal depicted promising results either as anticancer drugs or in the treatment of other diseases.[120] Both chemical and thermal stability of the carbene-metal bond toward air and moisture are of great interest in the development of novel drugs to improve the overall stability of metallodrugs. Considering the harsh conditions encountered *in vivo*, namely highly acidic or reducing media and reactive agents, the C-M bond stability is essential to avoid any unwanted event and prevent premature drug inactivation. The ease of derivatization and fast optimization of NHCs precursors allow fine-tuning of both steric and electronic properties by simple modification of either their backbone or N-substituents. This is of major importance to efficiently adapt the versatility of metal complexes and improve both physicochemical properties and reactivity in biological media. Finally, the bulky and strongly bound NHC ligand is

expected to remain attached to the platinum and thus to induce a different mechanism of antitumor action to access polyvalent drugs.

3) Anticancer NHC-Pt(II) complexes

Coordination of NHC ligands to platinum centre displayed a shorter carbene-Pt bond[121] compared with heteroatoms, therefore indicating a possible inertness of this lesion toward inactivation by blood proteins. Thus, several novel NHC-Pt(II) complexes synthesized by oxidation of [(NHC)Pt^0(dvtms)] precursors and subsequent ligand exchange [122,123] have been evaluated as anticancer agents by the group of Marinetti.[119] *Trans* NHC-platinum complexes demonstrated promising activities standing up against the presumption that *cis* configuration is mandatory for competent anticancer drugs.

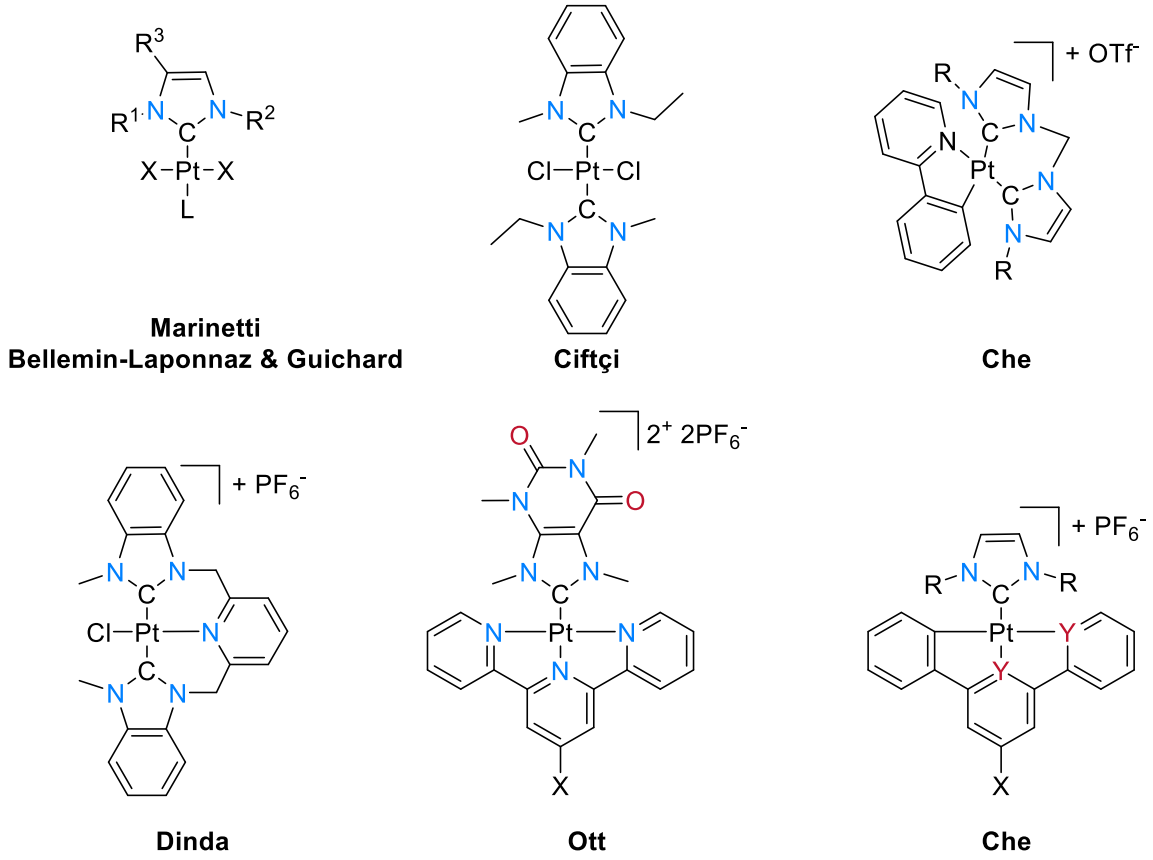

Scheme 5: Selected NHC-Pt(II) complexes investigated for anticancer applications

Preliminary trends could be drawn out of investigated complexes, namely the low amine influence as well as the superiority of iodide complexes toward cancer cells compared to bromide or even nitrate complexes.[119] Moreover, *trans* configured homobimetallic NHC-Pt complexes displayed potencies in the micromolar range and did not cross react with cisplatin on resistant cancer cell line.[124] Detailed investigation of the mechanism highlighted different behaviour from cisplatin since tested NHC-Pt(II) complexes promoted apoptosis through a caspase 3 and 7 independent pathway and was confirmed by the translocation of apoptosis inducing factors and caspase 12.[124] Remarkably, while selected NHC-Pt(II) complexes proved to accumulate up to 10 folds more than cisplatin in the nucleus, no cytotoxicity improvement was reached.[124] This was suggested to be due to either low ability in chelating DNA or easy removal of Pt-DNA adducts by the defence system. Finally, contrarily to cisplatin which induces accumulation at the S/G2, NHC-Pt complexes failed at inducing cell cycle arrest though this seems to be related to the overall drug nature rather than the NHC ligand as other NHC-metal complexes successfully induce cell cycle arrest.[124]

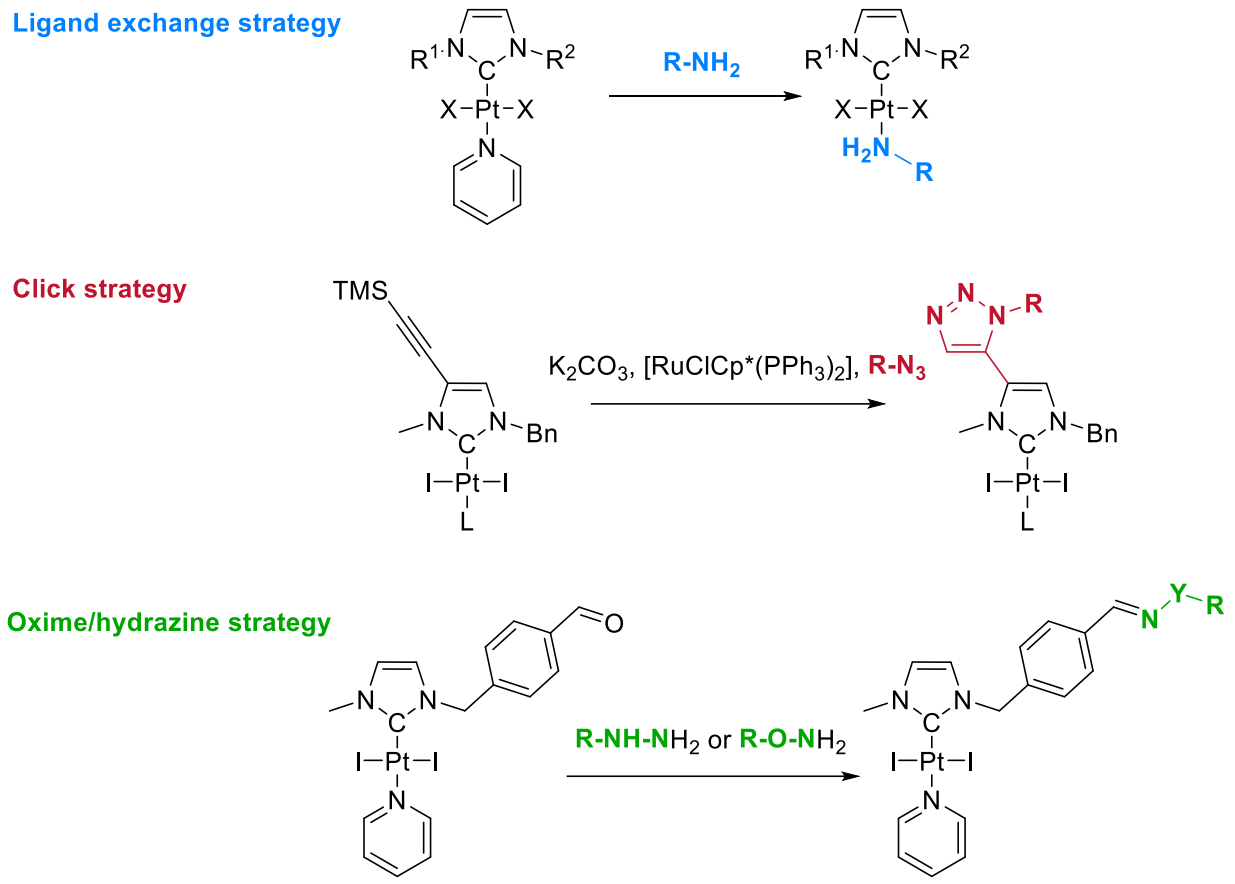

Scheme 6: Post-functionalization strategies developed by our group

A large range of functionalized NHC-Pt(II)-amine complexes have been synthesized in our group following a tuneable and high yielding pathways (Scheme 6).[117,125,126] Indeed, subsequently to one-pot imidazolium deprotonation and coordination to platinum salt, pyridine-ligand exchange allowed easy diversity enhancement. Efficient pyridine displacement was rendered possible by the high *trans* influence of the carbene which weakens the Pt-N bond. Therefore, post-functionalization by ligand exchange with various amino acids and peptides has been widely explored.[127] Very promising results were reached with peptide-functionalized complexes which IC_{50} reached the range of micromolar and in some cases nanomolar concentrations. Moreover, a luminescent complex where emission may be switched on or off depending on the *trans* ligand has been developed in our group to potentially gain deeper knowledge in the interactions of NHC-Pt(II) complexes with DNA.[117] Post-functionalization on NHC's backbone is also possible by click reaction of an alkyne-NHC-Pt(II) complex with external azide (*i.e.* Huisgen reaction).[118] The

most remarkable example is an oestradiol NHC-Pt(II) conjugate designed to access active targeting and which proved somewhat more cytotoxic than cisplatin *in vitro* (Scheme 7).[128] Finally, pH sensitive hydrazine or oxime bonds have been introduced on the NHC's backbone to explore selective targeting and controlled release of bioactive ligands.[129,130] Interestingly, while the combination of NHC-Pt complex with metronidazole favourably compared with cisplatin, neither pyrimidium nor urea conjugation promoted dual action *in vitro*. Until now, all targeted NHC-Pt(II) complexes (Scheme 7) have been tested *in vitro* and *in vivo* studies are needed to evaluate their selectivity toward biological receptors.

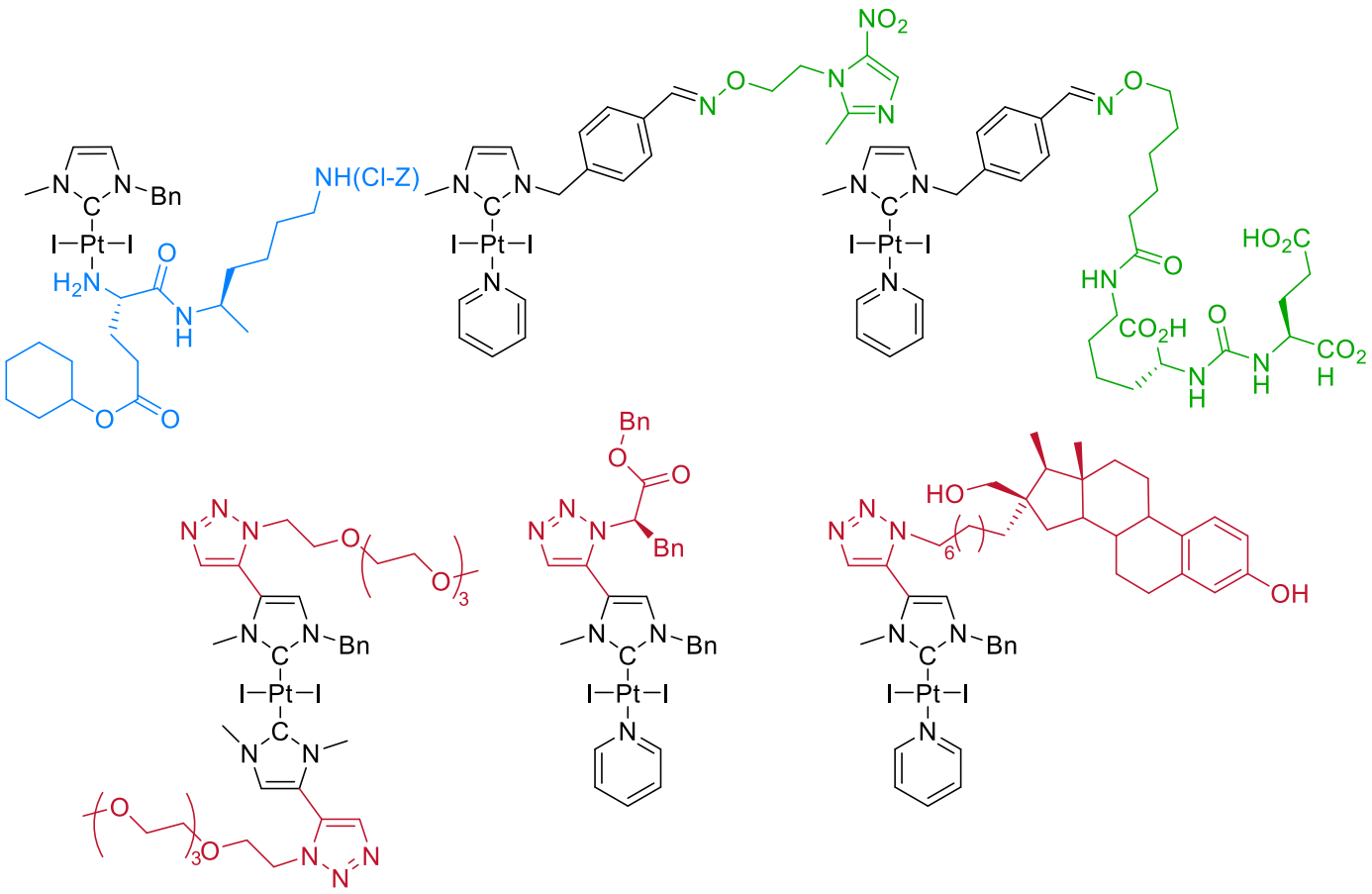

Scheme 7: Selected examples of potent drugs synthesized by post-functionalization strategies

Finally, while the field of NHC-Pt(II) anticancer drugs is very recent, numerous complex architectures have been reported with particularly impressive potencies toward selected diseases such as antileshmanian properties,[131,132] luminescent cores for investigation of the intracellular biodistribution[133,134] or telomeric targeting by G-quadruplex conjugation.[135]

III. Platinum(IV) prodrugs

After decades of investigation on complex ligand architecture on Pt(II) derivatives, recently the attention was turned on the nature of the platinum centre and in particular Pt(IV) derivatives.[136,137,138] While it was often considered as a challenger for anticancer activities, it showed very interesting clinical results. Its molecular structure differs from Pt(II) as the d^6 platinum(IV) adopts an octahedral geometry providing increased inertness toward ligand exchange and offers more opportunities for pharmacological properties fine tuning. This improved stability toward biomolecules allows for greater drug uptake and prevent off-target interactions. Platinum(IV) complexes are considered as a prodrug thanks to their metabolization into cells which involves their bioreduction into a pharmacologically active Pt(II) drug.[141,139] This mechanism has been investigated using several techniques such as elemental imaging of single cell,[140] X-ray absorption near edge structure (XANES)[141] and synchrotron radiation-induced X-ray emission (SRIXE)[142] to confirm drug internalization and release.[143]

1) Pt(IV) in clinical study

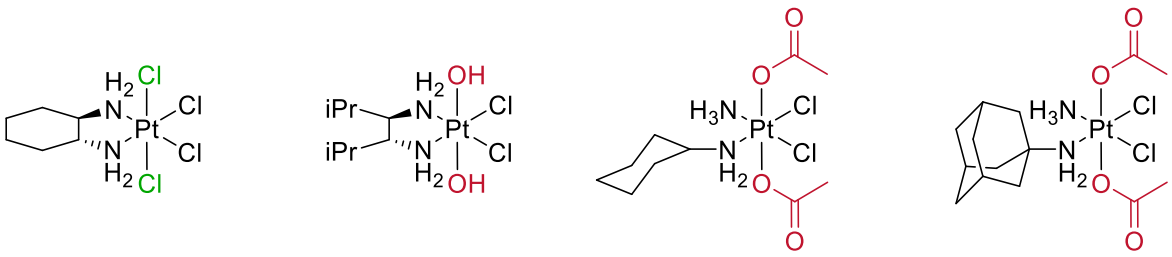

Scheme 8: Structure of platinum(IV) complexes which entered clinical trials

Several Pt(IV) prodrugs entered clinical trials though all of them were recently dismissed due to either severe side effects or low overall survival benefit. Ormaplatin and Iproplatin proved fairly cytotoxic and induced moderate side effects, though nephrotoxicity[144] and myelosuppression[145] respectively remain major issues. Good antineoplastic activity, oral availability and weaker side

effects were reported for LA-12, yet no overall benefit was observed.[146] The highly lipophilic satraplatin (also known as JM-216) based on a modified cisplatin scaffold depicted potencies that compared favourably with cisplatin both *in vitro* and *in vivo*. Its bulky cyclohexylamine ligand is believed to more efficiently overwhelm the DNA-Pt adducts repair process, though some resistance features still appeared.[147] Oral administration allowed up to 10-folds increased inhibition of cancer proliferation compared to intravenous administration.[148] In preclinical phase, six different metabolites where identified, the Pt(II) precursor being the most abundant.[149] Up to 93% of the injected satraplatin was found irreversibly bound to plasma proteins.[150] In clinical trials no neurotoxicity, ototoxicity or nephrotoxicity were observed thus emphasizing its clinical benefit. Nevertheless, FDA refused its market launching due to a too low overall survival benefit.[151]

2) Strategies developed to access efficient platinum release and high cytotoxicity

a. Oxidation of Pt(II) precursors and further derivatization

So far mostly Pt(IV) complexes following the SAR,[86] namely derivatives functionalized with two *cis*-amine ligands, and only scarce examples of phosphine derivatives have been reported for chemotherapy.[152,153] This is probably due to the old assumption that among all the requirements to access highly cytotoxic Pt(IV) derivatives, the presence of at least one ligand possessing a hydrogen bond donor function was necessary.[154]

Numerous architectures have been investigated for either biomedical application or investigation of catalytic processes and fully reviewed recently.[155,156,160] However, most oxidation pathways rely on oxygen peroxide-mediated oxidation of the Pt(II) centre (Scheme 9).[157] The presence of L ligands with hydrogen bonding substituents has been suggested to be of importance for efficient platinum oxidation.[158] Several examples of $[L_2PtCl_4]$ complexes were also obtained by use of chlorine gas or hypervalent iodine, which is more easily handleable. Theoretical investigation of Pt(IV) complexes following the SAR rule highlighted a trend for chloride complexes to be more active than the hydroxide ones.[159] Finally, only few examples

deal with the oxidative addition of a C-X bond and its involvement in catalytic processes. However, in the case of Pt(IV) prodrugs, hydroxo complexes were preferred as starting material for further development warranting either increased lipophilicity or selective binding to cancer cells (Scheme 10).

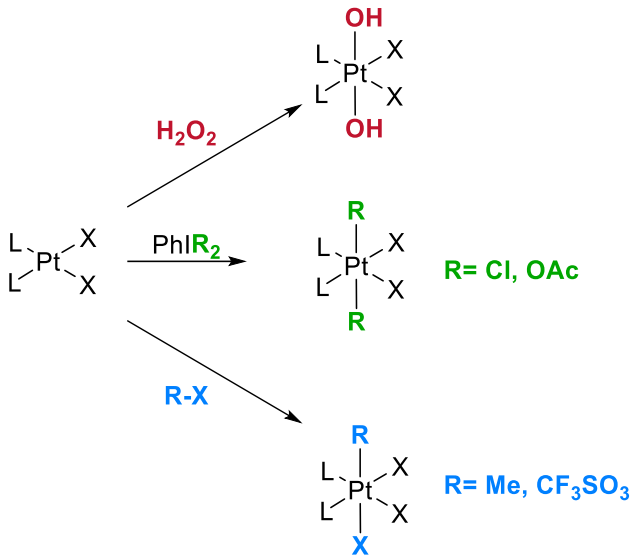

Scheme 9: Common oxidation pathways for the synthesis of Pt(IV) complexes[160]

A large chemistry has been developed around the functionalization of both equatorial -OH ligands by outer-sphere ligand-based reactivity with electrophiles, namely esters or succinic anhydride (Scheme 10), thus opening access to bis-carboxylate or bis-succinate-Pt(IV) complexes.[160] Interestingly, the stereochemistry is retained during reaction with equatorial hydroxo ligands. Post-functionalization of equatorial ligands is the key step for multiple derivatizations with targeting moiety, chromophores or even organic drug binding.[155,156]

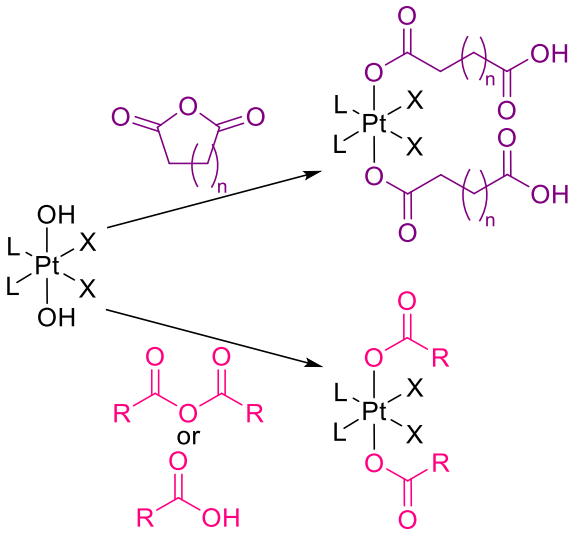

Scheme 10: Main outer-sphere ligand based reactivity

b. Strategies developed for efficient Pt(IV) prodrug activity

Equatorial ligands post-functionalization allowed large variation of physicochemical properties such as lipophilicity which was suggested to promote high cytotoxicity.[161,162] Fluorescein (FITC) conjugation confirmed Pt(IV) intracellular uptake and subsequent reduction probably due to increased GSH concentration prior excretion through a lysosomal pathway.[163] Similarly, equatorial grafting of bioactive ligands[164,165,166,167] is of interest to promote improved anticancer activity through synergistic effect by Pt(IV) reduction and equatorial ligands release *in cellulo*.

In the family of dual-action prodrugs, the functionalization of a cisplatin scaffold with two additional dichloroacetate (DCA) equatorial ligands proved conclusive as high potency where observed toward cisplatin resistant cancer cells.[167] A Pt(IV)-chalcone bioconjugate expected to sensitise cancer cells to platinum based chemotherapy effectively induced p53 activation, yet moderate potencies where detected.[168] Ibuprofen was conjugated to cisplatin scaffold and effectively overcame cell resistance though moderate dual-action was observed.[169,170] Remarkably, Gibson highlighted the difference of efficient concentration between organic drugs and platinum based chemotherapy which explains some failure encountered in the use of dual-action prodrugs.[171] Pt(IV) functionalization with targeting moieties[172,173] and peptides[173]

effectively induced HMGB1 overexpression expected to increase cell sensitization, yet only moderate potency improvement was observed.[172]

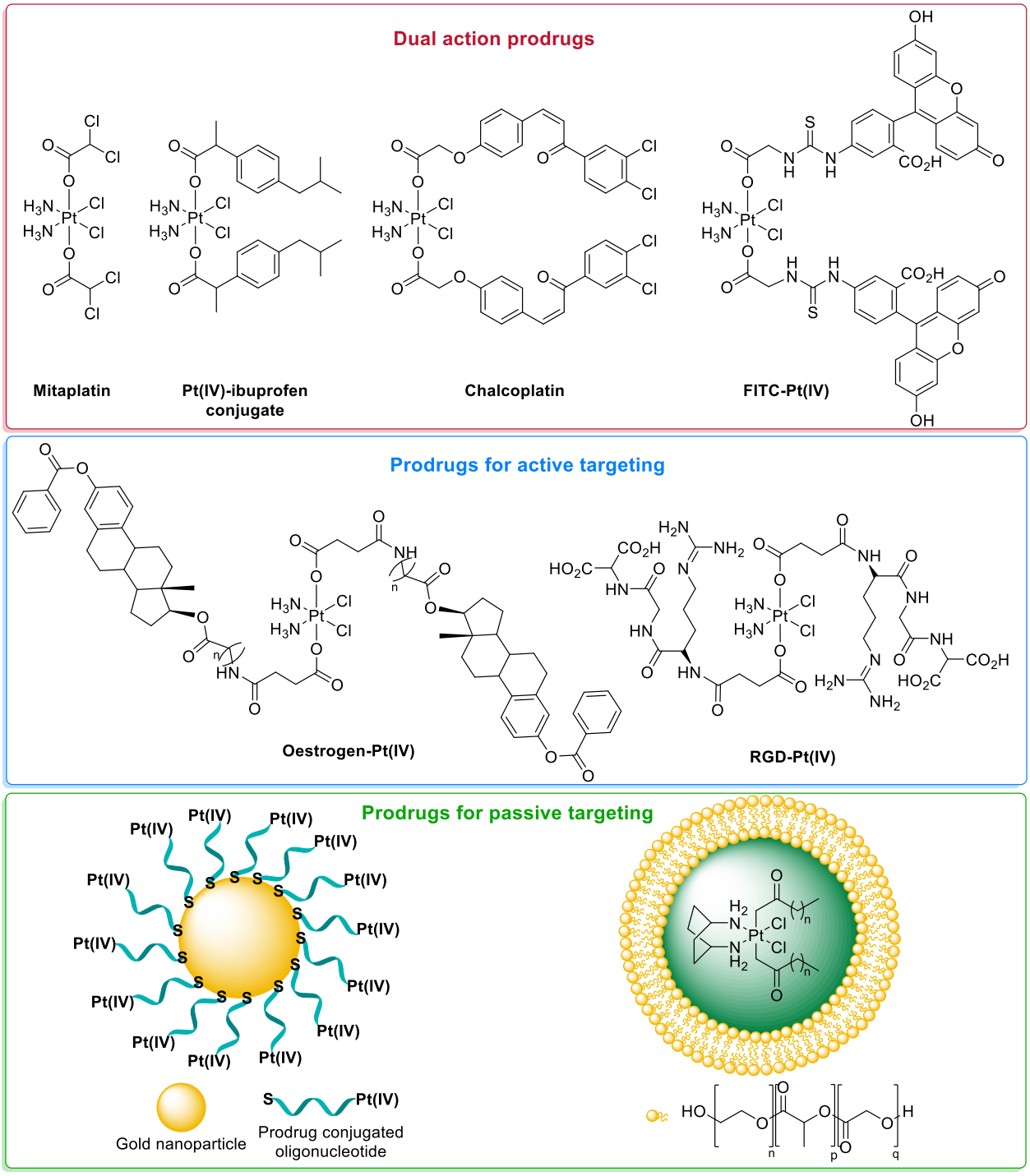

Scheme 11: Examples of Pt(IV) complexes developed for anticancer application

Furthermore, Pt(IV) based nanodelivery is a blossoming strategy[155] allowing physico-chemical properties fine tuning, high tumour accumulation and possibility to combine radiosensitization or medical imaging.[174,175] Passive targeting through Pt(IV) grafting on silica nanoparticles proved successful as 80-fold higher potencies where obtained compared to the free complex.[176] Pt(IV) combination to carbon nanotubes induced moderate cytotoxicities,[177] though platinum accumulation in liver and kidneys proved drastically decreased thus lowering kidney toxicity.[178] Liposomal formulation of Pt(IV) prodrugs highlighted improved cytotoxic and selective anticancer activity[179] and reduced overall toxicity.[180]

IV. Toward the next generation of NHC-Pt drugs

The high potential of NHC-platinum derivatives as cytotoxic agents has already been widely assessed though, the influence of the metal oxidation degree remains underexplored. Only few examples of stable NHC-Pt(IV) are reported in the literature and none of them has been investigated for biological applications (Scheme 12).[181-188] Yet, the upgrade of successful Pt(II) derivatives following the SAR rules into Pt(IV) prodrugs appeared as a breakthrough in the field of platinum-based chemotherapy as less toxic and sometimes more active anticancer agents where developed this way. Accordingly, the improvement of NHC ligands combination to high valent Pt(IV) centre will be discussed in the present manuscript.

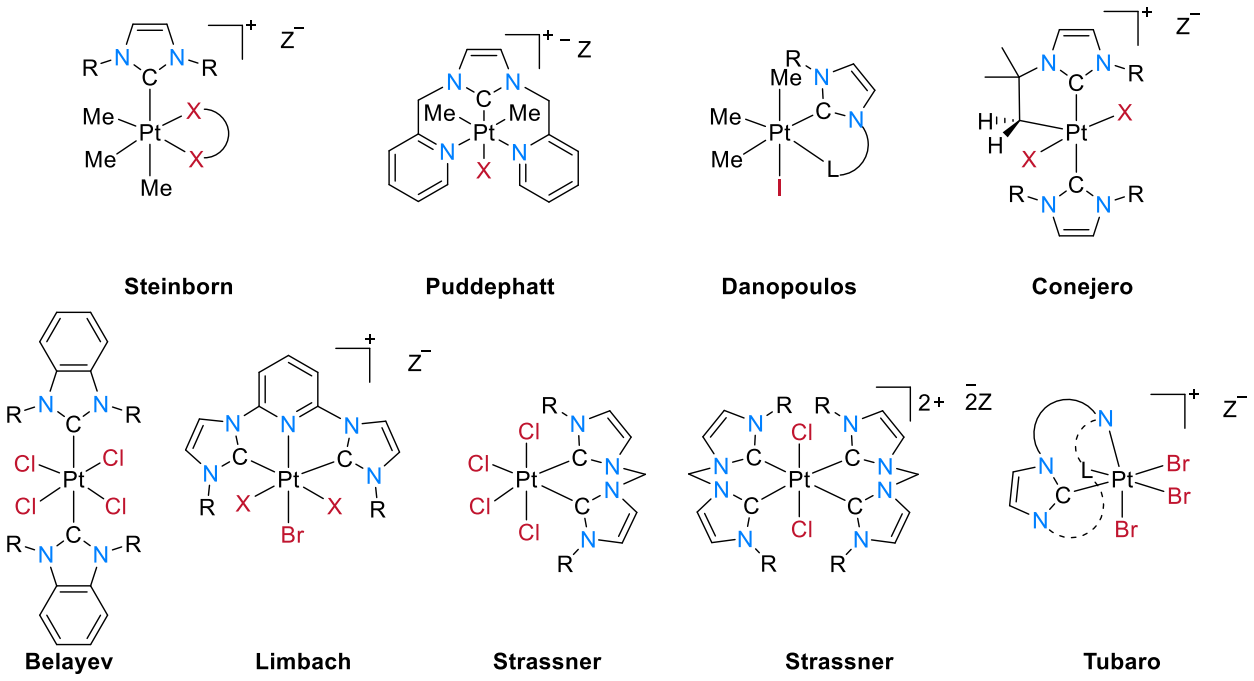

Scheme 12: Isolated stable mono- and bis-NHC-Pt(IV) complexes[181,182,183,184,185,186,187,188]

Based on this literature overview and in order to enhance the chemical diversity available for NHC-Pt anticancer agents, we aimed at designing NHC-platinum complexes displaying novel metabolization pathways to efficiently circumvent resistance mechanisms. Therefore, modular synthetic pathways based on easy and reproducible reactions have been developed for the improvement of cytotoxic NHC-platinum complexes. The potential of these novel NHC-Pt derivatives at inducing high cytotoxic activity while overcoming mechanisms of resistance associated with cisplatin treatment will be discussed in the two following chapters (2 & 3). Finally, the combination to nanodelivery devices has been envisioned to improve NHC-platinum uptake while limiting side effects will be emphasized in the chapter 4.

Chapter 2: Exploration of the functionalization of NHC-platinum(II) complexes

The development of modular and versatile approaches to introduce chemical diversity is of great importance in the field of drug development. This chapter details the one-step synthesis of simple platinum derivatives of the general formula [(NHC)PtX_2(pyridine)] with X = Cl, Br or I, while varying the electronic and steric properties of the N-heterocyclic carbene. Further ligand exchange strategy has been developed to introduce novel features such as lipophilic amines or pnictogen-based cytotoxic ligands by taking advantage of the labile pyridine in *trans* position to the NHC. Finally, their anticancer efficiency has been evaluated toward a range of cancer cell lines.

I. Synthesis and characterization of Pt(II)-NHC complexes with nitrogen-based ligands

1) *From imidazolium salts to pyridine-Pt(II)-NHC complexes*

All imidazolium salt presented herein were synthesized by N-alkylation with halogenoalkanes and purified by recrystallization according to a reported procedure.[189] Subsequent coordination to the platinum centre was achieved according to a straightforward synthesis developed in our laboratory.[117] The reaction of platinum with 1.2 equivalents of imidazolium salt deprotonated *in situ* by addition of an excess of base with halogen salt in pyridine led to complexes of the general formula [(NHC)PtX_2(pyridine)] with X = Cl, Br, or I after one night under reflux. Subsequent purification by chromatography on silica gel afforded the expected complexes as yellow powders in good yields. This synthetic pathway could be applied to a broad range of derivatives and as detailed below numerous variations could be achieved to enhance diversity.

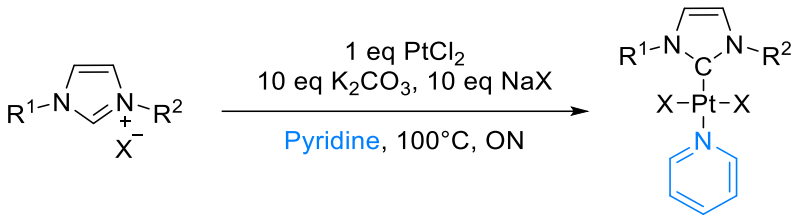

Scheme 13: General synthesis of NHC-Pt(II) precursors (X = Cl, Br, I)

The whole family of [(NHC)PtX_2(pyridine)] complexes could be easily characterized by ^{1}H and ^{13}C NMR. Successful NHC coordination was ensured by the disappearance of the characteristic resonance peak associated with the imidazolium salt proton on the ^{1}H NMR spectra. The apparition of a signal around 130 to 140 ppm in ^{13}C NMR is a signature for the carbene resonance in *trans* [(NHC)$Pt^{II}X_2$(pyridine)] complexes.

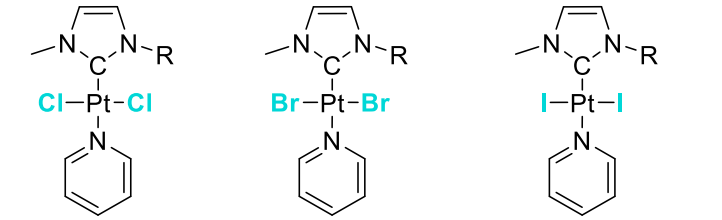

R = Bn, **1** (24%) R = Bn, **3** (52%) R = Bn, **5** (72%)
C_5H_{11}, **2** (26%) C_5H_{11}, **4** (43%) C_5H_{11}, **6** (51%)

Scheme 14: Yield dependence on halogen ligand

Variation of the halogen coordinated to the platinum centre can be easily achieved according to the procedure detailed in scheme 13 by using sodium iodide, bromide or chloride. The corresponding bis chloride-, bromide- or iodide-platinum complexes **1**-**2**, **3**-**4** or **5**-**6** could be isolated in moderate to good yield depending on the nature of the halogen ligand (Scheme 14). Higher yields obtained for the iodide-complexes can be attributed to the soft characters of both platinum and iodine atoms compared to harder bromine and chlorine. To note, the purification of the chloride complexes appeared somewhat difficult due to the presence of the

[$Cl_2Pt(pyridine)_2$] impurity which polarity on silica gel was similar to our complex. We next focused on iodide derivatives mostly because they showed better biological activities.[119]

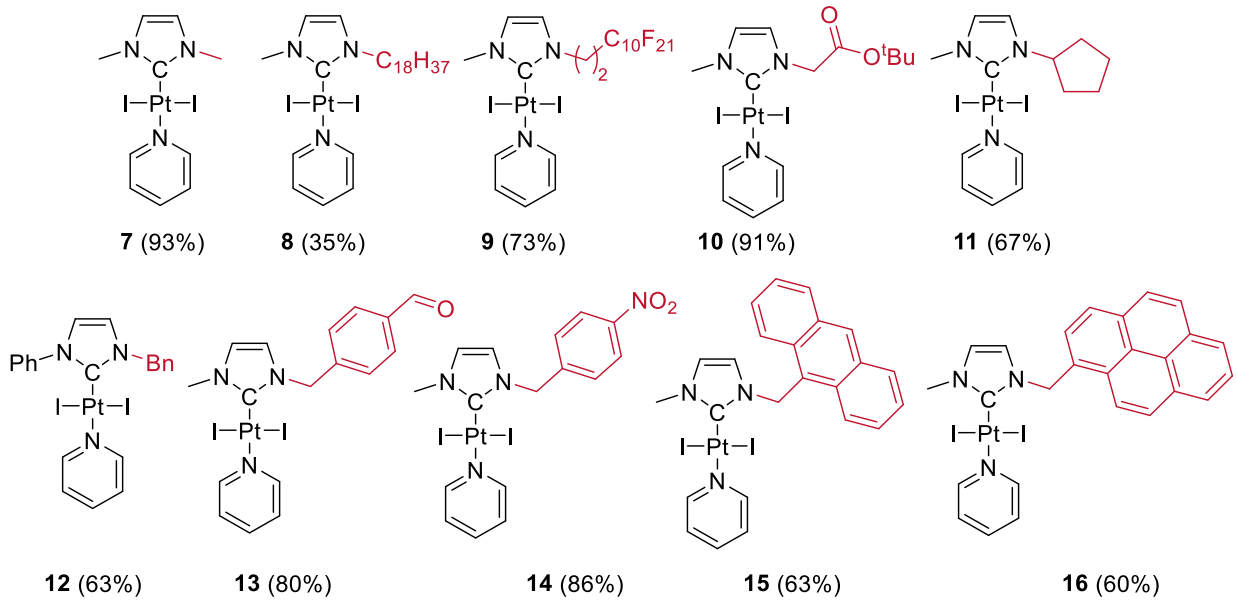

Scheme 15: Variation of N-substituents on [(NHC)PtI_2(pyridine)] precursors and isolated yields

N-substituents have been varied to increase the diversity of precursors available for further oxidation studies. Special emphasis has been placed on lipophilic substituents, namely linear or cyclic alkyl chains in addition to fluorinated alkyl chain in **7-11**. To note, the coordination yield drops when increasing the chain length on N-substituents. Moreover, intercalating moieties, namely anthracene in **15** and pyrene in **16**, have also been used in order to increase the overall cytotoxicity and allow near UV luminescence for *in vitro* tracking. For diversity enhancement, the aldehyde complex **13** is of interest as it could be further conjugated to either complementary drug or targeting moieties and allow synthesis of bioconjugated NHC-Pt(IV) complexes.

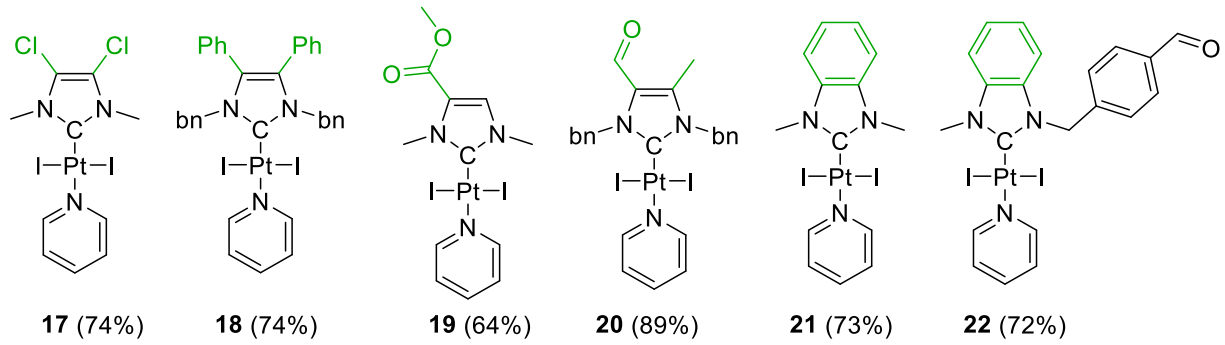

17 (74%) **18** (74%) **19** (64%) **20** (89%) **21** (73%) **22** (72%)

Scheme 16: Variation of the NHC backbone and isolated yields

Modification of the NHC backbone has also been investigated with the aim to fine-tune both the hindrance and electronic density available at the carbene when coordinated to the platinum centre (Scheme 16). Various NHC-Pt(II) complexes that could allow further oxidation of the metal center have been successfully synthesized in good yields as detailed in scheme 16 (**17**-**22**). Neither aldehyde nor ester reactive functions proved sensible to reaction conditions, thus complexes **19**, **20** and **22** could be further used for functionalization by oxime ligation or peptidic coupling. Surprisingly, while the complex **19** proved highly stable both in solid state and in solution, similar complexes bearing either benzyl of alkyl chain substituent proved somewhat less stable and led to complex degradation byproducts in solution.

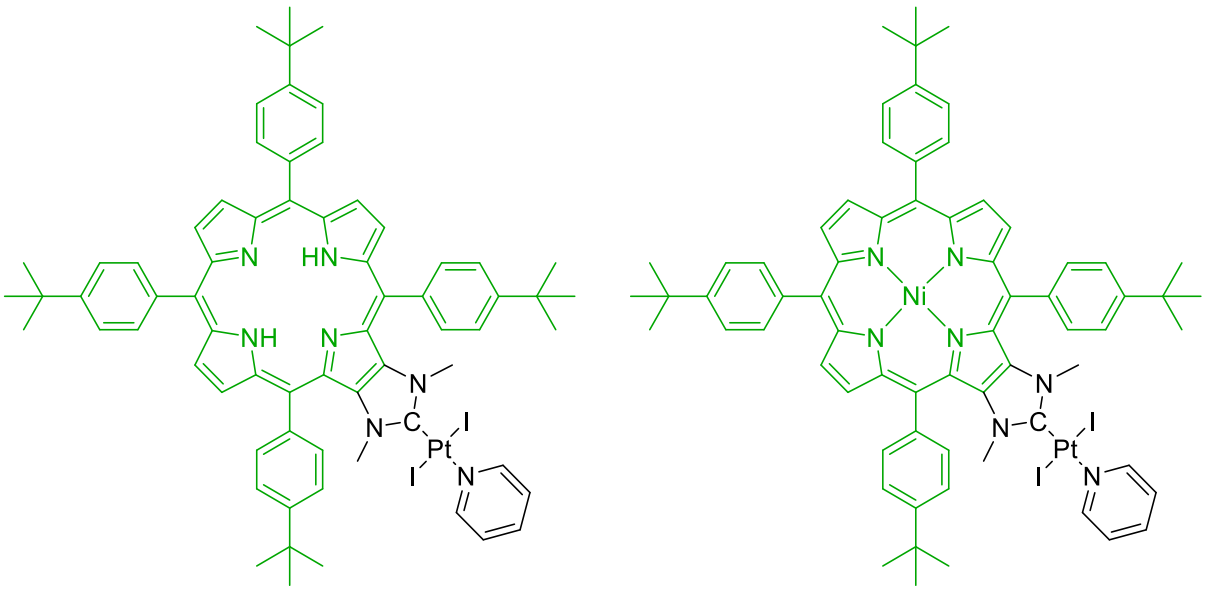

23 (52%) **24** (41%)

Scheme 17: Platinum complexes bearing porphyrin-modified NHC backbone

The straightforward procedure developed in our laboratory[118] allowed use of more complex ligand precursors since two porphyrin-modified imidazolium salts synthesized by Dr S. Richeter (Institut Charles Gerhardt, Montpellier) efficiently afforded the NHC-Pt(II) complexes **23** and **24** as red powders (Scheme 17). Signal shifts observed in ^{1}H NMR proved similar to other derivatives of the [(NHC)PtI$_2$(pyridine)] family. To note, the characteristic broad singlet observed at -2.84 ppm in the ^{1}H NMR spectrum of **23** corresponding to both pyrrolic amine protons confirmed that the porphyrin ring remained metal-free. In ^{13}C NMR, the carbenic carbon signal was found around 149 ppm in both cases, which suggests a lower electronic density at the carbene compared to complexes of the same family as **5** which were found at around 135 ppm. Interestingly, the strong electronic delocalization in the porphyrin ring favours a strong absorption up to 550 nm in UV and should therefore be of interest in the aim to unravel mechanistical aspects in biology by time dependent biodistribution and so forth.

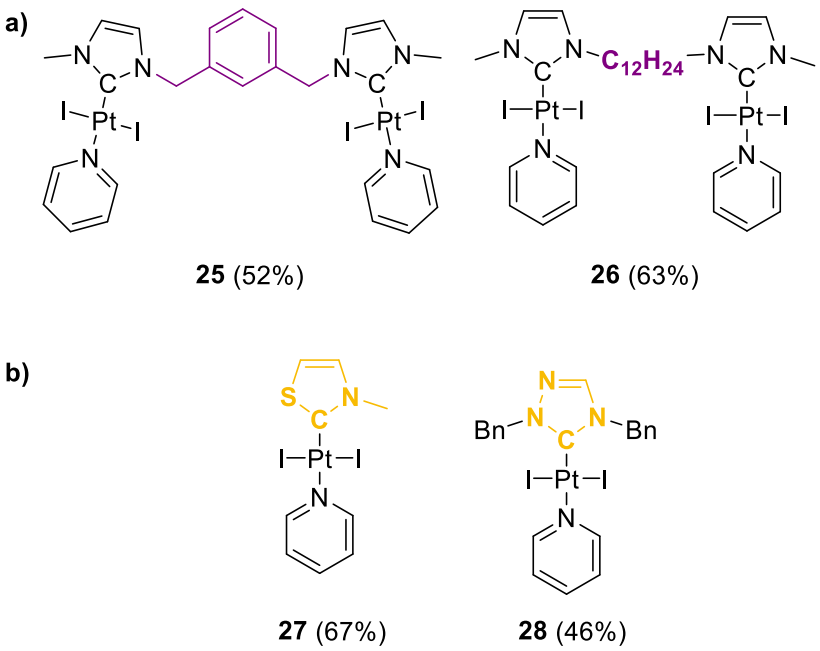

Scheme 18: Complex architectures based on a) homo-bimetallic NHC-Pt(II) precursors, b) non-N-heterocyclic carbenes-Pt(II) complexes

The formation of homo-bimetallic complexes proved possible starting from bis-imidazolium salts though both complexes **25** and **26** where obtained in moderate yields (Scheme 18). In ^{1}H NMR, the integration of coordinated pyridine signals confirmed the homo-bimetallic structure rather than chelating coordination on one platinum centre.

Finally, the influence of both thioimidazole and triazole toward the electronic stabilization of NHC-Pt complexes has been explored by coordination of two non-N-heterocyclic carbenes according to the same procedure as described in Scheme 13. Both *trans* thioimidazol- and triazole- platinum complexes **27** and **28** respectively, have successfully been obtained as yellow powders and proved stable in both solid state and solution. While the replacement or addition of heteroatom in the carbene backbone is expected to provide a difference in electron donation to the platinum centre in **27** and **28** respectively, only moderate signal shift is observed in ^{1}H NMR compared to the family of [(NHC)PtI_2(pyridine)] precursors.

Therefore, the procedure for platinum(II) synthesis proved to easily adapt to a large range of complex architectures and functional groups introduced on the NHC ligand. This allows easy diversity enhancement in the synthesis of NHC-Pt(II) precursors which will be further used for oxidation in NHC-Pt(IV) derivatives.

The molecular structure of several [(NHC)PtI_2(pyridine)] complexes could be determined by X-ray diffraction; some selected examples are presented in Figure 5. All NHC-Pt(II)-pyridine complexes display specific features as a *trans* configuration of the coordinated pyridine to the NHC ligand with the expected square planar geometry at the platinum centre. Both iodide ligands are facing each other in a *trans* configuration and point perpendicularly toward the NHC ligand plane. This possibly indicates interactions between the lone pairs of electrons on the iodide ligands and the formally antibonding p orbital of the NHC carbon atom. This is supported by the interatomic distances C_{NHC}···I with both iodides of ~ 3.25 Å compared to the sum of the van der Waals raddi for both carbon iodide (~ 3.68 Å).

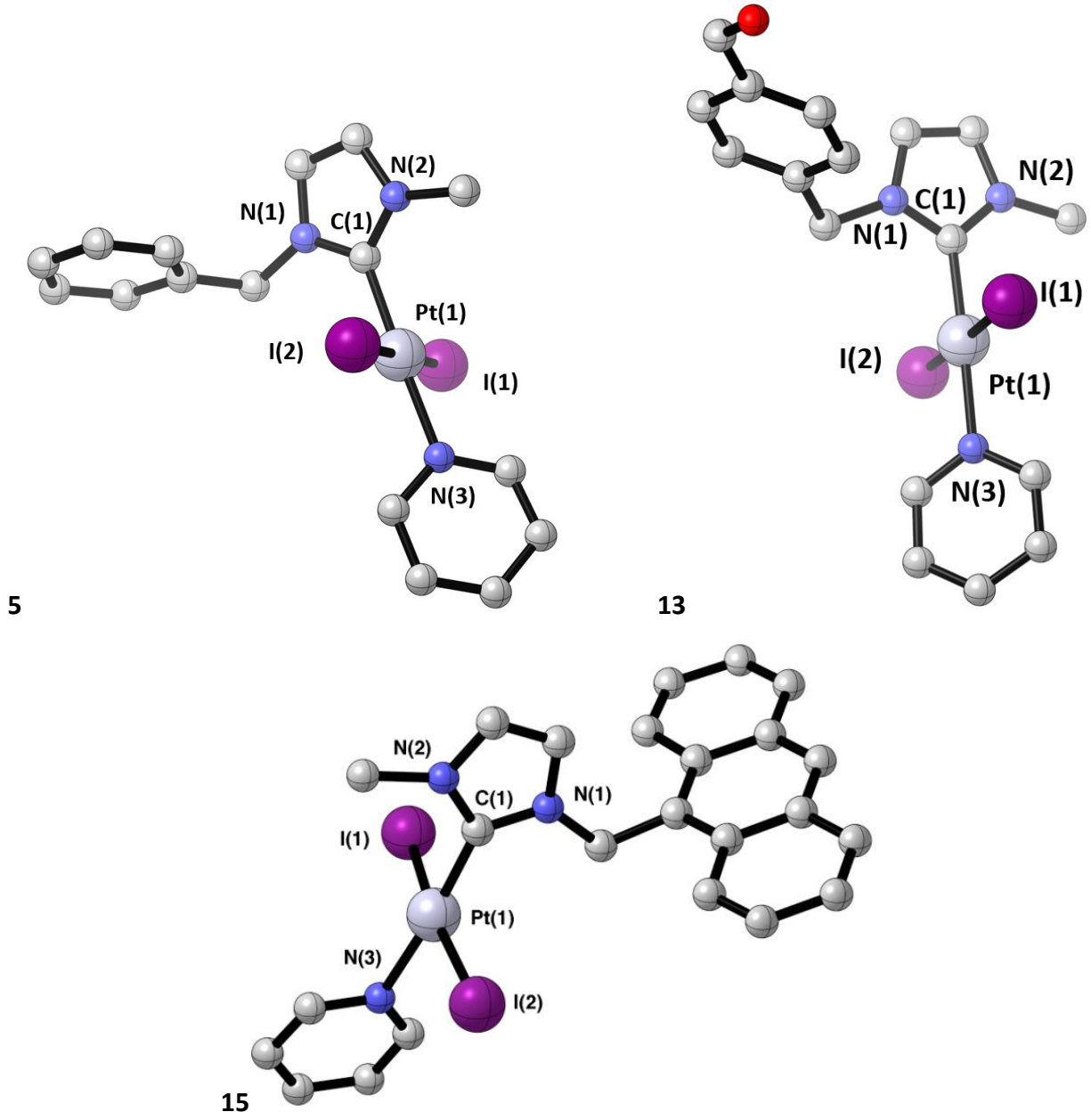

Figure 12: Structure of selected *trans* [(NHC)PtI$_2$(pyr)] complex **5**, **13** and **15**.[125] Selected bond distances [Å] and angles [°]: **5** Pt(1)–C(1), 1.974(7); Pt(1)–N(3), 2.094(6); Pt(1)–I(1), 2.5934(5); Pt(1)–I(2), 2.6025(5); C(1)-Pt(1)-I(1), 89.4(2); N(3)-Pt(1)-I(2), 90.4(2); I(1)-Pt(1)-I(2), 178.40(2); **13** Pt(1)–C(1), 1.981(6); Pt(1)–N(3), 2.091(4); Pt(1)–I(1), 2.5918(4); Pt(1)–I(2), 2.6031(4); C(1)-Pt(1)-I(1), 88.58(15); N(3)-Pt(1)-I(2), 90.50(12); I(1)-Pt(1)-I(2), 176.944(16); **15** Pt(1)–C(1), 1.961(4); Pt(1)–N(3), 2.088(3); Pt(1)–I(1), 2.5732(3); Pt(1)–I(2), 2.6013(3); C(1)-Pt(1)-I(1), 87.72(10); N(3)-Pt(1)-I(2), 91.76(9); I(1)-Pt(1)-I(2), 172.401(14).

2) Post-functionalization by ligand exchange with nitrogen-based ligands

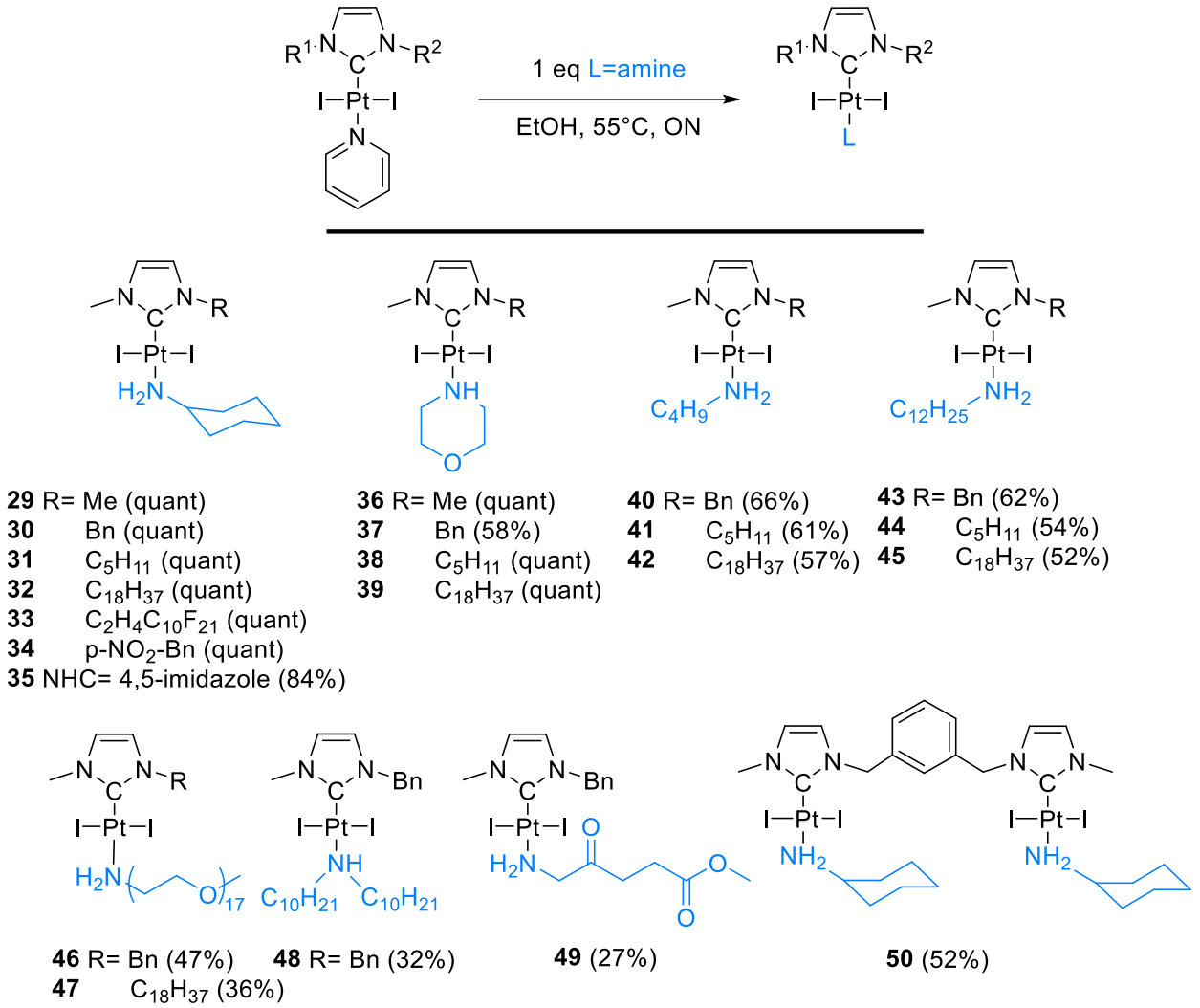

Scheme 19: Lipophilic NHC-Pt(II) precursors obtained by ligand exchange

Next post-functionalization of the NHC-Pt-pyridine complex was achieved to increase the lipophilicity of the complexes by simple pyridine displacement using various amines (*i.e.* ligand exchange), as shown on Scheme 19.[117] Both steric hindrance and electron density at the nitrogen proved to affect yields for this ligand exchange step. To note, no tested tertiary amine derivative allowed successful displacement of the pyridine ligand. Both simple cyclohexylamine and morpholine could successfully replace the pyridine in a large variety of derivatives **29**-**39**

and **50**. Two different lengths of alkyl chains were also used to fine-tune de lipophilic properties of formed complexes **40**-**45**. In the aim to access water-solubility an aminopolyethlyleneglycol of 750 Da was also used to selectively displace the pyridine and form complexes **46** and **47**. Finally, the clinically tested methylaminolevulinate (MAL) has been combined to the NHC-Pt(II) moiety and led to the derivative **49** which could be of interest as a dual therapeutic agent promoting DNA chelation and concomitant photodynamic therapy (PDT).

3) Evaluation of the lipophilicity of NHC-Pt(II) complexes

Lipophilicity is a major parameter which has been suggested to favourably impact both drug uptake and cytotoxicity. It can be evaluated by determination of (logP) which corresponds to the concentration ratio of the compound in octanol over water: (logP) = log $[complex]_{oct}/[complex]_{water}$ P representing the partition coefficient of a molecule between water and the organic solvent). A (logP) of 1.8 is considered as sufficient to allow efficient oral uptake. Therefore, lipophilicity measurements were conducted for some selected NHC-Pt(II) complexes using the shake-flask method in a mixture of water-PBS with octanol shaken for 72 h at 37 °C. After additional 24 h for solution equilibration, concentration of the complexes in both phases could be determined by UV absorbance spectroscopy. The calculated (logP) values for selected compounds are reported in Figure 6.

All tested complexes proved far more lipophilic than the cisplatin and thus improved drug uptake is expected to arise. The most lipophilic complex was compound **8** containing a C_{18} alkyl chain on the NHC backbone with a (logP) value of 0.56. The overall order of lipophilicity follows the sequence **8** > **48** > **46** > **43** > **40** > **6** > cisplatin thus confirming that more lipophilic ligands efficiently improve the lipophilicity of $[(NHC)PtI_2L]$ complexes. This trend highlighted a greater lipophilicity when increasing the alkyl chain length.

Complex	**6**	**8**	**Cisplatin[190]**	
	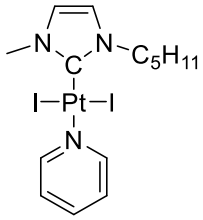	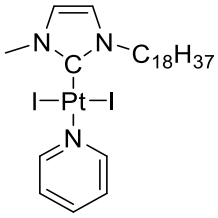		
logP	-0.95	0.56	-2.21	
Complex	**40**	**43**	**46**	**48**
	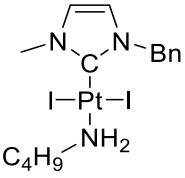	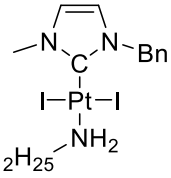	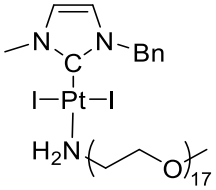	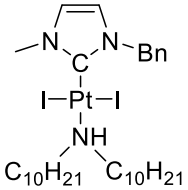
logP	-0.14	0.11	0.15	0.51

Figure 13: LogP values for selected compounds

II. Exploration of pnictogen synergy with NHC-Pt(II) complexes

1) Synthesis of neutral and cationic pnictogen functionalized Pt(II)-NHC complexes

While the easily available [(NHC)PtX$_2$] moiety has been established as a useful molecular building-block to generate libraries of anticancer analogues, so far exploration of the periodic table has been limited to nitrogen-based moieties. Indeed, while phosphine proved highly attractive for catalysis,[191,192] only few derivatives of NHC-Pt combined with phosphorous have been reported[193] and investigated *in vitro*.[194] Even less reports can be found when going down in group 15 with only one report of arsenic based carbene-platinum complexes by Lappert[195] and to the best of our knowledge, no report of NHC-Pt-As. Considering antimony, only scarce examples by O'Halloran widely explored the anticancer properties of Pt-Sb complexes and reported encouraging synergistic effects. While both arsenic and antimony have been dismissed

for biological application for dozen years due to their bad repute, this chemistry has for long been used in antique medicine to treat various diseases. Moreover, recent promising results obtained with organic arsenic based drugs renewed interest in theses derivatives,[196] especially with FDA approval of Trisenox (As_2O_3) to treat leukaemia.

Therefore, we highlighted the combination of pnictogens with NHC-Pt building block to access dual anticancer drugs.[197] The reaction of one equivalent of triphenylphosphine, triphenylarsine or triphenylstibine with the pyridine Pt precursor afforded the corresponding neutral [(NHC)$PtI_2(PnPh_3)$] complexes with Pn = phosphorous, arsine or antimony in high yields (up to 92% for **51c**, Scheme 20). Excess of pnictogen ligand did not improved yields and rather favoured the formation of homoleptic cationic species. Reaction of bismuth according to the same procedure failed at displacing the labile pyridine and only starting materials could be recovered. Finally, lower yields obtained for complexes **52a-c** bearing an anthracene moiety arise from lower precursor reactivity in addition to poor stability over silica gel.

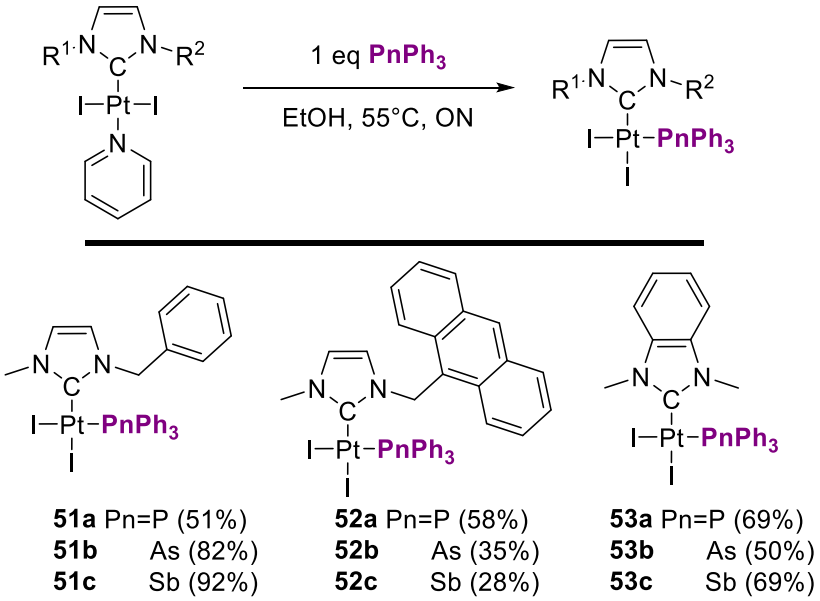

Scheme 20: Pyridine substitution on NHC-Pt(II) precursors with PPh_3, $AsPh_3$, or $SbPh_3$

All formed complexes adopted a *cis* configuration contrasting with the *trans* selectivity observed in the case of NHC-Pt complexes bearing nitrogen-based ligands. Easy characterization using ^1H

NMR confirmed a full conversion by total disappearance of proton resonance signals corresponding to coordinated pyridine. All N-CH_3 and N-CH_2 protons are found deshielded compared to their NHC-Pt pyridine counterparts. Moreover, the presence of bulky ligands in *cis* position seems to restrict the NHC-Pt rotation as evidenced by the desymmetrization of N-CH_2 protons, underlying their different environment. ^{31}P NMR also confirmed the *cis* configuration of the phosphorous atom at the platinum centre by resonance as a triplet signal with $^{1}J_{Pt\text{-}P}$ ~ 3664-3688 Hz. Carbenic carbon signal resonated around ~ 150 ppm in ^{13}C NMR which accounts as a fingerprint signal for *cis*-imidazolylidene platinum complexes.

Molecular structures obtained by X-ray diffraction confirmed a square planar geometry at the platinum centre, and the NHC ligand was always found pointing perpendicularly to the square plane, likely to minimise repulsive interactions. All neutral and cationic complexes bearing monodentate ligands adopted a *cis* conformation with respect to the NHC, as confirmed by crystal structure analysis in Figure 7.

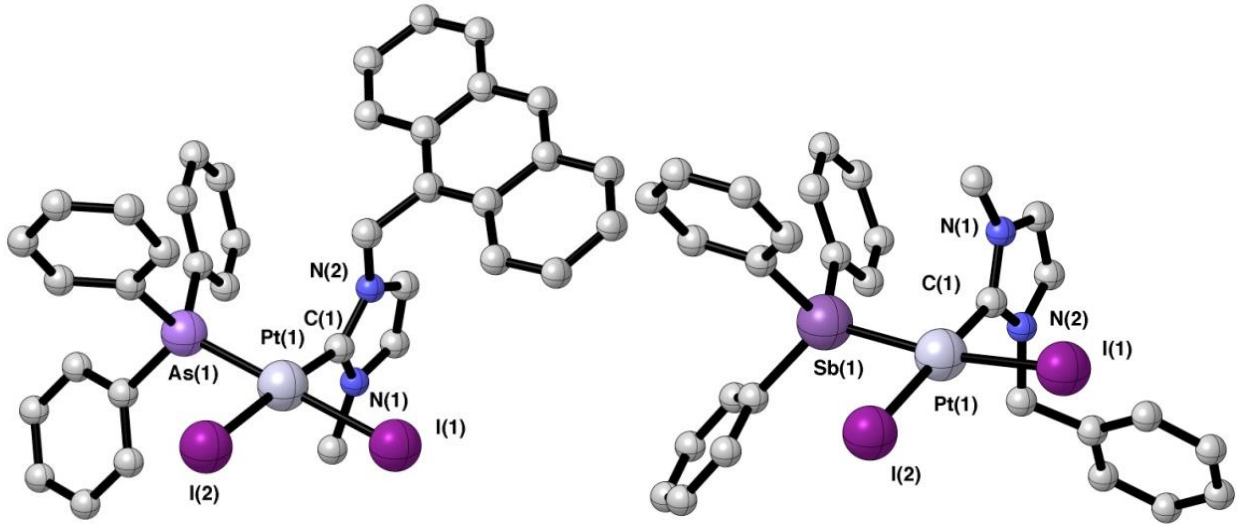

Figure 14: Molecular structure of selected arsine and antimony neutral complexes **52b** (*left*) and **51c** (*right*). Selected bond lengths [Å] and angles [°]: **52b** Pt(1)–C(1), 1.991(6); Pt(1)–I(1), 2.6263(5); Pt(1)–I(2), 2.6488(4); Pt(1)–As, 2.3551(6); C(1)–Pt(1)–I(2), 175.46(16); As(1)–Pt(1)–I(1), 179.75(2); **51c** Pt(1)–C(1), 1.983(9); Pt(1)–I(1), 2.6490(7); Pt(1)–I(2), 2.6374(6); Pt(1)–Sb(1), 2.5066(6); C(1)–Pt(1)–I(2), 176.8(2); Sb(1)–Pt(1)–I(1), 169.56(2).

The strong *trans* effect of the carbene is clearly seen on *cis* NHC-Pt-As complex **52b** for example as the Pt-I bond for the iodide ligand in *trans* position to the NHC [2.6553(5) Å] is significantly longer than to the arsine atom [2.6295(5) Å]. However, in the case of the complex **51c** with antimony, the *trans* effect of the Sb seems to be slightly higher than that of NHC since *trans* to the NHC, the Pt-I is 2.6374(6) Å while *trans* to the antimony, the Pt-I is 2.6490(7) Å. Moreover, no significant carbene-platinum bond length change is observed when varying the NHC backbone ca. 1.99 Å, thus underlying a minor influence toward the electron density at the metal centre. Interestingly, in the solid state, both arsine and stibine complexes bearing the anthracene moiety are stabilized by a CH-π intramolecular bond (3.055 Å) with a phenyl ring on the pnictogen. Similar behaviour appeared in the case of the benzimidazolin-2-ylidene Pt series where a CH-π intramolecular bond of 3.69 Å was found between the two ligands, namely the pnictogen phenyl ring and the NHC backbone.

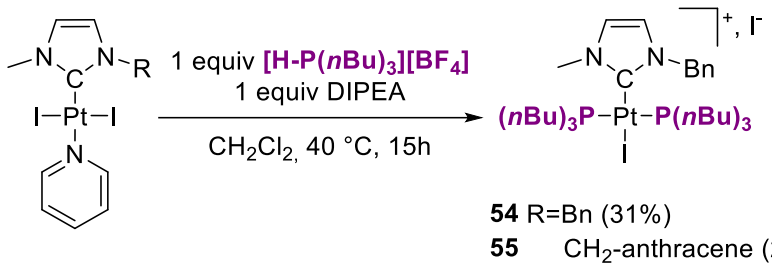

Scheme 21: Phosphonium pathway to access NHC-Pt-phosphine complexes **54** and **55**

Despite all our attempts, no suitable crystal of NHC-Pt complex bearing a triphenylphosphine ligand could be afforded; we thus focused on the use of tributyl phosphine ligand. The phosphonium salt [HP(*n*Bu)$_3$][BF$_4$] was used for the *in situ* generation of tributylphosphine ligand to further easily access to NHC-Pt-phosphine complexes with oxygen sensitive phosphorous ligands (Scheme 21).

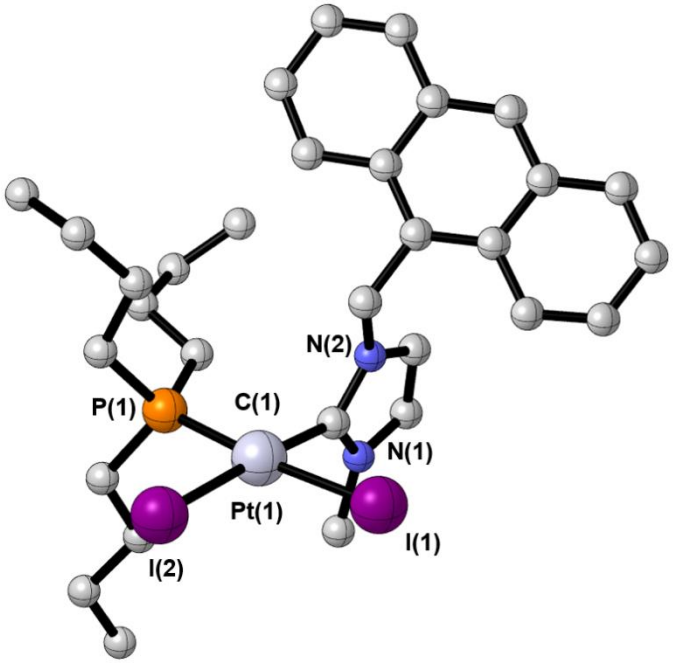

Figure 15: Molecular structure of the *cis* intermediate of 55. Selected bond lengths [Å] and angles [°]: Pt(1)–C(1), 1.965(9); Pt(1)–I(1), 2.668(7); Pt(1)–I(2), 2.6589(8); Pt(1)–P(1), 2.253(2); H(24A)–N(2), 2.651; H(24B)–N(1), 3.004; C(1)–Pt(1)–I(2), 176.8(3); P(1)–Pt(1)–I(1), 175.39(6).

Interestingly, using one equivalent of phosphonium salt, only the thermodynamically favoured bis-phosphine complex **54** or **55** could be obtained. This was confirmed by ^{31}P NMR where the coupling constant $J_{P\text{-}Pt}$ were of the same order as previously described *cis,cis* cationic complexes (2196 Hz for **54**). Further attempts to synthesize the mono-phosphine complex under milder conditions led to drastic conversion decrease. However, we could isolate few crystals of the expected neutral complex which is the intermediate to generate complex **55** (Figure 8). Both C-Pt bond and Pt-P bond proved in the same range as previously crystallized NHC-Pt-P complexes ($d_{C\text{-}Pt}$ = 1.965 Å, $d_{Pt\text{-}P}$ = 2.253 Å for **55**). Remarkably, the Pt-I bond proved longer in *trans* position to the phosphine than to the NHC and reveals a greater *trans* effect of the phosphine ($d_{Pt\text{-}Itrans}$ = 2.6683 Å, $d_{Pt\text{-}P}$ = 2.6589 Å).

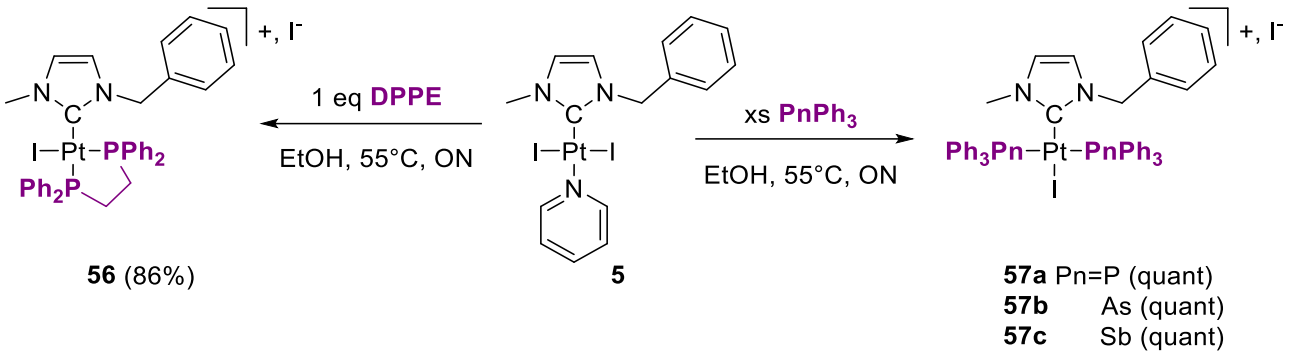

Scheme 22: Synthesis of both *cis-cis* and *cis-trans* cationic complexes **56** and **57**

Reaction of an excess of pnictogen ligands (up to 10 equivalents) successfully afforded cationic $[(NHC)PtI(PnPh_3)_2]^+[I^-]$ complexes **57a-c** in quantitative yield (Scheme 22). ^{31}P NMR of complex **57a** displayed a single signal at 13.06 ppm confirming the equivalence of both coordinated phosphorous. Moreover, the coupling constant of around 2500 Hz was consistent with two *trans* phosphorous atoms facing each other. The crystallization of cationic NHC-Pt-pnictogen derivatives proved difficult as obtained crystals were of insufficient quality to allow full refinement of the structure by X-ray diffraction. However, basic connectivities could be ascertained when considering the structure in Figure 9 of the complex **57a**. Preliminary results suggested a slightly longer carbene-platinum bond in the cationic complex when compared to its neutral counterpart. This could be attributed to the greater steric hindrance around the metal centre due to both triphenylphosphine groups compared to iodide.

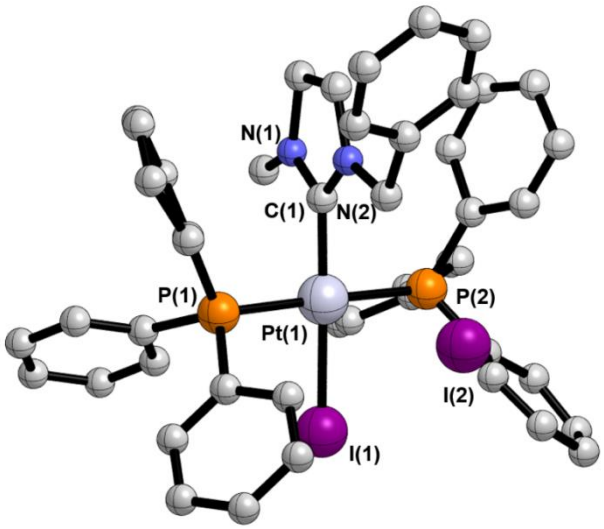

Figure 16: Molecular structure of cationic complex **57a**

Bidentate ligand such as DPPE also promoted the formation of cationic Pt complex **56** and neither κ^1 monometallic species nor bridged bimetallic complex were observed. The ^{31}P NMR spectrum displayed a typical AB system thus suggesting the non-equivalence of both coordinated phosphorous atoms and confirmed by both coupling constants $^1J_{Pt\text{-}P\textit{trans}}$ = 2221 Hz and $^1J_{Pt\text{-}P\textit{cis}}$ = 3306 Hz.[198,199]

2) Anticancer properties of pnictogen-functionalized Pt(II)-NHC complexes

Finally, cytotoxicity measurements were performed to investigate the possible synergistic effect of platinum centre with pnictogen (Figure 10). In this goal, MTS assay was used to measure cell metabolism and determine the half-inhibitory concentration expressed in µM in comparison to cisplatin. Three representative cancer cell lines (HCT116, colon cancer cell; MCF7, breast carcinoma; PC3, for prostate adenocarcinoma) were used to determine the biological profile in distinct environments, especially prostate cancer which is nowadays treated with cisplatin and MCF7 which is poorly sensitive to cisplatin. One healthy cell line (MRC5, human foetus cell lung) served to investigate possible specific targeting for cancer cells of selected drug candidates. To note, cisplatin activity toward healthy cells was not determined *in vitro* since this drug is known to target cellular DNA without distinction.

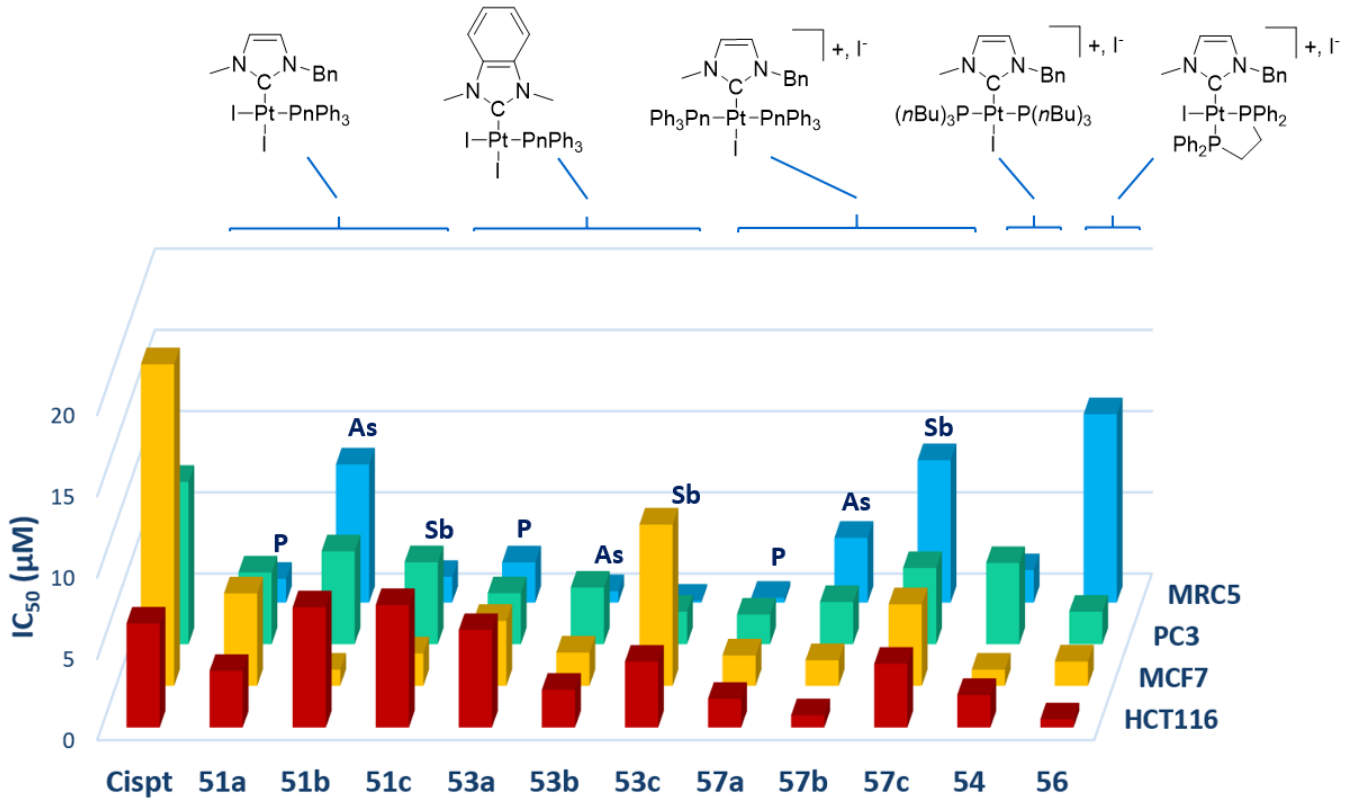

Figure 17: Half inhibitory concentrations (IC_{50} in µM) of the selected compounds against a range of human cell lines[200]

Interesting activities were obtained for most complexes that exerted similar or higher potencies than cisplatin for selected cancer cell lines. Remarkably, all tested NHC-Pt-pnictogen complexes depicted greater activity toward PC3, and even more significantly toward MCF7 where complexes **51b** and **56** were up to 20-fold more active than the cisplatin reference. Results for healthy cells MRC5 treated with our novel complexes proved more mixed since mainly the lipophilic cationic complexes (**54**, **56** and **57a-c**) proved more potent toward cancer. This result might underline the importance of a greater lipophilicity to improve drug uptake. The improved drug uptake of lipophilic drug candidates might explain their greater cytotoxicity toward cancer cells compared to their neutral counterparts. However, while all complexes appeared as efficient alternative to cisplatin *in vitro*, neither selectivity toward cancer cells nor synergistic effect could be observed.

III. Conclusion

A library of pnictogen-functionalized NHC-Pt(II) complexes have been successfully synthesized and characterized. We encompassed here the versatility of our method for post-functionalization of NHC-Pt precursors by easy and high yielding pyridine substitution. Coordination proved highly selective as only *trans* NHC-Pt-amine complexes were afforded. Moreover, the cytotoxicity of these derivatives was already ascertained in our group. Therefore, encouraged by these results, we extended the scope of this modular method to other pnictogens, namely phosphine, antimony and stibine ligands. Remarkably, only *cis* NHC-Pt-pnictogen complexes were obtained which contrasts with the *trans* selectivity observed for NHC-Pt-amine derivatives. Cationic complexes could also be obtained by adjusting the number of pnictogen equivalents, thus affording selectively the *cis*-*cis* complexes except when using DPPE ligand. Accordingly, cytotoxicity of several selected compounds was established toward a range of cancer cell lines and compared to cisplatine. While no synergistic effect could be observed, all tested NHC-Pt(II) complexes compared favourably with cisplatin. Altogether, these examples highlighted the post-functionalization of NHC-Pt derivatives as a method of choice to generate a library of cytotoxic complexes whose biological features could be easily tuned according to the introduced pnictogen ligands. Although cytotoxic drug candidates were successfully developed, possible *in vivo* platinum poisoning and deactivation remains a major issue to solve. Therefore, investigation of more inert NHC-Pt(IV) prodrugs has been suggested as a powerful strategy to tackle this problem.

Chapter 3: Novel NHC-Pt(IV) prodrugs: Synthesis and anticancer application

NHCs proved to be valuable ligands in the development of anticancer metallodrugs by improving the overall stability particularly when combined to platinum as highlighted by several groups including us.[117-119] Moreover, considering the promising results obtained with Pt(IV) derivatives as evidenced by the number of prodrugs that entered clinical trials, we decided to investigate the potential of platinum(IV) compounds stabilized by NHC ligands. Indeed, while scarce examples were reported for catalysis purpose, positive anticancer effect is expected to arise from this new class of compounds. Therefore, this chapter emphasizes the synthesis of NHC-Pt(IV) complexes and their evaluation as potential anticancer agent. Complexes of the general formula [(NHC)PtX_4L] will be considered, X being either chloride or bromide ligand. Moreover, since many reports suggest lipophilicity to positively affect cytotoxicity, the synthesis has been adapted to include lipophilic moieties. Full characterization will be detailed herein and ^{195}Pt NMR will be specially emphasized as a highly specific method of characterization. Accordingly, their potencies will be discussed and compared to cisplatin while considering their respective solution stability. Finally, preliminary biological mechanistic studies will be presented to emphasize the peculiar action mode of these NHC-Pt(IV) prodrugs.

I. Synthesis and characterization of NHC-Pt(IV) complexes

1) Synthesis and characterization of [(NHC)$PtBr_4$(pyridine)] complexes

Complete conversion of [(NHC)PtI_2(pyridine)] precursors into the corresponding bromide Pt(IV) species was achieved after 5 minutes exposure with a slight excess of bromine Br_2 at 0°C in dichloromethane (Scheme 23).[201] The desired *trans* [(NHC)$PtBr_4$(pyridine)] complexes could

further be isolated in quantitative yield by simple precipitation using pentane. Remarkably, excess of bromine promoted radical bromation as evidenced by the molecular structure presented in the experimental part. Selective bromation at the 4-position of the imidazole ring was observed under these conditions. Therefore, further syntheses were conducted using strictly two equivalents of bromine and a large range of complexes could be synthesized (Scheme 24). All Pt(IV) NHC complexes were stable under air in the solid state or in chlorine solvents. However, the pyridine functionalized Pt(IV)-NHC complexes displayed poor solubility in all organic solvents. Characterization by ^{1}H NMR showed that all formed complexes displayed a general signal shift to lower field which proved typical for such [(NHC)PtBr$_4$L] complexes. To note, the resonance signals were found shifted of up to 0.9 ppm for protons in *ortho* position of the pyridine compared to their NHC-Pt(II) precursors. Moreover, typical features were also noticed leading to more complex signal splitting patterns due to coupling with the ^{195}Pt isotope. As expected, chemical shifts to lower field were also observed by ^{13}C NMR spectroscopy while carbenic signals were observed at ca. δ 109–120 ppm.

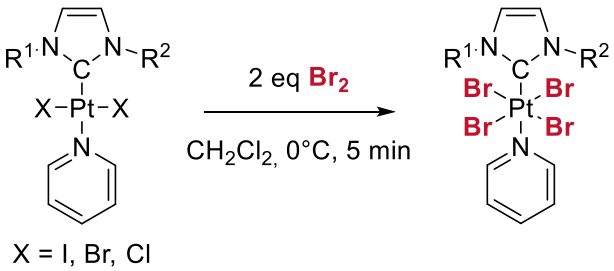

Scheme 23: Selective synthesis of *trans* [(NHC)PtBr$_4$(pyridine)] complexes

Remarkably, this procedure has been successfully applied to the variation of N-substituents as both linear and cyclic lipophilic chains proved inert toward bromation and selective oxidation of the platinum(II) centre into platinum(IV) complexes **58**-**67** was achieved in high yield. Neither fluorinated chain **61**, nor pyridyl moiety **58**-**67** or even the ester functional group **63** were affected by unwanted reaction which is encouraging for further post-functionalization. Similarly, neither inductive nor mesomeric attractive moieties on the NHC proved to disturb the platinum oxidation and complexes **66**-**67** were obtained in excellent yield. Nevertheless, the oxidation

with bromine of NHC-Pt(II) precursors bearing NHC functionalized with extended aromatic cycles as anthracene and pyrene failed at affording pure material due to the bromation on the aromatic positions which proved to occur concomitantly to platinum oxidation.

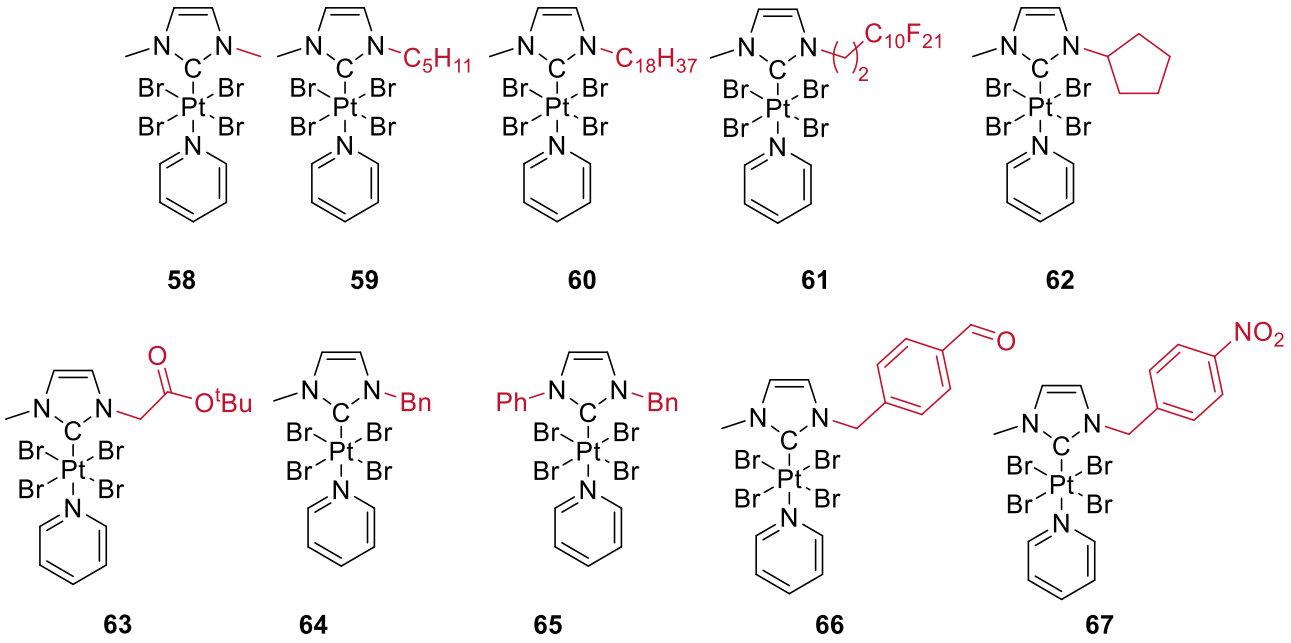

Scheme 24: Synthesis of [(NHC)PtBr$_4$(pyridine)] complexes with various N-substituents in NHC ligand (yield: 96-99%)

The selective oxidation of *trans* carbene-Pt-pyridine precursors proved successful thus affording Pt(IV) complexes **68**-**72** bearing various inductive or mesomeric attractive moieties in the position 4 or 5 of the NHC (Scheme 25). No significant chemical shift was observed by ^{1}H NMR for N-substituents protons in NHC-Pt(IV) derivatives **68**-**72** (δ = 4.45 ppm in **70** and 4.46 ppm in **71**), suggesting a weak electronic communication through nitrogen atoms with substituents in position 4 and 5 of the NHC backbone. To note, the signal shift in ^{13}C NMR corresponding to the carbenic carbon proved higher in the benzimidazole derivative **68** with $\delta_{C\text{-}Pt}$ = 133.9 ppm compared to other NHC-Pt(IV) complexes which range around 110-120 ppm. Due to the low solubility of **72**, ^{1}H-^{13}C HMBC were recorded instead or regular ^{13}C NMR and no information could be obtained for the carbon resonance peak corresponding to the carbene.

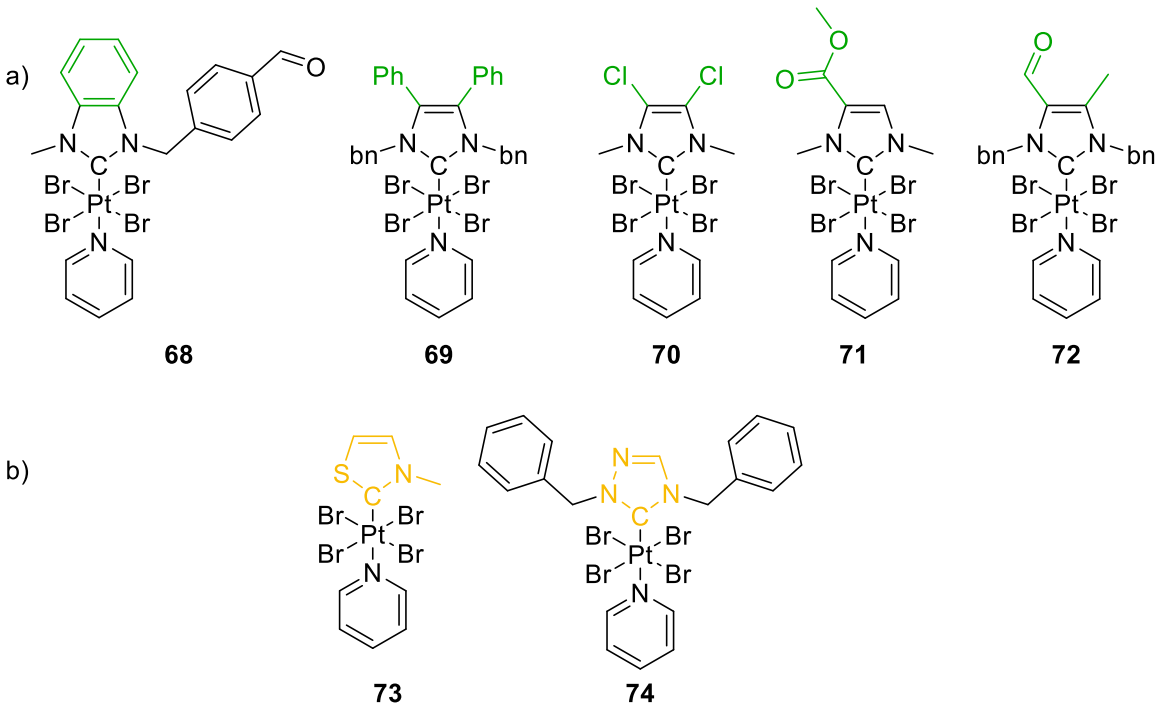

Scheme 25: Structural modification on the carbene backbone on platinum(IV) derivatives

(isolated in 99% yield in all cases)

Finally, the oxidation with bromine of both thiazolylidene and triazolylidene-Pt(II) precursors successfully afforded the corresponding complexes **73** and **74** in good yields though characterization proved difficult for **73** due to very low solubility in most organic solvents. Common signal shift to lower field was also observed for non-NHC functionalized Pt(IV) complexes as shown with the complex **74** where the N-CH_2 signal is of δ = 6.35 (δ = 5.85 ppm for the NHC-Pt(II) derivative **28**). Moreover, the presence of an electronegative nitrogen atom in the 4-position of the NHC's backbone induced overall moderate shift of 0.2 ppm in ^{1}H NMR compared to the NHC-Pt(IV) complex **64** bearing methyl- and benzyl- groups (for N-CH_2 protons, δ_{64} = 6.09 ppm). The carbenic carbon signal was found deshielded at δ_{74} = 119.5 ppm compared to **64** which is δ_{64} = 109 ppm, confirming a change in the electronic density compared to NHC-Pt(IV) complexes.

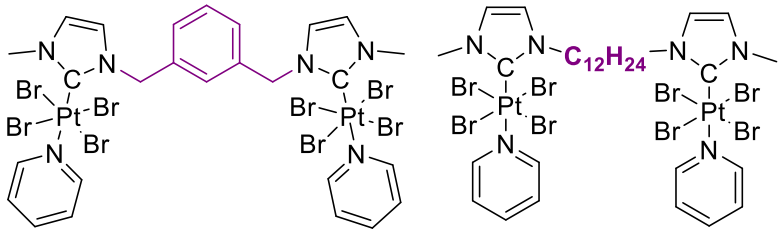

75 (99%) **76** (76%)

Scheme 26: Homobimetallic platinum(IV) complexes

The oxidation of two homo-bimetallic NHC-Pt(II) complexes has been attempted by adapting the amount of bromine and successfully afforded **75** and **76** in excellent yields (Scheme 26). As for the monometallic Pt(IV) complexes, all proton resonance signals were found shifted to lower field in both ^{1}H and ^{13}C NMR. To note, both platinum centers proved to oxidize simultaneously and no trace of mixed Pt(II)/Pt(IV) complex could be observed by ^{1}H NMR.

To unambiguously establish the atom connectivities, single crystals of several NHC-Pt(IV) complexes were grown by slow diffusion in pentane/dichloromethane. The molecular structures of some examples are depicted in Figure 11. The complete selectivity of halogen-mediated oxidation was confirmed as only *trans* [(NHC)$PtBr_4$(pyridine)] were observed in all cases. Analysis of the molecular structure of the two complexes **64** and **72** confirmed the slightly distorted octahedral geometry at the Pt(IV) center with angles Br(1)-Pt-Br(2) of 85° and Br(1)-Pt-Br(4) angle of 95°. Both NHC and pyridine are within the same plane in the molecular structure of **64**, and the four bromines occupy axial positions. As expected to minimize the steric repulsions both N-substituents are part of the median plan and pointing in the middle of two bromines. Moreover, proton atoms in alpha position to the nitrogen atoms in the NHC are engaged in H-bonding with neighboring bromines in a similar fashion to the ones in α of the N(3) (2.562 Å to 2.806 Å). Interestingly, the Pt-Br(2) is slightly elongated and bent toward the formally empty p orbital at the carbene as suggested by the corresponding C-Br(2) bond through space which is 3.244 Å [distance to the Br(1), Br(3) and Br(4) being respectively 3.278 Å, 3.266 Å and 3.316 Å]. To note, oxidation with the bromine reagent systematically led to iodide replacement.

A) B)

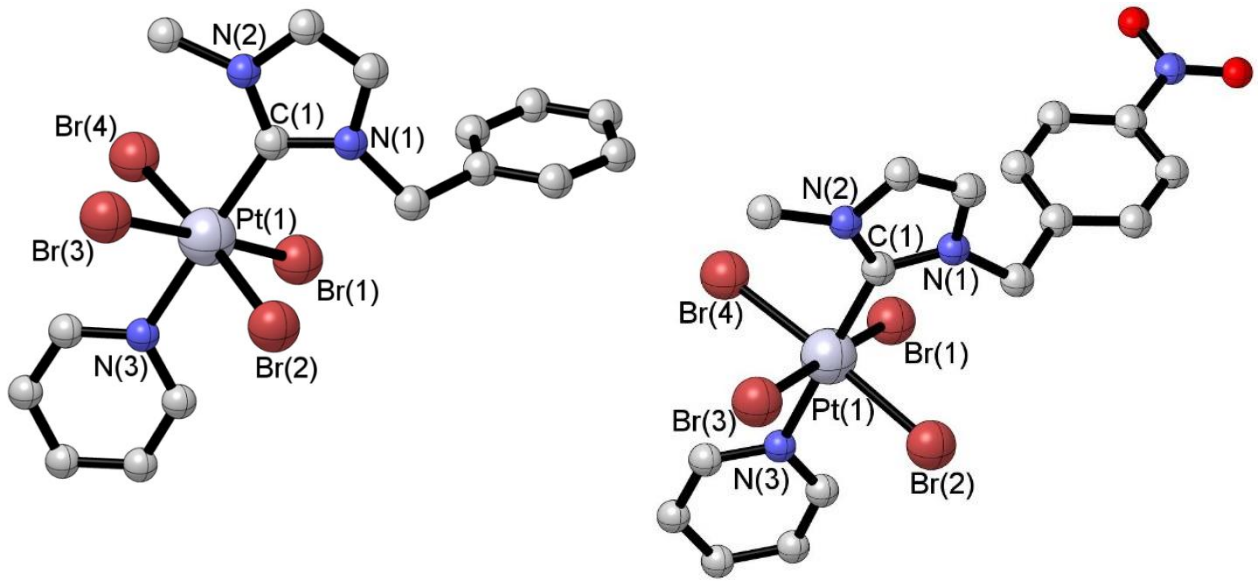

Figure 18: Molecular structures of trans [(NHC)PtBr$_4$(pyridine)] complexes **64** (A) and **67** (B). Selected bond distances [Å] and angles [°]: **64** C(1)–Pt(1), 2.065(11); Br(1)–Pt(1), 2.4728(14); Br(2)–Pt(1), 2.4806(12); Br(3)–Pt(1), 2.4767(14); Br(4)–Pt, 2.4746(12); N(3)–Pt(1), 2.135(9); C(1)–Pt(1)–N(3), 178.3(4); C(1)–Pt(1)– Br(1), 91.6(3); N(3)–Pt(1)–Br(4), 88.3(3); Br(1)–Pt(1)–Br(3), 176.07(4); Br(1)–Pt(1)– Br(4), 92.34(5). **67** C(1)–Pt(1), 2.057(8); Br(1)–Pt(1), 2.4882(8); Br(2)–Pt(1), 2.4657(8); Br(3)–Pt(1), 2.4615(8); Br(4)–Pt, 2.4839(8); N(3)–Pt(1), 2.128(6); C(1)–Pt(1)–N(3), 179.2(3); C(1)–Pt(1)–Br(3), 92.9(2); N(3)–Pt(1)–Br(4), 88.76(17); Br(1)–Pt(1)–Br(3), 175.29(3); Br(1)–Pt(1)– Br(4), 85.80(3).

Remarkably, when comparing the NHC-Pt(IV) complexes with their Pt(II) counterparts, it appeared that both C-Pt and Pt-N bonds were longer in the octahedral NHC-Pt(IV) form than in the square planar NHC-Pt(II) complexes (typical value was $d_{C\text{-}Pt}$ = 1.97 Å in Pt(II) and raised in Pt(IV) to $d_{C\text{-}Pt}$ ~ 2.05 Å). Similarly, the N-Pt bonds which elongate from $d_{N\text{-}Pt}$ = 2.09 Å in Pt(II) to $d_{C\text{-}Pt}$ = 2.12 Å in Pt(IV) which is consistent when considering the bulk increase around the metal due to two additional ligands.

2) Synthesis and characterization of lipophilic [(NHC)PtBr$_4$L] complexes

As for NHC-Pt(II) complexes, it appeared that the labile character of the pyridine *trans* to the NHC could be exploited to perform ligand exchange and allowed easy diversity generation in NHC-Pt(IV) metallodrug candidates (Scheme 27). Therefore, the use of selected amines as solvent efficiently afforded quantitatively the corresponding [(NHC)PtBr$_4$L] complexes as red oils. The disappearance of signals corresponding to the coordinated pyridine in ^{1}H NMR accounted for the complete ligand exchange while the proton resonance peak of N-CH$_3$ at ~ 3.8 ppm confirmed that the Pt(IV) centre was not reduced.

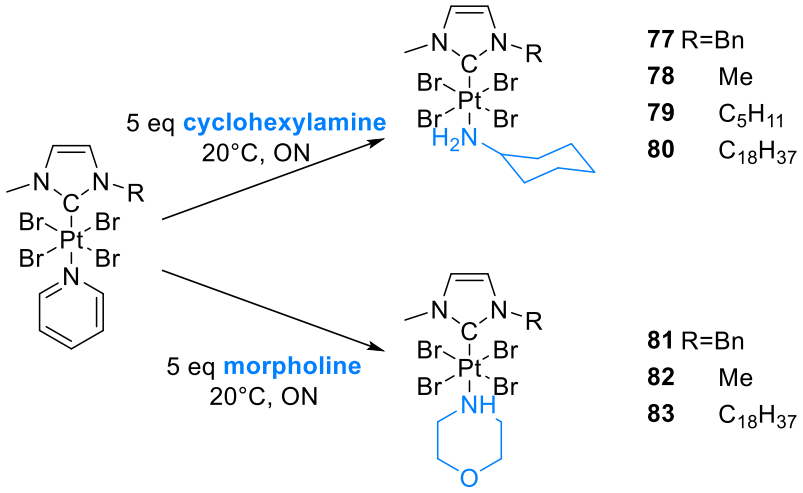

Scheme 27: Post-functionalization with lipophilic amine as ligands (97-99% yield)

Although more lipophilic NHC-Pt(IV) complexes could successfully be obtained using neat conditions, only a few range of amines are available as liquid at room temperature, thus limiting the functional diversity available. Therefore, the synthetic pathway involving oxidation of NHC-Pt(II) precursors functionalized with butylamine, dodecylamine and so forth (**29**-**50**) has been used to access highly lipophilic NHC-Pt(IV) complexes **84**-**92** (Scheme 28). All complexes could be easily characterized by both ^{1}H and ^{13}C NMR and displayed the characteristic global signal shift to lower field for NHC-Pt(IV) complexes. Only the carbenic carbon which is found around about 112-115 ppm depending on the amine ligand akin to the pyridine functionalized Pt(IV)-NHC complexes.

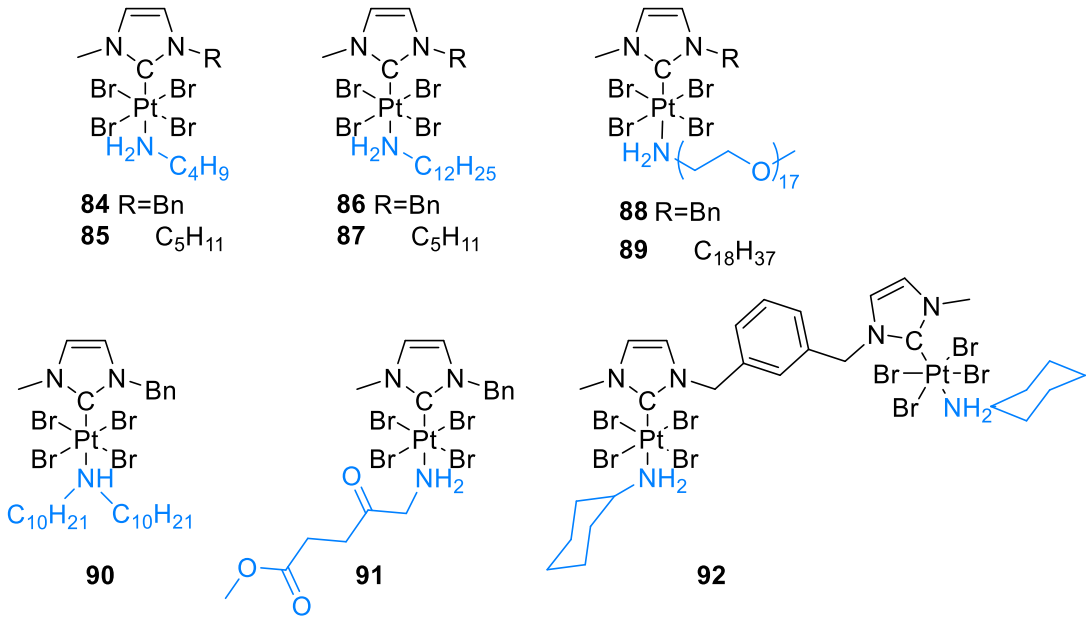

Scheme 28: Lipophilic NHC-Pt(IV) complexes obtained by direct oxidation of [(NHC)PtI_2L] complexes with L = primary or secondary amine ligand (99% yield in all cases)

As expected, selected lipophilic amines proved inert toward bromation under reported conditions, thus allowing large variations at the platinum centre. Most protons signals in ^{1}H NMR were found slightly shielded of around 0.1 ppm in the case of primary and secondary amines **77**-**92** compared to their [(NHC)$PtBr_4$(pyridine)] counterpart **64**. To note, oxidation of the *cis* NHC-Pt(II)-pnictogen derivatives promoted the concomitant formation of numerous species and neither increased dilution nor longer reaction times favoured the formation of a single isomer. Furthermore, (logP) measurements have been carried in order to evaluate the lipophilicity of selected NHC-Pt(IV) complexes and compare with their Pt(II) counterparts. However, due to Pt(IV) reduction occurring concomitantly to the 72 h stirring in octanol/water solution, no clear results could be obtained.

Two NHC-Pt(IV) complexes bearing lipophilic amines **77** and **81** respectively were grown as single crystals suitable for X-ray diffraction studies by slow diffusion in pentane/dichloromethane (Figure 12). Akin to their counterparts bearing a pyridine moiety,

both complexes selectively adopted a distorted octahedral geometry with the amine ligand in *trans* position to the NHC. Remarkably both Pt(IV) complexes displayed significant bonds elongation compared to their Pt(II) precursors, evidence of the steric prevalence toward electronic parameters.[202] However, the N-Pt bond distance did not vary much depending on the σ-donation of the amine ligand. The interaction between the shortened bromine and the empty p orbital at the carbene was even more pronounced for **77** where the distance is 3.182 Å. On the contrary, in **81** no Pt-Br bond length elongation was noticed, yet slight interaction with the carbene was still noticed with a distance through space of 3.238 Å.

A) B)

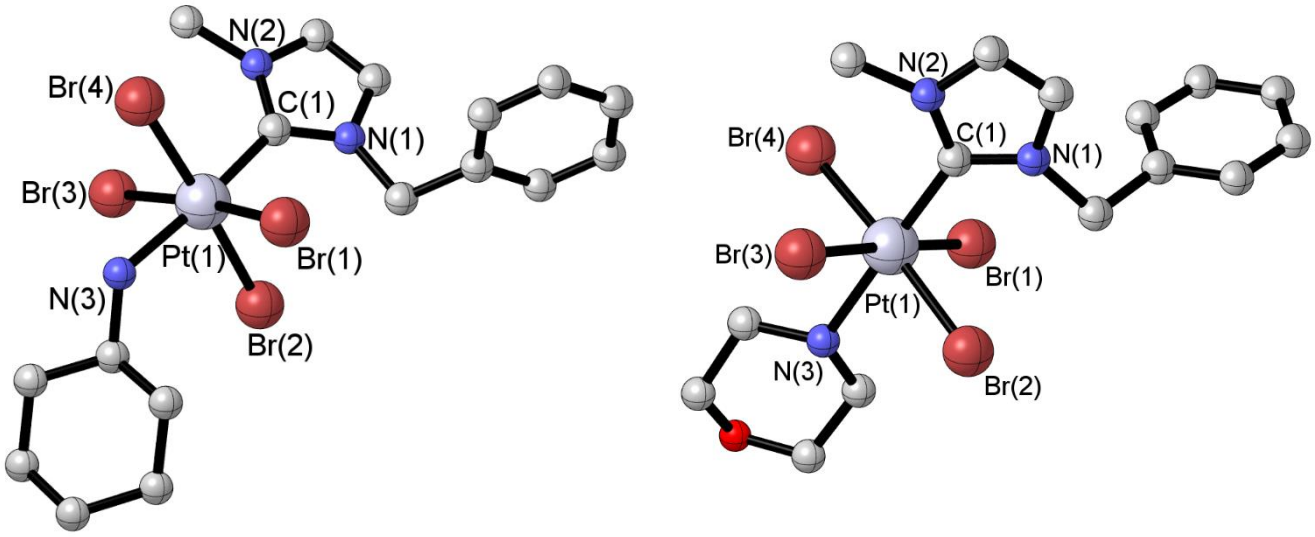

Figure 19: Molecular structures of moderately lipophilic [(NHC)PtBr4(pyridine)] complexes **77** (A) and **81** (B). Selected bond distances [Å] and angles [°]: **77** C(1)–Pt(1), 2.036(7); Br(1)–Pt(1), 2.4793(9); Br(2)–Pt(1), 2.4693(9); Br(3)–Pt(1), 2.4716(9); Br(4)–Pt, 2.4743(9); N(3)–Pt(1), 2.138(6); C(1)–Pt(1)–N(3), 175.7(3); C(1)–Pt(1)–Br(3), 95.0(2); N(3)–Pt(1)–Br(3), 88.3(2); Br(1)–Pt(1)–Br(3), 172.55(3); Br(1)–Pt(1)–Br(4), 93.99(3). **81** C(1)–Pt(1), 2.074(13); Br(1)–Pt(1), 2.4754(18); Br(2)–Pt(1), 2.4748(15); Br(3)–Pt(1), 2.4770(18); Br(4)–Pt, 2.4748(17); N(3)–Pt(1), 2.167(12); C(1)–Pt(1)–N(3), 175.1(5); C(1)–Pt(1)–Br(2), 92.0(4); N(3)–Pt(1)–Br(3), 85.9(4); Br(1)–Pt(1)–Br(3), 176.46(6); Br(1)–Pt(1)–Br(2), 93.47(6).

In conclusion, a wide range of [(NHC)PtBr$_4$L] complexes could be successfully synthesized in high yield by direct oxidation of NHC-Pt(II) precursors bearing diverse functional groups and fully

characterized. The molecular structure of several representative complexes functionalized with lipophilic amines confirmed their octahedral geometry and the oxidation with bromine proved regioselective as only *trans* complexes were observed by X-ray diffraction.

3) Synthesis and characterization of [(NHC)PtCl$_4$L]

Remarkably, a majority of platinum complexes that entered clinical trials are decorated with chloride ligands[4b] rather than bromide. Access to the chloride family [(NHC)PtCl$_4$L] proved successful by oxidation using the *freshly* prepared hypervalent iodine reagent PhICl$_2$[203] again in excellent yield (Scheme 29). The mechanism is supposed to involve light activated dissociation of a chlorine radical and subsequent oxidation at the platinum centre.[204] The expected [(NHC)PtCl$_4$(pyridine)] complexes were isolated as light yellow powders by precipitation with pentane. All [(NHC)PtCl$_4$L] complexes displayed overall signals deshielding in both ^{1}H NMR and ^{13}C NMR, similarly to their bromide counterparts, though the observed shift is less significant since *ortho* protons on the pyridine moiety and N-methyl protons are found deshielded up to 0.6 and 0.4 ppm respectively compared to their Pt(II) precursors. To note, these pyridine functionalized Pt(IV)-NHC complexes proved poorly soluble in all organic solvents and thus characterization by ^{13}C NMR proved difficult. Still, interesting trends could be observed as carbon signals deshielding except for the carbenic carbon which was found around 110 to 115 ppm as previously underlined in section 3.I.1 for bromide complexes.

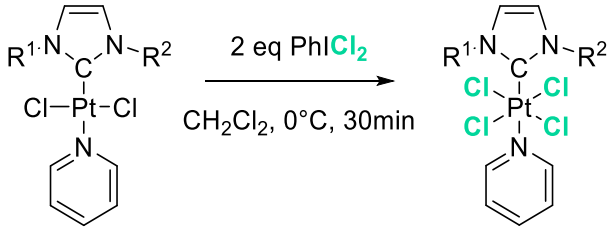

Scheme 29: Hypervalent iodine-mediated oxidation of Pt(II) precursors in [(NHC)PtCl$_4$(pyridine)] complexes

To note, the oxidation step proved somewhat more sensitive to the platinum environment and surrounding ligands when using hypervalent iodine compared to bromine. Difficulties in the oxidation of NHC-Pt complexes using iodobenzene dichloride have already been reported by Strassner who failed in oxidizing a cationic tetra-NHC platinum complex with bromine as the counter-ion.[205] The formation of Br-Pt(IV) derivatives is very likely to be preferred to Cl-Pt(IV) for thermodynamic reasons based on the low affinity of soft Pt^{IV} toward hard chlorine. Therefore, NHC-Pt(II) precursors bearing chloride ligands were preferred to iodide for direct oxidation with $PhICl_2$ oxidant. Moreover, chloride Pt(IV) complexes are known to favour chlorination of alkenes which might also explain side reactions observed during the synthesis.[206] Scheme 30 displays all synthesized [(NHC)$PtCl_4$(pyridine)] complexes.

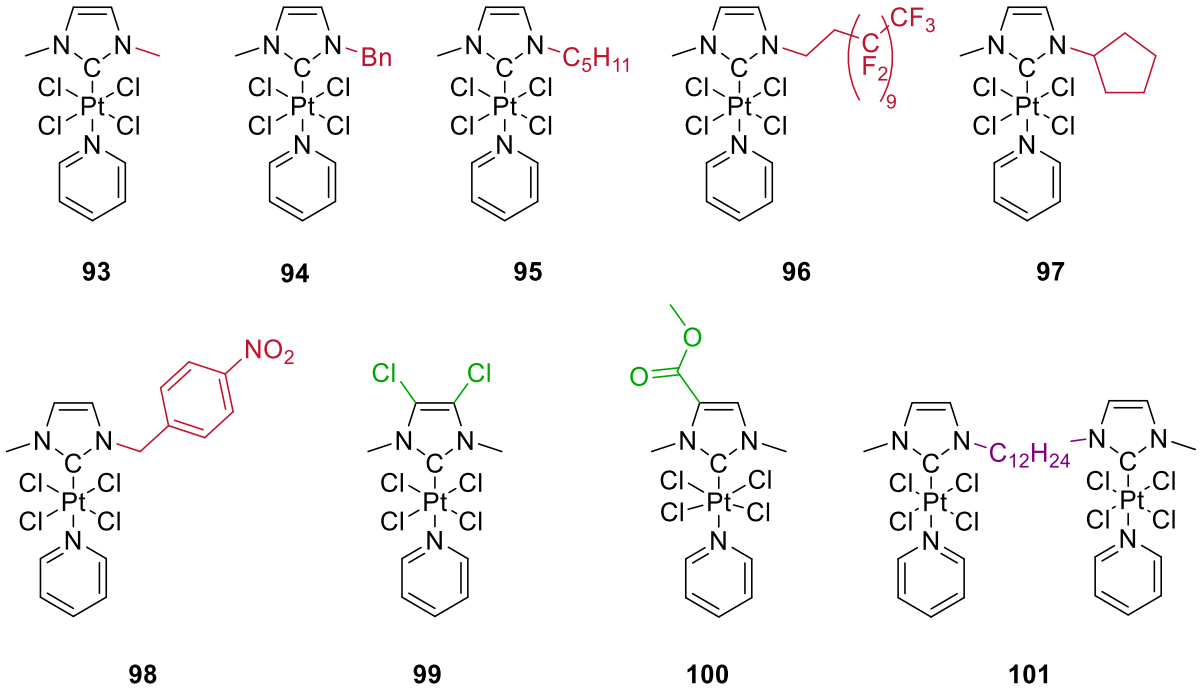

Scheme 30: Successfully synthesized [(NHC)$PtCl_4$(pyridine)] complexes (92-99% yield)

Both complexes **94** and **98** bearing aromatic rings and moderately lipophilic complexes **95**, **96** and **97** were afforded in good yield and similarly to their bromine counterparts **64** and **73**, benzylic protons for both complexes **94** and **98** appeared as singlet in ^{1}H NMR. Moreover, while

99 proved easily oxidized and stable for over a week in chlorine solvents, **94** was somewhat less stable and quickly decomposed in solution within days. Finally, the homobimetallic complex **101** could be obtained similarly also in high yield. Unfortunately, the range of functional groups stable under oxidative addition remained limited since neither precursors bearing ester **8** and aldehydes **11** and **18** nor NHC-Pt(II) complexes bearing anthracene **13** and pyrene **14** could be oxidized without the formation of numerous by-products. Finally, the oxidation using $PhICl_2$ of both thioimidazol- and triazol- complexes **23** and **24** respectively proved difficult and only complex mixtures were observed. Moreover, the rapid reduction of NHC-Pt(IV) complexes into their Pt(II) counterparts on silica gel, emphasized above prevented purification through column chromatography and recrystallization attempts were unsuccessful.

The direct oxidation of Pt(II) precursors bearing lipophilic amines using $PhICl_2$ following the same procedure as their pyridine counterparts successfully afforded the highly soluble $[(NHC)PtCl_4L]$ complexes **102**-**106** (Scheme 31). Although complete conversion of Pt(II) precursor was observed by ^1H NMR, the lipophilic complexes **104**-**106** were isolated in moderate yield probably due to their low solubility in pentane, thus preventing full complex recovery even by centrifugation.

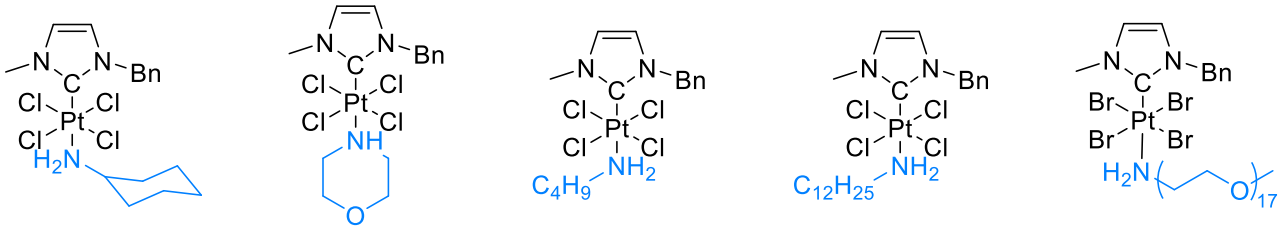

102 (96%) **103** (96%) **104** (52%) **105** (47%) **106** (35%)

Scheme 31: Lipophilic and highly soluble $[(NHC)PtCl_4L]$ complexes

Comparison between ^1H and ^{13}C NMR spectra of both NHC-Pt(IV) complexes and their precursors highlighted similar trends as their pyridine counterparts with an overall signal

deshielding of up to 0.6 ppm. Again, carbenic carbons were found shifted of over 30 ppm to higher field suggesting an increased electronic density at the carbene.

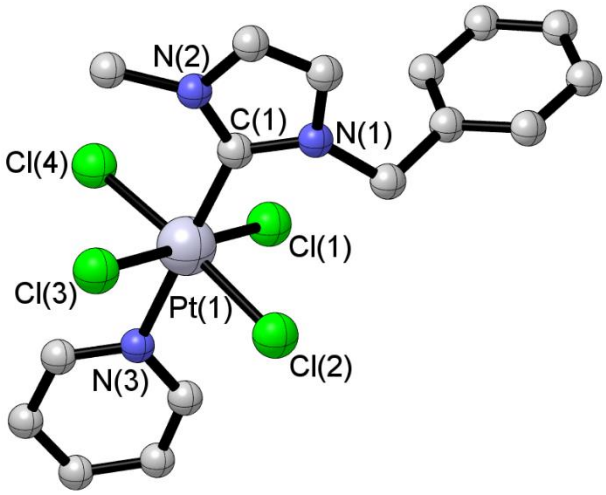

Figure 20: Molecular structure of [(NHC)$PtCl_4$(pyridine)] complex **94.** Selected bond distances [Å] and angles [°]: C(1)–Pt(1), 2.034(11); Cl(1)–Pt(1), 2.329(3); Cl(2)–Pt(1), 2.327(3); Cl(3)–Pt(1), 2.336(3); Cl(4)–Pt, 2.330(3); N(3)–Pt(1), 2.127(9); C(1)–Pt(1)–N(3), 178.4(4); C(1)–Pt(1)–Cl(2), 91.6(4); N(3)–Pt(1)– Cl(2), 89.2(3); Cl(2)–Pt(1)–Cl(4), 177.34(12); Cl(1)–Pt(1)–Cl(4), 91.85(12).

Moreover, single crystal of the [(NHC)$PtCl_4$(pyridine)] complex **94** could be grown by slow diffusion in pentane/dichloromethane. Its molecular structure confirmed the octahedral geometry around the Pt(IV) centre surrounded by the four chloride ligands in a slightly distorted square plan. No major modification of the overall structure is observed compared to the bromide complex **64** (Figure 11), suggesting chloride ligands to have little impact on the whole structure. Only C-Pt bond is smaller than in bromide counterpart according to chlorine's smaller Van der Waals radii with $d_{C\text{-}Pt}Br$ = 2.066 Å and $d_{C\text{-}Pt}Cl$ = 2.034 Å.[18] H-bonding network was observed between N-substituents protons or *ortho*-pyridine protons and the four chlorine atoms.

In conclusion, several complexes of the general formula [(NHC)$PtCl_4$L] could be obtained and characterized; their physico-chemical and antiproliferative properties will be emphasized below in Section 3.II.1.

4) Toward oxidation of NHC-Pt(IV) complexes with oxygen-based oxidants

The majority of reports dealing with Pt(IV) drugs are based on the oxidation of cisplatin scaffold using hydrogen peroxide, yet neither diluted nor freshly concentrated H_2O_2 solution succeeded in oxidizing our selected NHC-Pt(II) precursors.[207] No positive influence could be observed when exposing the reaction mixture to light, higher reaction time or temperature. Similar behavior was already reported on bis-phosphine complexes[208] and the suggestion that proximate ligands promoting hydrogen bonding are necessary for successful oxidation with H_2O_2 might explain this failure.[209]

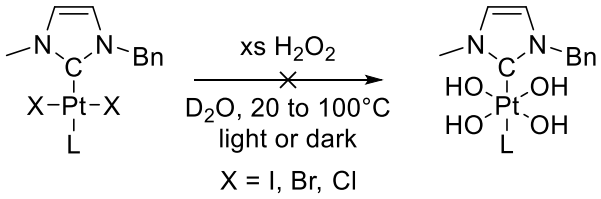

Scheme 32: Unsuccessful attempted oxidation of NHC-Pt(II) precursors using hydrogen peroxide

Many other one- or two-electron oxidants have been tested namely $PhI(OAc)_2$,[210] TEMPO, OXONE, tBuOOH, $KMnO_4$, $HClO_4$ and so forth, though oxidation met with failure in all cases. Several strategies were envisioned to favor halogen replacement by oxygen-based ligands, namely *in situ* deprotonation of chelating ligands like *acac*, halogen abstraction by silver triflate or freshly synthesized silver malonate salt. However, all attempts met with failure as the redox reaction prevailed and only Pt(II) product could be isolated concomitantly with degradation.

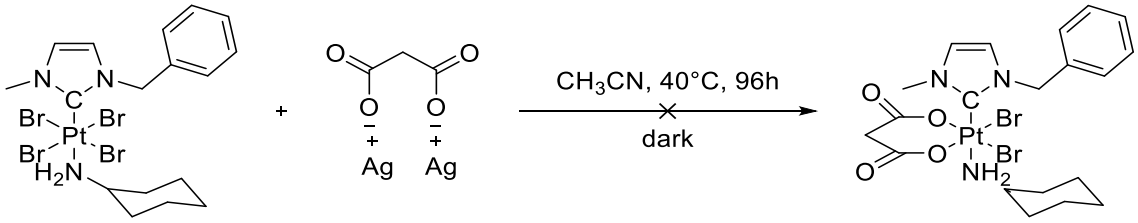

Scheme 33: Unsuccessful ligand exchange with silver malonate salt on NHC-Pt(IV) complex

Reasons explaining the failure of oxygen-based ligands coordination to NHC-Pt complexes remain unknown at the moment and could be due to either steric or electronic parameter. Hence, post-functionalization with free carbene as reported by Steinborn could be a fair solution, otherwise electrochemical synthesis could be envisioned in the future.[184]

5) C-X activation on NHC-Pt(II) precursors

As presented in the introduction, literature reports on NHC based Pt(IV) complexes mainly deal with spontaneous oxidative addition of a C-X bond. However using similar procedures, none of the *trans* [(NHC)PtI_2(pyridine)] precursors investigated successfully promoted activation of trimethylsilyl bromide, methyl iodide, methyl magnesium bromide or 5-(trifluoromethyl)dibenzo-thiophenium tetrafluoroborate even after up to 96 h reaction.

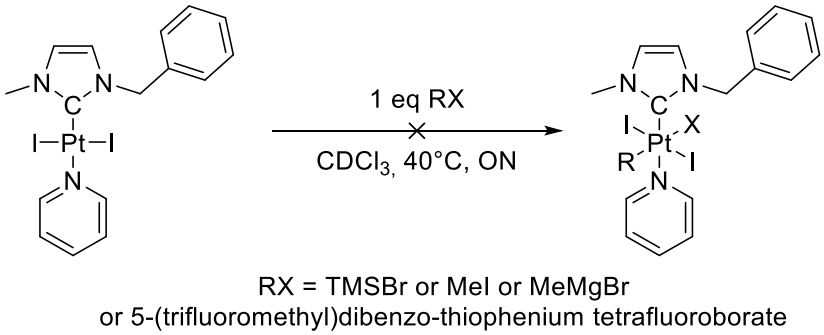

Scheme 34: Unsuccessful attempted oxidative addition at the platinum centre

These results together highlighted the electronic specificity of the redox couple NHC-Pt(II)/Pt(IV) compared to the multitude of other platinum compounds reported up to now and endorsed us in further investigating this family of complexes.

6) ^{195}Pt NMR spectroscopy

The ^{195}Pt isotope which nuclear spin is I = 1/2 and natural abundance about 34% has become a highly versatile probe to study platinum chemistry by NMR. Typical for heavy atoms, the chemical shift range of ^{195}Pt is large (about 13 000 ppm) thus exploration for a signal shift can rapidly become tedious without the assistance of DFT calculations. [211,212] Yet, Huynh recently suggested ^{195}Pt NMR chemical shifts to be indicative of the electron density at the metal centre based on systematic comparative analysis of the ^{195}Pt NMR resonances for complexes which only differed in the NHC ligands.[213] Therefore, to get further insights in the electronic parameters of [(NHC)PtX$_4$(amine)] complexes, both direct ^{195}Pt and indirect ^{1}H-^{195}Pt HMQC NMR measurements have been undertaken in $CDCl_3$ at 20°C considering the solvent and temperature effects on ^{195}Pt shift (a 107 ppm signal deshielding was observed for **95** in d_6-DMSO compared to $CDCl_3$).

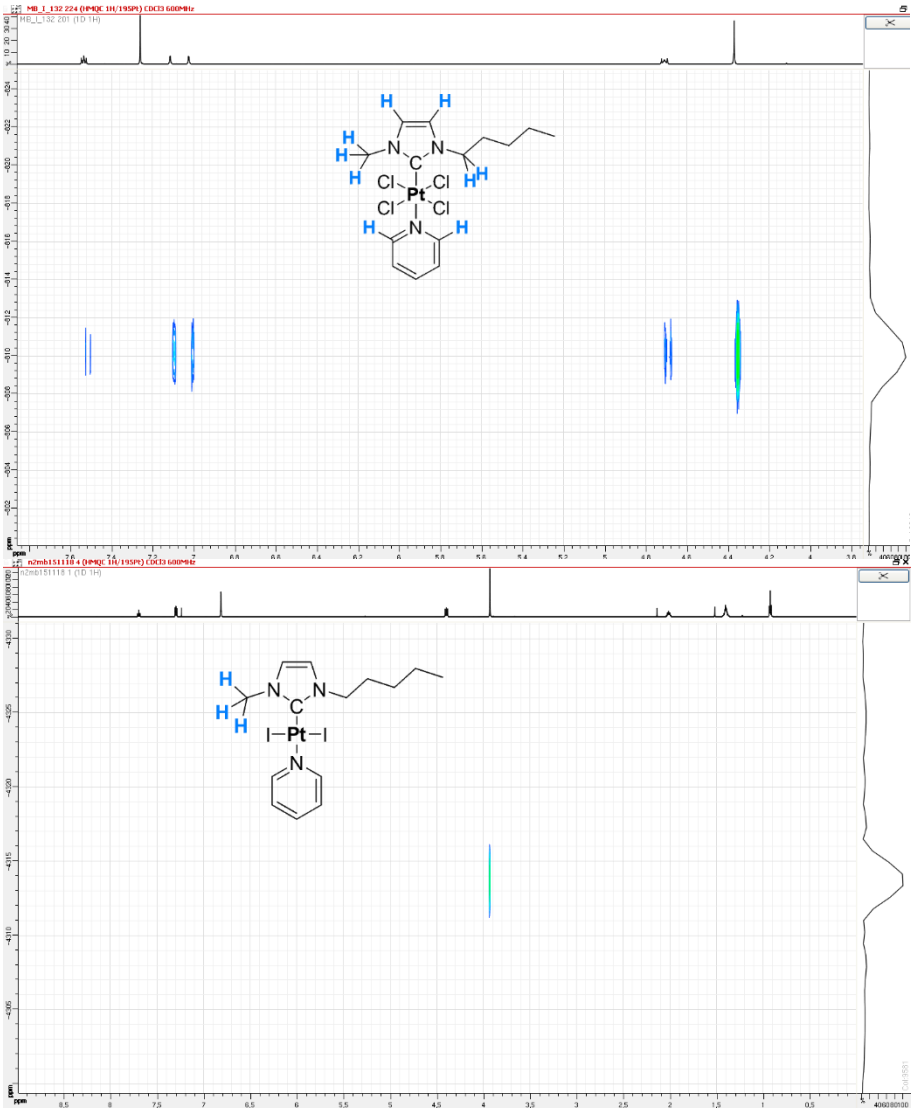

Figure 21: Selected examples of ^{1}H-^{195}Pt NMR spectra of **95** (*above*) and **6** (*below*) highlighting the proton coupling in long range with the platinum centre. Observed signals in ppm ($CDCl_3$): **95** 4.35 (N-CH_3), 4.70 (N-CH_2), 4.75 (N-CH_2), 7.0 (CH_{im}), 7.10 (CH_{im}), 7.50 (CH_{pyr}), 7,55 (CH_{pyr}); **5** 3.9 (N-CH_3).

^{1}H-^{195}Pt HMQC NMR have been acquired for most complexes and highlighted the coupling of protons in $^{3}J_{H\text{-}Pt}$ and $^{4}J_{H\text{-}Pt}$ with the Pt(IV) centre thus emphasizing a stronger communication through the nitrogen atom compared to the Pt(II) centre where only N-CH_3 protons are coupling in $^{4}J_{H\text{-}Pt}$ (Figure 14).

Remarkably, specific trends were deduced from chemical shift measurements on NHC-Pt complexes, the most obvious was the large shift from below -3300 ppm to either -2000 or -800 ppm when oxidizing NHC-Pt(II) precursors into [(NHC)$PtBr_4$L] complexes or their chloride counterparts respectively. These values seem to act as finger print for this family of complexes considering the range of complexes investigated. Moreover, for both Pt(IV)/Pt(II) complexes a significant platinum shift dependence was observed depending on the halogen ligand and correlated with the different stabilities of both chloride and bromide families. To note, the shifts of both *cis* NHC-Pt^{II}-DMSO complexes displayed negligible shift from bromide **107** to chloride **108** compared to *trans* NHC-Pt-L complexes (Δδ = 5 ppm). Furthermore, Figure 15 displayed the ^{195}Pt NMR signal shift dependence on either the NHC ligand backbone or its *trans* ligand in [(NHC)$PtBr_4$L] complexes and highlighted a moderate influence of the *trans* amine modification from the [(NHC)$PtBr_4$(pyridine)] derivative **64** to its cyclohexylamine and morpholine counterparts **84** and **85** respectively. This suggest a minor contribution to the platinum shift of *trans* ligand compared to the *cis* ligand. Finally, the variation of the NHC backbone seemed to moderately influence the platinum signal shift and was coherent with the low signal shift for carbenic carbon in ^{13}C NMR, suggesting a low influence on the metal centre.

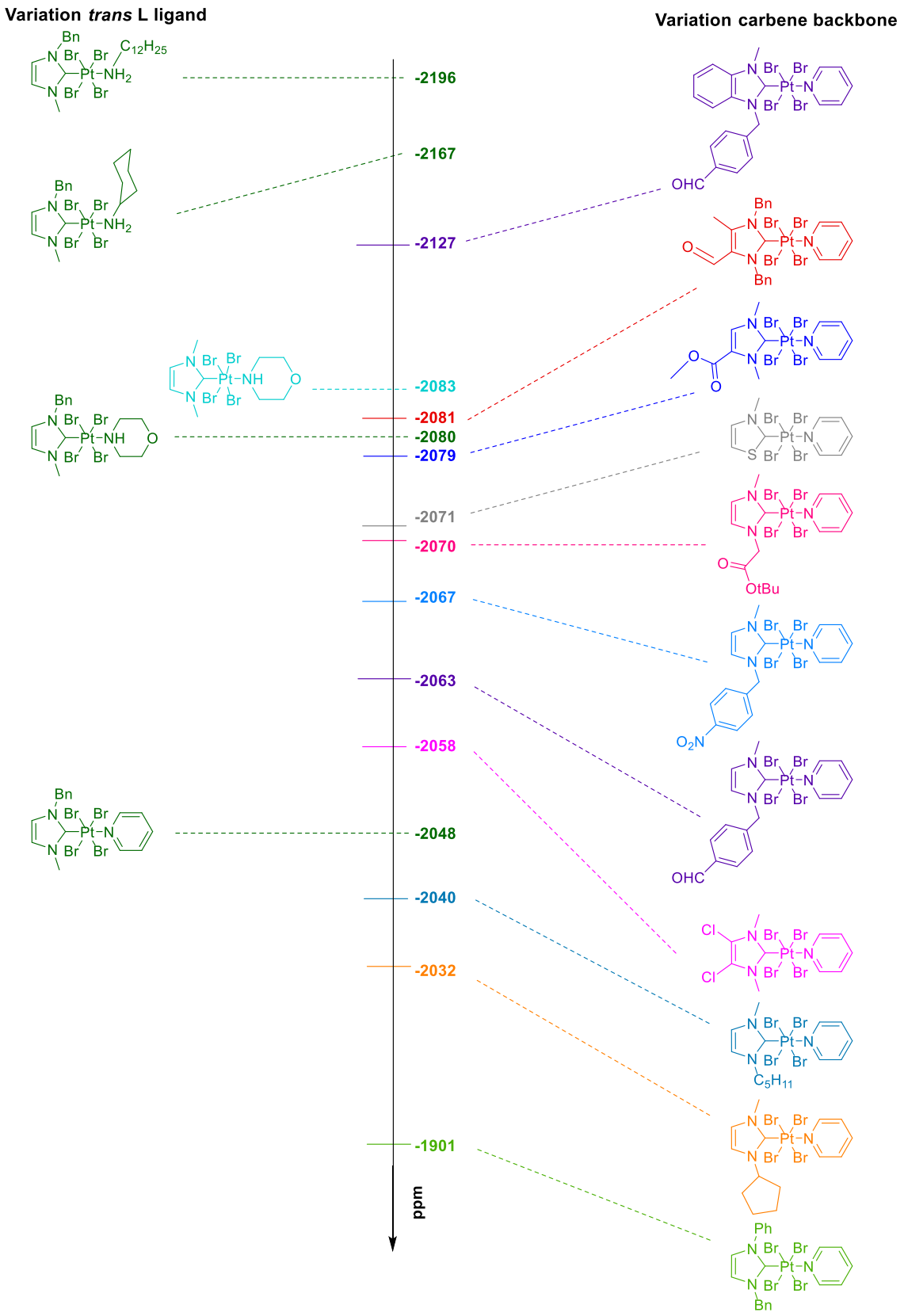

Figure 22: Platinum shift of various NHC-Pt complexes in ^{195}Pt NMR (in $CDCl_3$)

II. NHC-Pt(IV) prodrugs: stability and drug release

1) Stability of NHC-Pt(IV) complexes in organic solvent and mice serum

As previously mentioned, the novel family of NHC-Pt(IV) complexes developed herein have been designed to provide enhanced cytotoxicity toward cancer cells and stability toward deactivation processes in serum media. However, drug stability should be investigated prior *in vivo* investigation to confirm its inertness until it reaches its target. Best-selling cisplatin is an interesting illustration of the issue encountered with platinum drug due to its interaction with the solvent and poor stability in the blood stream.[214,215] Indeed, numerous side effects noticed after the injection of cisplatin are partly due to its poor stability in biological environment. Moreover, in drug screening, stock solutions are often prepared using DMSO as solvent at high concentration. Yet, the highly nucleophilic sulfur atom from DMSO is able to coordinate numerous metals by ligand displacement. Such unfortunate event is not only damageable due to structure modification so as electronic and steric change, but more importantly can affect drug's cytotoxicity and biodistribution. Indeed, DMSO has been shown to lower the potency of cisplatin toward cultured thyrocytes[216] and several reports recently stressed the importance to evaluate the possible interaction between investigated drug candidates and DMSO.[215,217,218] Therefore, prior to investigation of anticancer properties, the stability of selected NHC-Pt(IV) complexes have been evaluated toward a DMSO/H_2O solution.

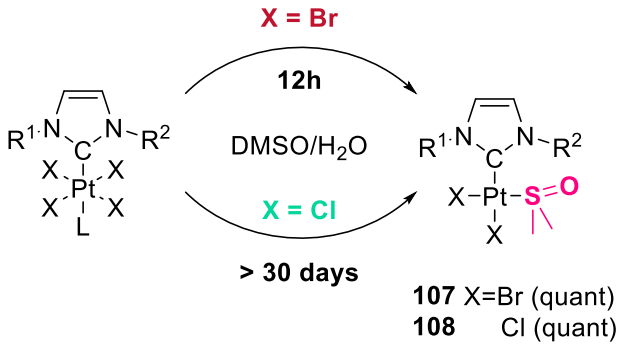

Scheme 35: Stability of (NHC)PtX_4(amine) complexes in DMSO/H_2O (C = 10^{-3}M, 20°C)

It appeared that both families of NHC-Pt(IV) complexes reacted in the presence of DMSO to form new NHC-Pt(II)-DMSO species which were isolated and compared to synthetically obtained [(NHC)PtX_2(DMSO)] complexes **107** and **108** (X = Br, Cl). This evolution could preliminary be studied by UV and ^{1}H NMR measurement on a 8 mmol solution of the selected complex in a 4/1 solution of d_6-DMSO/D_2O until full NHC-Pt(IV) consumption. Conversions were calculated based on the signal integration corresponding to pyridine protons in *ortho* position (Figure 16). The reduction of NHC-Pt(IV) complexes could be precisely followed by either decrease in UV of the band λ = 359 nm or by ^{1}H NMR analysis in which disappearance of the resonance peak for *ortho* protons of coordinated pyridine and apparition of free pyridinium signal attested for the formation of Pt(II)-DMSO compound **108** (Figure 16).

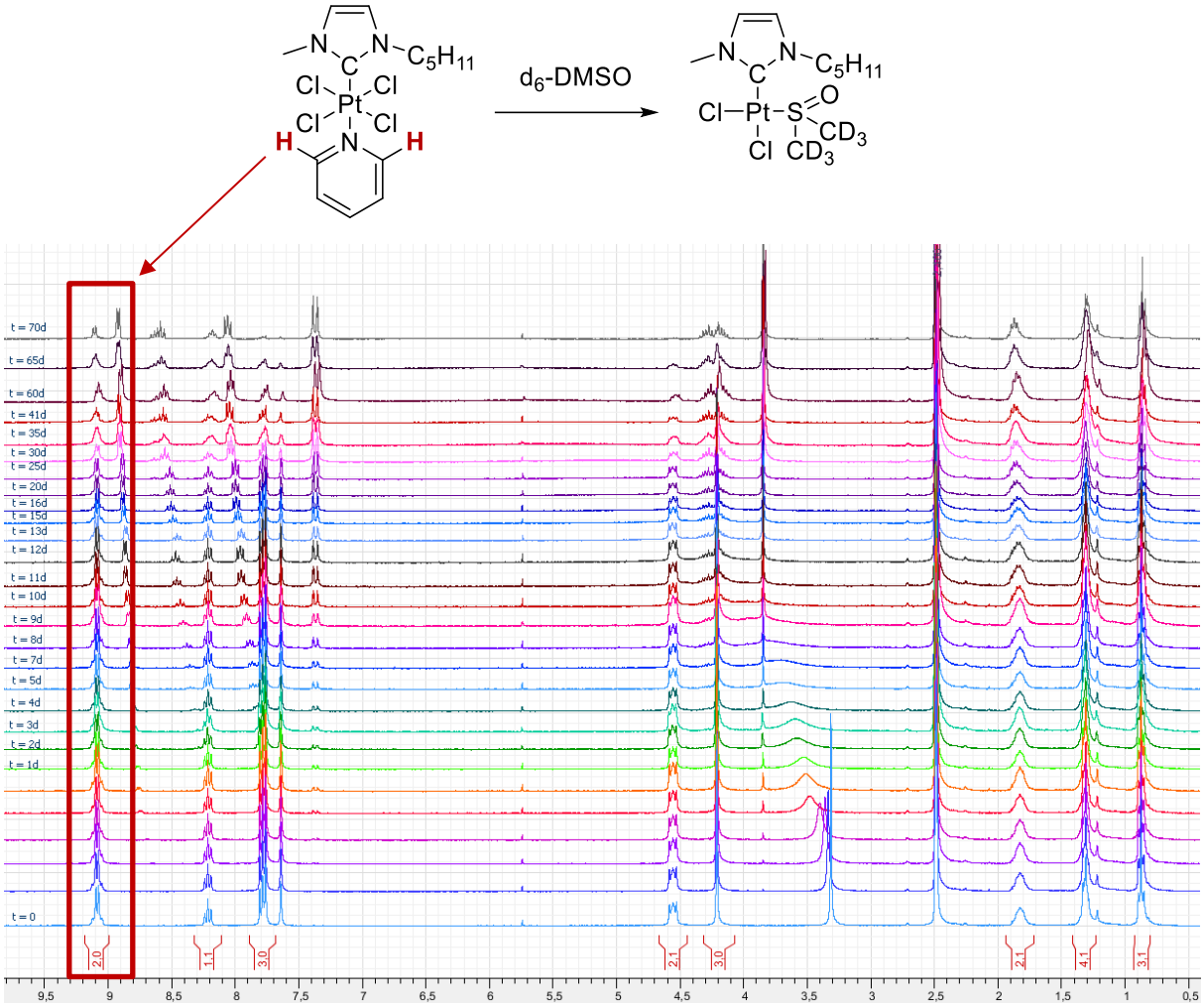

Figure 23: Reaction progress with platinum complex **95** at 20°C in d-$_6$DMSO over 70 days

A series of reaction progress with various NHC-Pt(IV) complexes in DMSO has been conducted by ^{1}H NMR. Remarkably, all [(NHC)$PtBr_4$L] complexes were fully converted to NHC-Pt(II)-DMSO within hours even for **77** bearing the more σ-donating cyclohexylamine ligand despite the stability of its Pt(II) counterpart **30** in DMSO. Contrastingly, the family of [(NHC)$PtCl_4$L] complexes proved far more stable as full reduction required several weeks. Such a huge difference in inertness has already been investigated for other Pt(IV) complexes and inertness has been suggested to be highly dependent on the nature of the axial ligands.[219] In the end, the great stability of the [(NHC)$PtCl_4$L] family is an excellent opportunity for further analysis in biological media as unwanted reaction should not have strong incidence toward obtained results. Unfortunately, no intermediate of the reaction between NHC-Pt(IV) complexes and DMSO could be observed at the NMR time scale. A follow-up of this reaction has been conducted in the presence of spin-traps (TEMPO or ascorbic acid), yet no significant change could be noticed in both cases which might suggest that no radical was involved in this process. Although the formation of pyridinium was noticed, a possible mechanism might involve spontaneous eliminative reduction of bromine, subsequent hydrolysis in hydrogen bromide and finally protonation of the free pyridine. However, up to now no evidence of such mechanism has been observed. Other reduction processes have already been reported for Pt(IV) prodrug candidates, as thermal or photoinduced reduction.[220]

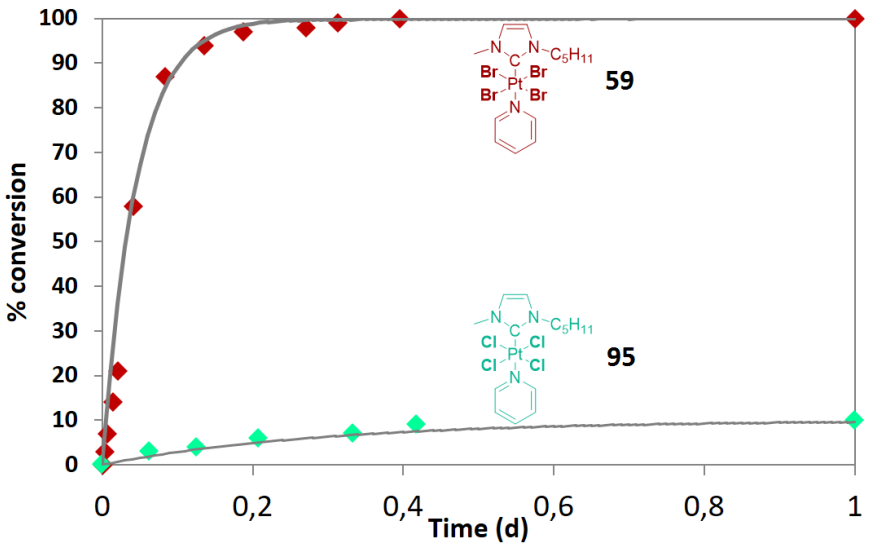

Figure 24: General trends observed in the conversion percentages of NHC-Pt(IV)-amine complexes into NHC-Pt(II)-DMSO as a function of time in a DMSO/H_2O mixture

To note, the less coordinating solvent DMF is usually a great alternative to DMSO in the preparation of stock solutions, however as already discussed the low solubility of our NHC-Pt(IV) prodrug candidates in DMF prevented its use as alternative solvent.

The stability of NHC-Pt(IV) complexes in biological media has been evaluated by solubilizing the selected complex **59** in mouse serum at 37 °C for 72 h. However, ^{1}H NMR on the extract proved inconclusive due to the multiple proteins overlapping characteristic NHC-Pt(IV) signals. A secondary followed-up experiment has been performed using UV-vis spectroscopy in a mixture of 9/1 of DMSO/mice serum containing the complex **59**. The band intensity decrease at 380 nm suggested a full consumption of the NHC-Pt(IV) prodrug candidate within 30 minutes, which is reasonable for further use in biological application since the half-life stability in blood of cisplatin is $t_{1/2}$ = 21.6 min[221] while satraplatin is $t_{1/2}$ = 6.3 min.[222] MALDI mass analysis failed at giving additional insight on the formed metabolites as only heavy protein fragments were observed which might suggest complex trapping into the hydrophobic cavities of proteins as already evidenced for cisplatin[223] and other platinum compounds.[224,225,226] Similarly, in ^{195}Pt NMR no signal corresponding to the NHC-Pt(IV) complex **59** or its reduction product **107** could be observed, which might suggest the formation of other metabolites or trapping of the complex into protein thus disturbing signal acquisition.

2) Investigation of the NHC-Pt(IV) reduction process by biological reducing agent

It is nowadays widely accepted that a two-electron bioreduction of Pt(IV) prodrugs *in vivo* is necessary to release the active drug and promote anticancer activity toward cancer cells (Figure 18).[227,228] As previously reviewed in the introduction, numerous sulphur containing molecules and proteins encountered within the serum and hypoxic tumors can be responsible for the Pt(IV)/Pt(II) redox process.[229] Reduced glutathione (GSH) is a common reducing biomolecule largely present in the blood with a concentration in healthy patients is ranging around 680-2500 µM in the blood and 2-11 µM in the plasma.[230,231] It has been widely used as a representative

model for preliminary investigation of NHC-Pt(IV) bioreduction in the literature (*i.e.* 1:2-25 Pt/reducing agent ratio, r.t. to 37 °C).[232,233,234]

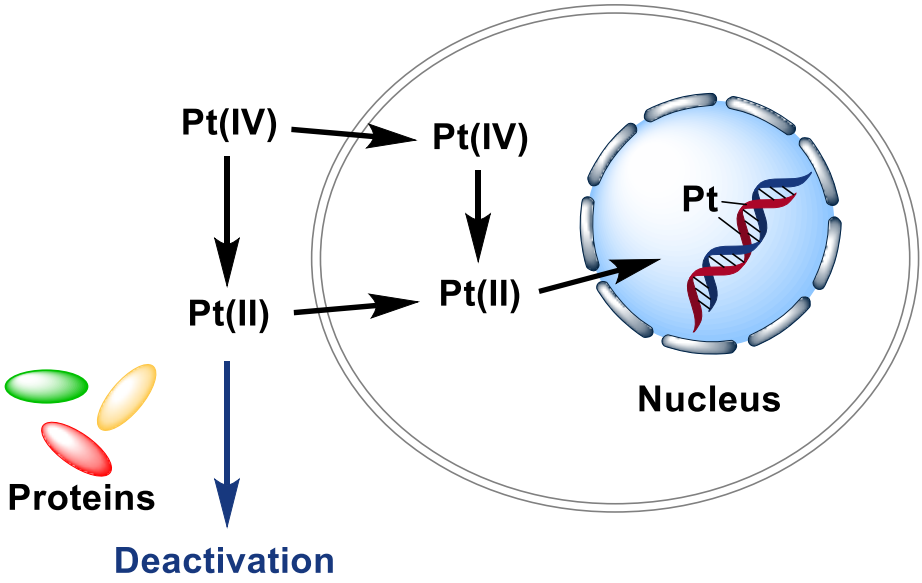

Figure 25: Proposed mechanism of action for Pt(IV) prodrugs

Therefore, we decided to conduct a ^{1}H NMR follow-up of the highly stable complex **95** with two different GSH/Pt ratio, *i.e.* 1/1 and 10/1. Bioreduction of **95** by glutathione proved to be complete within 48 h which matches the requirements for efficient Pt(II) drug release. Moreover, only the reduction product [(NHC)PtX$_2$(pyridine)] was observed by ^{1}H NMR, thus suggesting that no GSH-Pt adduct formation occured in parallel to the bioreduction which contrasts with platinum poisoning reported for cisplatin.[235,236,237] To note, while GSH failed at displacing the pyridine ligand, smaller thiols as the ethylthiol proved to bind NHC-Pt complexes, suggesting great influence of the steric parameter toward coordination.

Other biological reducing agents have been evaluated for the bioreduction of NHC-Pt(IV) prodrug candidates, namely ascorbate which concentration in blood plasma is 50-150 µM[238,239] and methionine, under similar conditions and in a 1/1 ratio of Pt/reducing agent. Again, only the expected NHC-Pt(II)-pyridine compound was formed and no side reaction occured contrarily to the group of Natile which noticed a dependence of the reduction product upon the nature of

reducing bio-molecule.[240] Moreover, slower reduction was observed for both methionine and ascorbate compared to the GSH which is coherent with literature.[241]

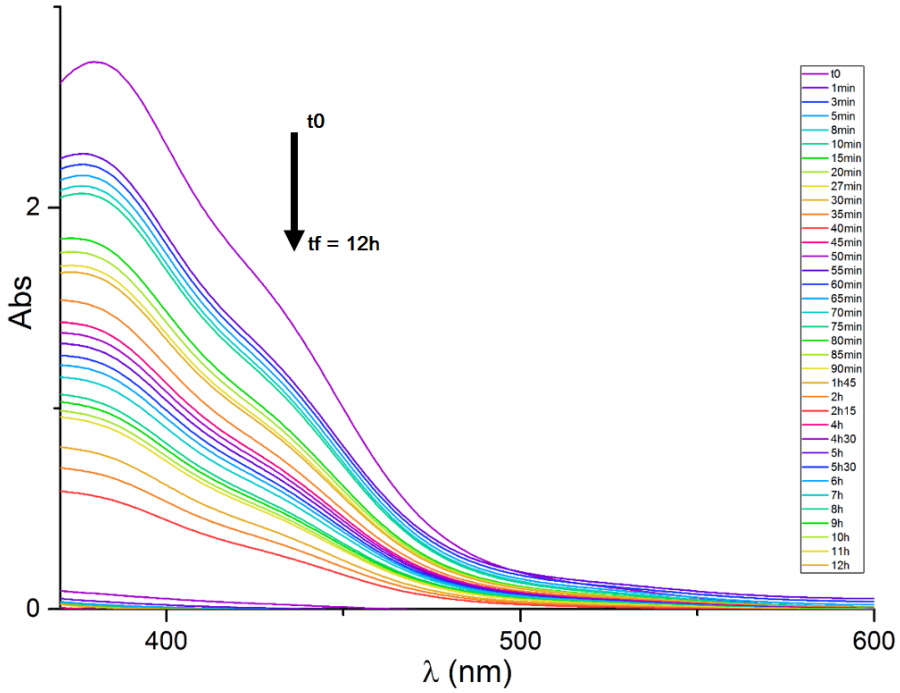

Figure 26: Reduction of **95** by methionine in DMSO solution (10^{-3}M, 20°C)

Complex	Reducing agent	Pt/red ratio	$t_{1/2}$ (h)	t_{final} (j)
	GSH	1/10	5.5	1.5
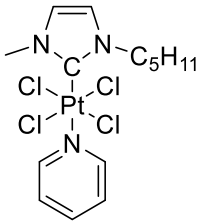	GSH	1/1	10.5	3
	Sodium ascorbate	1/1	1.2	1
	Methionine	1/1	5.7	4

Scheme 36: Kinetic of reduction of **95** depending on the nature of biological reducing agent

Observed reduction kinetics of NHC-Pt(IV) complexes compare favorably with other Pt(IV) prodrugs reported which reduction kinetic is rather of the order of minutes than hours.[242,243,244]

Therefore, these investigations validated the possibility of drug release in great time scale of [(NHC)$PtCl_4$(pyridine)] compounds in a solution mimicking biological media. Moreover, NHC-Pt(IV) prodrug candidates appeared to be sufficiently kinetically inert to prevent early hydrolysis and other unwanted side reactions with biological material.

3) Electrochemical investigations

Potency of Pt(IV) complexes is highly dependent on the redox properties of the Pt(IV)/Pt(II) couple. Indeed, when the Pt(IV) reduction potential is shifted toward negative values, the active Pt(II) species release is slow, resulting in lower cytotoxicity. On the other hand, an increase of the Pt(IV) reduction potential will promote early drug release, thus allowing metalloprotein-mediated deactivation. Reduction potentials $E_{Pt(IV)/Pt(II)}$ of both NHC-Pt(IV) complexes and the oxidation of their Pt(II) precursor were investigated by cyclic voltammetry (CV). The experiments were performed in a regular three-electrode cell using a glassy carbon working electrode and Pt electrodes as counter electrode and pseudo-reference electrode in acetonitrile solution containing 0.1 M $TBAPF_6$ as supporting electrolyte (Figure 20). All experiments were performed at room temperature. In the following, the potential axes are referred to the ferrocenium/ferrocene redox potential as recommended by IUPAC when working in organic solvents.

Figure 20 presents voltammograms obtained at a scan rate of 100 $mV.s^{-1}$ for [(NHC)PtX_4(pyridine)] complexes with X = Br or Cl as well as [(NHC)PtX_2(pyridine)] complexes with X = I, Br or Cl. To note, the synthesis of [(NHC)PtI_4(pyridine)] complex met with failure and thus investigation remained restricted to NHC-Pt(IV) complexes **59** and **95**. NHC-Pt(IV) complexes undergo a two-electron metal-centered reduction during the cathodic potential scan as exemplified by **59** where the reduction potential is E_{red} = -0.55 V. It should be mentioned that the halide ligands released during NHC-Pt(IV) reduction are oxidized at lower potential than the one of the NHC-Pt(II) reoxidation (Figure 20B), making the NHC-Pt(II) reoxidation wave difficult

to observe in the CV. Reduction potentials are very similar for both [(NHC)$PtBr_4$(pyridine)] and [(NHC)$PtCl_4$(pyridine)] complexes, though the 0.1 V negative shift for **95** correlates with its improved stability in solution (Figure 20A). Since the halide oxidation occurs at a lower potential than the one of the Pt(II) species, the oxidation of [(NHC)PtX_2(pyridine)] complexes was also investigated (Figure 20B). The oxidation of NHC-Pt(II) into NHC-Pt(IV) occurs at ~ 1.2 V for both [(NHC)$PtBr_4$(pyridine)] and [(NHC)$PtCl_4$(pyridine)] complexes. To note, the wave displayed at 0.25 V for [(NHC)PtI_2(pyridine)] complex **6** is attributed to the oxidation of I^- into I_2 followed by the oxidation of the iodide ligands into most probably IO_4^- species which might be one of the reason for the low stability of the iodide-Pt(IV) species. During the cathodic potential scan the NHC-Pt(IV) species formed from the oxidation of NHC-Pt(IV) precursors bearing either chlorine or bromine are reduced around -0.5 V, their iodine counterpart **6** exhibiting a reduction potential lower (E_{red} = -1 V for **6** and E_{red} = -0.5 V for [(NHC)$PtCl_2$(pyridine)] **2**).

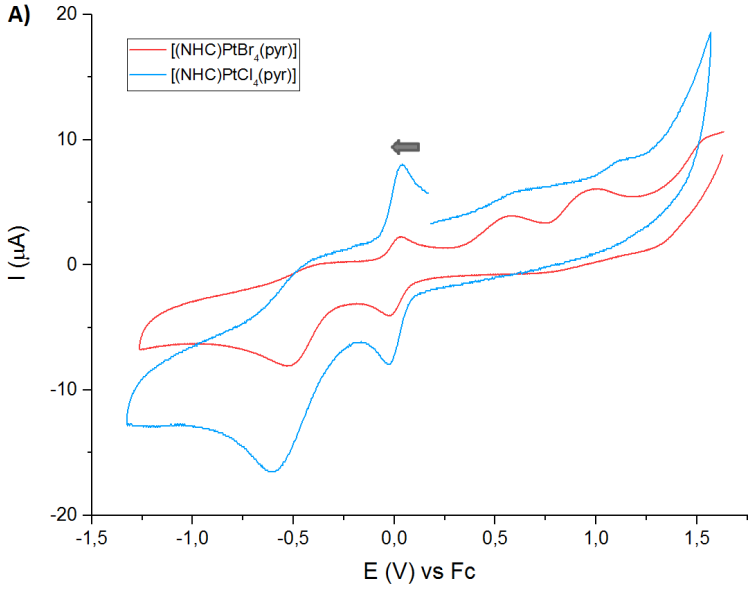

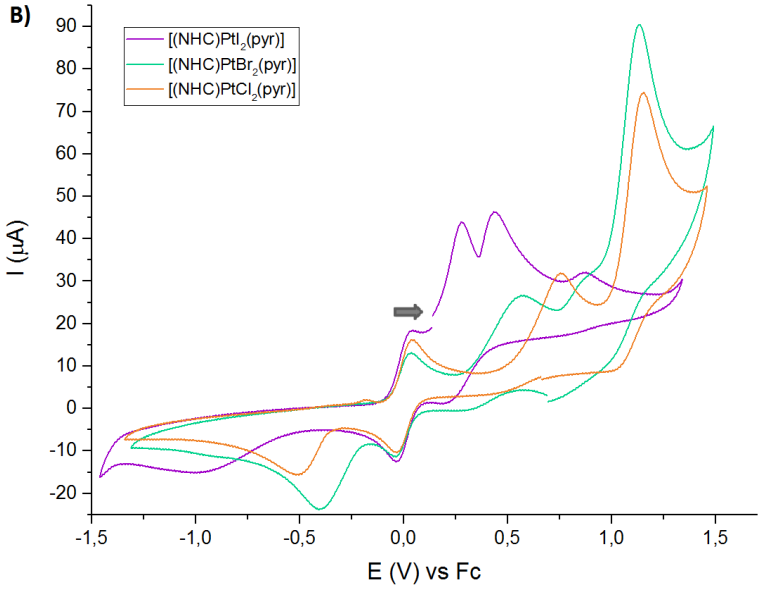

Figure 27: Cyclic voltammetry in 0.1 M $TBAPF_6$ and acetonitrile solution at a scan rate of 100 $mV.s^{-1}$ on A) NHC-Pt(IV) complexes **59** and **95**, B) NHC-Pt(II) complexes **2**, **4** and **6**

Entry	95	59	2	4	6
	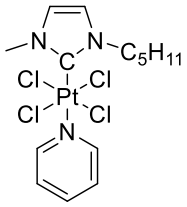	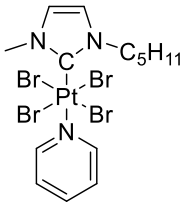	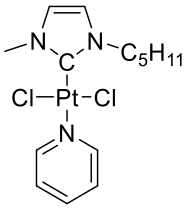	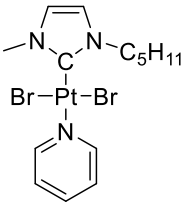	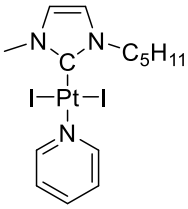
In CH_3CN, E_{red} (V)	-0.65	-0.55	-0.50*	-0.40*	~ -1.0*
In CH_3CN, E_{ox} (V)	1.17**	1.0V**	1.2	1.2	0.9V**
In DMSO, E_{red} (V)	-0.65	-0.45	ND	ND	ND

Figure 28: Peak potential of Pt(II)/Pt(IV) complexes in acetonitrile or DMSO at room temperature

* Potential corresponding to the reduction peak attributed to the Pt(IV) species generated during the anodic scan

** Potential corresponding to the oxidation peak attributed to the Pt(II) species generated during the anodic scan

In order to gain more insights on the reactivity of NHC-Pt(IV) complexes in DMSO, cyclic voltammetry has been performed in DMSO using the same parameters as previously mentioned above (Figure 22). While no reduction potential modification was observed for **95** when solubilized in either acetonitrile or DMSO, drastic reduction potential shift was observed for **59** as E_{red} = -0.55 V in acetonitrile and goes up to E_{red} = -0.4 V in DMSO (Figure 21). This suggests that **59** is more easily reduced in DMSO compared to other solvents and confirms the observed rapid reduction in DMSO/H_2O solution observed by ^1H NMR and UV-vis.

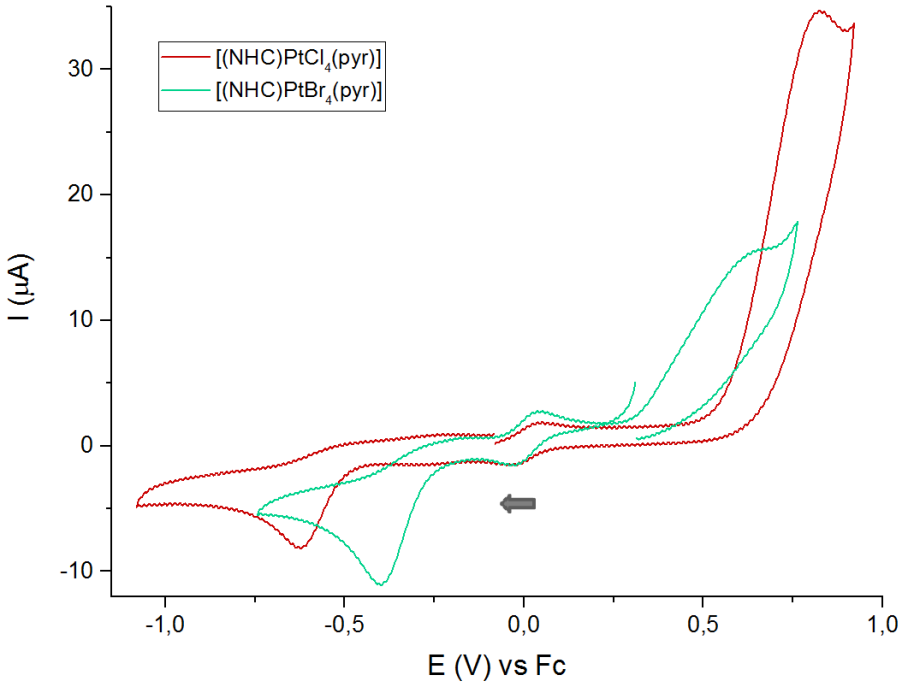

Figure 29: Cyclic voltammetry on both bromine and chlorine NHC-Pt(IV) complexes **59** and **95** respectively in DMSO at a scan rate of $mV.s^{-1}$

In order to investigate the role of water in the formation of the NHC-Pt(II)-DMSO species, voltammograms have been acquired on both bromine and chlorine NHC-Pt(IV) complexes **59** and **95** respectively in a mixture of DMSO while progressively adding small amounts of water (Figure 23). Upon water addition, the intensity of the reduction peaks decreases while the reduction potential shifts toward higher values. The rapid solution bleaching observed for the [(NHC)$PtBr_4$(pyridine)] complex **59** correlates with full conversion to the NHC-Pt(II)-DMSO species **107** within minutes. However, while only slow solvation of **95** is observed in DMSO

solution, sudden solution bleach is observed subsequently to the water addition which seems to promote full conversion to the NHC-Pt(II)-DMSO complex **108** (reduction potentials of both species are found at E_{red} = -0.65 V for **95** and E_{red} = -0.45 V for **108**). Interestingly, the presence of water seems to have a major influence on the reaction kinetic since months were necessary to promote Pt(IV) reduction for **95** in dry d_6-DMSO while minutes allowed full reduction in the presence of water; which is in line with reported observation for oxaliplatin.[218]

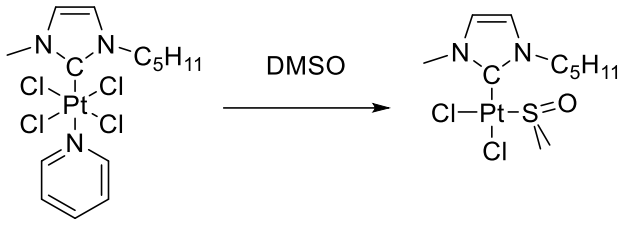

95 **108**

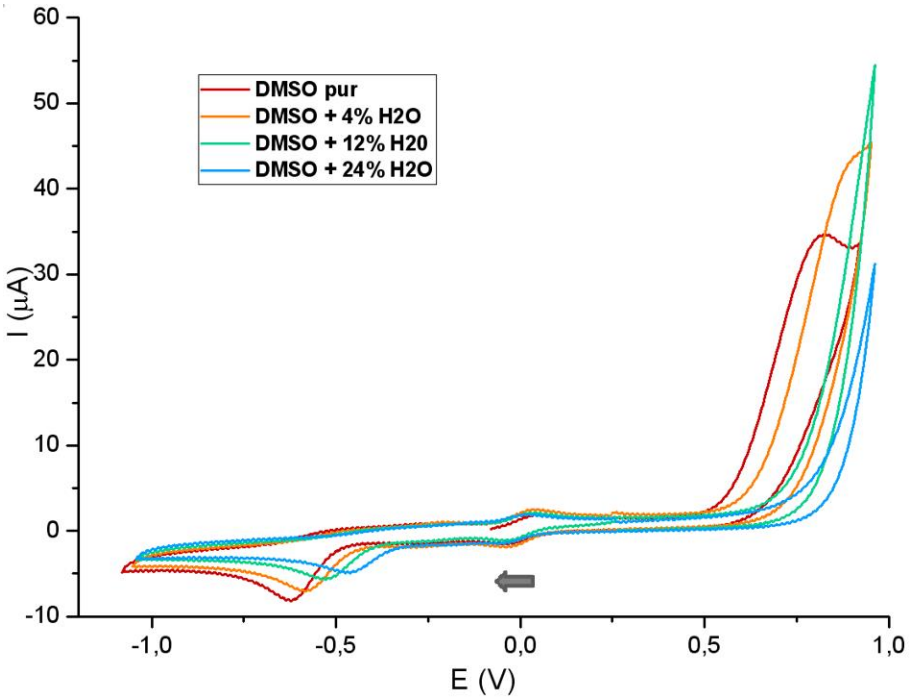

Figure 30: Cyclic voltammetry on bromine NHC-Pt(IV) complex **59** at a scan rate of 100 mV.s^{-1} in a 0.1 M $TBAPF_6$ solution of a) DMSO, b) 95%DMSO/5%H_2O, c) 85%DMSO/15%H_2O, d) 76%DMSO/24%H_2O

Finally, the reduction process of NHC-Pt(IV) complexes **59** and **95** in the presence of glutathione as a model for reducing biomolecule has been investigated by cyclic voltammetry in DMSO. No reduction potential shift is observed for both **59** and **95** as in the presence of water but

decrease of the intensity of the reduction wave suggests the progressive conversion of the NHC-Pt(IV) starting materials into their Pt(II) counterparts. Moreover, within the time scale used for this experiment, no formation of the solvation product **107** is observed, thus confirming the full NHC-Pt(IV) reduction to its Pt(II) counterpart. Altogether, these results confirm trends previously observed by ^{1}H NMR suggesting reduction of NHC-Pt(IV) complexes to be preferred to solvation in the presence of GSH. This additional experiment thus reinforces the possibility for Pt(IV) reduction *in vitro* and *in vivo* and Pt(II) drug release to further exert cytotoxicity.

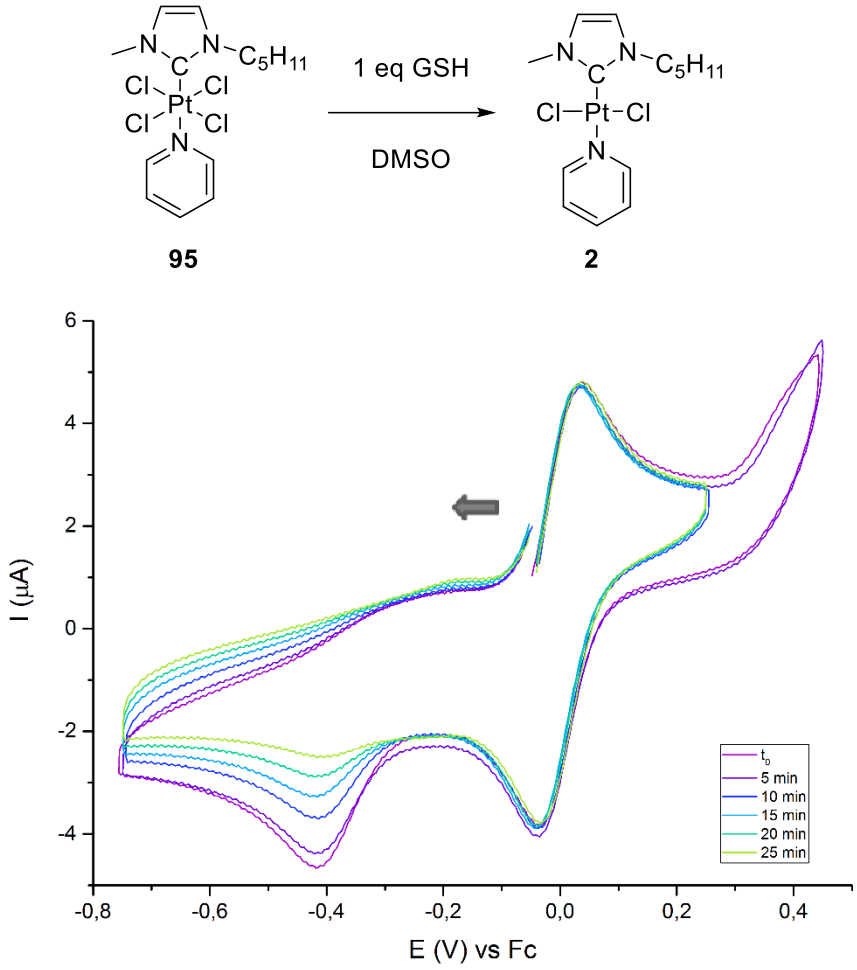

Figure 31: Evolution complex **59** in a DMSO solution with 0.1 M $TBAPF_6$ in the presence of one equivalent of GSH by cyclic voltammetry at 100 $mV.s^{-1}$

III. Anticancer activity and mechanism of action of NHC-Pt(IV) prodrugs

The family of NHC-Pt(IV) complexes appeared to be very promising within the frame of drug development according to their high yielding synthesis and modulation possibilities. While both bromide and chloride families depicted somewhat moderate to extremely low solvation rate in DMSO, their high inertness toward thiol-mediated deactivation and slow reduction kinetic in *in vivo* like media are promising properties in the development of Pt(IV) prodrugs. Altogether, previous investigations highlighted the potential of NHC-Pt(IV) complexes in the fight against cancer.

1) Cytotoxicity of selected NHC-Pt(IV) prodrug candidates

The anticancer activities of some selected NHC-Pt(IV) compounds (Scheme 37) have been evaluated *in vitro* toward three human cancer cell lines, namely HCT116, MCF7 and PC3 treated at several platinum concentrations for 72h and compared to cisplatin (Figure 37). The percentage of viable cells was determined by MTS assay and allowed measurement of half inhibitory concentration (IC_{50}) defined as the maximal concentration of a drug needed to inhibit a given biological process by half. All experiments were performed in triplicate at Imagif, Gif sur Yvette (Chapter 5).

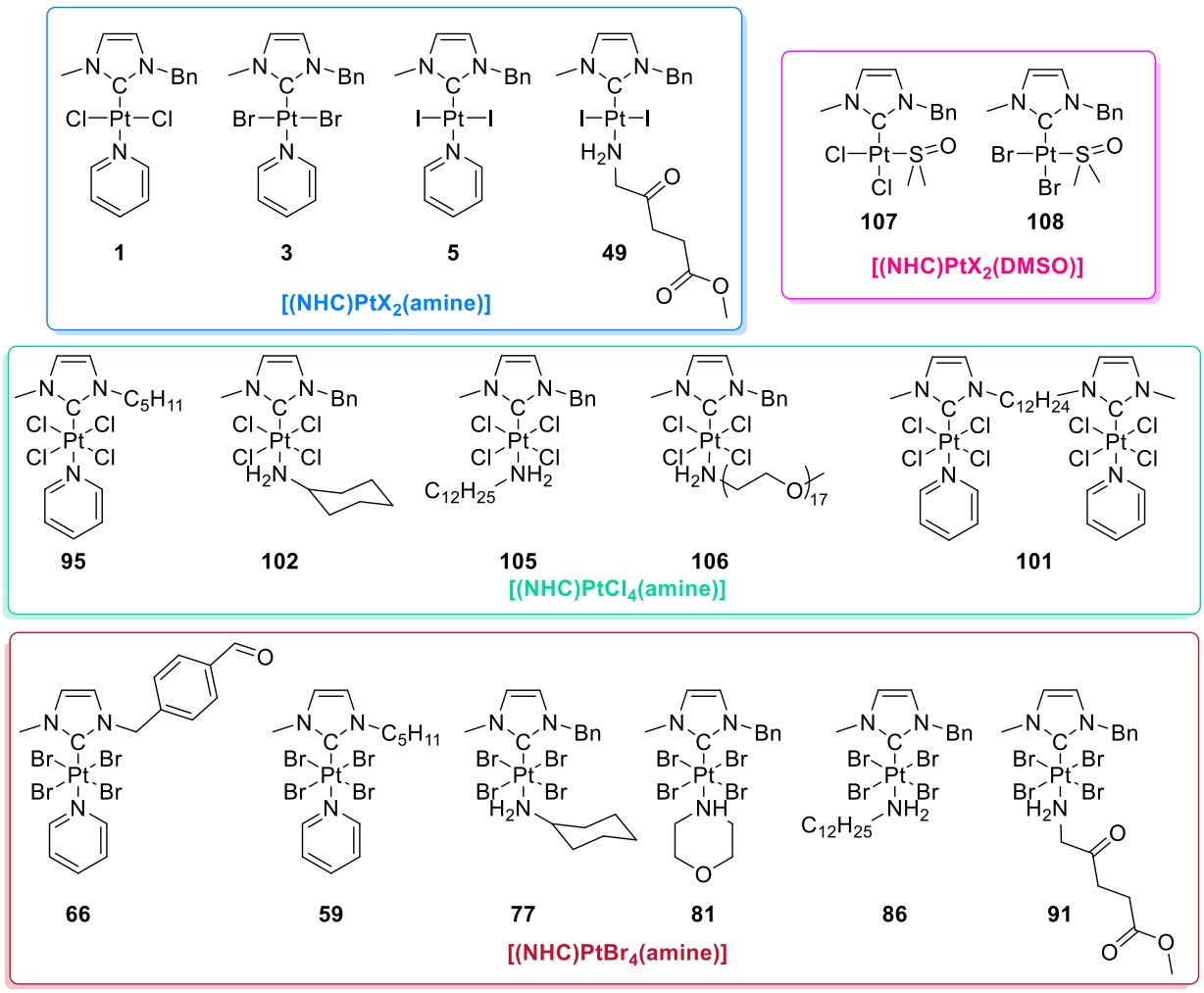

Scheme 37: Selected NHC-Pt complexes for *in vitro* anticancer studies

Among the tested NHC-Pt(II) derivatives, the three [(NHC)PtX$_2$(pyridine)] complexes **1**, **3** and **5** displayed greater cytotoxic activity than cisplatin as anticipated considering the effectiveness of NHC-Pt(II) combination already widely explored by our group, though the iodine complex is the most potent. The novel methyl-aminolevulinate functionalized precursor **49** has also been tested and shows IC$_{50}$ values that favorably compare with the clinically used cisplatin. This compound is of interest for further application in photodynamic therapy, expecting to access a synergistic effect with the platinum centre. The four NHC-Pt(II) complexes were used as a reference to evaluate the possible benefit gained by oxidizing these well-established anticancer drugs into NHC-Pt(IV) prodrugs.

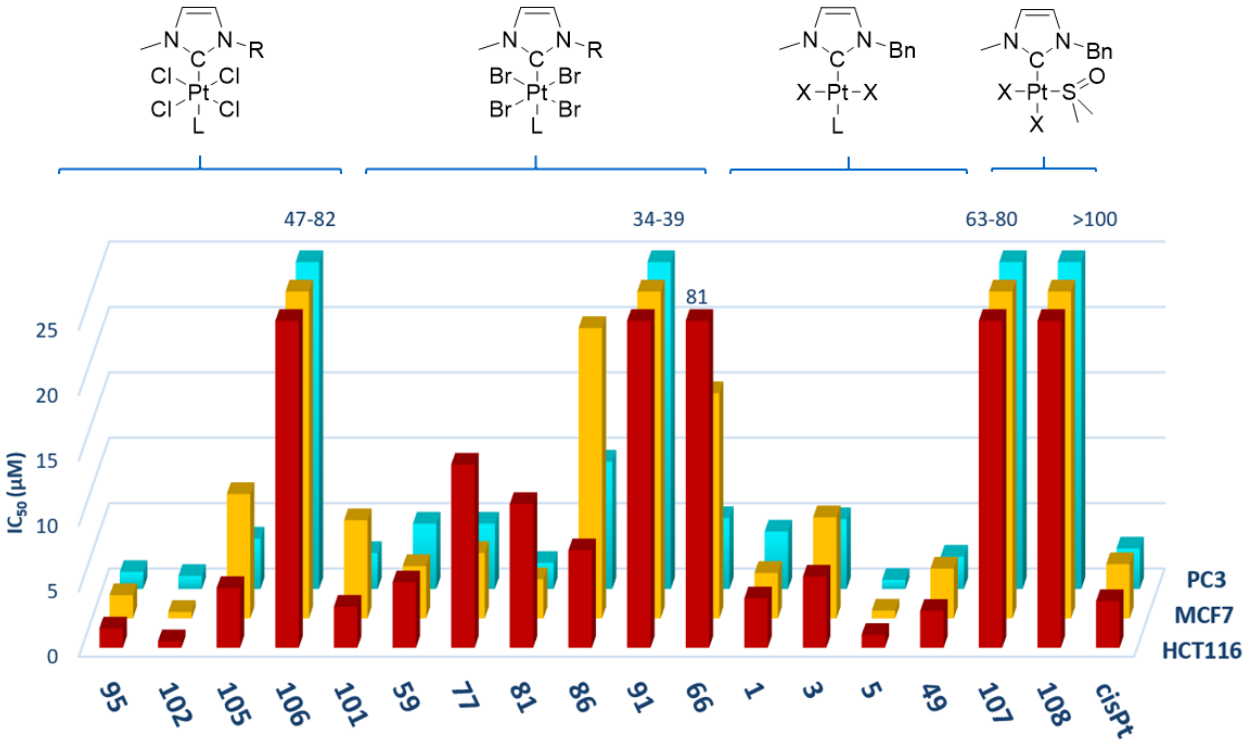

Figure 32: Half inhibitory concentrations IC_{50} (in µM) of selected compounds toward colon cancer cell HCT116, breast carcinoma MCF7 and prostate adenocarcinoma PC3

Interestingly, most NHC-Pt(IV) complexes displayed anticancer activities within the same range as cisplatin, though the chloride family **95**-**101** seemed to promote more efficient cancer cell death than [(NHC)$PtBr_4$L] complexes **66**-**91**. Indeed, **95** complex depicted IC_{50} of almost 1.5 µM on the three cancer cell lines and **102** was even found one order of magnitude more active than the cisplatin. Only the complex **106** bearing a polyethyleneglycol chain in *trans* position to the NHC appeared to be less active than other tested chloride NHC-Pt(IV) complexes. Remarkably, results presented in Figure 25 did not suggest improved potencies along with the greater lipophilicity. However, this has already been reported for other Pt(IV) complexes and a more comprehensive drug screening would be necessary to disregard the lipophilicity as a valuable parameter to tune for efficient NHC-Pt(IV) drug development.[245] The family of [(NHC)$PtBr_4$L] complexes depicted mixed activities and were typically found ranging around ~ 5-15 µM. The MAL-functionalized complex **91** which was tested under regular conditions for biological analysis promoted moderate cytotoxicity as IC_{50} = 35-39 µM toward the three cancer cell lines.

However, no complementary experiment exposing the cancer cell lines to a source of light has been undergone, which might result in higher potencies thanks to photodynamic therapy on the MAL moiety and its metabolites. The complex bearing an aldehyde-functionalized NHC backbone **66** appeared even less cytotoxic depicting only moderated anticancer activities. However, such results were not unexpected considering the somewhat modest stability of the bromide NHC-Pt(IV) family discussed above. Indeed, both **107** and **108** complexes bearing a DMSO moiety are not toxic under tested conditions up to 100 µM.

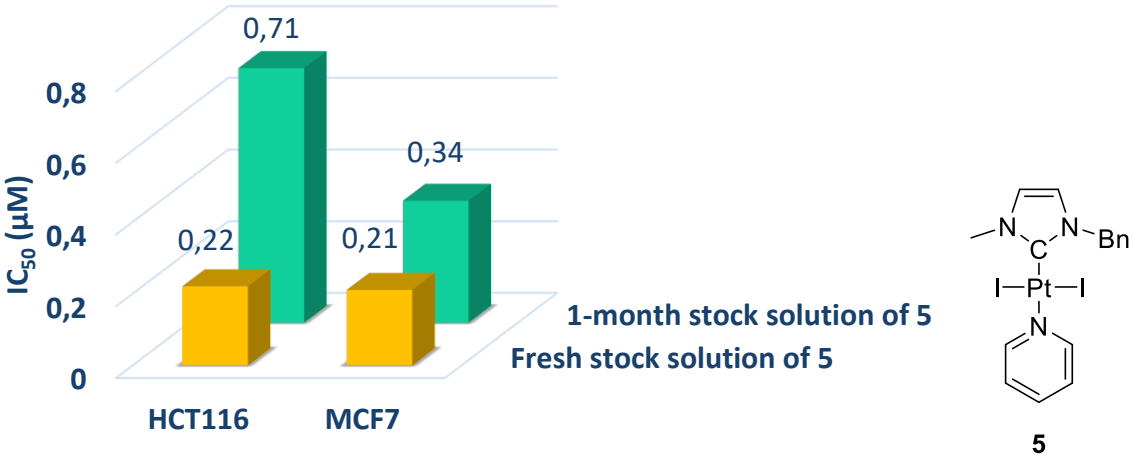

Figure 33: Influence of stock solution preparation toward half inhibitory concentrations on **5**

Moreover, the influence of experimental conditions has been assessed by determining the IC_{50} of both freshly prepared and one-month old stock solutions of **5** toward both HCT116 and MCF7 cancer cell lines (Figure 26). Remarkably, the IC_{50} values proved up to three times higher on HCT116 cancer cells treated with old stock solution, thus emphasizing the influence of experimental conditions used toward the reliability of cytotoxicity results. Therefore, taking into consideration both the low stability of [(NHC)$PtBr_4$L] complexes and inefficiency of their Pt(II)-DMSO byproduct **107**, moderated potencies observed in Figure 25 should no longer be an issue if stabilized with a liposomal formulation for example.

Finally, when considering the range of tested NHC-Pt(IV) complexes, overall encouraging results have been obtained even toward breast cancer (MCF7 cell line) which is known to be less

sensitive to platinum based chemotherapy. Several [(NHC)$PtCl_4$L] complexes proved significantly cytotoxic, some of them appearing even more potent than their Pt(II) precursors, thus suggesting the occurrence of complementary anticancer pathways to a simple reduction into Pt(II). Accordingly, more work is necessary in order to stabilize the bromide family and envisioned strategies to achieve it will be further exposed in chapter 4.

2) *Efficiency of NHC-Pt(IV) complexes toward cisplatin resistant cell lines*

Altogether, previous results highlighted the potential of NHC-Pt(IV) complexes as effective anticancer agents toward several human cancer cell lines, yet the major issue in the field of platinum-based chemotherapy remains the acquired and intrinsic resistance of cancer. Therefore, to determine whether NHC-Pt(IV) could substitute cisplatin in the treatment of resistant cancers, the cytotoxicity of prodrug candidate **95** has been evaluated toward both regular and mutated cancer cells which developed acquired resistance to cisplatin based chemotherapy by inactivation of caspase-3 dependent apoptosis pathways (A2780 and A2780R respectively). To note, the capsase-3 has been proposed to be responsible for cleavage of the DNA fragmentation factor (DFF), thus activating apoptosis factors.

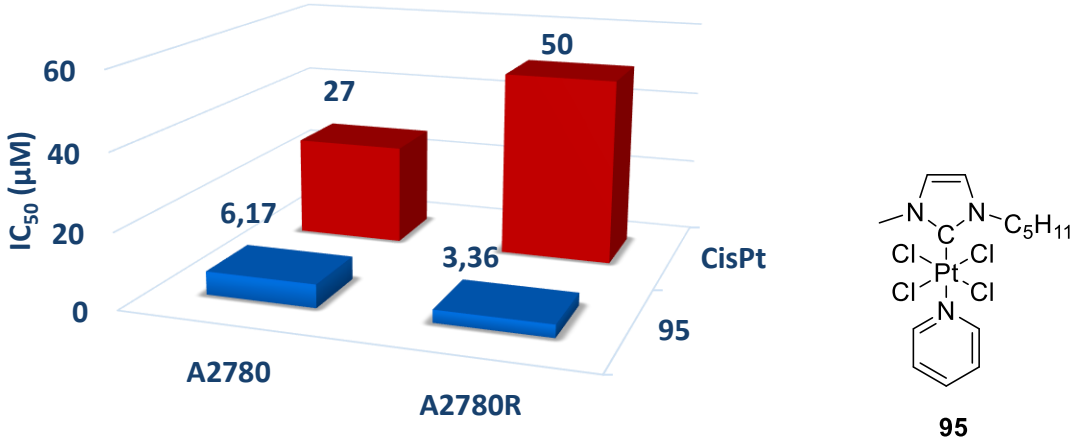

Figure 34: IC_{50} measurement for **95** compared to cisplatin[246] toward A2780 and A2780R cell lines

As expected, the cytotoxicity of cisplatin toward the resistant cell line A2780R is reduced by almost a factor two compared to A2780, thus confirming the drug inefficiency at providing complete anticancer activity when the caspase-3 dependent apoptosis pathway is inactivated. On the contrary, the treatment of A2780 cell line with our complex **95** seemed of the same order toward the resistant cell line A2780R as A2780 (IC_{50}*A2780* = 6.17 µM and IC_{50}*A2780R* = 3.36 µM). Moreover, the resistance factor calculated as R = IC_{50}*A2780R*/ IC_{50}*A2780* proved to be below 1 (R_{95} = 0.54) thus confirming that compound **95** efficiently overcomes this mechanism of acquired resistance. Therefore, altogether these results pointed out the efficiency of **95** toward cisplatin resistant cancer cell line A2780R and would need to be confirmed toward a larger range of cisplatin resistant cancers. Moreover, more solid investigations would be necessary to confirm a caspase-3 independent pathway for the cytotoxicity of **95**.

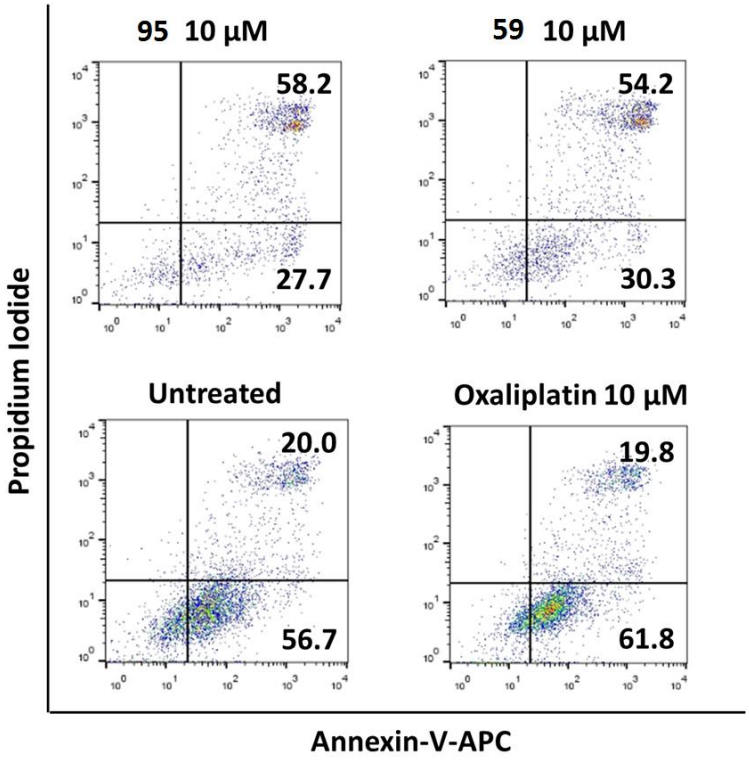

Figure 35: Evaluation of apoptosis on HCT116 p53 KO cell lines after treatment with **95**, **59** or oxaliplatin at indicated concentrations (24 h of incubation). After treatment, cells were labelled Annexin V-APC and Propidium Iodide and analysed by flow cytometry. Significant flow cytometry dot plots showing apoptosis induction are represented. The percentage of early apoptotic cells (Annexin V^+/PI^-) and late apoptotic cells (Annexin V^+/PI^+) are indicated.

The caspase-3 apoptosis pathway is supposed to be activated through a p53-mediated cell death,[247,248,249] p53 being a tumour antigen supposed to preserve genome integrity by inducing cell cycle stop at the G1/S phase and subsequent apoptosis. [250,251] Therefore, a complementary mechanistic investigation has been performed in collaboration with Pr S. Fournel (Faculté de Pharmacie de Strasbourg) to determine whether NHC-Pt(IV) complexes promote their anticancer activity through a p53 dependent pathway. The cancer cell line HCT116p53KO where the p53 gene is rendered inactive has been treated alternatively with our complexes **59** and **95** or oxaliplatin serving as a reference for clinically used chemotherapy. The inhibition percentage appeared to be within the same range between blanc sample and platinum chemotherapy reference oxaliplatin which suggests that oxaliplatin failed at inducing cancer cell death when the p53 pathway is inactivated thus confirming its inefficiency at overcoming resistance phenomenon. On the other hand, both NHC-Pt(IV) complexes seemed to promote cell inhibition of the same order toward p53 deficient cancer cells (Figure 28), though IC_{50} values previously reported on HCT116 suggested the chloride complex **95** to promote greater anticancer activity than **59** (IC_{50} = 1.48 µM for **95** and IC_{50} = 5 µM for **59**). Finally, these results supported that NHC-Pt(IV) complexes behave following a different pathway from cisplatin-like drugs and thus might be promising anticancer drugs to overcome resistance associated with cisplatin.

3) Binding experiments

Numerous reports highlighted DNA as the primary target for cisplatin and the formation of platinum-DNA adducts has for long been admitted as the major event responsible for its high *in vivo* cytotoxicity. Interestingly, several groups already suggested Pt(IV) to be capable to bind nucleobases.[252,253,254] Therefore binding experiments have been undertaken with two selected NHC-Pt(IV) complexes **59** and **95** which have been reacted in either ethanol or DMSO or DMF solutions with one equivalent of either guanine or adenine at 37 °C for 96h and compared to their Pt(II) precursor **6**. ^{1}H NMR analysis of the extract revealed that no nucleobase coordination occurs at the platinum centre for **59** and **95** and instead a mixture of reduction products and

starting material are obtained in all cases, so as the low valent platinum complex **6**. Others have already reported similar trends in the chemistry of platinum-based complexes[255,256] though several reports of Pt(IV)-mediated nucleobase oxidation are found in literature.[257,258,259] Accordingly, these preliminary results should be considered cautiously according to the difference between free nucleobase and DNA chain *in vivo*. To gain more knowledge into the binding affinity of NHC-Pt complexes, complementary investigation on their reactivity toward DNS should be considered. Moreover, at the moment selected [(NHC)PtI_2(pyridine)] drugs are under investigation in collaboration with Dr S. Harlepp (Institut de Physique et Chimie des Matériaux de Strasbourg) to evidence the formation of Pt-DNA adducts using optical tweezers. Finally, though the cytotoxic NHC-Pt compounds failed at binding nucelobases, other cellular compartments might be preferred targets for NHC-Pt(IV) complexes than DNA.

4) Mitochondria as an alternative target: from ROS generation to mitochondria dependent cytotoxic pathway

Mitochondria is the cellular compartment in charge of cells respiration and furnishes energy to cells through glucose oxidation. Oxidative stress in cellular tissue is a common process that lead to oxidative damage[260] by redox homeostasis disruption in the mitochondria and has been widely exploited in the field of metal-based anticancer drug.[261] Transition metals and particularly platinum drugs like cisplatin[262] or Pt(IV) derivatives[263,264,265,266,267] contribute to the death of mitochondria by *in situ* generation of radical oxygen species (ROS), namely superoxide ($O2^{\bullet -}$), hydrogen peroxide (H_2O_2), hydroxyl radical ($OH^{\bullet}$) and so forth.[268] Platinum derivatives also disturb the redox balance by interacting with the glutathione thus promoting cell cycle disruption and apoptosis.[269] Therefore, oxidative stress investigations have been undertaken on two selected NHC-Pt(IV) compounds **59** and **95** in addition to the NHC-Pt(II) complex **6**, and compared to oxaliplatin and staurosporine as a reference for ROS active drugs.[270] HCT116 cancer cells were treated with selected drug candidates at various concentrations for 13 h at 37 °C and subsequent incubation with MitoSox a mitochondrial superoxide indicator allowed quantification of cells whom mitochondria express ROS.

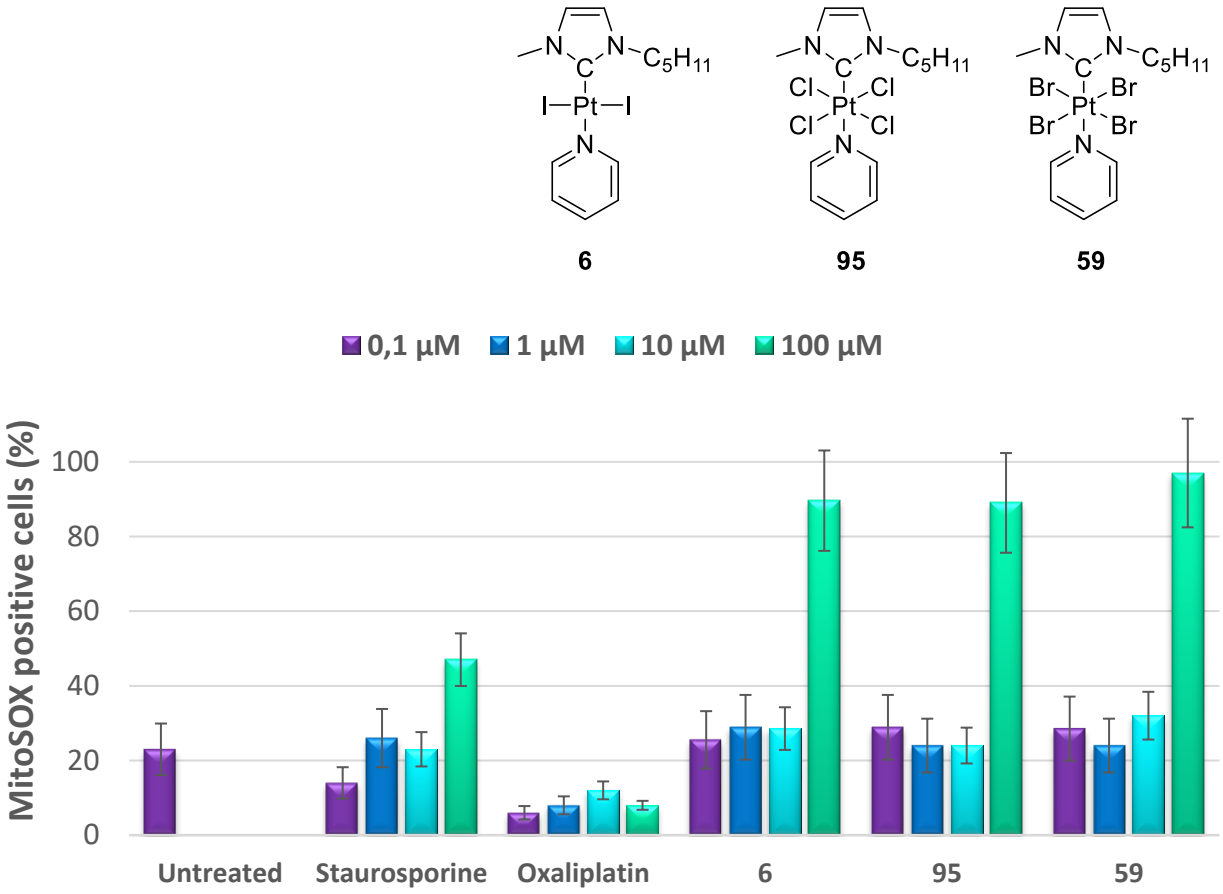

Figure 36: ROS production after cells treatment with selected compounds

Results confirmed the efficiency of NHC-Pt complexes at generating ROS in mitochondria and compared favorably with staurosporine at low concentration (~ 30% at 0.1 µM, 1 µM and 10 µM). Moreover, they appeared to be dose-dependent since important increase in ROS sensitized cells was observed at 100 µM (up to two-fold more positive cells than staurosporine), though no significant increase in ROS production was detected for NHC-Pt(IV) derivatives **59** and **95** compared to the NHC-Pt(II) complex **6**. In addition, only negligible effect is observed in cells treated with oxaliplatin, thus confirming a cancer cell death pathway that did not involve mitochondria. These results confirmed the mitochondria as a target for platinum-NHC based cytotoxicity since high stress levels were observed.

However, several enzymes act as guardian for the redox homeostasis and usually restore the intracellular redox balance, therefore a secondary experiment has been performed using the same compounds to ensure their efficiency at overwhelming the antioxidant system and induce cell death. Similarly to the previous experiments, cells have been treated with the selected compounds and exposed to MitoTracker which is a dye that labels mitochondria within living cells based on the mitochondrial membrane potential, thus allowing differentiation between the populations of live and dead mitochondria.[271]

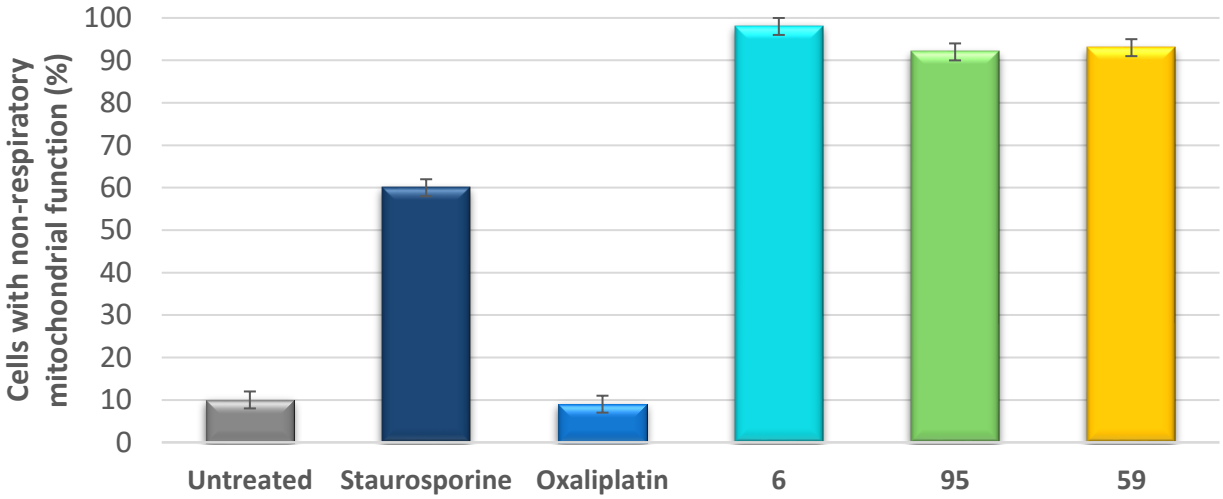

Figure 37: Mitochondria respiration activity after cells treatment with selected compounds (C = 100 µM)

Results depicted in Figure 30 confirmed the potential of both NHC-Pt(IV) and NHC-Pt(II) anticancer agents at stopping the respiratory activity in mitochondria. Interestingly, high percentage of mitochondria death was observed for all NHC-Pt(IV) tested complexes **59**, **95** and their precursor **6** up to two-fold higher than staurosporine while oxaliplatin failed at inducing mitochondrial death. This observation is in line with previous MitoSOX experiment since identical percentage of cells expressing ROS were found dead in the MitoTracker assay. The comparison between Figure 29 and Figure 30 therefore confirmed the efficiency of the combination of NHC to platinum for exerting potency *via* a mitochondria dependent pathway.

In conclusion, both tested NHC-Pt(IV) prodrug candidates **59** and **95** as well as the [(NHC)PtI_2(pyridine)] complex **5** equally promoteed the generation of radical oxygen species and

efficiently induced mitochondrial death. Remarkably, neither the nature of the halogen at the platinum centre nor the different stabilities between **59** and **95** seemed to impact their activity toward mitochondria contrarily to IC_{50} measurements previously reported in Section 3.III.1. Finally, the family of NHC-platinum complexes proved to successfully induce anticancer activity according to a different pathway from the clinically used oxaliplatin, therefore highlighting their potential in the treatment of cisplatin-resistant cancers.

IV. Conclusion

This chapter emphasized the synthesis of a library of high valent NHC-platinum prodrug candidates. Several straightforward synthetic pathways have been described herein to allow easy and modular access to a range of [(NHC)PtX_4L] derivatives with X corresponding to either bromide or chloride ligand. We also extended the scope to highly lipophilic NHC-Pt(IV) complexes by taking advantage of the *trans* pyridine lability. Characterizations are reported with special highlight on the use of ^{195}Pt NMR which proved to be a powerful tool in the evaluation of the platinum environment in both NHC-Pt(IV) and NHC-Pt(II) complexes. A full investigation of their stability properties toward DMSO and toward selected reducing bio-molecules validated the concept of prodrugs. The potency of this innovative family of complexes was evaluated toward several cancer cell lines and proved generally more active than the clinically used cisplatin. Encouraged by these results, a comprehensive investigation of mechanisms involved in their cytotoxic activity has been performed. Selected derivatives revealed promising efficiency at promoting cancer cell death in several cisplatin-resistant cell lines and a mechanism involving stress generation in mitochondria has been uncovered. Thus, we generated a chemical library of cytotoxic NHC-Pt(IV) prodrug candidates with promising potencies toward both regular and cisplatin resistant cancer cells.

Chapter 4: Nanodelivery of NHC-platinum complexes

Side effects associated to cisplatin-based cancer treatment have been suggested to arise from the formation of protein-platinum adducts which disrupt biological processes.[272,273] Therefore, nanodelivery devices have raised a huge interest to limit side reactions and access highly cytotoxic and biocompatible drugs for selective cancer targeting and individualized treatment.[274] However, numerous parameters are highly dependent on the nanoparticle choice, namely the route of administration, the mechanism for drug release and so forth. Therefore, we describe here four strategies to combine the cytotoxic NHC-Pt moieties to nanodelivery devices with the aim to improve selective drug uptake and lower side effects. The first part deals with NHC-platinum complexes covered by a biocompatible protein. The synthesis, characterization and drug release were then explored to ascertain the efficient drug delivery to cancer cells. Finally, their biological activities have been investigated and compared to free drugs. The second part of this chapter emphasizes preliminary developments of a liposomal formulation for NHC-platinum drugs and their anticancer activities. The next part is dedicated to the synthesis and comprehensive biological evaluation of biocompatible polymers functionalized with cytotoxic NHC-Pt moieties. Several synthetic pathways were used to enhance diversity by combination with chromophore or targeting moieties and their anticancer activity will be discussed. Finally, the synthesis of gold nanoparticles and preliminary investigation of their biocompatibility are detailed along attempts of drug conjugation.

I. Proteins as biocompatible carrier

Among dozens of proteins known to bind cisplatin and other platinum based complexes, human serum albumin (HSA) is of importance. Indeed, albumin is the main blood protein and regulates osmotic blood pressure.[275] HSA usually binds a large amount of injected platinum,[276] and this

strong affinity has been exploited for numerous applications ranging from surface functionalization, biosensors, deactivation of selected proteins relevant for defined pathologies and so forth.[277] However, large proteins can also be used as drug carrier to improve its circulation time in blood and tumour accumulation thanks to the enhanced permeability and retention effect (EPR).[278,279] Therefore, taking advantage of the high affinity of platinum complexes for albumin, its use as a biocompatible cargo for hydrophobic NHC-Pt complexes has been investigated herein to access selective drug delivery.[280,281]

1) State of the art: albumin in drug delivery

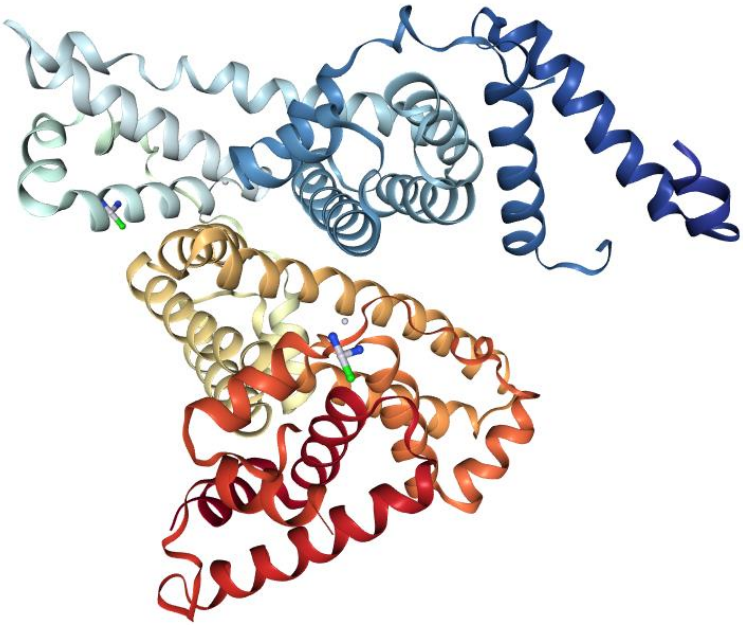

Figure 38: Structure of the human serum albumin complexed with cisplatin[282]

Human serum albumin (HSA) is the most abundant protein in blood[283] and serum (up to 40-45 $g.L^{-1}$) and composed of a single chain of 585 amino acids.[284] This protein is in charge of osmotic blood pressure regulation as well as lipids transport. The Sudlow's site I in HSA is known as a common locus for interaction with hydrophobic drugs such as cisplatin.[285,286] Yet contrarily to

other proteins, while HSA usually binds a large amount of injected platinum, such phenomenon is not irreversible and slow platinum release has been reported.[287] Moreover, FDA approved the use of the biocompatible HSA for pharmaceutical applications as illustrated by Levemir, Victoza and Ozoralizumab drugs.[289] Therefore, taking advantage of the high affinity of platinum complexes for albumin,[288] its use as a biocompatible carrier has been suggested.[289,290] This strategy allowed improvement of drug stability and proved promising to treat brain tumours as an alternative to clinically used drugs which usually fail at crossing the blood-brain barrier.[291]

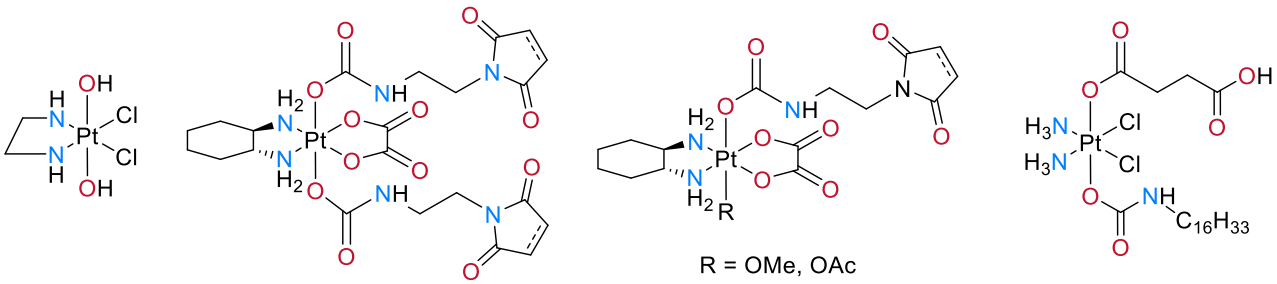

Sadler 1999 **Keppler 2013** **Keppler 2016** **Lippard 2014**

Scheme 38: Structure of Pt(IV) complexes designed to selectively bind to albumin[287,292,293,294]

Several Pt(IV) derivatives have been reported to bind to albumin by either covalent bonding of a maleimide moiety to the free thiol of Cys34[292,293] or non-covalent binding.[294,287] Such combination prevented side reactions at the metal centre[278] in addition to improve blood stability and cytotoxicity compared to free Pt(IV) complexes.[295] The authors therefore suggested that administration of the performed macromolecular drug is preferred.[287] Remarkably, the combination of a mono-functionalized maleimide containing platinum(IV) complex to HSA allowed successful mice recover thanks to both long time frames of disease stabilization and tumour inhibition by apoptosis.[293] However, all described Pt(IV) complexes covered with albumin follow the SAR rule, thus combination of NHC-Pt(IV) derivatives to albumin would be of interest for anticancer applications.

2) NHC-Pt(IV) uptake by bovine serum albumin

For our investigations, bovine serum albumin (BSA) was used instead of HSA since only a negligible difference of two amino acids exists between them. The combination of NHC-Pt motif to albumin protein was achieved by slow addition of a freshly prepared solution of NHC-Pt complex in DMSO to a BSA mixture in PBS/DMSO in a 18/1 ratio. The solution was allowed to settle for two complementary hours at 37 °C to ensure complete platinum uptake. The BSA concentration was maintained constant at 2.5×10^{-6} M for all experiments. This procedure could be extended from the [(NHC)PtX_2(pyridine)] compounds **2** and **4** to both [(NHC)PtX_4(pyridine)] complexes **59** and **95**. Various Pt/BSA ratio from 5/1 to 1/5 where investigated thus easily affording a range of macromolecules **109**-**112** (Scheme 39).

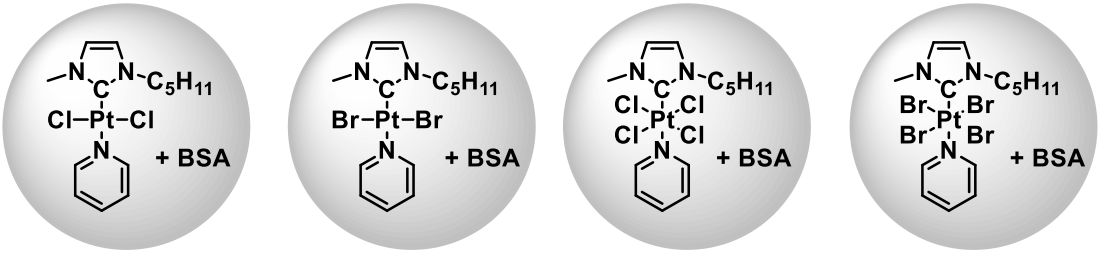

Scheme 39: General structure of NHC-Pt-BSA macromolecules **109**-**112** synthesized in various Pt/BSA ratio (5/1, 2/1, 1/1, 1/2, 1/5)

Unfortunately, ^{1}H NMR of the macromolecule proved inconclusive as no NHC-Pt characteristic peak could be observed due to overlapping with broad signals from the BSA. Nevertheless, complete adsorption of complexes **2**, **4**, **59** and **95** could be confirmed by disappearance of the characteristic MLCT band at 380 nm of NHC-Pt on UV spectra. Moreover, UV spectra confirmed the good stability in solution of these albumin-based nanodevices over a week.

UV spectroscopy is a common analysis technique to investigate protein structural changes and discover the formation of a protein-drug adduct.[296,297] Indeed, the UV spectrum of BSA displays

overlapping bands with a maximum intensity at λ = 280 nm corresponding to the π→π* transitions of aromatic residues, namely tryptophan, tyrosine and phenylalanine.[298] Therefore, UV analysis of the macromolecules **109**-**112** with a 1Pt/1BSA ratio at a BSA concentration of $2.5x10^{-6}$ M were carried in a 9/1 mixture of H_2O/DMSO (Figure 32).

All macromolecules loaded with NHC-Pt drugs displayed an increase in their maximum of absorption, thus confirming an interaction between platinum complexes and the protein. Moreover, both macromolecules **109** and **111** loaded with chlorine-platinum derivatives promote the most important absorbance increase in addition to blue shift (λ_{BSA} = 277 nm while $\lambda_{\mathbf{111}}$ = 269 nm). This seem to suggest a strong static interaction between the NHC-Pt derivative and aromatic moieties in the BSA.[299,300] Finally, no protein unfolding was observed by UV-vis measurement, thus suggesting that no BSA unfolding occur in the presence of NHC-Pt complexes.[301]

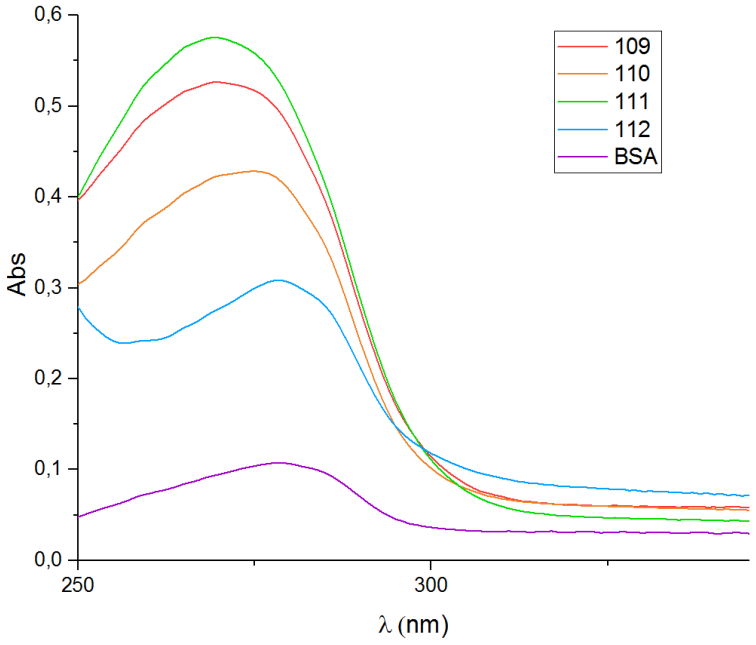

Figure 39: Evaluation of the interaction of NHC-Pt(II) complexes **2**, **4** and NHC-Pt(II) complexes **59**, **95** with BSA by UV (1Pt/1BSA ratio)

To ensure efficient drug release, the mixture of BSA-Pt **110** was dialyzed over one litre of water for three days and dialysate was lyophilized and analysed by ^{1}H NMR. The spectra displayed identical resonance signals to the NHC-Pt(II) complex **2**, thus confirming efficient release from the protein of the intact drug.

Finally, the efficiency of NHC-Pt combination to the albumin carrier at promoting anticancer activity has been explored by mean of IC_{50} measurements on both HCT116 and PC3 cancer cells and compared to cisplatin and free NHC-Pt complexes (Figure 33).

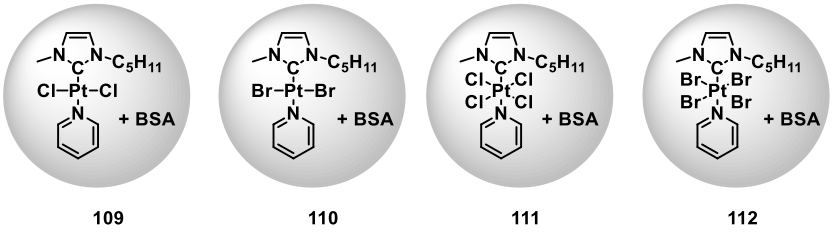

109 110 111 112

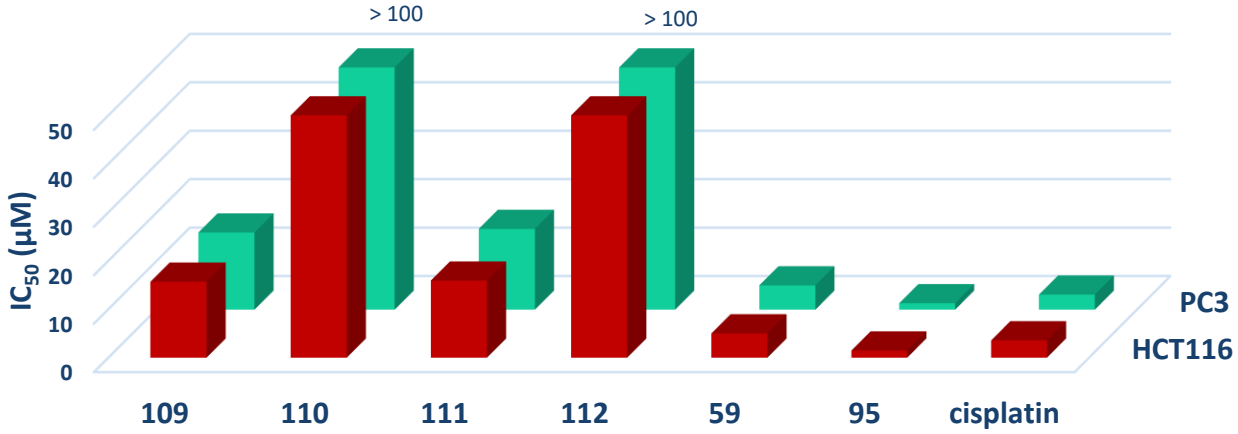

Figure 40: IC_{50} values of NHC-Pt-albumin macromolecules **109**-**112** toward HCT116 and PC3 human cancer (IC_{50} expressed in µM)

Remarkably, the cytotoxicities displayed in Figure 33 proved to be highly dependent the nature of the halogen ligand at the platinum centre rather than the oxidation state of the metal. Indeed, while both macromolecules **109** and **111** bearing bromine ligands displayed moderate

activities toward both cancer lines (IC_{50} of ~ 16 µM), the macromolecules **110** and **112** proved inefficient at promoting cancer cell death. The encapsulation of NHC-Pt compounds into the albumin did not improve cytotoxicity compared to free drugs. Finally, no variation was observed in the potencies displayed by the Pt(IV) macromolecule **111** and its Pt(II) analogue **109** which tends to suggest that prodrug **59** reduction occurs when wrapped into the protein within the time scale of *in vitro* experiment.

3) Conclusion

In conclusion, the use of albumin as a carrier for NHC-Pt complexes has been investigated by varying both the nature of the halogen ligands at the metal and the platinum oxidation degree which proved to greatly influence drug stability. Moreover, the ratio of platinum complex per protein can be easily tuned and affords a large range of nanodelivery devices which proved stable in solution over a week. The efficient drug uptake was easily confirmed by UV-vis measurements which suggest NHC-Pt complexes to be located in the albumin hydrophobic pockets near tryptophan moieties. Finally, *in vitro* cytotoxicity investigation highlighted contrasting results between the nanodevices bearing chlorine derivatives of NHC-Pt complexes which failed at inducing cell death and both bromine macromolecules **109** and **111** which exerted moderate potencies. Accordingly, *in vivo* potency measurements would be necessary to investigate the gain of covering NHC-Pt complexes with albumin toward both the side effects decrease and cancer cell targeting.

II. Liposomal formulation

Liposomes are synthetic spherical vesicles composed of amphiphilic molecules which self-aggregate and form a phospholipid bilayer envelope. They are biocompatible and

biodegradable, and offer the possibility to encapsulate either hydrophobic or sensitive drugs and deliver them to targeted cancer cells without promoting side effects. The easy variation of their physiological properties by modification of the lipid nature, size or particle charge raised considerable interest in the last decades, several liposomal formulations being already used in clinics.[302] Therefore, we synthesized NHC-Pt complex **48** functionalized with a lipophilic didecylamine to favour its incorporation into the anionic liposomes concomitantly to a mixture of phospholipids, namely phosphatidylcholine, phosphatiydylglycerol and cholesterol. The liposomal formulation using 5% of the [(NHC)PtI_2(didecylamine)] complex **48** has been investigated in collaboration with Pr S. Fournel (Faculté de Pharmacie de Strasbourg). Self-aggregation into spherical liposomes of ~ 60-70 nm using the technique of lipid film hydration proved successful as confirmed by DLS measurements. Moreover, preliminary cytotoxicity experiments seem to suggest that NHC-platinum loaded liposomes promoted viability inhibition of HCT116 cancer cells over a complex concentration of 30 µM.

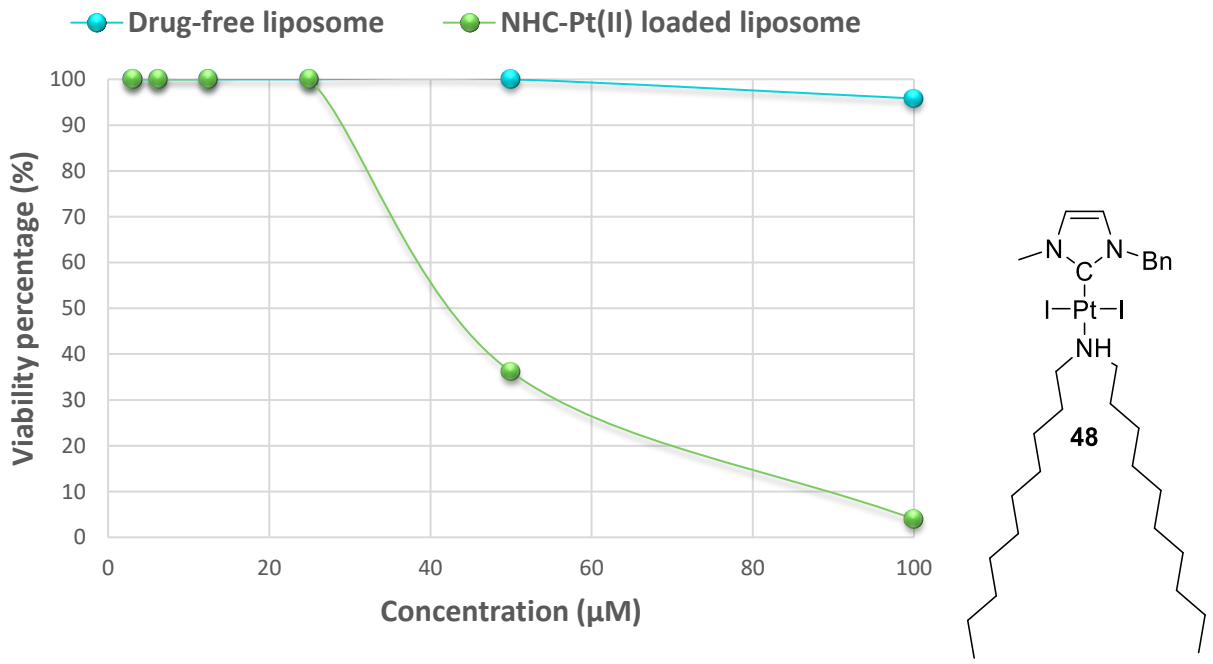

Figure 41: Viability percentage of HCT116 cancer cell lines treated with drug free liposome (blue), liposome loaded with 5% of NHC-Pt complex **48** (green)

Complementary investigation of the influence of drug loading ratio and comparison to the free drug are currently underway in order determine the optimal NHC-platinum loading and evaluate the possible gain in both stability and anticancer activity. In the end, the liposome loading with the [(NHC)$PtBr_4$L] complex **90** would be evaluated in order to overcome stability issue and ultimately afford highly cytotoxic drug.

III. Biocompatible and water-soluble polycationic Pt(II)-NHC macromolecules

As emphasized in the introduction, numerous strategies have been developed in order to circumvent side effects associated with cisplatin-based chemotherapy. Among them, drug delivery based on polymeric assemblies has raised massive interest to protect the platinum centre from side reactions and to promote selective platinum accumulation to cancer cells through EPR effect.[303] Among them, polyethylenimine (PEI) is a well-established biocompatible polymer used as an efficient transfecting agent.[304] It can be obtained by straightforward synthesis based on either aziridine polymerization or acidic hydrolysis of functionalized oxazoline moieties. The potential of PEI to transfect DNA has first been highlighted by the group of Behr[305] and further extended to a wide number of biological material for gene delivery.[306] The peculiar proton-sponge ability of PEI resides in its network of protonable nitrogen atoms depending on the surrounding pH. Indeed, these amino groups have a pKa of 5.5 which easily allow formation of a polycationic system capable to condensate with DNA or other biological material by electrostatic interactions. *In* vivo, this polycationic macromolecule is expected to target cells thanks to electrostatic interaction with the negatively charged phospholipid cellular membrane. Drug delivery is believed to occur through cell endocytosis of the drug-PEI nanoparticle. Endosomal escape is favoured by the action of enzymes (ATPase) which acidify the media within the nanoparticle thus promoting PEI protonation and elongation.[307] Subsequent osmotic swelling provoke a rupture of the endosomal membrane and drug release into the cytoplasm (Figure 35).[308]

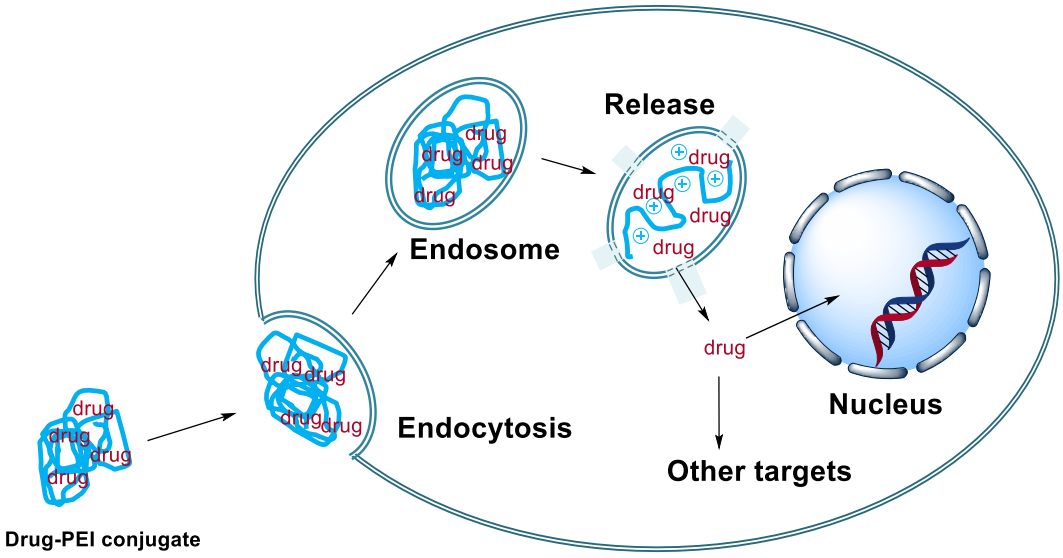

Figure 42: Gene delivery principle using polyethylenimine as transfecting agent

Therefore, we envisioned the functionalization of PEI chains with NHC-Pt cytotoxic moieties to access biocompatible and water-soluble macromolecular drugs for efficient and selective intracellular platinum delivery.

1) Background in the development of PEI-platinum conjugates within our group

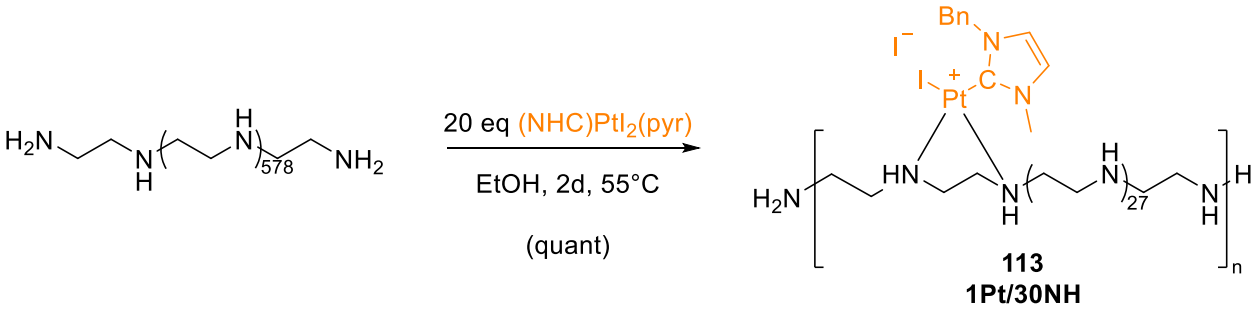

Scheme 40: Synthesis of the NHC-Pt-PEI conjugate **113** through ligand exchange (Pt/NH ratio of 1/30)

A straightforward functionalization of either linear or branched polyethylenimine with various ratio of NHC-Pt moieties based on ligand exchange of a [(NHC)PtI_2(pyridine)] precursor has been

developed by our group to generate quantitatively a library of NHC-Pt-PEI macromolecules (Scheme 40).[309] The self-assembly of the polycationic complex **113** (1Pt/30NH ratio) into soft nanoparticles of ~ 100 nm has been evidenced by cryo-EM analysis.

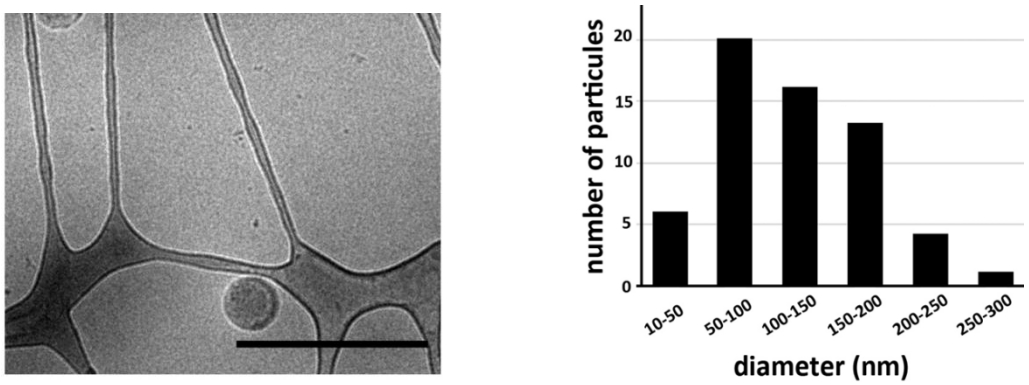

Figure 43: Cryo-EM observation of free PEI and **113**[309]

The *in vitro* anticancer investigations of NHC-Pt-PEI macromolecules confirmed their potential as great cancer cell inhibition toward several cancer cell lines were observed for all tested features. Among the tested molecules varying PEI weight and the platinum loading, the derivative **113** where a 25k Da PEI chain was functionalized with NHC-Pt moieties bearing benzyl and methyl N-substituents in a 1Pt/30NH ratio displayed the highest anticancer activity.

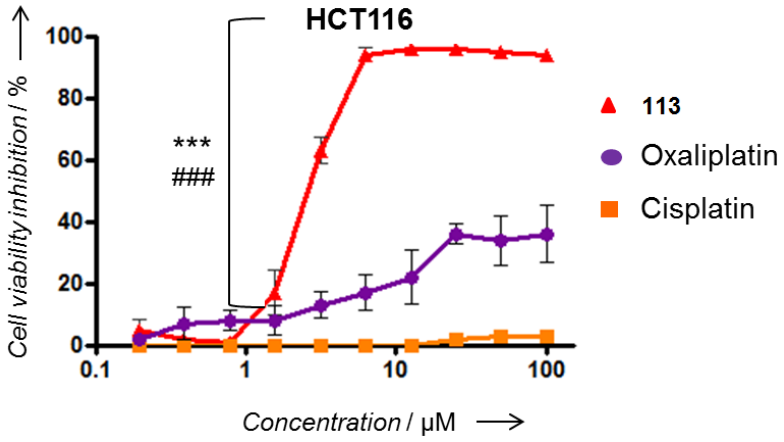

Figure 44: Cell viability on HCT116 treated alternatively with oxaliplatin, cisplatin and **113**[309]

A complementary *in vitro* analysis confirmed the potential of the **113** macromolecule which displayed higher potencies than the two clinically used cisplatin and oxaliplatin (Figure 37). Similar trends were observed *in vivo* on nude mice which were administered the **113** cytotoxic complex. Indeed, greater tumour volume control and lower side effects have been observed compared to mice treated with oxaliplatin which suffered haemorrhagic events (Figure 38). Complementary *in vivo* work on immunocompetent mice confirmed the efficiency of NHC-Pt-PEI complexes at promoting high anticancer activity despite the possible immune response.

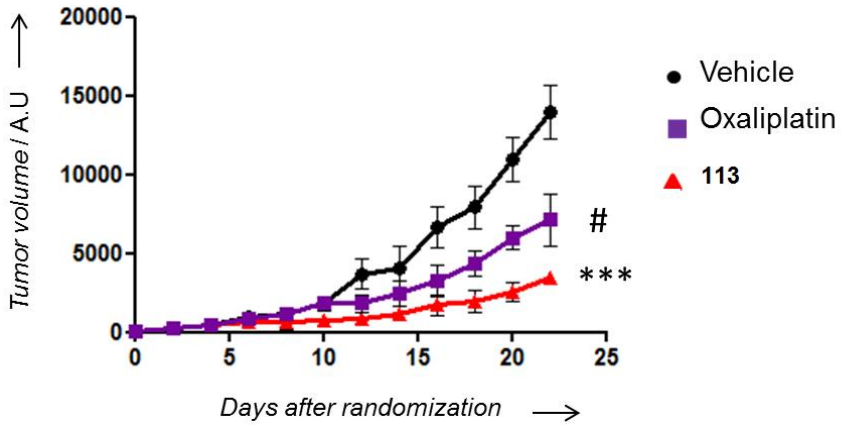

Figure 45: Antitumor effect on nude mice bearing HCT116 xenografts of **113** and oxaliplatin injected in vehicle at 5 µmol/kg[309]

A drug biodistribution study has been performed by ICP-MS measurement of platinum into several cellular compartments of cancer cells treated with the NHC-Pt-PEI complex **113** and compared to oxaliplatin (Figure 39). This confirmed the successful drug internalization in addition to suggest greater platinum uptake in the mitochondria for **113** rather than the nucleus which is the main target for oxaliplatin. Therefore, NHC-Pt-PEI derivatives do not seem to promote cancer cell death according to a cisplatin-like mechanism. Finally, the formation of ROS in the mitochondria of cancer cell death due to treatment with NHC-Pt-PEI complexes has been evidenced, thus confirming the occurrence of a parallel mechanism of cytotoxicity induced by these novel macromolecules.

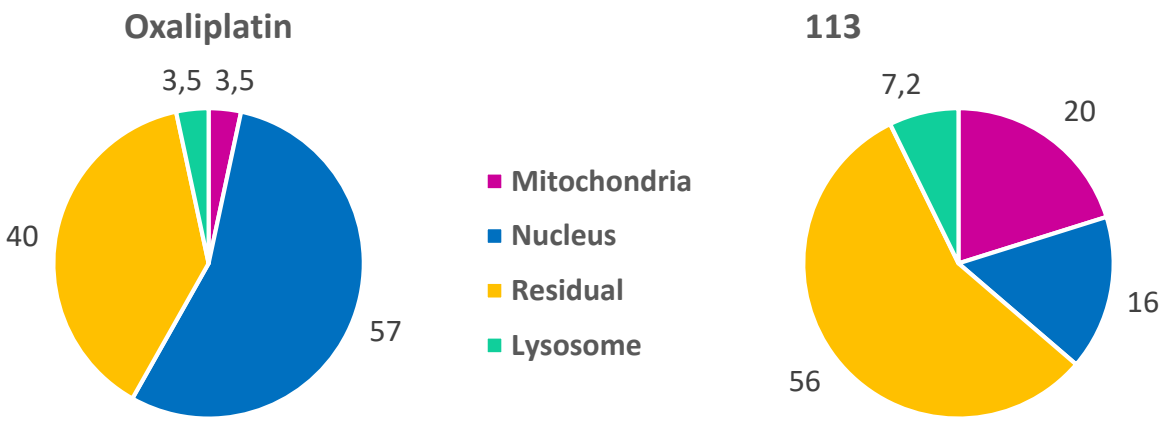

Figure 46: Cellular uptake of **113** and oxaliplatin in HCT116 cells[309]

In conclusion, the novel combination of NHC-platinum to the water-soluble and biocompatible PEI has proved to be an asset to efficiently inhibit cancer cell proliferation both *in vitro* and *in vivo* without inducing visible side effects. The self-organization in spherical soft particles has been evidenced by cryo-EM and might account for their high cytotoxicities, though the large size polydispersity remains to be tackled. Biodistribution investigation by ICP-MS highlighted a different localization compared to the clinically used oxaliplatin and motivated the examination of a mitochondrial pathway for cytotoxicity.[309]

2) Diversity enhancement by functionalization of NHC-Pt-PEI conjugates

Several structural modifications on the NHC-Pt-PEI conjugates have already been investigated in our group. Variation of the NHC backbone, the polymer molecular weight or the platinum loading provided interesting results for further anticancer drug development. The modification of both terminal amino-groups has been envisioned to fine tune physico-chemical properties without disturbing the self-arrangement previously observed. This section will detail their

synthesis, characterization and evaluation of their luminescence for further *in vitro* time followed biodistribution. To note, only PEI of 25k Da has been used in this series of experiment.

Previous investigations on the variation of platinum loading highlighted **113** bearing a 1Pt/30NH ratio as the more potent combination thanks to its higher chemical similarity with free PEI compared to macromolecules bearing a 1Pt/10 or 20 NH ratio.[308] However, we theorized that the ideal balance between the cytotoxic platinum centres and the chain polarization might involve a lower Pt/NH ratio. Accordingly, two NHC-Pt-PEI complexes **114** and **115** have been synthesized according to the synthesis described in Scheme 40 by decreasing the platinum loading to 1Pt/40NH and 1Pt/50NH (Scheme 41). An additional NHC-Pt-PEI conjugate **116** with very low platinum loading down to 1Pt/100NH has also been obtained. Such low platinum loading should only induce minor polarization and hindrance on the polymeric chain thus behaving similarly to free PEI in solution while promoting cytotoxic activity thanks to attached NHC-Pt moieties. All complexes were quantitatively obtained as sticky white solids.

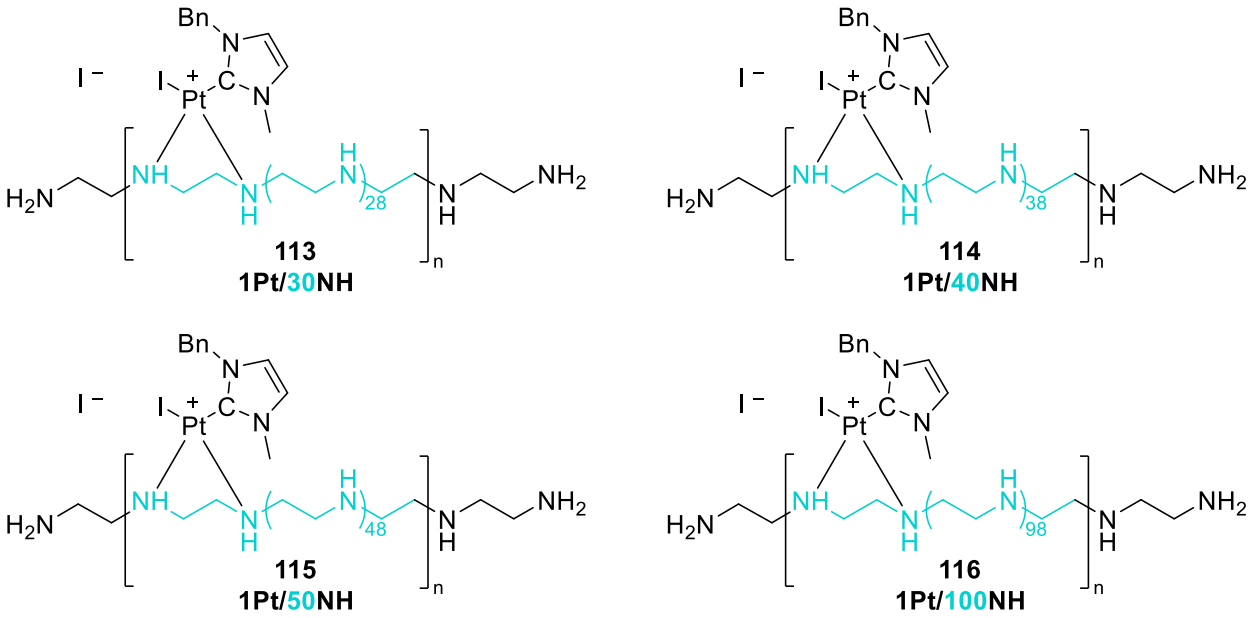

Scheme 41: Three NHC-Pt-PEI conjugates with low platinum loading (quantitative yield)

In complement of ^{1}H and ^{13}C NMR characterizations, the three complexes have been formulated in an EtOH/H_2O solution in a 1/9 ratio at 10^{-5} M concentration and DLS measurement have been performed. While the **113** serving as a reference effectively provided spherical vesicles of ~ 100 nm as previously reported, none of the newly formed conjugate formed large particles. Instead, only amorphous objects were observed, which suggests the cationic charge decrease along the polymeric chain to prevent their self-assembly in solution. The potency of the three complexes have been examined *in vitro* and compared to NHC-Pt-PEI conjugates with higher platinum loading in collaboration with Pr S. Fournel (Faculté de Pharmacie de Strasbourg). The percentages of cancer cell inhibition are shown in Figure 40 and confirm the most potent complex to be **113**. Indeed, the inhibition efficiency appeared to drop proportionally to the platinum loading as **114** was less efficient than its counterpart bearing a 1Pt/30NH ratio. To note, results obtained for **115** with a 1Pt/50NH ratio seem inconsistent with the observed trend when moving from **113** to **116** and thus should not be considered.

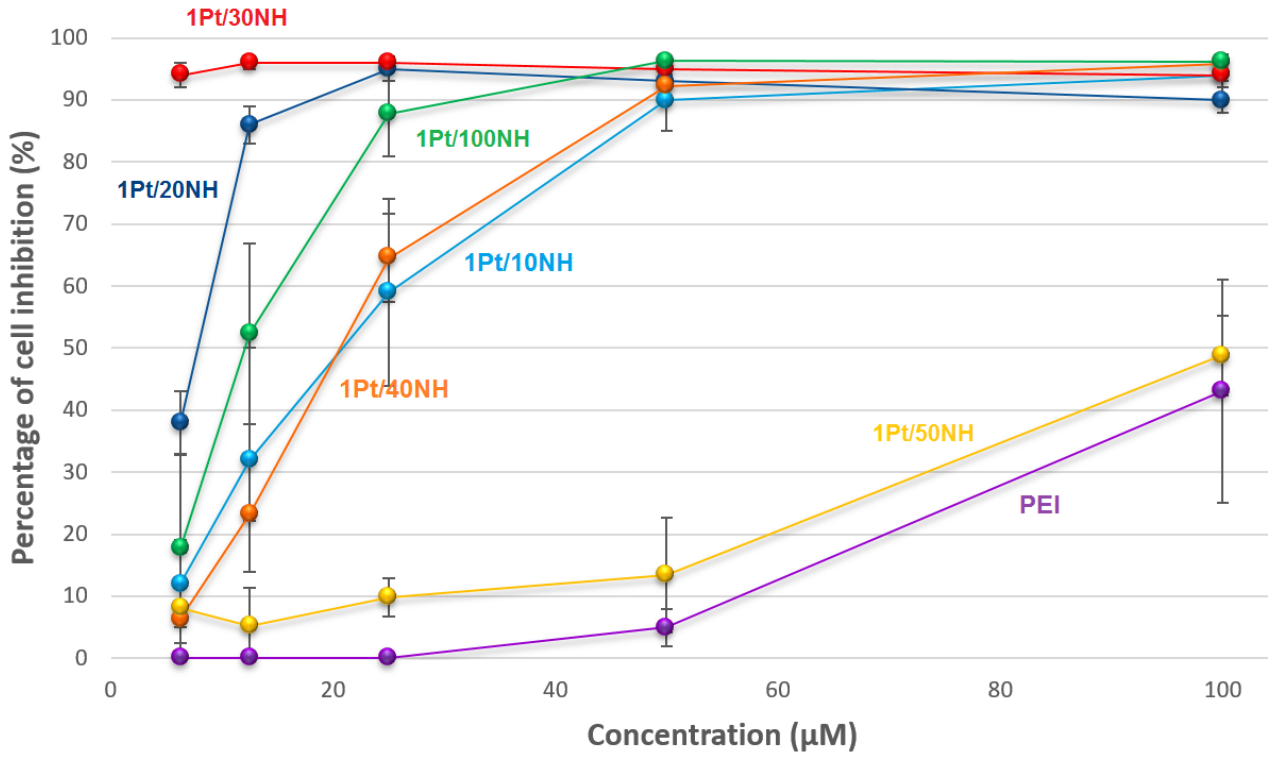

Figure 47: Percentage of cell inhibition of a HCT116 cancer cell line depending on the platinum loading on the polymeric chain

Biological investigations detailed above confirmed the Pt/NH ratio of 1/30 to be the ideal balance between the number of platinum centres to exert efficient anticancer activity and the cationic charge amount and distribution along the PEI. The correlation between the vesicular self-arrangement failure and lower cancer cell inhibition of **114**-**116** complexes seems to confirm the importance of the formation of nanometric spherical soft nanoparticles for improved potency. However, whether this phenomenon protects platinum moieties from deactivation or favour drug uptake remains to be investigated.

A strategy based on peptidic coupling between the amino group at the end of PEI chain and carboxylic acid derivatives has been developed to allow easy diversity enhancement at the polymer extremities (Scheme 42). After 30 min reaction between excess of both N-hydroxysuccinimide (NHS) and N-(3-dimethylaminopropyl)-N'-ethylcarbodiimide (EDCI) with two equivalents of selected carboxylic acid in ethanol, one equivalent of PEI was added and required additional stirring for up to three days at room temperature to be complete as confirmed by the carboxylic acid moiety consumption followed by TLC. Subsequent removal of coupling reagents was achieved by multiple centrifugation of the concentrated mixture dropped into diethyl ether. This strategy proved efficient for various moieties and allowed easy and quantitative generation of diverse functionalized polymers.

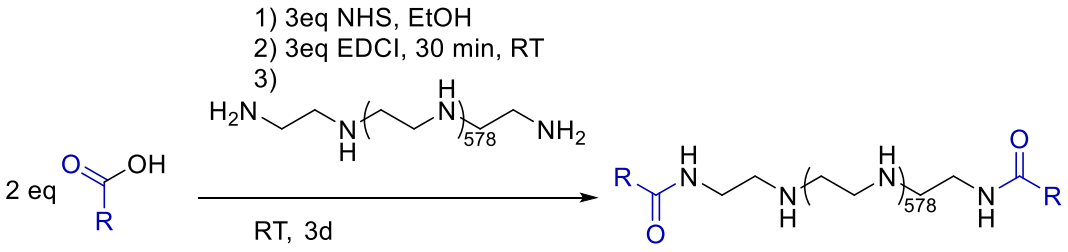

Scheme 42: General synthesis for amide formation on polyethylenimine

As previously highlighted, the formation of spherical vesicles most probably accounts for the high cytotoxicity of NHC-Pt-PEI macromolecules. The addition of highly hydrophilic polyethylene

glycol (PEG) has been anticipated to help in the shape and size control of NHC-Pt-PEI self-arrangement and favour the formation of a well-defined vesicle. Accordingly, taking into consideration the molecular weight of selected PEI (25k Da), two heavy PEG chains have been selected, namely a 750 Da and 3000 Da, and attached according to synthesis presented in scheme 42. Both PEG-PEI-PEG copolymers **117** and **118** were obtained quantitatively as sticky colourless oils (Scheme 43). The combination of long alkyl chain at both extremities of the PEI also quantitatively afforded the conjugate **119** and is expected to further allow the micellar formulation of well-defined nano-sized soft particles. Finally, adamantyl moieties have been attached onto the PEI chain in quantitative yields and obtained as a colourless oil **120**. Adamantyl group is known to promote host-guest interaction with cyclodextrin rings and is thus of great interest for further post-functionalization,[310,311] in particular in the field of material dedicated to biological use.[312,313]

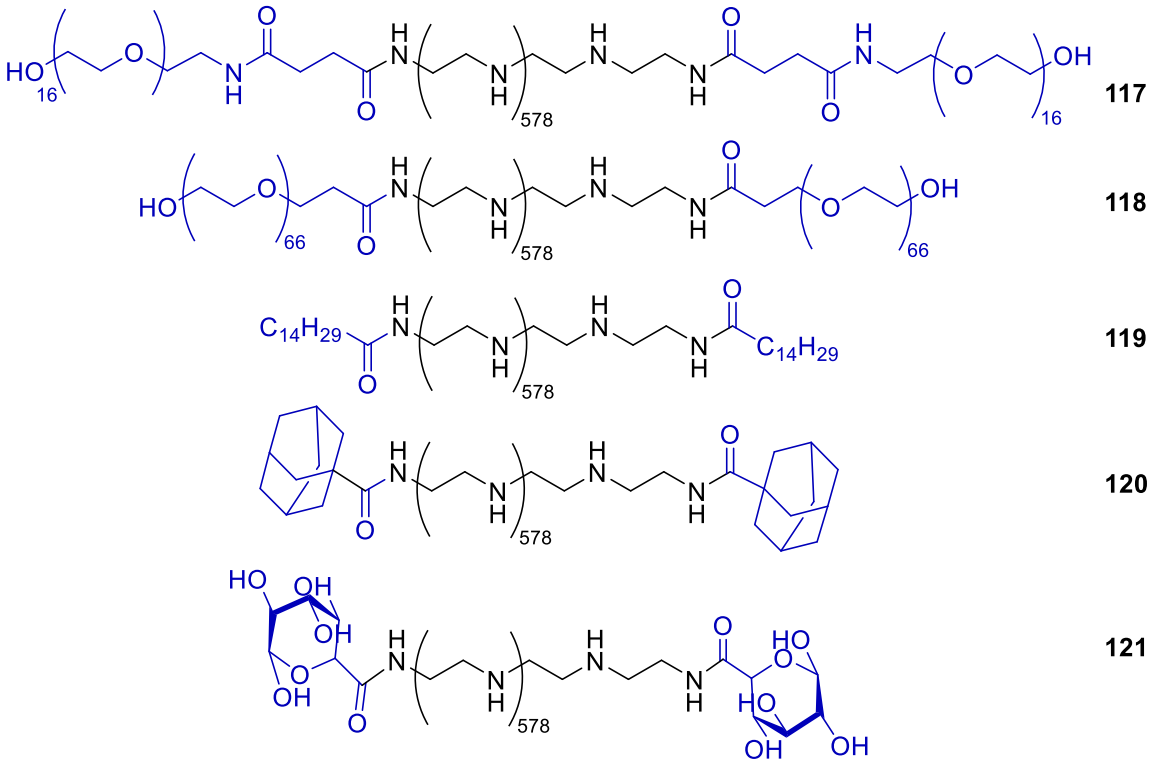

Scheme 43: PEI based copolymers functionalized with hydrophilic and lipophilic polymers **117**-**121** (quantitative yields)

Another strategy is based on π-extended moieties which could interact through π-stacking and are expected to form monodisperse particles. The small π-extended anthracene is of interest for biological investigations owing to its fluorescence properties under UV light. Moreover, several moieties bearing π-extended networks have been highlighted as good DNA chelating agents and might therefore appear as complementary anticancer moieties. Hence, peptidic coupling of the 9-carboxylic anthracene allowed quantitative isolation of **122** as a yellow sticky solid which proved fluorescent under UV light both in solid state and in solution (Scheme 43). Similarly, both fluorene and the highly green fluorescent coumarin have been chemically linked to the linear PEI chain for subsequent coordination to platinum. While the sticky oil **123** obtained after fluorene coupling proved poorly luminescent under UV light, the well-established fluorescent agent coumarin yielded a highly fluorescent bright yellow oil **124** under 365 nm UV exposure. The successful coupling of carboxylic acid in all newly synthesized PEI derivatives could be ascertained by ^{1}H NMR despite the large molecular weight difference between both amides groups and the long polymeric chain. Proton integration supported the efficient grafting of two moieties per PEI chain and proved particularly easy for polymers **122**, **123** and **124** which aromatic proton signals could be found in the PEI-protons free area of around 7.5 ppm. The presence of carbon resonance peak around 176 ppm in ^{13}C NMR which is characteristic of amide carbons also accounted for the successful PEI functionalization. Finally, the fluorescence of **124** has been confirmed at a concentration of 10^{-7} M in ethanol.

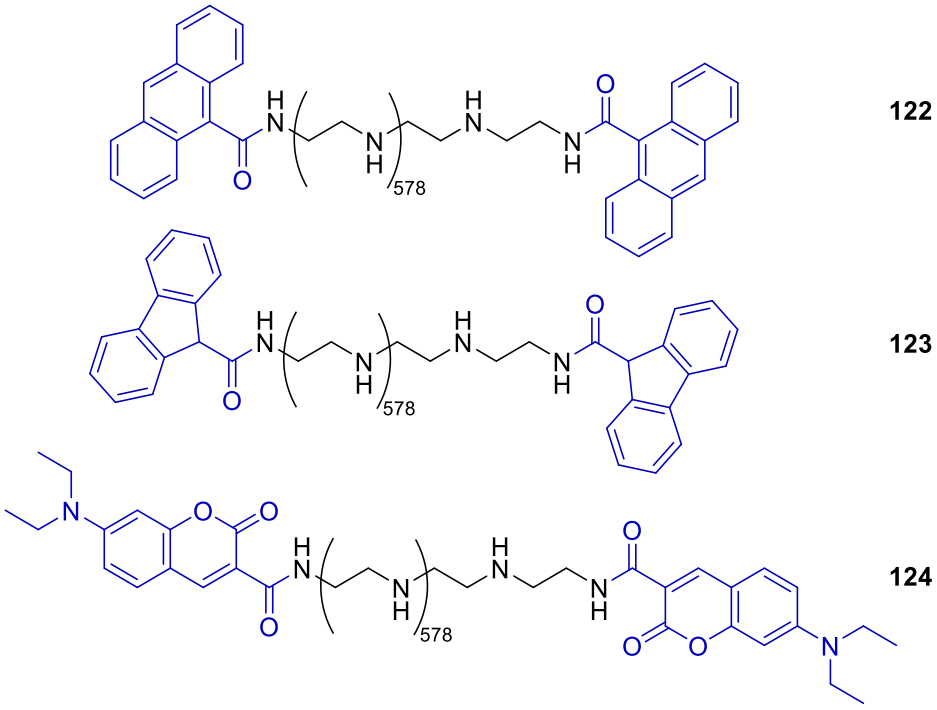

Scheme 44: Luminescent functionalized PEI derivatives (quantitative yields)

All functionalized polymers **117**-**124** were reacted in ethanol with 20 equivalents of the [(NHC)PtI_2(pyridine)] precursor **5** bearing both methyl- and benzyl- N-substituents, corresponding to a final 1Pt/30NH ratio, for two days at 55°C (Scheme 45). Subsequent polymer isolation could be achieved by precipitation in diethyl ether and centrifugation. Similarly to **113**, in ^{1}H NMR characteristic signals corresponding to the imidazolium protons resonance were observed in the PEI-protons free area within 6.5-7 ppm, the aromatics proton signals being around 7.5 ppm while N-substituents are found at $\delta_{N\text{-}CH2}$ = 6.5 and $\delta_{N\text{-}CH3}$ = 4 ppm.

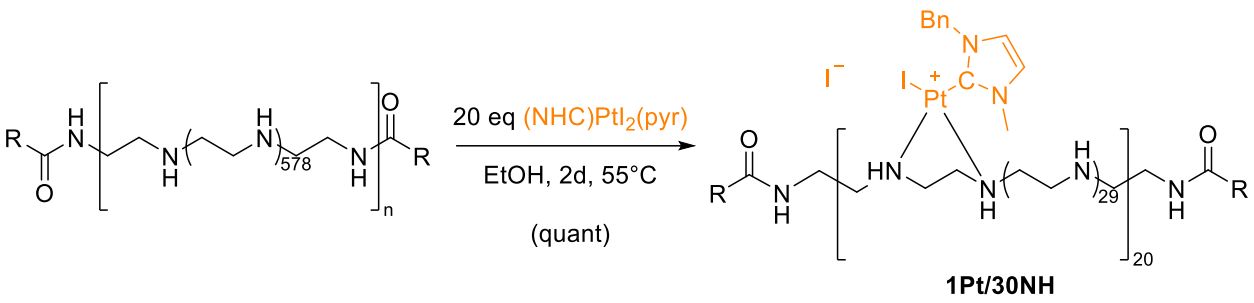

Scheme 45: General synthesis of NHC-Pt-PEI conjugates, prepared from *trans* [(NHC)PtX_2(pyridine)] (NHC = 3-benzyl-1-imidazolilydene) **5**

The PEG-PEI-PEG copolymers **117** and **118** both underwent successful coordination of the NHC-Pt moieties affording **125** and **126** quantitatively, thus suggesting that no polymer folding occurs in solution due to both 750 Da and 3000 Da hydrophilic PEGs (Scheme 46). To note, the solubility in ethanol solution decreased as the PEG molecular weight increased. On the contrary, PEI derivatives **127**-**129** which platinum coordination occurred smoothly in quantitative yield, proved highly soluble in ethanol.

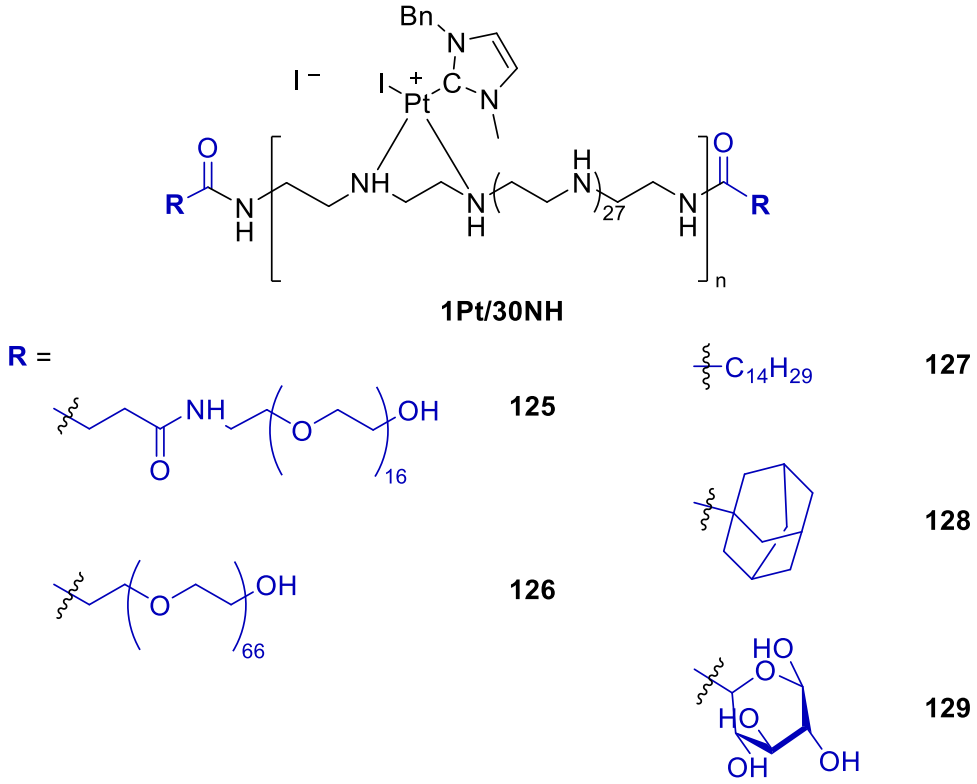

Scheme 46: Successfully synthesized NHC-Pt-functionalized PEI conjugates (quantitative yield)

The three anthracene-, fluorene- and coumarin- functionalized PEI **122**-**124** could be successfully reacted with the NHC-Pt precursor **5** and clean metallopolymers **130**, **131** and **132** respectively were obtained in quantitative yields after multiple centrifugations in diethyl ether (Scheme 47). While overlapping of most NHC characteristic protons with fluorescent aromatic moieties was observed in ^{1}H NMR, ligand exchange at the platinum centres could be ascertained thanks to the N-methyl protons found as a singlet at around 4 ppm. This characteristic signal was also used for quantification of the platinum amount actually grafted. To note, no luminescence decrease has been observed in solution after polymer functionalization with multiple platinum centres, and the coumarin functionalized complex **132** proved once more the most luminescent derivative and promising for further *in vitro* biodistribution investigation.

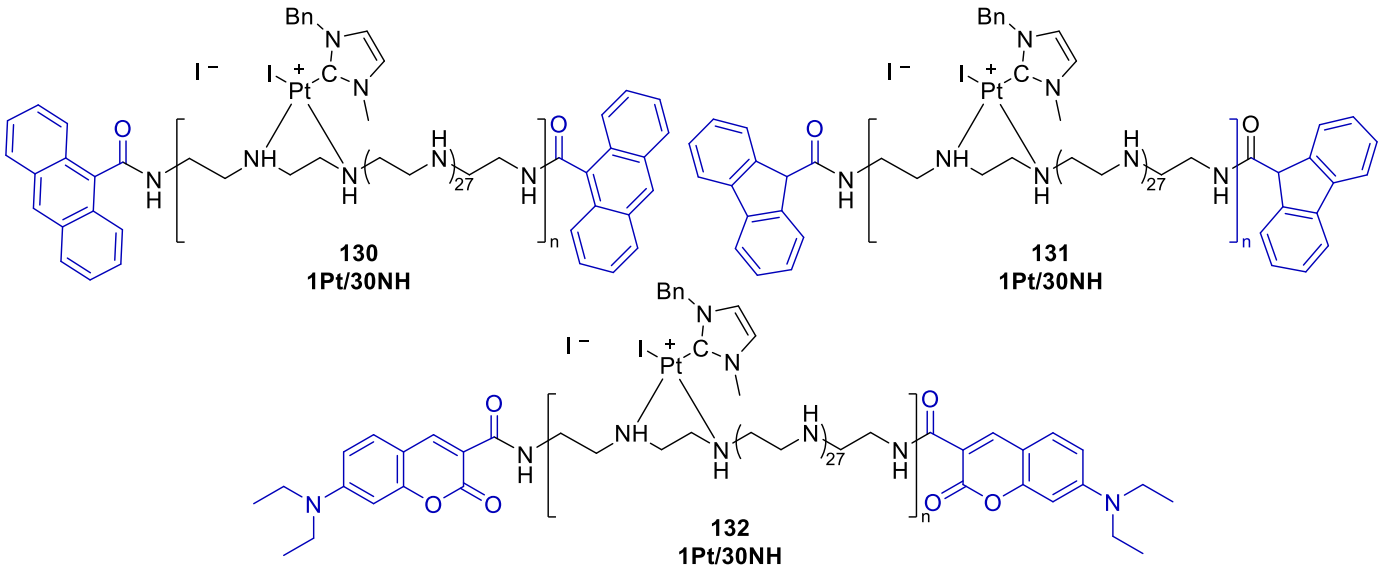

Scheme 47: Luminescent NHC-Pt-PEI conjugates obtained in quantitative yields

The possible spontaneous formation of soft-nanoparticles similar to **113** in an ethanol/water solution has been investigated by DLS at a pH of 7 for all the novel metallopolymers **125**-**132** and compared to the platinum-free polymers **113**-**124**. Under investigated conditions no vesicles formation is noticed for the functionalized polymers **125**-**132**. This suggests that combination of the polycationic NHC-Pt-PEI macromolecules with hydrophilic/lipophilic moieties or functional groups known to favour π-stacking failed at forcing a self-arrangement into

vesicular system. However, this could be explained by the high polymer molecular weight compared to the weak H-bonding and π-stacking forces that would be involved in the formation of soft-nanoparticles in these neutral species.

Nevertheless, only few is known about the *in vitro* and *in vivo* behaviour and fate of the NHC-Pt-PEI conjugates family. Accordingly, the linkage of the highly yellow luminescent fluorescein (FITC) which is well known in the study of biological systems and is suitable for *in vitro* microscopy imaging has been investigated. The reaction of one primary amine at the extremity of the PEI chain with the isothiocyanate fluorescein spontaneously occurred within three hours in a 1/2 mixture of DMSO/PBS at room temperature in the dark to prevent photobleaching (Scheme 48). Subsequent dialysis over large volume of PBS for one day followed by a lyophilization quantitatively yielded an intense yellow sticky solid **133**. To note, a parallel synthetic route involving PEI label with fluorescein prior to platinum coordination has been developed and allowed successful isolation of the same conjugate **133** and is expected to allow further development in milder conditions using more sensitive NHC-Pt motifs.

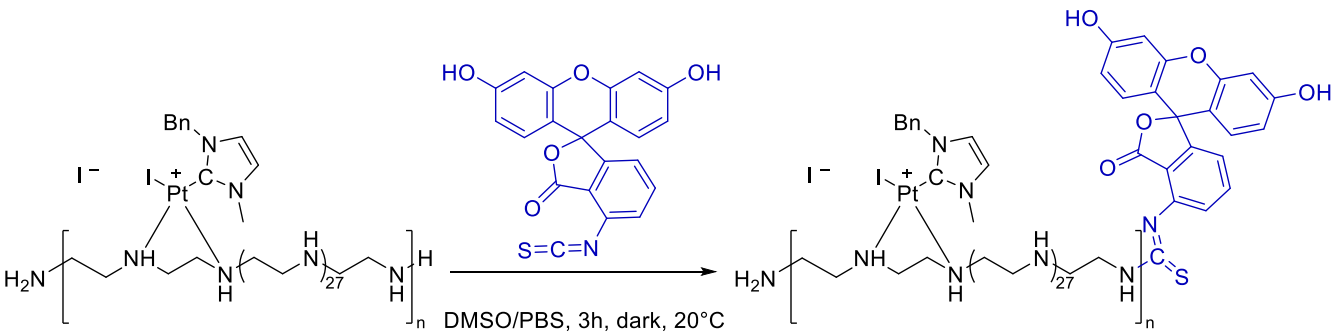

113 **133** **1Pt/30NH** (quant)

Scheme 48: NHC-Pt-PEI functionalization with luminescent fluorescein moiety

The fluorescein based conjugate **133** proved highly luminescent under UV light both in solution and solid state. Preliminary investigation of its fluorescence properties confirmed the excitation wavelength to be λ_{exc} = 495 nm and fluorescence emission λ_{em} = 520 nm (Figure 41). While no

excitation or emission shift is observed after fluorescein grafting onto the NHC-Pt-PEI conjugate, the fluorescence intensity is significantly decreased compared to free FITC. Though the emission intensity proved sufficient to allow observation of the conjugate by fluorescence microscopy.

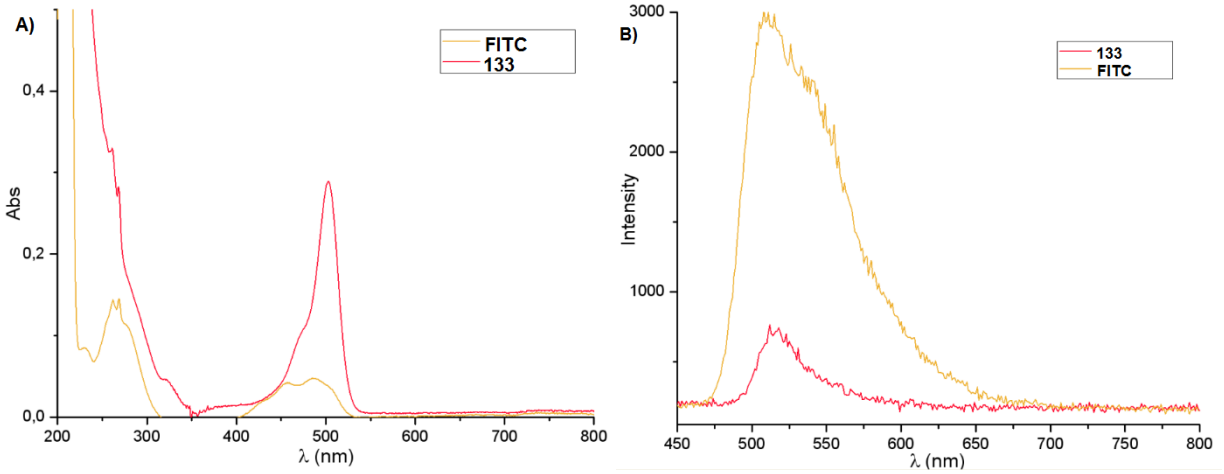

Figure 48: Spectra comparison between free fluorescein and NHC-Pt-PEI conjugate **133** by A) UV-vis spectra, B) fluorescence analysis at λ_{exc}= 495 nm (C = $5x10^{-6}$ M in ethanol)

The importance of drug biodistribution for improved drug efficiency has already been highlighted in the introduction. The fate of this fluorescein based NHC-Pt-PEI conjugate **133** when exposed to cancer cells *in vitro* has been investigated by epifluorescence in collaboration with Pr S. Fournel (Faculté de Pharmacie de Strasbourg). The Figure 42A shows the analyzed cells observed by epifluorescence under white light while B) displays the same area under UV light. This comparison suggests successful internalization of the fluorescein conjugated complex **133** as fluorescence spectrum B) perfectly matches the cells observed in A). Moreover, no disseminated fluorescence can be observed thus confirming that drug do not randomly bind biological material. A comprehensive investigation of the drug uptake depending on the cellular comparment and time-followed is currently underway and should provide more knowledge in the fate of NHC-Pt-PEI compounds during and after completing cytotoxic activity.

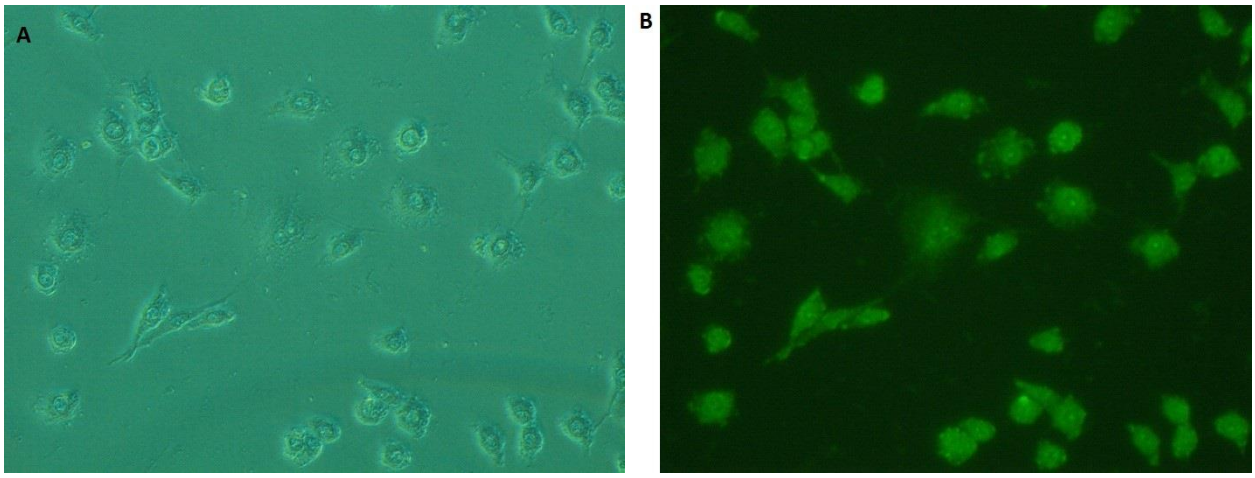

Figure 49: View of cancer cells treated with **133** by epifluorescence microscopy under A) white light, B) UV light at λ = 365 nm

However, drug functionalization with bulky chromophore might slightly modify its physico-chemical properties and consequently both its biodistribution and fate. Therefore, these observations should be considered carefully and supported by complementary analysis such as colocalization study or ICP-MS measurement.

In order to determine whether the functionalization with chromophores modify the drug uptake, the combination of **113** with a different chromophore has been investigated and its *in vitro* distribution has been compared to the previously synthesized NHC-Pt-PEI-FITC derivative **133**. We selected the epicocconone motif which is a natural compound intrinsically non-fluorescent. However, its intense red fluorescence after intermolecular ring-opening with amine groups (Scheme 49), and especially with proteins, raised it as a powerful staining agent in biological investigations under the brand name of Lavapurple.[314] The major asset of the epicocconone family is its huge stokes shift as exemplified by Lavapurple which λ_{em} = 610 nm is found almost a hundred nanometers above with λ_{exc} = 520 nm.

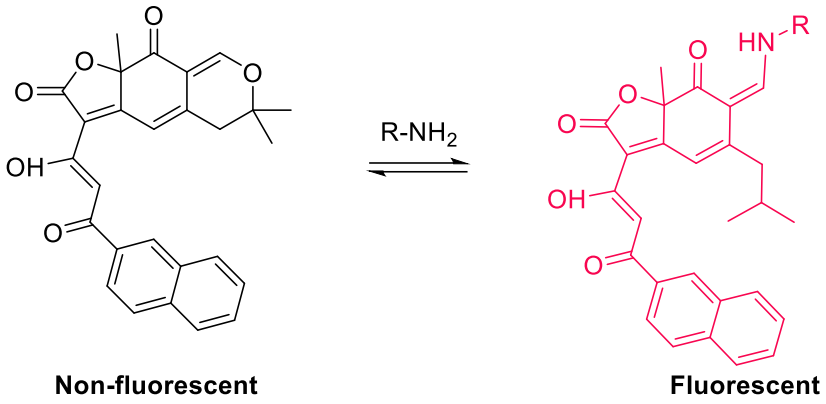

Scheme 49: Mechanism for the reaction of epicocconone derivatives with amines

We investigated here the combination of PEI with an epicocconone derivative presented in Scheme 49 which has been synthesized by the group of Dr X. Franck (IRCOF, Université de Rouen).

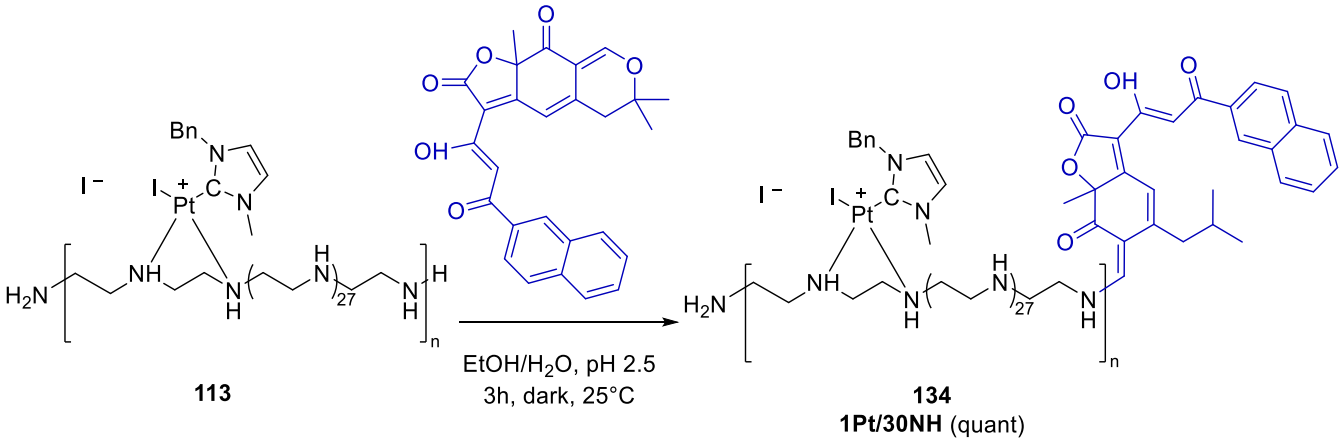

Scheme 50: Synthetic pathway for **134** by intermolecular ring opening for epicocconone grafting on the **113** conjugate

Ring opening of the epicocconone moiety in the presence primary amines of the prefunctionalized **113** successfully promoted chromophore conjugation, thus affording **131** as a red oil in quantitative yields (Scheme 50). ^{1}H NMR confirmed the successful epicocconone conjugation since aromatic protons resonance signals could be observed in the area from 7 to 8

ppm and UV-vis spectrum displayed two absorption bands at 269 nm and 420 nm, characteristic of the epicocconone moiety. One intrinsic limitation in the use of epicocconone derivatives is their rapid photobleaching which has been previously reported to reach 83% fluorescence lost within 19 minutes[315] in addition to its pH dependent stability which maximum is pH 2.5.[316]

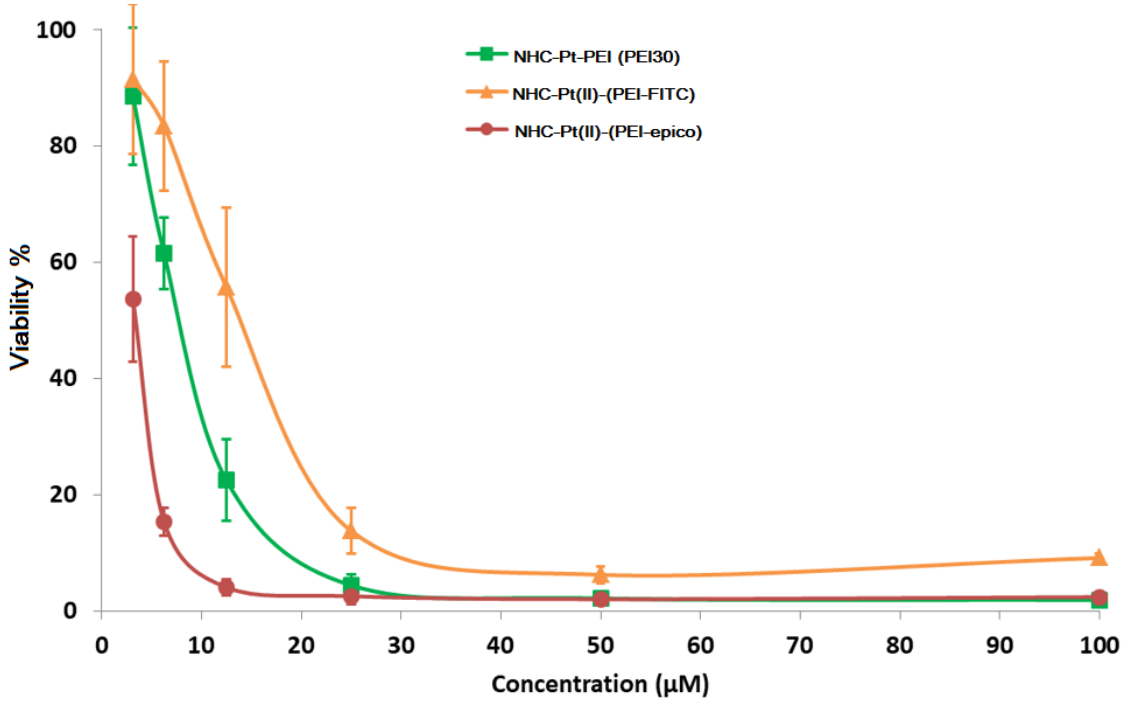

Figure 50: Viability percentages determined on HCT116 cancer cell line after treatment with **113** (green), **133** (orange) or **134** (red)

Finally, preliminary cytotoxicity experiments have been conducted in collaboration with Pr S. Fournel (Faculté de Pharmacie de Strasbourg) on HCT116 cancer cells treated alternatively with **113** as a reference, the conjugate **133** bearing fluorescein and **134** functionalized with epicocconone. Remarkably, despite the pH dependent stability of **134** the cytotoxicities presented in Figure 43 suggested comparable anticancer properties with the **113** while the fluorescein conjugate **133** is found slightly less cytotoxic. These results confirmed the potency of both metallopolymers functionalized with either fluorescein or epicocconone moieties, and thus encouraged us to investigate their *in vitro* biodistribution.

The introduction of a chromophore on the NHC-platinum motif by strong covalent bond has been envisioned to follow NHC-Pt release from the PEI *in vitro*, and explore its biodistribution and compare with the fluorescent polymer **133**. Moreover, the carbene-platinum bond is believed to be exceptionally stable toward biological media, thus marking the NHC ligand appeared as a straightforward method to follow the platinum fate *in vitro* without inducing major electronic and steric modifications at the metal centre.

Fluorescein binding through condensation of the 6-aminofluorescein on the aldehyde derivative **13** has been investigated according to previously reported procedure.[317] However, the complex **13** proved inert toward condensation even in presence of an excess of fluorescein (Scheme 51). This lack of reactivity has previously been observed in our lab in the case of large and rigid molecules and might explain the failure of fluorescein condensation under mild conditions.

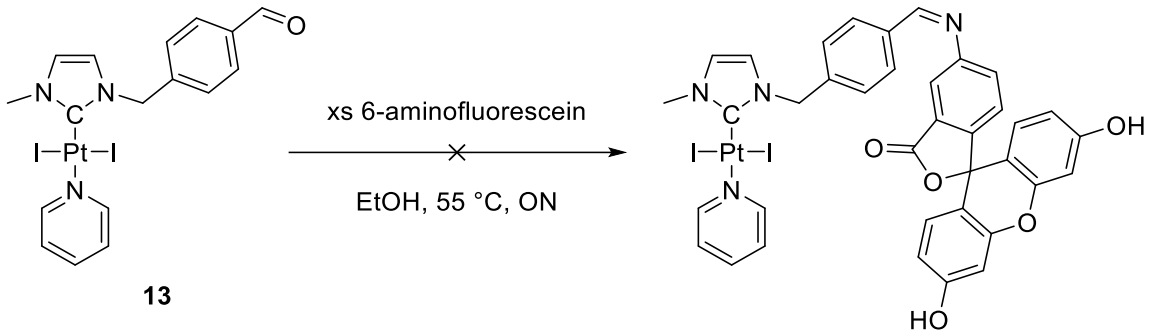

13

Scheme 51: Attempted synthesis of fluorescein condensation with the aldehyde derivative **13**

Similar attempts by condensation of fluorescein-6-isothiocyanate on a [(NHC)PtI_2(pyridine)] precursor bearing an ethanol N-substituant developed in our group also failed and only starting materials could be recovered.[318]

Therefore, chromophore conjugation onto the NHC ligand through click reaction has been investigated according to previously reported procedure (Scheme 52).[118] First reaction step

involved the catalytic reaction of $[Cp^*RuCl(PPh_3)_2]$ complex with the alkyne $[(NHC)PtI_2(pyridine)]$ derivative **135** in dry THF. Subsequent addition of a 3.5 excess of 7-azido-4-methylcoumarin and 2 h reflux yielded the desired intense yellow complex **133** which has been reacted with PEI without intermediary purification. Complexation of the coumarin-functionalized NHC-Pt moiety has next been achieved using a 1Pt/30NH ratio and three days under dark conditions proved necessary for full platinum precursor consumption and quantitative recovery of NHC-Pt-PEI conjugate **137** by centrifugation.

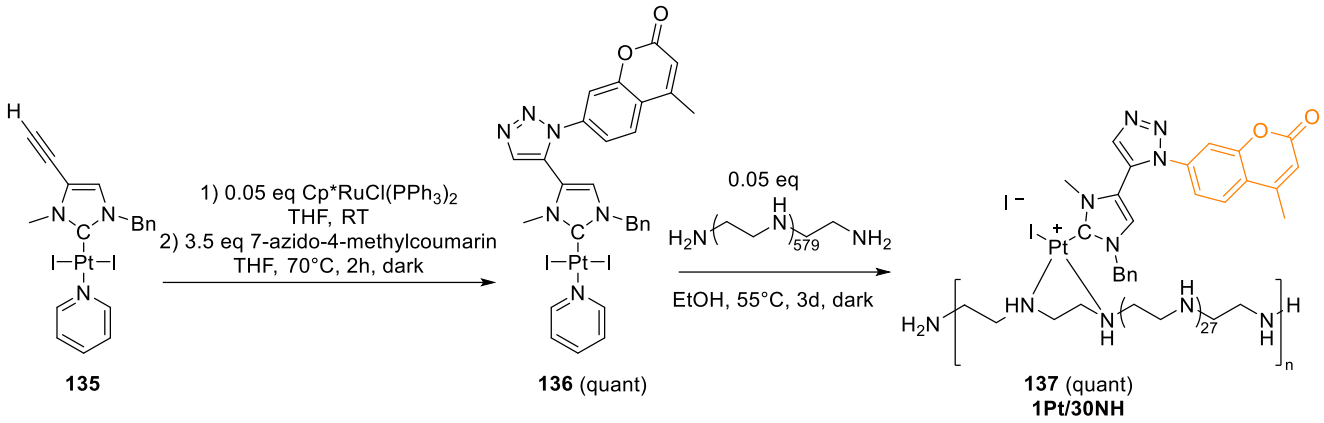

Scheme 52: Functionalization of the NHC-platinum complex **135** with fluorescent coumarin derivative by click reaction and subsequent quantitative ligand exchange of **136** with PEI to afford **137**

This strategy successfully allowed the synthesis of a NHC-Pt-PEI conjugate with chromophore binding through the highly stable triazol- moiety which should allow successful *in vitro* monitoring of the platinum biodistribution and colocalization study with complexes **133** and **134**.

In addition, the coordination of a non-metallated porphyrin-modified NHC-Pt moiety has been attempted by reacting in ethanol the precursor **23** using a 1Pt/30NH ratio similarly to the procedure described in scheme 40. However, despite a one week long reflux conversion remained uncomplete and only moderate amount of porphyrin-NHC-Pt-PEI conjugate **138** was isolated as confirmed by ^{1}H NMR and UV analysis (Scheme 53 and Figure 44).

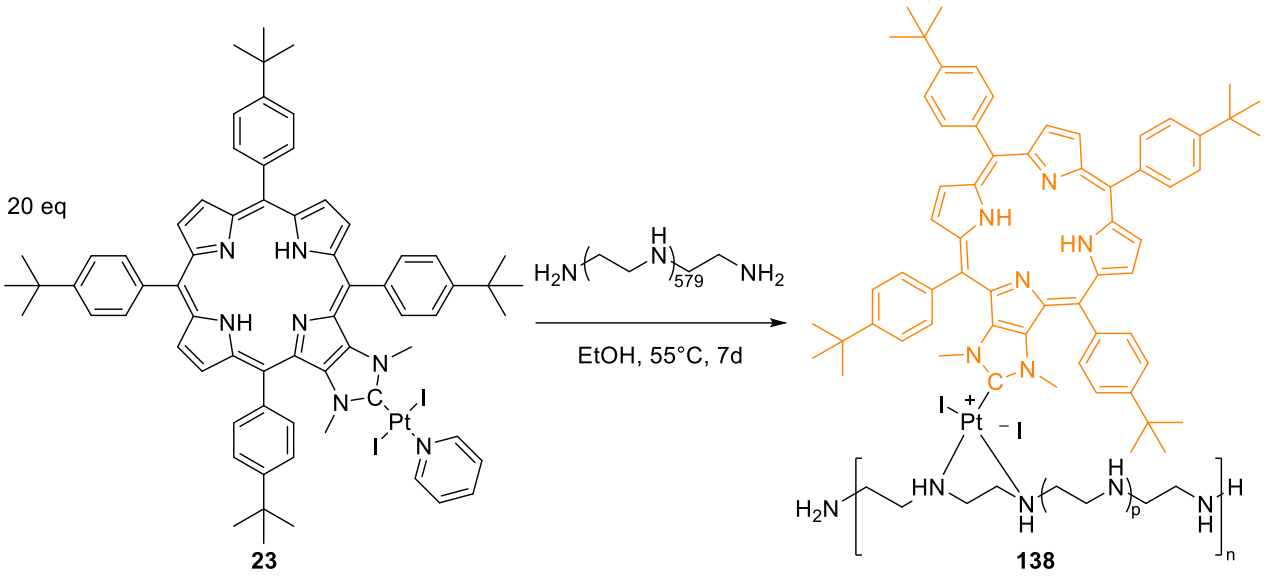

Scheme 53: Coordination of a NHC-Pt precursor **23** bearing a porphyrin modified NHC backbone to PEI

Similarly, the coordination of **24** proved uncomplete though successful coordination of a moderate amount of porphyrin moiety affording **139** as a deep red oil was ascertained by ^{1}H NMR and UV-vis analysis (Scheme 54 and Figure 44). Accordingly, *in vitro* cytotoxicity experiments should be carried on both porphyrin-functionalized macromolecules **138** and **139** to confirm their efficiency at promoting cancer cell death prior to colocalization study with the complex **137**.

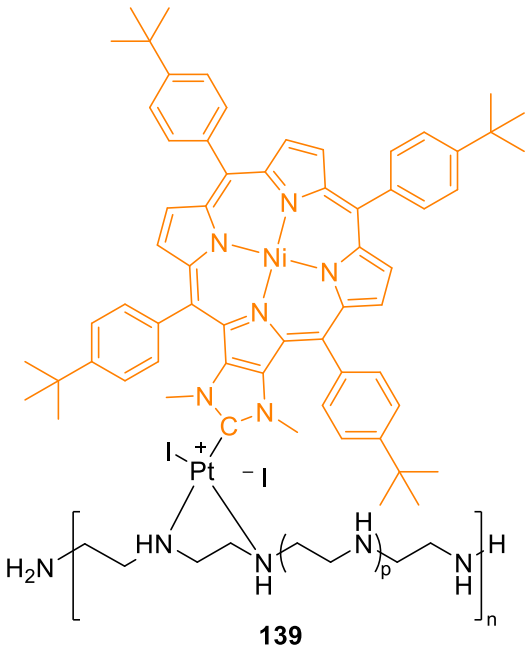

139

Scheme 54: NHC-Pt-PEI conjugate **139** functionalized with a nickel metallated porphyrin-NHC backbone

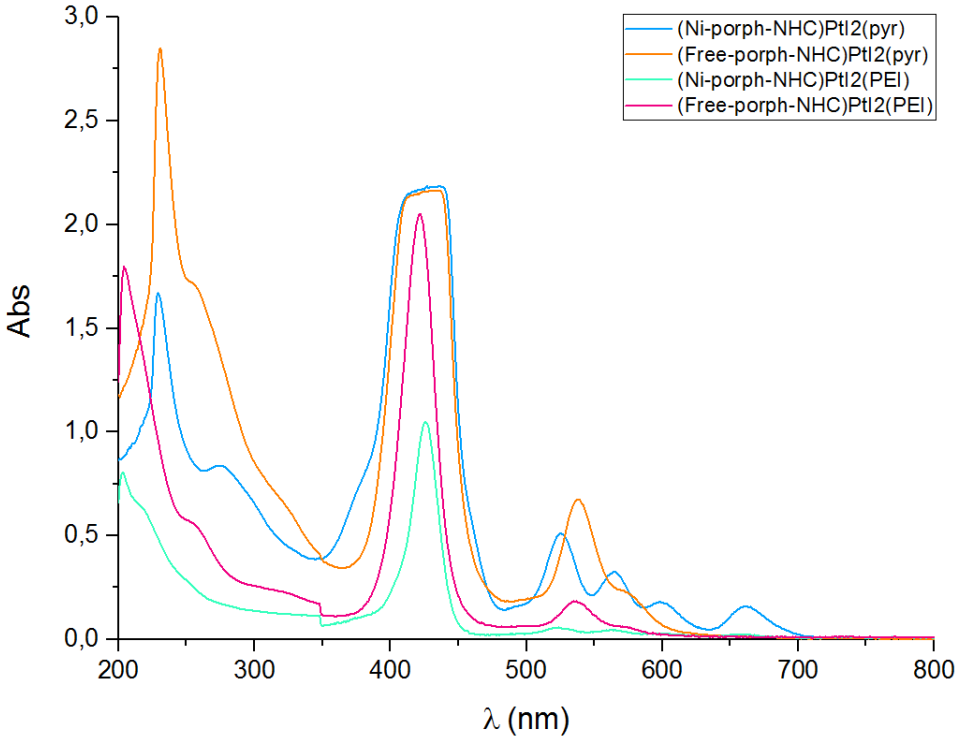

Figure 51: UV-vis spectra of porphyrin-NHC-Pt precursors **23** and **24** compared to their conjugate with PEI **138** and **139**

In the development of new NHC-Pt-PEI analogues, the incorporation of moieties targeting the cancer cells surface proteins would be a major step to access efficient and selective drug delivery. Indeed, vectorised drugs are expected to exclusively bind proteins expressed at the surface of a defined type of cancer cells and therefore promote selective drug uptake. A very promising targeting peptide called HB-19 has been developed in the groups of J. -P. Briand and A. Hovanessian.[319] It is known to specifically target the nucleoline in charge of vasculature development required for cancer cell growth.[320,321] Moreover, the HB-19 peptide itself exerts cancer cell inhibition which might act synergistically in combination with platinum centre.[322] A thiol derivative of HB-19 has been synthesized and provided by Dr G. Guichard (IECB, CNRS-Université de Bordeaux) and we therefore developed a novel strategy to allow simple thiol grafting on NHC-Pt-PEI conjugates.

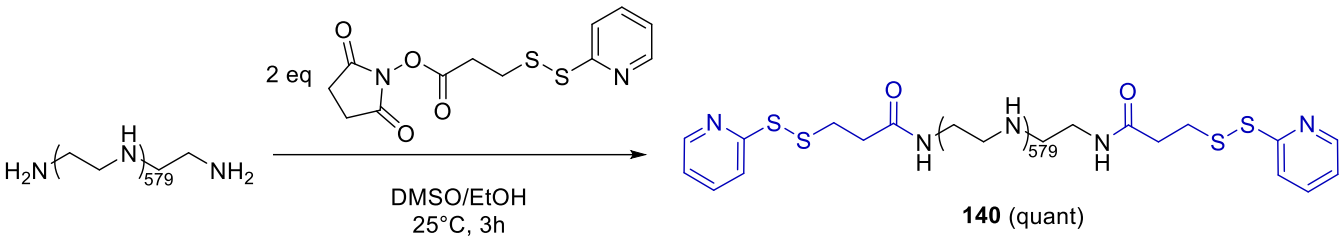

Scheme 55: PEI activation with SPDP fragment

PEI functionalization using two equivalent of the activated succinimidyl 3-[2-pyridildithio)propionate] (SPDP) has been achieved within 3 h at 25 °C by adaptation of a reported procedure.[323] The nucleophilic substitution on the N-succinimide moiety was ensured by ^{1}H NMR as pyridyl protons of **140** were observed over 7 ppm in the PEI protons free area. Similarly, ^{13}C NMR displayed carbon resonance signals characteristic of pyridyl and carbonyl carbons visible around 120 ppm and 165 ppm respectively.

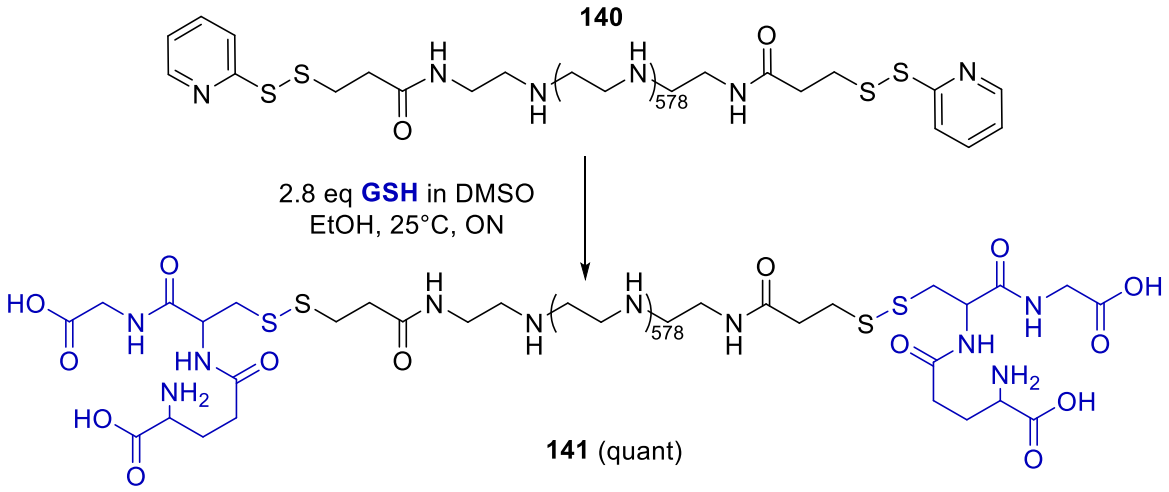

Scheme 56: Thiol exchange with GSH on the activated SPDP-PEI macromolecule **140**

Further conjugation of thiol derivatives on the polymer **140** has first been investigated with the small glutathione as a thiol model prior to HB-19 binding. The thiol exchange has been successfully achieved within a night at 25 °C in ethanol by reaction with slight excess of glutathione (Scheme 56). Precipitation by centrifugation in diethyl ether allowed successful recovery of the colourless oil **141** in quantitative yields. Full thiol exchange was supported by ^{1}H and ^{13}C NMR where pyridyl characteristic signals disappeared. Moreover, apparition of additional protons signals over 5 ppm attested for the conjugation of glutathione moieties.

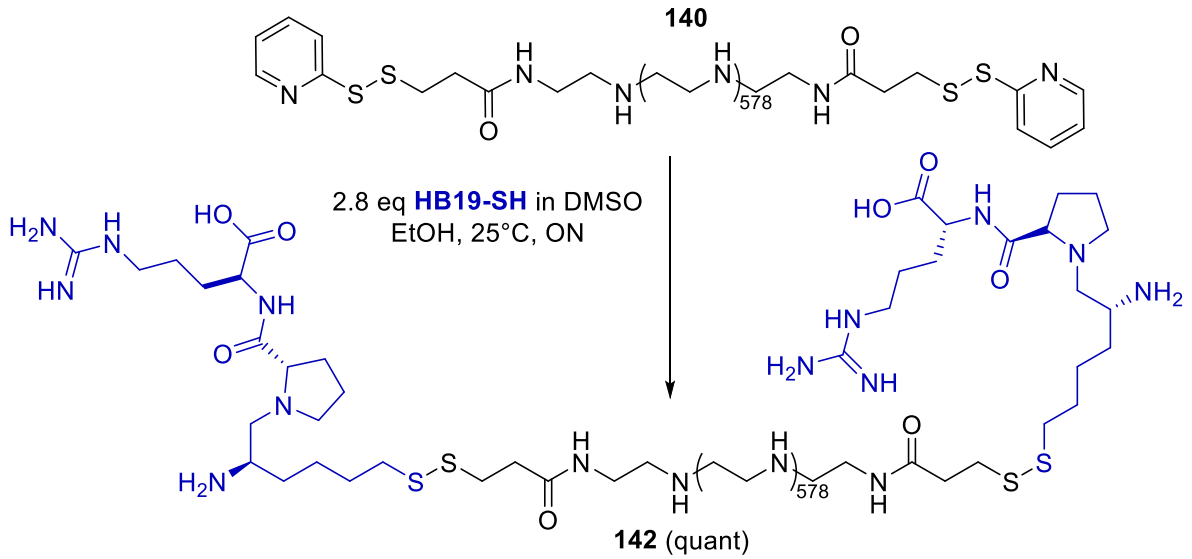

Scheme 57: Thiol exchange with HB19-SH on the activated SPDP-PEI macromolecule **140**

Encouraged by the successful functionalization of PEI chain with the glutathione, similar synthetic pathway has been applied to the targeting moiety HB-19 (Scheme 57). The novel conjugate **142** bearing the HB-19 peptide has been synthesized in a straightforward manner and quantitatively afforded as a colourless oil. The presence of new proton resonance signals over 5 ppm in ^{1}H NMR confirmed the thiol exchange with HB-19.

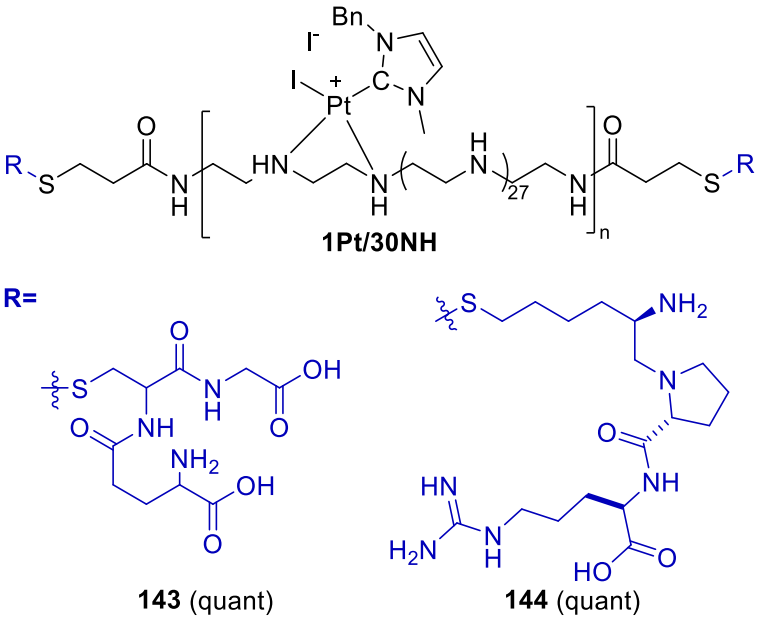

Scheme 58: Thiol functionalized NHC-Pt-PEI conjugates **143** and **144**

Finally, efficient platinum coordination in a 1Pt/30NH ratio on PEI derivatives **141** and **142** has been achieved according to the synthetic pathway reported in Scheme 40. Quantitative reaction afforded the NHC-Pt-PEI conjugate **143** bearing glutathione moieties or **144** bearing HB-19 as a sticky solid (Scheme 58). Successful platinum coordination for both **143** and **144** polymers has been confirmed by appearance of NHC characteristic signals around 4 ppm for N-methyl moiety and 7 ppm for the imidazole ring in addition to the disappearance of proton resonance signals corresponding to the coordinated pyridine in ^{1}H NMR. Finally, the novel NHC-Pt-PEI conjugate functionalized with a targeting moiety HB-19 remains to be evaluated *in vitro* as anticancer agent and its efficiency at targeting surface overexpressed nucleoline will be the matter of future studies.

3) Conclusion

Various strategies have been developed to allow alternatively pre- or post-functionalization of the cytotoxic NHC-Pt-PEI conjugate in excellent yields. Successful chromophore grafting and platinum coordination have been confirmed by ^{1}H NMR for all derivatives presented herein and UV techniques supported the polymer functionalization with all chromophores envisioned. A convenient two steps synthesis has been developed to allow tuneable conjugation of sulphur containing targeting moieties such as HB-19 which is expected to improve drug uptake. Moreover, while the PEI functionalization at both extremities appeared to prevent self-organization into vesicular systems, some selected examples proved to undergo comparable potencies as the highly cytotoxic complex **113** with a 1Pt/30NH ratio. Finally, preliminary *in vitro* investigations of the biodistribution of fluorescent metallopolymers supported the successful complex internalization which is of importance to promote efficient anticancer activity. Complementary experiments are currently underway to determine whether the expected platinum release from the PEI indeed occurs and allows platinum entry into the nucleus to promote cell apoptosis *via* a DNA platination.

IV. Gold nanoparticles for the delivery of NHC-Pt

1) Gold nanoparticles for biomedical application

Encouraged by the great anticancer activities and negligible side effects observed both *in vitro* and *in vivo* for the NHC-Pt-PEI conjugates detailed above, their association with well-defined metal nanoparticles (NPs) appeared as a powerful strategy to upgrade these anticancer agents. Gold nanoparticles (AuNPs) are of particular interest for biomedical applications thanks to their high stability and biocompatibility.[324] Moreover, two preparations based on PEG coated gold nanoparticles, namely AurImmune™ and AuroLase™ have already been through clinical trials

and approved by the FDA.[325,326] The use of either branched or linear polyethylenimine with various molecular weights have already been investigated for purposes as transfecting agents,[327,328] chemiluminescence agents,[329] sensors and even contrast agents.[330,331] Several PEI coated gold nanoparticles successfully entered cell nucleus and proved promising as transfecting agent.[332] Therefore, the synthesis of PEI coated gold nanoparticles (PEI-AuNPs) as cargo and subsequent grafting of NHC-Pt moieties have been investigated to improve both drug uptake by passive diffusion and biocompatibility. Moreover, the combination of NHC-Pt-PEI to gold nanoparticles is expected to prevent side effects and allow further biodistribution study.

2) Synthesis and characterization of PEI coated gold nanoparticles

In the literature, numerous synthetic pathways have been reported to access gold nanoparticles stabilized by PEI, particularly direct synthesis by thermal reduction[332] using an additional reducing agent or by ligand exchange on gold nanoparticles previously synthesized according to Turkevich's method.[333] Under the guidance of Dr J.-L. Gallani (IPCMS, Université de Strasbourg), we developed two convenient procedures involving the spontaneous assembly of gold atoms by chloroauric reduction with tetrabutylammonium borane (TBAB) to form PEI-AuNPs with an average size diameter of 10.7 nm or 30.9 nm under mild conditions. To note, other reducing agents as sodium borohydride or ammonium citrate have been envisioned but further dismissed due to the large size polydispersity observed. Several parameters proved essential in the synthesis of well-defined spherical particles rather than amorphous objects, namely solvents, concentration and the amount of reducing agent. After optimization process, the formation of an intermediate specie by reaction of 0.02 equivalent of PEI with one equivalent of $HAuCl_3$ in water (C_{Au} = 6.4 mM) at 20 °C proved essential. Subsequent slow reduction with 0.001 equivalent of TBAB for one hour at 50 °C promoted the successful formation of monodisperse PEI-AuNPs. The visual evolution from brown to deep red is characteristic for the arrangement of dispersed gold aggregates into spherical NPs (Figure 45). Dialysis purification over 500 mL of

water with a 10k Da cut-off membrane allowed isolation of pure PEI-AuNPs after 24 h. To note, storage was restricted to water solution at 20 °C due to irreversible aggregation when lyophilized or stored at lower temperature. This procedure allowed the synthesis of PEI-AuNPs with an average size of ~ 10 nm in a reproducible manner and which proved stable for weeks. A second procedure has been developed to access larger PEI-AuNPs of ~ 30 nm diameter. Chloric acid reaction in water with 0.02 equivalent of PEI for 15 minutes prior to rapid addition of larger amount of TBAB up to 0.1 equivalent promoted the formation of spherical nanoparticles after 15 additional minutes at 20 °C. Subsequent dialysis over water proved necessary to remove unreacted reducing agent and prevent the formation of amorphous or discoidal particles.

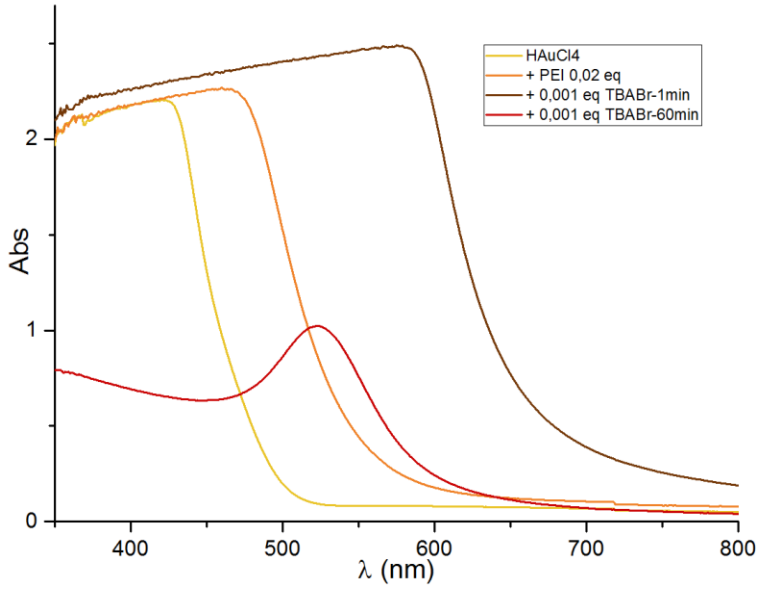

Figure 52: Follow-up of the ~10 nm PEI-AuNPs synthesis by UV

The intense band which maximum is λ_{abs} = 522 nm in UV spectra attested for the presence of a strong resonance plasmon characteristic of gold nanoparticles and thus confirmed the formation of spherical PEI-AuNPs. To note, a sharper peak suggested a more monodisperse size distribution of AuNPs. Dynamic light scattering (DLS) measurements have been performed to gain primary insight into the size distribution of synthesized PEI-AuNPs. It suggested the formation of either 10 nm or 30 nm average diameter size gold nanoparticles depending on the

procedure used. Complementary transmission electronic microscopy (TEM) has been performed to confirm the shape and diameter size distribution of gold nanoparticles afforded with the two previously detailed synthesis (Figure 46).

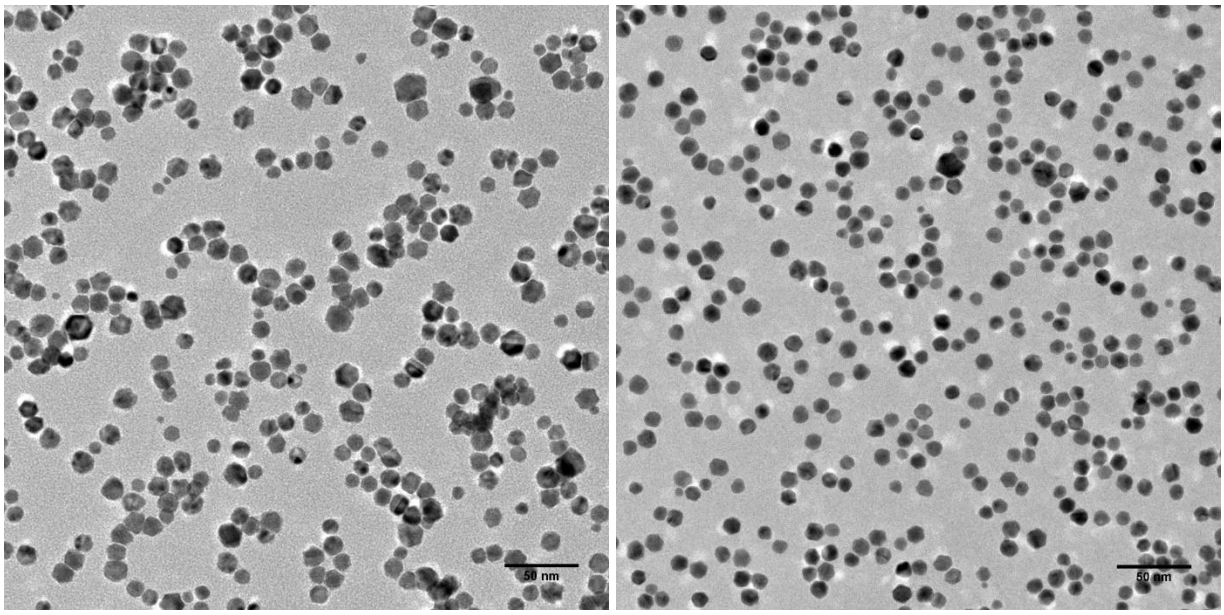

Figure 53: Typical TEM images of synthesized PEI-AuNPs with an average diameter of ~ 10 nm

The stability of metal nanoparticles over time and in biological environment is critical in the development of non-toxic nanodelivery devices to promote efficient passive cancer cell targeting. Both 10 nm and 30 nm PEI-AuNPs proved highly stable in water as confirmed by the strong plasmon resonance peak observed in UV-vis spectroscopy on solution stored at room temperature for one month. Their stability has also been regularly monitored by UV-vis spectroscopy when diluted alternatively in PBS solution and in the presence of mice serum. Remarkably, while 10 nm PEI-AuNPs proved moderately stable in PBS as slow aggregation could be seen over three days, no signal broadening or shift of the maximum absorption peak was observed in mice serum. This suggests a great colloidal stability in biological media. Moreover, 30 nm PEI-AuNPs also proved stable for days in both PBS solution and mice serum as suggested by UV-vis measurements. These results support the great stabilization of these AuNPs with the

PEI coating which contrasts with precedent reports suggesting linear PEI to form poorly stable conjugates with gold nanoparticles.[Erreur ! Signet non défini.]

While gold nanoparticles usually improve the pharmacokinetics and biodistribution of therapeutic molecules, their size and shape determine their *in vitro* and *in vivo* fate. Therefore, the cytotoxicity of both sizes of drug-free PEI-AuNPs developed in our laboratory has been evaluated toward three cancer cell lines by mean of IC_{50} measurements (Figure 47). Interestingly, the potency profiles proved to be dependent on the nanoparticle size since smaller nanoparticles (~ 10 nm) were non-toxic even at doses up to 400 µM. Distinctively, larger nanoparticles of ~ 30 nm exhibited low cytotoxicity toward all cancer cell lines. This is coherent with previous reports highlighting the biocompatibility of small gold nanoparticles stabilized by PEI.[332,334] Moreover, PEI-AuNPs are known to localize preferentially to the cell nucleus and faster exocytosis of smaller NPs might also account for their improved biocompatibility.[335] These results confirmed the potential of PEI-AuNPs developed herein for use as a biocompatible cargo for further nanodelivery of the cytotoxic NHC-Pt complexes.

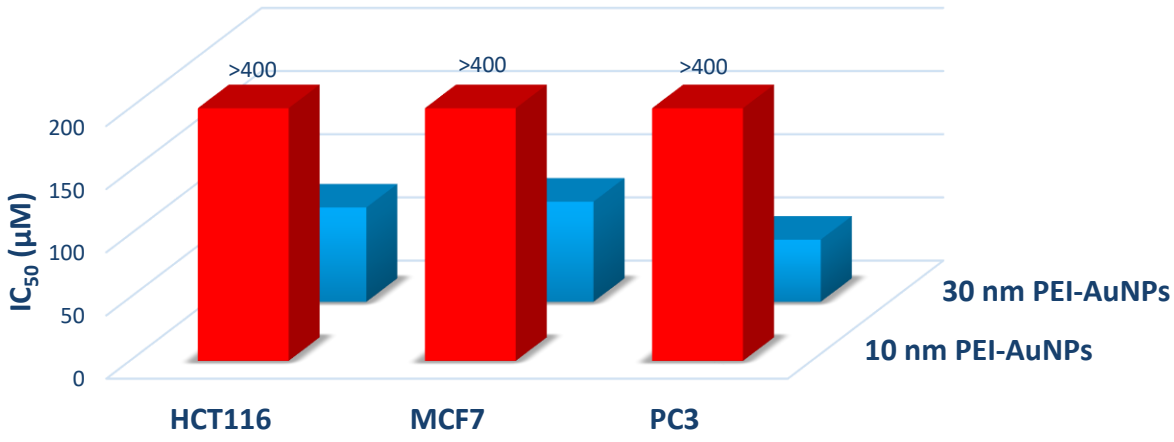

Figure 54: IC_{50} measurements on PEI coated gold nanoparticles of average size of 10 nm or 30 nm (IC_{50} based on gold mononuclear concentration)

Finally, the grafting of cytotoxic NHC-Pt moieties at the surface of the biocompatible PEI-AuNPs by ligand exchange has been attempted under numerous reaction conditions (temperature, solvent and reaction time). Unfortunately, all tested conditions either promoted an irreversible nanoparticles aggregation or failed at coordinating the platinum centre as confirmed by X-ray photoelectron spectroscopy (XPS). Accordingly, more development is needed to allow efficient grafting of NHC-Pt complexes at the surface of gold nanoparticles and the binding through a modified NHC backbone functionalized with thiol moiety might be a solution.

3) Conclusion

We successfully developed a reproducible synthetic strategy to access hydrophilic small gold nanoparticles stabilized by the biocompatible polyethylenimine. Interestingly, the PEI-AuNPs depicted great stability in saline solution and *in vitro* tests confirmed the biocompatibility of the smallest nanoparticles (~ 10 nm) which therefore appeared as promising cargo for further drug delivery. Comforted by previous achievement of the PEI functionalized with cytotoxic NHC-Pt moieties, and exploiting the high affinity of NHC-Pt for polyamines, coordination of well-established NHC-Pt complexes to gold nanoparticles has been investigated. While none of the strategies investigated to non-covalently bind NHC-Pt moieties to the nanoparticle proved successful, other paths are currently envisioned such as covalent binding of the NHC moiety to the nanoparticle through Au-S bond. Moreover, taking advantage of the positively charged synthesized nanoparticles, transfection with SiRNA will be envisioned to access gene therapy.[336]

General Conclusion

In this work, we reported on the synthesis of various platinum drug candidates functionalized with easily tuneable N-heterocyclic ligands to improve their stability and overcome resistance mechanism associated to platinum(II) based chemotherapy. We first envisioned the modification of platinum coordination sphere by simple ligand exchange for the development of a library of metallodrugs displaying promising anticancer activities.

Additionally, the upgrade of a large range of NHC-Pt(II) precursors also by simple oxidation using either bromine or $PhICl_2$ oxidants has been investigated to access NHC-Pt(IV) prodrug candidates. Comprehensive examination of the stability, drug release efficiency and anticancer activity of novel NHC-Pt(IV) complexes highlighted them as tremendous alternatives to cisplatin like drugs. Moreover, the occurrence of a parallel mechanism of action involving mitochondrial death by generation of oxidative stress successfully provided great cytotoxicity toward resistant cancers.

Furthermore, with the aim to access water-soluble and selective anticancer agents with improved cellular uptake, the combination of cytotoxic NHC-platinum moieties to various nanodelivery devices has been investigated. The use of natural albumin as a cargo appeared as a straightforward approach to allow biocompatible formulation of NHC-platinum complexes though preliminary *in vitro* tests were varied and further comprehensive drug screening is needed. Furthermore, liposomal formulation of an amphiphilic NHC-platinum complex successfully allowed drug release to promote cancer cell death. We also reported on the development of a family of polycationic NHC-Pt-PEI conjugates easily functionalized in high yields by modular approaches which offered the possibility to conjugate chromophores or targeting peptide to further improve their selectivity and potency. These macromolecules proved highly efficient at promoting cancer cell death either *in vitro* or *in vivo* and their mechanism of action and biodistribution are currently being unravelled by support of fluorescence microscopy.

Finally, we developed an easy and reproducible synthesis of two sizes of PEI coated gold nanoparticles though their functionalization with NHC-platinum derivatives requires additional investigation.

Encouraging results were obtained in the development of high valent NHC-Pt(IV) complexes and the synthesis of [(NHC)$PtCl_4$L] complexes based on oxidation using $PhICl_2$ could be extended to more complex structures. Moreover, the access to dual action derivatives combining selected organic drugs could be of interest for synergistic cytotoxicity. Furthermore, preliminary combination of cytotoxic NHC-Pt moieties to nanodelivery devices introduced new opportunities in the development of next generation of platinum anticancer agents. Next research efforts should be directed toward the development of safer nanoscale delivery devices in order to ultimately allow their clinical translation and use in personalized therapy. Indeed, combination of the promising NHC-Pt-PEI conjugate to synthetic peptides and proteins would allow improved potency by active targeting. Moreover, galenic formulation of the highly cytotoxic NHC-Pt-PEI conjugates could be investigated in combination with glucose to improve its bioavailability. Finally, NHC-Pt grafting onto AuNPs remains to be achieved and further decoration with biologically active moieties would give access to theranostic nanodevices for combined cancer therapy and treatment response follow up.

Chapter 5: Experimental part

1) General remarks

All manipulations of air and moisture sensitive compounds were carried out using standard Schlenk techniques under an argon atmosphere and solvents were purified and degassed following standard procedures. All reagents were purchased from commercial chemical suppliers (Acros, Alfa Aesar, TCI Europe and Rapp Polymer) and used without further purification. ^{1}H and ^{13}C Nuclear Magnetic Resonance (NMR) spectra were recorded on a Bruker Avance 300 or a Bruker Avance 500 spectrometer using the residual solvent peak as a reference ($CDCl_3$: δH = 7.26 ppm; δC = 77.16 ppm) at 295 K. HMQC ^{1}H–^{195}Pt spectra were recorded on a Bruker Avance 600 spectrometer using the residual solvent peak as a reference (H_2PtCl_6 in D_2O: δPt = 0 ppm) at the Institut de Chimie NMR Facility of the University of Strasbourg. The following abbreviations are used to classify the multiplicity of the observed signals: s = singlet, d = doublet, t = triplet, m = complex multiplet and bs = broad signal. UV-visible absorption spectra were recorded on a HITACHI U-3000 spectrophotometer, fluorescence spectra on a Photon Technology International MD-5020. Positive mode electrospray ionization mass spectra (ESI-HRMS) analyses have been carried out using microTOF (Bruker Daltonics). X-Ray diffraction studies were carried out at the Institut de Chimie X-ray Facility of the University of Strasbourg. Crystal data were collected at 173 K using MoKα graphite monochromated (λ = 0.71073 Å) radiation on a Nonius KappaCCD diffractometer. The structures were solved using direct methods with SHELXS97552 and refined against F2 using the SHELXL97 software. Non-hydrogen atoms were refined anisotropically. Hydrogen atoms were generated according to stereochemistry and refined using a riding model in SHELXL97. Dynamic light scattering (DLS) were performed on a VASCO γ from Cordouan Technologies.

2) Protocols of cell culture and proliferation assay

Cancer cell lines were obtained from the American Type Culture Collection (Rockville, MD, USA) and cultured according to the supplier's instructions. Human HCT116 colorectal carcinoma, MCF7 breast adenocarcinoma and PC3 prostate adenocarcinoma cells were grown in RPMI 1640 supplemented with 10% fetal calf serum (FCS) and 1% glutamine. Cell lines were maintained at 37 °C under a humidified atmosphere containing 5% CO_2. Cell growth inhibition was determined by an MTS assay according to the manufacturer's instructions (Promega, Madison, WI, USA). Briefly, the cells were seeded into 96-well plates (2.5 × 103 cells per well) containing 200 µL of growth medium. After 24 h of culture, the cells were treated with the tested compounds at different final concentrations. After 72 h of incubation, 40 µl of resazurin was added for 2 h before recording the absorbance at 490 nm with a spectrophotometric plate reader. The IC_{50} corresponds to the concentration of the compound that induces a decrease of 50% in the absorbance of drug-treated cells compared with untreated cells. Experiments were performed in triplicate.

3) Synthesis of functionalized imidazolium salts

- ***Procedure A: Synthesis of [(NHC)PtX$_2$(pyridine)] complexes***

All imidazolium salts are obtained using standard synthesis procedures in 250 mg to 1 g scale by alkylation of azole derivatives with excess halogenoalkane in CH_3CN overnight at 75 °C. After evaporation of the volatiles, the crude product is dissolved in a minimum amount of methanol, washed with diethyl ether and dried under reduced pressure to yield the imidazolium salt.

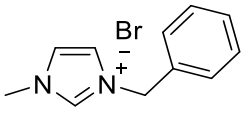

Synthesized according to procedure A. Yellow oil, yield 92%. ^{1}H NMR ($CDCl_3$, 300 MHz, 20 °C): δ 4.08 (s, 3H, N-CH_3), 5.58 (s, 2H, N-CH_2), 7.17 (s, 1H, CH_{im}), 7.23 (s, 1H, CH_{im}), 7.38-7.50 (m, 5H,

CH_{ar}), 10.79 (s, 1H, NC*H*N); ^{13}C NMR ($CDCl_3$, 75 MHz, 20 °C): δ 36.6 (N-CH_3), 52.8 (N-CH2), 122.1 (CH), 123.8 (CH), 128.8 (CH_{ar}), 129.1 (CH_{ar}), 129.2 (CH_{ar}), 133.2 (CH_{ar}), 136.6 (N*C*HN).

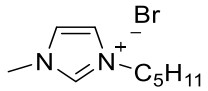

Synthesized according to procedure A. Colourless oil, yield 92%. ^{1}H NMR ($CDCl_3$, 300 MHz, 20 °C): δ 0.48 (t, *J*=6.9 Hz, 3H, CH_3), 0.94 (m, 4H, 2CH_2), 1.54 (quint, *J*=7.4 Hz, 2H, CH_2), 3.75 (s, 3H, N-CH_3), 3.96 (t, *J*=7.4 Hz, 2H, N-CH_2), 7.30 (t, *J*=1.8 Hz, 1H, CH_{im}), 7.43 (t, *J*=1.8 Hz, 1H, CH_{im}), 9.86 (s, 1H, NC*H*N); ^{13}C NMR ($CDCl_3$, 75 MHz, 20 °C): δ 13.5 (CH_3), 21.7, 27.8, 29.6 (CH_2), 26.3 (N-CH_3), 49.6 (N-CH_2), 122.1 (CH_{im}), 123.6 (CH_{im}), 136.5 (N*C*HN).

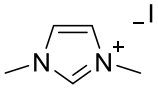

Synthesized according to procedure A. Yellow oil, quant. ^{1}H NMR (DMSO, 300 MHz, 20 °C): δ 3.83 (s, 6H, N-CH_3), 7.69 (d, *J*=1.6 Hz, 2H, CH_{im}), 9.08 (s, 1H, NC*H*N); ^{13}C NMR (DMSO, 75 MHz, 20 °C): δ 35.8 (N-CH_3), 123.3 (CH_{im}), 136.9 (N*C*HN).

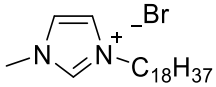

Synthesized according to procedure A. Colourless oil, yield 44%, ^{1}H NMR ($CDCl_3$, 300 MHz, 20 °C): δ 0.85 (t, *J*=6.6 Hz, 3H, CH3), 1.22 (m, 30H, CH_2), 2.11 (m, 2H, CH2), 4.11 (s, 3H, N-CH_3), 4.29 (t, *J*=7.5 Hz, 2H, N-CH_2), 7.36 (t, *J*=1.8 Hz, 1H, CH_{im}), 7.52 (t, *J*=1.8 Hz, 1H, CH_{im}), 10.44 (s, 1H, NC*H*N); ^{13}C NMR (CDCl3, 75 MHz, 20 °C): δ 14.1 (CH_3), 22.6, 26.2, 29.0, 29.3, 29.5, 29.7, 30.3, 31.9 (CH_2), 36.7 (N-CH_3), 50.2 (N-CH_2), 121.7 (CH_{im}), 123.5 (CH_{im}), 137.6 (N*C*HN).

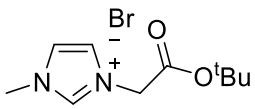

Synthesized according to procedure A. Colourless oil, quant. ^{1}H NMR ($CDCl_3$, 300 MHz, 20 °C): δ 1.52 (s, 9H, CH_3), 3.95 (s, 3H, N-CH_3), 5.19 (s, 2H, N-CH_2), 7.54 (s, 1H, CH_{im}), 7.64 (s, 1H, CH_{im}),

9.37 (s, 1H, NC*H*N); ^{13}C NMR ($CDCl_3$, 75 MHz, 20 °C): δ 28.0 (CH_3), 36.8 (N-CH_3), 50.8 (N-CH_2), 84.8 (O-C), 123.0, 123.8 (CH_{im}), 138.3 (N*C*HN), 164.9 (C=O).

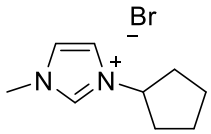

Synthesized according to procedure A. White solid, quant. ^{1}H NMR (d_6-DMSO, 300 MHz, 20 °C): δ 1.60-1.85 (m, 6H, CH_2), 2.15-2.17 (m, 2H, CH_2), 3.87 (s, 3H, N-CH_3), 4.78 (m, 1H, N-CH), 7.80 (s, 1H, CH_{im}), 7.92 (s, 1H, CH_{im}), 9.48 (s, 1H, NC*H*N); ^{13}C NMR ($CDCl_3$, 75 MHz, 20 °C): δ 23.0 (CH_2), 32.5 (CH_2), 35.7 (N-CH_3), 60.45 (N-CH), 121.1 (CH_{im}), 123.6 (CH_{im}), 135.7 (N*C*HN).

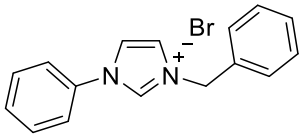

Synthesized according to procedure A. Yellow oil, quant. ^{1}H NMR ($CDCl_3$, 300 MHz, 20 °C): δ 5.55 (s, 2H, N-CH_2), 6.98-7.21 (m, 6H, 6H_{ar}), 7.40-7.53 (m, 4H, 4H_{ar}), 7.00 (t, *J*=1.8 Hz, 1H, CH_{im}), 7.82 (t, *J*=1.8 Hz, 1H, CH_{im}), 77.15 (t, *J*=1.8 Hz, 1H, NC*H*N); ^{13}C NMR ($CDCl_3$, 75 MHz, 20 °C): δ 52.9 (N-CH_2), 120.9 (CH_{im}), 121.2(CH_{ar}), 123.1 (CH_{im}), 129.0, 129.1, 129.7, 130.2 (CH_{ar}), 133.4 (C_{ar}), 134.2 (C_{ar}), 135.3 (N*C*HN).

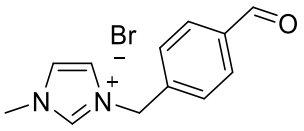

Synthesized according to procedure A. White solid, quant. ^{1}H NMR ($CDCl_3$, 300 MHz, 20 °C): δ 4.09 (s, 3H, N-CH_3), 5.80 (s, 2H, N-CH_2), 7.26 (CH_{im}), 7.30 (s, 1H, CH_{im}), 7.72 (d, *J*=8.1 Hz, 2H, CH_{ar}), 7.92 (d, *J*=8.1 Hz, 2H, CH_{ar}), 10.03 (s, 1H, CH_{im}), 10.87 (s, 1H, NC*H*N). MS (positive ESI): [M-Br]: calculated for $C_{12}H_{13}N_2O_1$: 201.10, found 201.10.

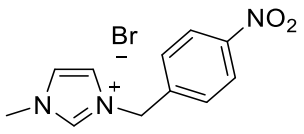

Synthesized according to procedure A. Light yellow solid, quant. ^{1}H NMR (DMSO, 300 MHz, 20 °C): δ 3.88 (s, 3H, N-CH_3), 5.65 (s, 2H, N-CH_2), 7.69 (d, *J*=8.6 Hz, 2H, 2CH_{ar}), 7.79 (t, *J*=1.7 Hz, 1H, CH_{im}), 7.86 (t, *J*=1.7 Hz, 1H, CH_{im}), 8.28 (d, *J*=8.6 Hz, 2H, 2CH_{ar}), 9.34 (s, 1H, NC*H*N); ^{13}C NMR (DMSO, 75 MHz, 20 °C): δ 36.0 (N-CH3), 50.8 (N-CH2), 122.5 (CH_{im}), 124.0 (CH_{ar}), 124.2 (CH_{im}), 129.5 (CH_{ar}), 137.1 (N*C*HN), 142.2 (C_{ar}), 147.5 (C_{ar}-NO_2).

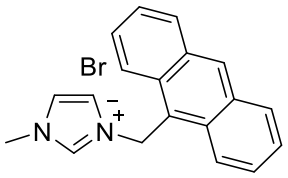

Synthesized according to procedure A. Yellow solid, quant. ^{1}H NMR (DMSO, 300 MHz, 20 °C): δ 3.72 (s, 3H, N-CH_3), 6.47 (s, 2H, N-CH_2), 7.61-7.70 (m, 6H, CH_{ar}+CH_{im}+NC*H*N), 8.21 (d, *J*=7.8 Hz, 2H, CH_{ar}), 8.44 (d, *J*=7.8 Hz, 2H, CH_{ar}), 8.82 (d, *J*=7.8 Hz, 2H, CH_{ar}).

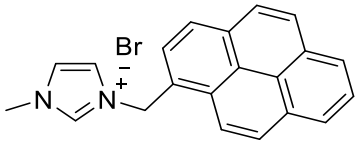

Synthesized according to procedure A. Light yellow solid, quant. ^{1}H NMR (DMSO, 300 MHz, 20 °C): δ 3.83 (s, 3H, N-CH_3), 6.24 (s, 2H, N-CH_2), 7.76 (t, *J*=1.7 Hz, 1H, CH_{im}), 7.90 (t, *J*=1.7 Hz, 1H, CH_{im}), 8.09-8.59 (m, 9H, H_{ar}), 9.23 (s, 1H, NC*H*N); ^{13}C NMR (d_6-DMSO, 75 MHz, 20 °C): δ 37.8 (N-CH_3), 51.8 (N-CH_2), 124.3, 124.5, 125.6, 125.8, 126.0, 127.1, 127.7, 127.9, 128.6, 129.2, 129.3, 129.9, 130.1, 130.5, 130.7, 132.0, 132.6, 133.4 (C_{ar} CH_{im}), 138.6 (N*C*HN).

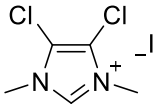

Synthesized according to procedure A. Yellow solid, quant. ^{1}H NMR (d_6-DMSO): δ 9.39 (s, 1H), 3.82 (s, 6H); ^{13}C NMR ($CDCl_3$, 75 MHz, 20 °C): δ 35.9 (N-CH_3), 116.8 (C_{im}), 137.4 (N*C*HN).

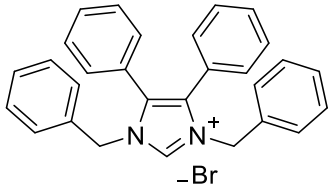

Synthesized according to procedure A. Dark brown solid, quant. ^{1}H NMR (d_6-DMSO): δ 5.41 (s, 4H, N-CH_2), 7.07-7.53 (m, 25H, CH_{ar}), 9.65 (s, 1H, NC*H*N).

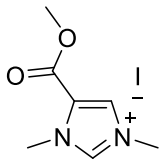

Synthesized according to procedure A. Yellow oil, yield 80%. ^{1}H NMR ($CDCl_3$, 300 MHz, 20 °C): δ 3.92 (s, 3H, OCH_3), 4.17 (s, 3H, NCH_3), 4.19 (s, 3H, NCH_3), 8,05 (bs, 1H, CH_{im}), 10.25 (s, 1H, NCHN); ^{13}C NMR ($CDCl_3$, 75 MHz, 20 °C): δ 37.1 (CH_3), 38.1 (CH_3), 53.3 (OCH_3), 124.3 (C_{im}), 128.9 (CH_{im}), 141.0 (N*C*HN), 157.7 (C=O).

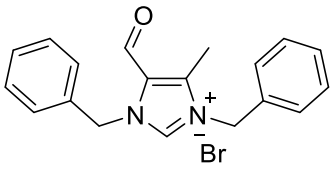

Synthesized according to procedure A. Oil, quant. ^{1}H NMR (DMSO, 300 MHz, 20 °C): δ 2.56 (s, 3H, CH_3), 5.55 (s, 2H, N-CH_2), 5.72 (s, 2H, N-CH_2), 7.35-7.49 (m, 10H, H_{ar}), 9.68 (s, 1H), 9.93 (s, 1H); ^{13}C NMR (DMSO, 75 MHz, 20 °C): δ 8.7 (CH_3), 49.9 (N-CH_2), 51.3 (N-CH_2), 125.8, 127.8, 128.1, 128.6, 128.8, 129.1, 133.3, 134.3, 139.8, 142.2 (Car + C_{im} + N*C*HN), 180.8 (CHO).

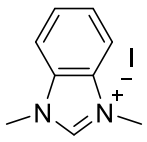

Synthesized according to procedure A. White solid, yield 73%. ^{1}H NMR ($CDCl_3$, 300 MHz, 20 °C): δ 4.17 (s, 6H, 2N-CH_3), 7.21-7.36 (m, 6H, $2H_{pyr}$, $4H_{Ar}$), 7.7 (t, *J*=7 Hz, 1H, $1H_{pyr}$), 9.07 (m, 2H, $2H_{pyr}$); ^{13}C NMR ($CDCl_3$, 75 MHz, 20 °C): δ 34.9 (N-CH_3), 109.9 (CH_{Ar}), 122.9 (CH_{Ar}), 125.1 (CH_{pyr}), 134.7

(C_{Ar}), 137.7 (CH_{pyr}), 149.9 (C-Pt), 153.6 (CH_{pyr}); HRMS (positive ESI): m/z calcd for $C_{14}H_{15}IN_3Pt$ [M-I] 546.9958; found 547.0036; m/z calcd for $C_{34}H_{29}IN_3PtCH_3CN$ [M-I + CH_3CN] 842.1319; found 842.1340. $C_{14}H_{15}I_2N_3Pt$ (674.19): calcd. C 24.94, H 2.24, N 6.23; found C 24.59, H 2.47, N 6.53.

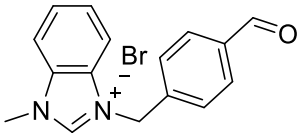

Synthesized according to procedure A. White solid, quant. ^{1}H NMR (DMSO, 300 MHz, 20 °C): δ 2.56 (s, 3H, CH_3), 5.55 (s, 2H, N-CH_2), 5.72 (s, 2H, N-CH_2), 7.35-7.49 (m, 10H, 10H_{ar}), 9.68 (s, 1H), 9.93 (s, 1H); ^{13}C NMR (DMSO, 75 MHz, 20 °C): δ 8.7 (CH_3), 49.9 (N-CH_2), 51.3 (N-CH_2), 125.8, 127.8, 128.1, 128.6, 128.8, 129.1, 133.3, 134.3, 139.8, 142.2 (C_{ar} + C_{im} + NC*H*N), 180.8 (CH_{im}O).

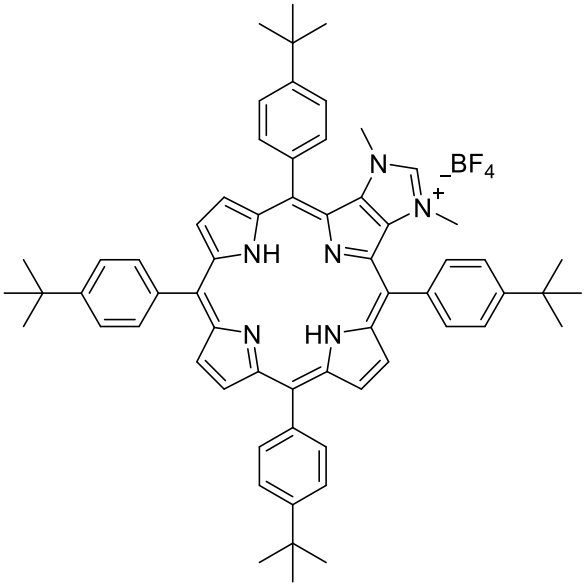

Synthesized according to reported procedure.[1] Red solid, ^{1}H NMR ($CDCl_3$, 300 MHz, 20 °C): δ -2.96 (bs, 2H, $NH_{pyrrole}$), 1.60 (s, 18H, H_{tBu}), 1.62 (s, 18H, H_{tBu}), 3.16 (s, 6H, N-CH_3), 7.80 (d, *J*=8.0 Hz, 4H, CH_{ar}), 7.91 (d, *J*=8.0 Hz, 4H, CH_{ar}), 8.17 (d, *J*=8.0 Hz, 4H, CH_{ar}), 8.36 (d, *J*=8.0 Hz, 4H, CH_{ar}), 8.75 (s, 2H, $H_{pyrrole}$), 8.94 (s, 4H, $H_{pyrrole}$), 9.20 (s, 1H, NC*H*N).

[1] J.-F. Lefebvre, M. Lo, D. Leclercq, S. Richeter *Chem. Commun.* **2011**, *47*, 2976-2978

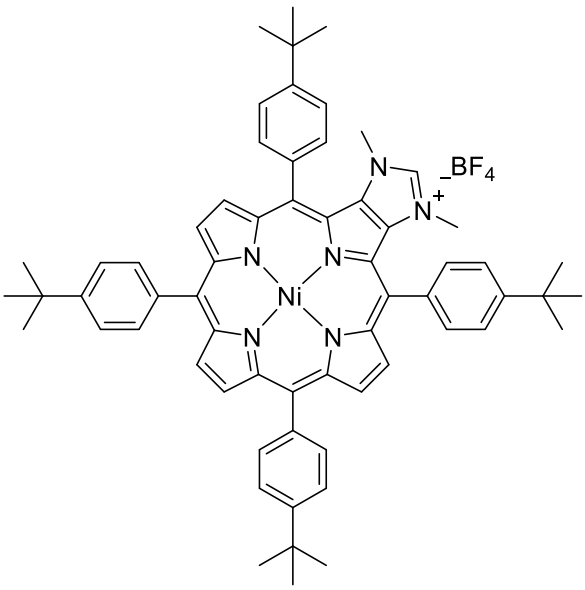

Synthesized according to reported procedure.[1] Red solid, ^{1}H NMR ($CDCl_3$, 300 MHz, 20 °C): δ 1.54 (s, 18H, H_{tBu}), 1.56 (s, 18H, H_{tBu}), 3.16 (s, 6H, N-CH_3), 7.71 (d, *J*=8.0 Hz, 4H, CH_{ar}), 7.79 (d, *J*=8.0 Hz, 4H, CH_{ar}), 7.94 (d, *J*=8.0 Hz, 4H, CH_{ar}), 8.05 (d, *J*=8.0 Hz, 4H, CH_{ar}), 8.68-8.74 (M, 6H, $H_{pyrrole}$), 9.24 (s, 1H, NC*H*N).

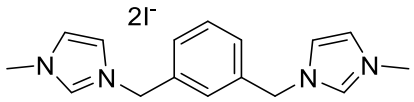

Synthesized according to procedure A. Oil, quant. ^{1}H NMR (DMSO, 300 MHz, 20 °C): δ 3.90 (s, 6H, N-CH_3), 5.53 (s, 4H, N-CH_2), 7.46 (m, 3H, CH_{ar}), 7.69 (s, 1H, CH_{ar}), 7.81 (t, *J*=1.7 Hz, 2H, CH_{im}), 7.94 (t, *J*=1.7 Hz, 2H, CH_{im}), 9.54 (s, 2H, NC*H*N); ^{13}C NMR ($CDCl_3$, 75 MHz, 20 °C): δ 36.0 (N-CH_3), 51.2 (N-CH_2), 122.2 (CH_{im}), 123.9 (CH_{im}), 128.4, 128.6, 129.5 (CH_{ar}), 135.6 (C_{ar}), 136.7 (N*C*HN)

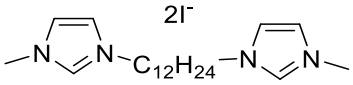

Synthesized according to procedure A. Oil, quant. ^{1}H NMR (MeOD, 300 MHz, 20 °C): δ 1.31-1.39 (m, 16H, CH_2), 1.97 (m, 4H, CH_2), 4.07 (s, 6H, N-CH_3), 4.41 (m, 4H, N-CH_2), 7.82 (s, 2H, CH_{im}), 7.91 (s, 2H, CH_{im}); ^{13}C NMR (MeOD, 75 MHz, 20 °C): δ 27.0 (CH_2), 29.9(CH_2), 30.3(CH_2), 30.4(CH_2), 31.1(CH_2), 37.0 (N-CH_3), 50.7 (N-CH_2), 123.6 (CH_{im}), 124.8 (CH_{im}), 137.7 (N*C*HN).

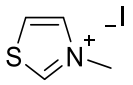

Synthesized according to procedure A. Oil, quant., ^{1}H NMR (DMSO, 300 MHz, 20 °C): δ 4.21 (s, 3H, N-CH_3), 8.32 (m, 1H, CH_{im}), 8.47 (m, 1H, CH_{im}), 10.11 (s, 1H, SC*H*N).

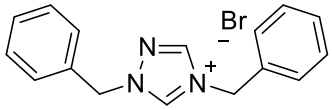

Synthesized according to procedure A. White solid, quant. ^{1}H NMR ($CDCl_3$, 300 MHz, 20 °C): δ 5.63 (s, 2H, N-CH_2), 5.76 (s, 2H, N-CH_2), 7.28-7.38 (m, 6H, $6H_{ar}$), 7.46-7.54 (m, 2H, $2H_{ar}$), 7.56-7.62 (m, 2H, $2H_{ar}$), 8.93 (s, 1H, CH_{im}N), 11.78 (s, 1H, NC*H*N); ^{13}C NMR ($CDCl_3$, 75 MHz, 20 °C): δ 52.0 (N-CH_2), 56.3 (N-CH_2), 129.2, 129.4, 129.5, 129.6, 129.9 (CH_{ar}), 131.7 (C_{ar}), 131.9 (C_{ar}), 142.6 (N*C*HN), 143.7 (N*C*HN).

2) Synthesis of NHC-Pt(II) complexes

- ***Procedure B: Synthesis of [(NHC)PtX$_2$(pyridine)] complexes***

The ligand precursor (imidazolium halide, 1.1 equiv.), $PtCl_2$ (1 equiv.), NaI (10 equiv.) and K_2CO_3 (10 equiv.) were suspended under argon in anhydrous pyridine (10 mL). The mixture was sonicated for 20 min, heated overnight at 100 °C, then concentrated under reduced pressure, dissolved in CH_2Cl_2, and filtered through a Celite plug. The residue was purified by silica gel chromatography (pentane/CH_2Cl_2, 1:1 to CH_2Cl_2) to afford the complex as a yellow powder.[2]

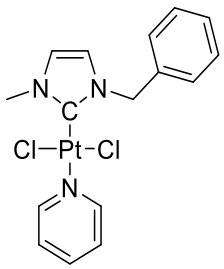

[2] E. Chardon, G. Dahm, G. Guichard, S. Bellemin-Laponnaz *Chem. Asian J.* **2013**, *8*, 1232-1242

1. *Synthesized according to procedure B.* Yellow solid, 23.3 mg, yield 24%. ^{1}H NMR ($CDCl_3$, 300 MHz, 20 °C): δ 4.09 (s, 3H, N-CH_3), 5.82 (s, 2H, N-CH_2), 6.63 (d, *J*=2.5 Hz, 1H, CH_{im}), 6.82 (d, *J*=2.5 Hz, 1H, CH_{im}), 7.31-7.39 (m, 5H, CH_{ar}), 7.46-7.50 (m, 2H, CH_{pyr}), 7.75 (m, 1H, CH_{pyr}), 9.03 (m, 2H, CH_{pyr}); HMQC ^{1}H–^{195}Pt NMR ($CDCl_3$, 64.2 MHz, 20 °C): δ – 3304 (m).

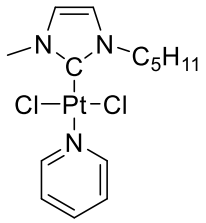

2. *Synthesized according to procedure B.* Yellow solid, 25.2 mg, yield 26%. ^{1}H NMR ($CDCl_3$, 300 MHz, 20 °C): δ 0.94 (t, *J*=6.5 Hz, 3H, CH_3), 1.42 (m, 4H, CH_2), 2.03 (m, 2H, CH_2), 4.09 (s, 3H, N-CH_3), 4.51 (m, 2H, N-CH_2), 6.85 (s, 2H, CH_{im}), 7.36 (M, 2H, CH_{pyr}), 7.76 (t, *J*=7.6 Hz, 1H, CH_{pyr}), 9.03 (m, 2H, CH_{pyr}).

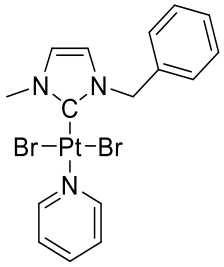

3. *Synthesized according to procedure B.* Yellow solid, 59.2 mg, yield 52%. 1H NMR ($CDCl_3$, 300 MHz, 20 °C): δ 4.11 (s, 3H, N-CH_3), 5.83 (s, 2H, N-CH_2), 6.64 (d, *J*= 2.1Hz, 1H, CH_{im}), 6.83 (d, *J*=2.1 Hz, 1H, CH_{im}), 7.27-7.53 (m, 7H, 5H_{ar} and 2H_{pyr}), 7.76 (tt, J_1=7.6 Hz, J_2=1.6 Hz, 1H, H_{pyr}), 9.04 (dt, J_1=5.0 Hz, J_2=1.6 Hz, 2H, 2H_{pyr}); ^{13}C NMR ($CDCl_3$, 75 MHz, 20 °C): δ 37.9 (N-CH_3), 54.2 (N-CH_2), 120.0 (CH_{im}), 122.4 (CH_{im}), 124.9 (C_{pyr}), 128.2 (CH_{ar}), 128.8 (CH_{ar}), 128.8 (CH_{ar}), 135.7 (C_{ar}), 137.7 (C_{pyr}), 138.2 (C-Pt), 152.6 (C_{pyr}); ^{13}C NMR (Acetone, 75 MHz, 20 °C): δ 37.1 (N-CH_3), 53.5 (N-CH_2), 120.3 (CH_{im}), 123.0 (CH_{im}), 125.1 (C_{pyr}), 127.9 (CH_{ar}), 128.5 (CH_{ar}), 128.8 (CH_{ar}), 136.8 (C_{ar}), 138.3 (C_{pyr}), 152.5 (C_{pyr}); HMQC ^{1}H–^{195}Pt NMR ($CDCl_3$, 64.2 MHz, 20 °C): δ – 3814 (m).

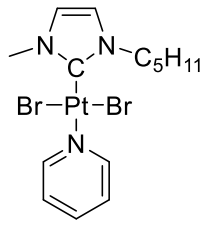

4. *Synthesized according to procedure B.* Yellow solid, 47.3 mg, yield 43%. ^{1}H NMR ($CDCl_3$, 300 MHz, 20 °C): δ 0.91 (t, *J*=6.7 Hz, 3H, CH_3), 1.38 (m, 4H, CH_2), 2.01 (m, 2H, CH_2), 4.02 (s, 3H, N-CH_3), 4.46 (m, 2H, N-CH_2), 6.82 (s, 2H, CH_{im}), 7.31 (t, *J*=7.0 Hz, 2H, CH_{pyr}), 7.73 (t, *J*=7.6 Hz, 1H, CH_{pyr}), 8.98 (m, 2H, CH_{pyr}); ^{13}C NMR ($CDCl_3$, 75 MHz, 20 °C): 14.0 (CH_3), 22.3 (CH_2), 28.7 (CH_2), 29.9 (CH_2), 37.8 (N-CH_3), 50.6 (N-CH_2), 120.4 (CH_{im}), 121.8 (CH_{im}), 124.9 (CH_{pyr}), 136.9 (C-Pt), 137.7 (CH_{pyr}), 152.5 (CH_{pyr}).

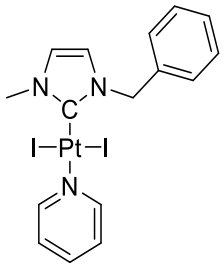

5. *Synthesized according to procedure B.* Yellow solid, 94.7 mg, yield 72%. ^{1}H NMR ($CDCl_3$, 300 MHz, 20 °C): δ 3.97 (s, 3H, N-CH_3), 5.72 (s, 2H, N-CH_2), 6.60 (s, 1H, CH_{im}), 6.82 (s, 1H, CH_{im}), 7.27-7.44 (m, 5H, H_{ar}), 7.52 (m, 2H, H_{pyr}), 7.74 (m, 1H, H_{pyr}), 9.09 (m, 2H, H_{pyr}); ^{13}C NMR ($CDCl_3$, 75 MHz, 20 °C): δ 38.3 (N-CH_3), 54.4 (N-CH_2), 119.8 (CH_{im}), 122.2 (CH_{im}), 124.8 (C_{pyr}), 128.3 (C_{ar}), 128.8 (C_{ar}), 129.1 (s, CH_{ar}), 135.4 (C_{pyr}), 136.3 (C-Pt), 137.5 (s, C_{pyr}), 153.7 (C_{pyr}); MS (positive ESI) [M-I]: calculated for $C_{16}H_{17}IN_3Pt$: 573.011, found 572.969. Microanalysis: Calculated for $C_{16}H_{17}I_2N_3Pt$: C, 27.44; H, 2.45; N, 6.00. Found: C, 26.97; H, 2.47; N, 5.82.

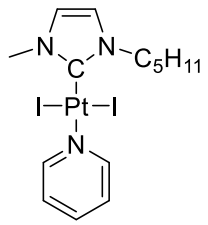

6. *Synthesized according to procedure B.* Yellow solid, 65 mg, yield 51%. ^{1}H NMR ($CDCl_3$, 300 MHz, 20 °C): δ 0.95 (t, *J*=6.7 Hz, 3H, CH_3), 1.41 (m, 4H, CH_2), 2.03 (q, *J*=7.6 Hz, 2H, CH_2), 3.94 (s, 3H, N-CH_3), 4.41 (t, *J*=7.6 Hz, 2H, N-CH_2), 6.83 (s, 2H, CH_{im}), 7.31 (t, *J*=6.7 Hz, 2H, H_{pyr}), 7.71 (tt, J_1=7.8 Hz, J_2=1.6 Hz, 1H, H_{pyr}), 9.02 (m, 2H, H_{pyr}); ^{13}C NMR ($CDCl_3$, 75 MHz, 20 °C): δ 14.1 (CH_3), 22.3 (CH_2), 28.9 (CH_2), 29.3 (CH_2), 38.4 (N-CH_3), 50.9 (N-CH_2), 120.4 (CH_{im}), 121.9 (CH_{im}), 125.0 (C_{pyr}), 135.1 (C-Pt), 137.5 (C_{pyr}), 153.7 (C_{pyr}). MS (positive ESI) [M-I]: calculated for $C_{14}H_{21}I_1N_3Pt_1$: 553.04, found 553.04, [M-I + CH3CN]: calculated for $C_{14}H_{21}I_1N_3Pt_1CH_3CN$: 594.07, found 594.07.

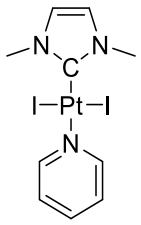

7. *Synthesized according to procedure B.* Yellow solid, 109.1 mg, yield 93%. ^{1}H NMR ($CDCl_3$, 300 MHz, 20 °C): δ 3.93 (d, *J*=0.7 Hz, 6H, N-CH_3), 6.82 (d, *J*=0.7 Hz, 2H, CH_{im}), 7.31 (t, *J*=6.8 Hz, 2H, H_{pyr}), 7.71 (td, J_1=7.6 Hz, J_2=0.7 Hz, 1H, H_{pyr}), 9.02 (m, 2H, 2H_{pyr}); ^{13}C NMR ($CDCl_3$, 75 MHz, 20 °C): δ 38.2 (N-CH_3), 121.9 (CH_{im}), 125.0 (C_{pyr}), 135.9 (C-Pt), 137.5 (C_{pyr}), 153.7 (C_{pyr}).

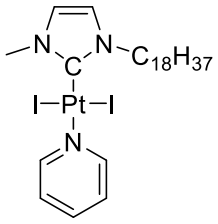

8. *Synthesized according to procedure B.* Yellow solid, 56.8 mg, yield 35%. ^{1}H NMR ($CDCl_3$, 300 MHz, 20 °C): δ 0.87 (t, *J*=6.7 Hz, 3H, CH_3), 1.25 (m, 30H, CH_2), 2.03 (m, 2H, CH_2), 3.95 (s, 3H, N-CH_3), 4.42 t, *J*=7.7 Hz, 2H, N-CH_2), 6.83 (s, 2H, CH_{im}), 7.31 (m, 2H, H_{pyr}), 7.71 (tt, J_1=7.7 Hz, J_2=1.6 Hz, 1H, H_{pyr}), 9.04 (m, 2H, H_{pyr}); ^{13}C NMR ($CDCl_3$, 75 MHz, 20 °C): δ 14.1 (CH_3), 22.7, 26.7, 29.2, 29.3, 29.5, 29.6, 29.7, 31.9 (CH_2), 38.3 (N-CH_3), 50.9 (N-CH_2), 120.8 (CH_{im}), 121.8 (CH_{im}), 124.9 (C_{pyr}), 135.1 (C-Pt), 137.3 (C_{pyr}), 153.7 (C_{pyr}).

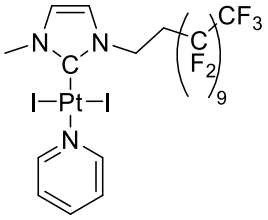

9. *Synthesized according to procedure B.* Yellow solid, 119.0 mg, yield 73%. ^{1}H NMR ($CDCl_3$, 300 MHz, 20 °C): δ 3.06 (m, 2H, CH_2), 3.95 (s, 3H, N-CH_3), 4.79 (t, *J*=7.7 Hz, 2H, N-CH_2), 6.89 (m, 2H, CH_{im}), 7.32 (t, *J*=6.9 Hz, 2H, H_{pyr}), 7.72 (t, *J*=7.7 Hz, 1H, H_{pyr}), 8.97 (m, 2H, H_{pyr}); ^{19}F-NMR ($CDCl_3$, 300 MHz, 20 °C): δ -126.3 (m, 2F), -123.3 (s, 2F), -122.9 (s, 2F), -121.9 (m, 10F), -113.5 (quint, *J*=16.2 Hz, 2F), -81.0 (t, *J*=10.0 Hz, 3F); ^{13}C NMR ($CDCl_3$, 75 MHz, 20 °C): δ 31.5 (t, *J*=21.3 Hz, CH_2), 38.5 (N-CH_3), 43.0 (N-CH_2), 104.1-115.8 (m, CF), 117.7 (t, *J*=32.4 Hz, CF), 119.0 (t, *J*=33.0 Hz, CF), 120.9 (CH_{im}), 122.6 (CH_{im}), 125.1 (C_{pyr}), 137.7 (C_{pyr}), 153.7 (C_{pyr}).

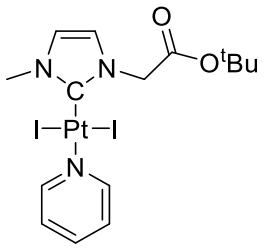

10. *Synthesized according to procedure B.* Yellow solid, 61.9 mg, yield 91%. ^{1}H NMR ($CDCl_3$, 300 MHz, 20 °C): δ 1.51 (s, 9H, $C(CH_3)_3$), 3.95 (s, 3H, N-CH_3), 5.22 (s, 2H, N-CH_2), 6.88 (d, *J*=2.1 Hz, 1H, CH_{im}), 7.00 (d, *J*=2.1 Hz, 1H, CH_{im}), 7.32 (t, *J*=6.7 Hz, 2H, H_{pyr}), 7.72 (tt, J_1=6.7 Hz, J_2=1.2 Hz, 1H, H_{pyr}), 9.02 (m, 2H, H_{pyr}); ^{13}C NMR ($CDCl_3$, 75 MHz, 20 °C): δ 28.2 (CH_3), 38.3 (N-CH_3), 52.1 (N-CH_2), 83.0 (O-C), 121.8, 122.2 (CH_{im}), 125.0 (C_{pyr}), 137.5 (C_{pyr}), 137.6 (C-Pt), 153.7 (C_{pyr}), 166.2 (C=O); MS (positive ESI) [M + Na]: calculated for $C_{15}H_{21}I_2N_3Pt_1O_2Na$ 746.9264, found 746.9299, [M_2 + Na]: calculated for $C_{30}H_{42}I_4N_6Pt_2O_4Na$ 1470.8627, found 1470.8629, [M-I]: calculated for $C_{15}H_{21}I_1N_3Pt_1O_2$ 597.0322, found 597.0371.

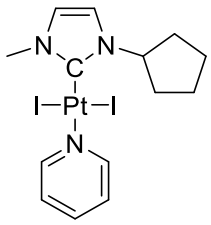

11. *Synthesized according to procedure B.* Yellow solid, 42.6 mg, yield 67%. ^{1}H NMR ($CDCl_3$, 300 MHz, 20 °C): δ 1.53-1.91 (m, 6H, CH_2), 2.41 (m, 2H, CH_2), 3.92 (s, 3H, N-CH_3), 5.77 (q, *J*=7.9 Hz, 1H, N-CH), 6.85 (m, 2H, CH_{im}), 7.30 (m, 2H, H_{pyr}), 7.71 (tt, J_1=7.7 Hz, J_2=1.6 Hz, 1H, H_{pyr}), 9.04 (m, 2H, H_{pyr}); ^{13}C NMR ($CDCl_3$, 75 MHz, 20 °C): δ 24.3 (CH_2), 33.1 (CH_2), 38.2 (N-CH_3), 61.3 (CH), 116.8 (CH_{im}), 122.5 (CH_{im}), 124.9 (C_{pyr}), 134.8 (C-Pt), 137.4 (C_{pyr}), 153.8 (C_{pyr}); MS (positive ESI) [M-e-]: calculated for $C_{14}H_{19}I_2N_3Pt$: 677.93, found 677.92, [M-2I-H]: calculated for $C_{14}H_{18}N_3Pt$: 423.11, found 423.11, [M-I]: calculated for $C_{14}H_{19}IN_3Pt$: 551.03, found 551.02.

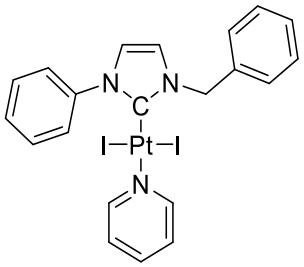

12. *Synthesized according to procedure B.* Yellow solid, 43 mg, yield 63%. ^{1}H NMR ($CDCl_3$, 300 MHz, 20 °C): δ 5.85 (s, 2H, N-CH_2), 6.76 (d, *J*=2.0 Hz, 1H, CH_{im}), 7.07 (d, *J*=2.0 Hz, 1H, CH_{im}), 7.22-7.66 (m, 11H, CH_{ar} + CH_{pyr}, overlap $CDCl_3$), 8.00 (m, 2H, H_{pyr}), 8.84 (m, 2H, H_{pyr}); ^{13}C NMR ($CDCl_3$, 75 MHz, 20 °C): δ 55.3 (N-CH_2), 120.6 (CH_{im}), 122.7 (CH_{im}), 124.9 (C_{pyr}), 126.5 (C_{pyr}), 126.9 (CH_{ar}), 128.6-129.0 (CH_{ar}), 129.5 (CH_{ar}), 135.3 (C_{ar}), 137.4 (CH_{ar}), 140.2 (N-C_{ar}), 153.8 (C_{pyr}). The carbene resonance peak could not be seen.

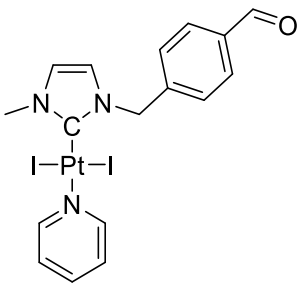

13. *Synthesized according to procedure B.* Yellow solid, 54.6 mg, yield 80%. ^{1}H NMR ($CDCl_3$, 300 MHz, 20 °C): δ 4.02 (s, 3H, N-CH_3), 5.83 (s, 2H, N-CH_2), 6.63 (d, *J*=2.1 Hz, 1H, CH_{im}), 6.88 (m, 1H, CH_{im}), 7.33 (m, 2H, H_{pyr}), 7.63 (m, 2H, H_{ar}), 7.73 (m, 1H, H_{pyr}), 7.90 (m, 2H, H_{ar}), 9.02 (m, 2H, H_{pyr}), 10.02 (s, 1H, CHO); ^{13}C NMR ($CDCl_3$, 75 MHz, 20 °C): δ 38.5 (N-CH_3), 54.2 (N-CH_2), 119.9 (CH_{im}), 122.8 (CH_{im}), 125.0 (C_{pyr}), 129.4 (C_{ar}), 130.2 (C_{ar}), 136.3 (C_{ar}), 137.5 (C_{pyr}), 137.7 (C-Pt), 142.2 (C_{ar}), 153.7 (C_{pyr}), 191.7 (CHO).

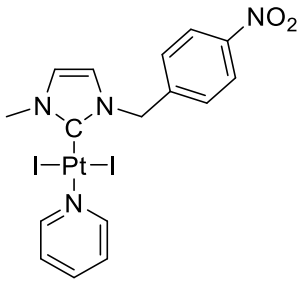

14. *Synthesized according to procedure B.* Yellow solid, 60.2 mg, yield 86%. ^{1}H NMR ($CDCl_3$, 300 MHz, 20 °C): δ 4.01 (s, 3H, N-CH_3), 5.85 (s, 2H, N- CH_2), 6.68 (d, *J*=2.1 Hz, 1H, CH_{im}), 6.92 (d, *J*=2.1 Hz, 1H, CH_{im}), 7.32 (t, *J*=7.0 Hz, 2H, H_{pyr}), 7.65 (d, *J*=8.7 Hz, 2H, H_{ar}), 7.72 (tt, J_1=7.8 Hz, J_2=1.6 Hz, 1H, H_{pyr}), 8.22 (d, *J*=8.7 Hz, 2H, H_{ar}), 8.99 (m, 2H, H_{pyr}); ^{13}C NMR ($CDCl_3$, 75 MHz, 20 °C): δ 38.6 (N-CH_3), 53.7 (N-CH_2), 120.2 (CH_{im}), 123.2 (CH_{im}), 124.1 (C_{ar}), 125.1 (C_{pyr}), 129.6 (C_{ar}), 137.7(C_{pyr}), 138.2 (C-Pt), 142.8 (C_{ar}), 147.9 (C_{ar}), 153.7 (C_{pyr}).

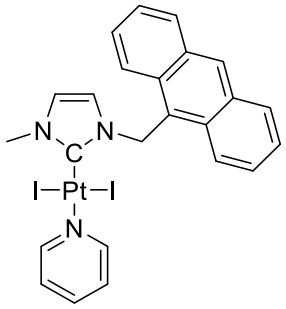

15. *Synthesized according to procedure B.* Yellow solid, 93.9 mg, yield 63%. ^{1}H NMR ($CDCl_3$, 300 MHz, 20 °C): δ 4.04 (s, 3H, N-CH_3), 5.98 (d, *J*=2.1 Hz, 1H, CH_{imid}), 6.58 (d, 2H, N-CH_2), 6.60 (d, *J*=1.8 Hz, 1H, CH_{imid}), 7.39 (m, 2H, $2CH_{pyr}$), 7.55 (m, 4H, $4H_{Anth}$), 7.77 (m, 1H, CH_{pyr}), 8.09 (d, *J*=7.8 Hz, 2H, $2H_{Anth}$), 8.46 (d, *J*=5.7 Hz, 2H, $2H_{Anth}$), 8.59 (s, 1H, H_{pyr}), 9.18 (m, 2H, $2H_{pyr}$) ppm; ^{13}C NMR

($CDCl_3$, 75 MHz, 20 °C): δ 38.5 (N-CH_3), 48.0 (N-CH_2), 119.8 (CH_{imid}), 121.4 (CH_{imid}), 124.6 (C_{pyr}), 124.7 (C_{Ar}), 125.6 (C_{Ar}), 127.6 (C_{Ar}), 129.2 (C_{Ar}), 129.5 (C_{Ar}), 131.5 (C_{Ar}), 131.6 (C_{Ar}), 131.7 (C_{Ar}), 135.7 (C_{pyr}), 137.6 (C_{pyr}), 153.9 (C_{pyr}); MS (positive ESI): m/z calcd for $C_{24}H_{21}IN_3Pt$ [M – I] 673.043; found 673.045. UV-vis (CH_2Cl_2): λ_{max} (ε, M^{-1} cm^{-1}) = 276 (9480), 334 (3490), 351 (5930), 368 (8890), 389 (8230) nm; Luminescent properties: λ_{exc} = 368 nm; λ_{em} = 400–470 nm. $C_{24}H_{21}I_2N_3Pt$ (800.35): calcd. C 36.02, H 2.64, N 5.25; found C 35.61, H 2.77, N 5.63.

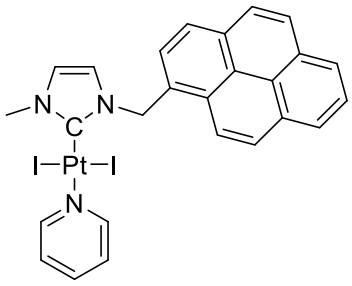

16. *Synthesized according to procedure B.* Yellow solid, 46.5 mg, yield 60%. ^{1}H NMR ($CDCl_3$, 300 MHz, 20 °C): δ 4.04 (s, 3H, N-CH_3), 6.26 (d, *J*=2.0 Hz, 1H, CH_{im}), 6.36 (s, 2H, N-CH2), 6.69 (d, *J*=2.0 Hz, 1H, CH_{im}), 7.35 (ddd, J_1= 7.6 Hz, J_2=5.2 Hz, J_3=1.3 Hz, 2H, $2H_{pyr}$), 7.74 (tt, J_1=7.6 Hz, J_2=1.5 Hz, 1H, $1H_{pyr}$), 7.99-8.26 (m, 8H, $8H_{ar}$), 8.55 (d, *J*=9.2 Hz, 1H, $1H_{ar}$), 9.12 (m, 2H, $2H_{pyr}$); ^{13}C NMR ($CDCl_3$, 75 MHz, 20 °C): δ 38.6 (N-CH_3), 53.6 (N-CH_2), 120.1, 121.9 ($CH_{im}CH$), 124.0, 124.7, 125.0, 125.1, 125.7, 125.8, 126.4, 127.5, 127.7, 128.2, 128.9, 129.1, 130.0, 131.0, 131.3, 132.1 (C_{ar} + C_{pyr}), 136.1 (C-Pt), 137.6 (C_{pyr}), 153.9 (C_{pyr}).

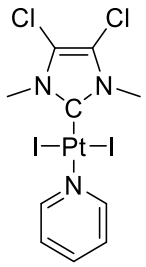

17. *Synthesized according to procedure B.* Yellow solid, 48.1 mg, yield 74%. ^{1}H NMR ($CDCl_3$, 300 MHz, 20 °C): δ 3.97 (s, 6H, N-CH_3), 7.34 (ddd, J_1=7.6 Hz, J_2=5.0 Hz, J_3=1.3 Hz, 2H, H_{pyr}), 7.74 (tt, J_1=7.7 Hz, J_2=1.5 Hz, 1H, H_{pyr}), 9.01 (m, 2H, H_{pyr}); ^{13}C NMR ($CDCl_3$, 75 MHz, 20 °C): δ 36.5 (N-CH_3), 116.1 (C_{im}), 125.0 (C_{pyr}), 137.7 (C_{pyr}), 153.7 (C_{pyr}); MS (positive ESI) [M-I]: calculated for

$C_{10}H_{11}Cl_{2}I1N_3Pt_1$: 565.9014, found 565.8937, [M-I + CH_3CN]: calculated for $C_{10}H_{11}Cl_2I_1N_3Pt_1CH_3CN$: 606.9280, found 606.9159.

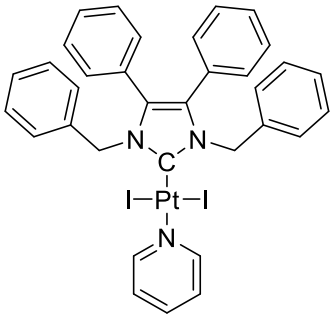

18. *Synthesized according to procedure B.* Yellow solid, 51.9 mg, yield 74%. ^{1}H NMR ($CDCl_3$, 300 MHz, 20 °C): δ 5.94 (s, 4H, N-CH_2), 6.93-7.02 (m, 4H, H_{ar}), 7.05-7.33 (m, 18H, H_{ar} + H_{pyr}), 7.68 (tt, J_1=7.7 Hz, J_2=1.6 Hz, 1H, H_{pyr}), 8.94 (m, 2H, H_{pyr}); ^{13}C NMR ($CDCl_3$, 75 MHz, 20 °C): δ 53.8 (N-CH_2), 124.9 (C_{pyr}), 127.3 (C_{im}), 128.1 (C_{im}), 128.2 (C_{ar}), 128.5 (C_{ar}), 128.6, 130.8 (C_{ar}), 132.5, 136.3 (C_{ar}), 137.4 (C_{pyr}), 138.2 (C-Pt), 153.8 (C_{pyr}); MS (positive ESI) [M-I]: calculated for $C_{34}H_{29}I_1N_3Pt_1$: 801.1051, found 801.1014, [M-I+CH_3CN]: calculated for $C_{34}H_{29}I_1N_3Pt_1CH_3CN$: 842.1317, found 842.1240.

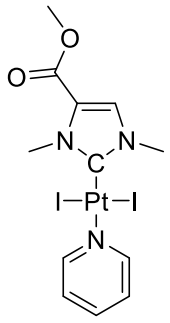

19. *Synthesized according to procedure B.* Yellow solid, 99 mg, yield 64%. ^{1}H NMR ($CDCl_3$, 300 MHz, 20 °C): δ 3.83 (s, 3H, CH_3), 3.99 (s, 3H, CH_3), 4.27 (s, 3H, N-CH_3), 7.32 (m, 1H, CH_{pyr}), 7.53 (s, 1H, CH_{im}), 7.73 (m, 1H, CH_{pyr}), 8.99 (m, 1H, CH_{pyr}); ^{13}C NMR ($CDCl_3$, 75 MHz, 20 °C): δ 37.9 (CH_3), 38.9 (N-CH_3), 52.1 (N-CH_2), 124.3 (C_{im}), 125.1 (C_{pyr}), 128.7 (CH_{im}), 137.8 (C_{pyr}), 143.8 (C-Pt), 153.7 (C_{pyr}), 158.9 (C=O).

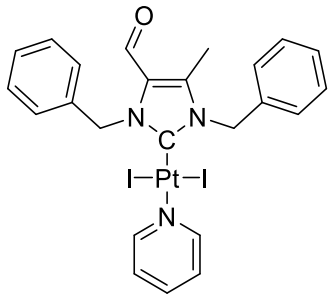

20. *Synthesized according to procedure B.* Yellow solid, 68.4 mg, yield 89%. ^{1}H NMR ($CDCl_3$, 300 MHz, 20 °C): δ 2.24 (s, 3H, CH_3), 6.07 (s, 2H, N-CH_2), 6.27 (s, 2H, N-CH_2), 7.21-7.63 (m, 12H, H_{ar} and H_{pyr}), 7.68 (tt, J_1=7.6 Hz, J_2=1.5 Hz, 1H, 1H_{pyr}), 8.93 (m, 2H, 2 H_{pyr}), 9.47 (s, 1H, CHO); ^{13}C NMR ($CDCl_3$, 75 MHz, 20 °C): δ 10.3 (CH_3), 53.7 (N-CH_2), 54.1 (N-CH_2), 124.9 (C_{pyr}), 127.6, 127.7, 127.9, 128.2, 128.4 (C_{ar}), 128.5 (C_{im}), 128.9 (C_{ar}), 134.4 (C_{ar}), 135.8 (C_{ar}), 137.7 (C_{pyr}), 142.0 (C_{im}), 147.1 (C-Pt), 153.5 (C_{pyr}), 176.7 (CHO); MS (positive ESI) [M_2 + Na]: calculated for $C_{48}H_{46}I_4N_6NaO_2Pt_2$: 1658.9054, found 1658.9061, [M + Na]: calculated for $C_{24}H_{23}I_2N_3NaOPt$: 840,9473, found 840.9451, [M+H]: calculated for $C_{24}H_{23}I_2N_3OPtH$: 818,9653, found 818.9620, [M-I + CH_3CN]: calculated for $C_{26}H_{26}IN_4OPt$: 732,07996, found 732.0810, [M-I]: calculated for $C_{24}H_{23}IN_3OPt$: 691,0530, found 691.0540, [M-I2-H]: calculated for $C_{24}H_{22}N_3OPt$: 563,1407, found 563.1443.

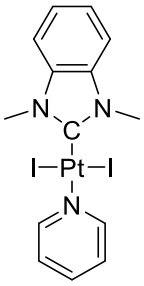

21. *Synthesized according to procedure B.* Yellow solid, 46 mg, yield 73%. ^{1}H NMR ($CDCl_3$, 300 MHz, 20 °C): δ 4.17 (s, 6H, 2N-CH_3), 7.21-7.36 (m, 6H, 2H_{pyr}, 4H_{ar}), 7.7 (t, J=7 Hz, 1H, 1H_{pyr}), 9.07 (m, 2H, 2H_{pyr}); ^{13}C NMR ($CDCl_3$, 75 MHz, 20 °C): δ 34.9 (N-CH_3), 109.9 (CH_{ar}), 122.9 (CH_{ar}), 125.1 (CH_{pyr}), 134.7 (C_{ar}), 137.7 (CH_{pyr}), 149.9 (C-Pt), 153.6 (CH_{pyr}); HRMS (positive ESI): m/z calcd for $C_{14}H_{15}IN_3Pt$ [M- I] 546.9958; found 547.0036; m/z calcd for $C_{34}H_{29}IN_3PtCH_3CN$ [M – I + CH_3CN]

842.1319; found 842.1340. $C_{14}H_{15}I_2N_3Pt$ (674.19): calcd. C 24.94, H 2.24, N 6.23; found C 24.59, H 2.47, N 6.53.

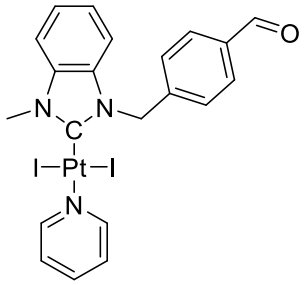

22. *Synthesized according to procedure B.* Yellow solid, 52.6 mg, yield 72%. ^{1}H NMR ($CDCl_3$, 300 MHz, 20 °C): δ 4.38 (s, 3H, N-CH_3), 6.28 (s, 2H, N-CH_2), 7.00-7.15 (m, 2H, CH_{ar}), 7.23-7.43 (m, 4H, CH_{ar}), 7.66-7.88 (m, 5H, CH_{ar}), 9.02 (m, 2H, CH_{pyr}), 9.98 (s, 1H, NC*H*N); ^{13}C NMR ($CDCl_3$, 75 MHz, 20 °C): δ 34.8 (N-CH_3), 52.2 (N-CH_2), 110.4 (C_{im}), 111.1 (C_{im}), 123.4 (C_{ar}), 123.5 (C_{ar}), 125.1 (C_{pyr}), 128.4 (C_{ar}), 130.2 (C_{ar}), 133.7 (C_{pyr}), 135.3 (C-Pt), 136.2 (C_{ar}), 138.1 (C_{ar}), 142.2 (C_{ar}), 152.6 (C_{pyr}), 191.8 (CHO).

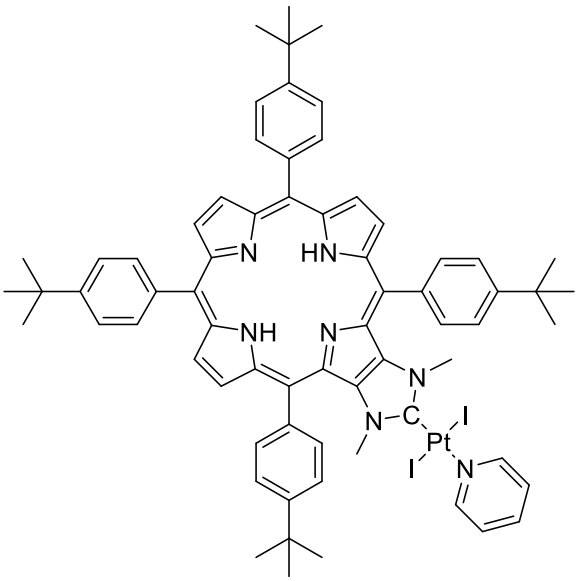

23. *Synthesized according to procedure B.* Dark red-green solid, 15 mg, yield 52%. ^{1}H NMR ($CDCl_3$, 500 MHz, 20 °C): δ -2.84 (bs, 2H, $NH_{pyrrole}$), 1.62 (s, 18H, H_{tBu}), 1.64 (s, 18H, H_{tBu}), 3.40 (s, 6H, H_{NMe}), 7.30 (m, 2H, H_{pyr}*meta*), 7.71 (tt, J_1=7.6 Hz, J_2=1.5 Hz, 1H, H_{pyr}*para*), 7.80 (d, *J*=8.2 Hz, 4H, H_{ar}), 7.91 (d, *J*=8.2 Hz, 4H, H_{ar}), 8.20 (d, *J*=8.2 Hz, 4H, H_{ar}), 8.44 (d, *J*=8.2 Hz, 4H, H_{ar}), 8.73 (s,

2H, $H_{pyrrole}$), 8.85 (d, *J*=5.1 Hz, 2H, $H_{pyrrole}$), 8.90 (d, *J*=5.1 Hz, 2H, $H_{pyrrole}$), 9.04 (m, 2H, H_{pyr}*ortho*); ^{13}C NMR ($CDCl_3$, 160 MHz, 20 °C): δ 1.2, 31.8, 35.1, 35.2, 37.6, 117.5, 121.1, 124.0, 125.0, 125.1, 128.3, 128.5, 134.2, 135.2, 136.8, 137.4, 138.8, 139.5, 142.9, 148.1 (C-Pt), 150.9, 152.4, 154.0; ESI-HRMS $C_{69}H_{71}I_2N_7Pt$ [M + H] $^+$: calc 1435.351; found 1435,348; UV-vis (CH_2Cl_2) λ_{max} (nm): 231, 433, 539.

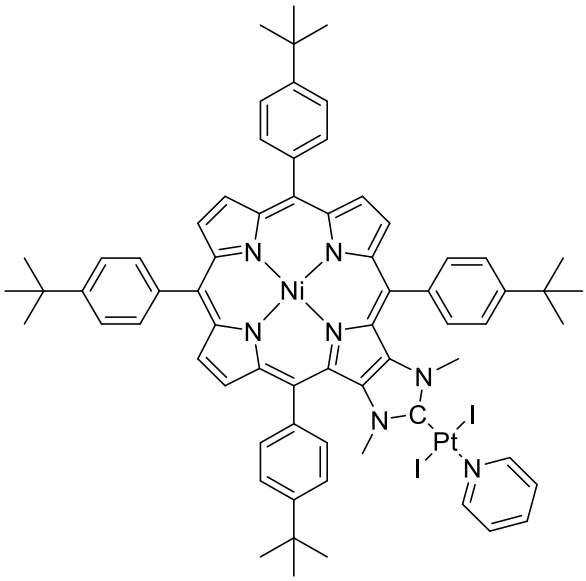

24. *Synthesized according to procedure B.* Dark red-green solid, 12.2 mg, yield 41%. ^{1}H NMR ($CDCl_3$, 500 MHz, 20 °C): δ 1.56 (s, 18H, H_{tBu}), 1.57 (s, 18H, H_{tBu}), 3.36 (s, 6H, H_{NMe}), 7.31 (m, 2H, H_{pyr}*meta*), 7.70 (d + m, *J*=8.2Hz, 5H, H_{ar} + H_{pyr}*para*), 7.78 (d, *J*=8.2 Hz, 4H, H_{ar}), 7.95 (d, *J*=8.2 Hz, 4H, H_{ar}), 8.08 (d, *J*=8.2 Hz, 4H, H_{ar}), 8.65 (q, J_1=5.5 Hz, J_2=5.3 Hz, 4H,), 8.69 (s, 2H, $H_{pyrrole}$), 9.03 (m, 2H, H_{pyr}*ortho*); ^{13}C NMR ($CDCl_3$, 160 MHz, 20 °C): δ 1.81, 31.7, 35.0, 35.2, 37.9, 115.8, 120.3, 124.2, 125.0, 125.1, 126.8, 132.2, 132.4, 132.7, 134.1, 135.2, 137.3, 137.9, 141.2, 142.9, 143.5, 144.5, 149.9 (C-Pt), 151.0, 152.5, 154.1; ESI-HRMS $C_{69}H_{71}I_2N_7PtNi$ [M + H] $^+$: calc 1491.265; found 1491,264; UV-vis (CH_2Cl_2) λ_{max} (nm): 229, 433, 525.

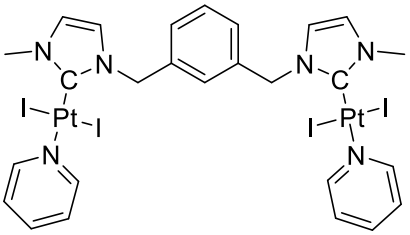

25. *Synthesized according to procedure B.* Yellow solid, 64.6 mg, yield 52%. ^{1}H NMR ($CDCl_3$, 300 MHz, 20 °C): δ 3.98 (s, 6H, N-CH_3), 5.74 (s, 4H, N-CH_2), 6.77 (s, 2H, CH_{im}), 6.86 (s, 2H, CH_{im}), 7.33 (t, *J*=6.7 Hz, 4H, H_{pyr}), 7.41 (t, *J*=7.7 Hz, 1H, H_{ar}), 7.55 (d, *J*=7.7 Hz, 2H, H_{ar}), 7.64 (s, 1H, H_{ar}), 7.72 (td, J_1=7.7 Hz, J_2=1.5 Hz, 2H, H_{pyr}), 9.03 (m, 4H, H_{pyr}); ^{13}C NMR ($CDCl_3$, 75 MHz, 20 °C): δ 38.4 (N-CH_3), 54.1 (N-CH_2), 120.4, 122.5 (CH_{im}), 124.9 (C_{pyr}), 128.8-129.3 (C_{ar}), 136.1 (C_{ar}), 136.3 (C-Pt), 137.5 (C_{pyr}), 153.5 (C_{pyr}); MS (positive ESI) [M + H]: calculated for $C_{26}H_{28}I_4N_6Pt_2H$: 1322.7910, found 1322.7953, [M-I]: calculated for $C_{26}H_{28}I_3N_6Pt_2$: 1194.8787, found 1194.8878, [M-I-C_5H_5N]: calculated for $C_{21}H_{23}I_3N_5Pt_2$: 1115.8364, found 1115.8524, [M-I-2C5H5N]: calculated for $C_{16}H_{18}I_3N_4Pt_2$: 1036.7941, found 1036.8088, [M-I-H-2C_5H_5N]: calculated for $C_{16}H_{17}I_2N_4Pt_2$: 908.8819, found 908.8875.

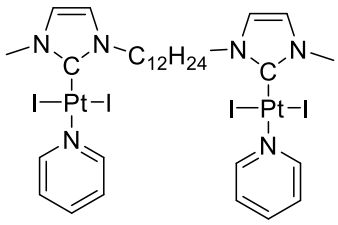

26. *Synthesized according to procedure B.* Yellow solid, 82.1 mg, yield 63%. ^{1}H NMR ($CDCl_3$, 300 MHz, 20 °C): δ 1.27-1.48 (m, 16H, CH_2), 2.04 (m, 4H, CH_2), 3.95 (s, 6H, N-CH_3), 4.42 (t, *J*=7.5 Hz, 4H, N-CH_2), 6.86 (s, 4H, CH_{im}), 7.33 (ddd, J_1=7.7 Hz, J_2=5.0 Hz, J_3=1.4 Hz, 4H, H_{pyr}), 7.73 (tt, J_1=7.7 Hz, J_2=1.6 Hz, 2H, H_{pyr}), 9.03 (m, 4H, H_{pyr}); ^{13}C NMR ($CDCl_3$, 75 MHz, 20 °C): δ 26.7-29.5 (CH_2), 38.3 (N-CH_3), 50.8 (N- CH_2), 120.4 (CH_{im}), 121.9 (CH_{im}), 124.9 (C_{pyr}), 134.9 (C-Pt), 137.5 (C_{pyr}), 153.6 (C_{pyr}).

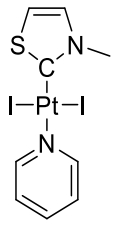

27. *Synthesized according to procedure B.* Yellow solid, 29.6 mg, yield 67 %. ^{1}H NMR ($CDCl_3$, 300 MHz, 20 °C): δ 4.17 (s, 3H, N-CH_3), 7.34 (ddd, J_1=7.7 Hz, J_2=5.0 Hz, J_3=1.6 Hz, 2H, H_{pyr}), 7.43 (d, J=3.9 Hz, 1H, CH_{im}), 7.50 (d, J=3.9 Hz, 1H, CH_{im}), 7.74 (tt, J_1=7.7 Hz, J_2=1.6 Hz, 1H, H_{pyr}), 9.00 (m, 2H, H_{pyr}); ^{13}C NMR ($CDCl_3$, 75 MHz, 20 °C): δ 44.5 (N-CH_3), 124.7 (C_{pyr}), 125.2, 135.9 (CH_{im}), 137.9 (C_{pyr}), 153.9 (C_{pyr}), 167.1 (C-Pt); MS (positive ESI) [M + Na]: calculated for $C_9H_{10}I_2N_2PtSNa$: 649.8195, found 649.8199, [M-I]: calculated for $C_9H_{10}I_1N_2Pt_S$: 499.9252, found 499.9234, [M-I+CH_3CN]: calculated for $C_9H_{10}I_1N_2Pt_S$ CH_3CN: 540.9518, found 540.9480.

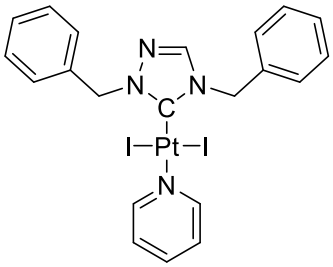

28. *Synthesized according to procedure B.* Yellow solid, 81.1 mg, yield 46%. ^{1}H NMR ($CDCl_3$, 300 MHz, 20 °C): δ 5.72 (s, 2H, N-CH_2), 5.85 (s, 2H, N-CH_2), 7.20-7.80 (m, 14H, H_{ar} + CH_{im} + H_{pyr}), 9.03 (m, 2H, H_{pyr}); ^{13}C NMR ($CDCl_3$, 75 MHz, 20 °C): δ 53.0 (N- CH_2), 56.5 (N- CH_2), 125.1 (CH_{ar}), 128.4 (CH_{ar}), 128.6 (CH_{ar}), 129.0 (CH_{ar}), 129.2 (CH_{ar}), 129.3 (CH_{ar}), 129.4 (CH_{ar}), 133.6 (C_{ar}), 134.5 (C_{ar}), 137.8 (C_{pyr}), 142.2 (C_{ar} + CH_{im} + C_{Pyr}), 143.7 (C-Pt), 153.7 (C_{pyr}).

- **Procedure C: Ligand exchange on NHC-Pt(II)-pyridine complexes**

The [(NHC)PtI_2(pyridine)] complex (10 mg, 1 equiv.) was reacted with the amine ligand (5 equiv.) in EtOH (2 mL) at 50 °C overnight. The resulting mixture was concentrated under reduced pressure, then dissolved in dichloromethane and subsequently precipitated by addition of pentane to afford the complex as light yellow powders in quantitative yield.

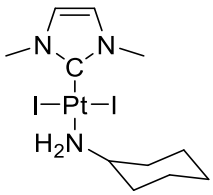

29. *Synthesized according to procedure C.* Yellow solid, 25.6 mg, quant. ^{1}H NMR ($CDCl_3$, 300 MHz, 20 °C): δ 1.13-1.30 (m, 5H, CH_2), 1.73-1.78 (m, 3H, CH_2), 2.25 (m, 2H, CH_2), 2.88 (m, 2H, NH_2), 3.21 (m, 1H, CH), 3.83 (s, 6H, N-CH_3), 6.78 (s, 2H, CH_{im}); ^{13}C NMR ($CDCl_3$, 75 MHz, 20 °C): δ 24.9 (CH_2), 25.4 (CH_2), 35.9 (CH_2), 38.0 (N-CH_3), 54.8 (N-CH_2), 121.7 (CH), 139.5 (C-Pt).

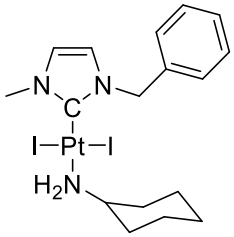

30. *Synthesized according to procedure C.* Yellow solid, 15.4 mg, quant. ^{1}H NMR ($CDCl_3$, 300 MHz, 20 °C): δ 0.96-1.32 (m, 5H, CH_2), 1.39-1.77 (m, 5H, CH_2), 2.71-3.00 (m, 2H, NH_2), 3.08-3.29 (m, 1H, CH), 3.81 (s, 3H, N-CH_3), 5.51 (s, 2H, N-CH_2), 6.47 (d, *J*=1.8 Hz, 1H, CH_{im}), 6.69 (d, *J*=1.9 Hz, 1H, CH_{im}), 7.29-7.50 (m, 5H, H_{ar}); ^{13}C NMR ($CDCl_3$, 75 MHz, 20 °C): δ 24.9 (CH_2), 25.3 (CH_2), 35.9 (CH_2), 38.1 (N-CH_3), 54.4 (N-CH_2), 54.9 (CH), 119.9 (CH), 122.2 (CH), 128.3 (C_{ar}), 128.8 (C_{ar}), 129.1 (C_{ar}), 135.5 (C_{ar}), 139.9 (C-Pt). HRMS (positive ESI) [M-I]: Calculated for $C_{17}H_{25}IN_3Pt$ 593.074, found 593.071. Microanalysis: Calculated for $C_{17}H_{25}I_2N_3Pt$: C, 28.35; H, 3.50; N, 5.83. Found: C, 27.98; H, 3.42; N, 5.56.

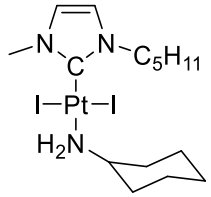

31. *Synthesized according to procedure C.* Yellow solid, 15.4 mg, quant. ^{1}H NMR ($CDCl_3$, 300 MHz, 20 °C): δ 0.92 (t, *J*=6.7 Hz, 3H, CH_3), 1.15-1.39 (m, 9H, CH_2), 1.61 (m, 1H, CH_2), 1.75 (m, 2H, CH_2), 1.97 (m, 2H, CH_2), 2.26 (m, 2H, CH_2), 2.89 (bs, 2H, NH_2), 3.24 (m, 1H, H_2N-C*H*), 3.84 (s, 3H, N-CH_3), 4.31 (m, 2H, N-CH_2), 6.79 (s, 2H, CH_{im}); ^{13}C NMR ($CDCl_3$, 75 MHz, 20 °C): δ 14.1 (CH_2),

22.4 (CH_2), 24.9 (CH_2), 25.4 (CH_2), 28.9 (CH_2), 29.5 (CH_2), 36.0 (N-CH_3), 38.2 (CH_2), 50.8 (H_2N-CH), 54.9 (N-CH_2), 120.4 (CH_{im}), 121.8 (CH_{im}), 138.7 (C-Pt).

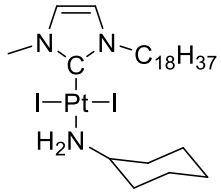

32. *Synthesized according to procedure C.* Yellow solid, 15.3 mg, quant. ^{1}H NMR ($CDCl_3$, 300 MHz, 20 °C): δ 0.87 (t, 3H, *J*=6.5 Hz, CH_3), 1.25 (m, 30H, CH_2), 1.61 (m, 1H, CH_2), 1.75 (m, 2H, CH_2), 1.96 (m, 2H , CH_2), 2.28 (m, 2H, CH_2), 2.90 (bs, 2H, NH_2), 3.25 (m, 1H, N-CH), 3.84 (s, 3H, N-CH_3), 4.30 (m, 2H, N-CH_2), 6.78 (s, 2H, CH_{im}); ^{13}C NMR ($CDCl_3$, 75 MHz, 20 °C): δ 14.2 (CH_3), 22.8 (CH_2), 26.8 (CH_2), 29.3 (CH_2), 29.4 (CH_2), 29.5 (CH_2), 29.6 (CH_2), 29.7 (CH_2), 29.8 (CH_2), 29.8 (CH_2), 31.0 (CH_2), 32.0 (CH_2), 38.3 (CH_2), 49.9 (CH_2), 50.6 (CH_2), 50.9 (CH_2), 53.5 (N-CH_3), 68.6 H_2N-CH), 68.9 (N-CH_2), 120.4 (CH_{im}), 121.9 (CH_{im}), C-Pt could not be seen.

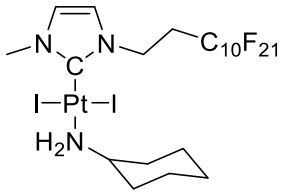

33. *Synthesized according to procedure C.* Yellow solid, 15.1 mg, quant. ^{1}H NMR ($CDCl_3$, 300 MHz, 20 °C): δ 1.10-1.40 (m, 8H, CH_2), 1.62-1.79 (m, 4H, CH_2), 2.25-2.29 (m, 2H, CH_2), 2.95 (m, 2H, NH_2), 3.24 (m, 1H, CH), 3.86 (s, 3H, N-CH_3), 4.86 (m, 2H, N-CH_2), 6.85 (m, 2H, CH_{im}); ^{19}F NMR ($CDCl_3$, 75 MHz, 20 °C): δ -126.1 (m, 2F), -123.3 (m, 2F), -122.7 (m, 2F), -121.5 (m, 11F), -113.4 (m, 2F), -80.7 (m, 2F).

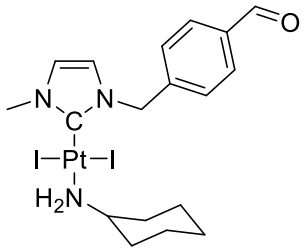

34. *Synthesized according to procedure C.* Yellow solid, 15.4 mg, quant. ^{1}H NMR ($CDCl_3$, 300 MHz, 20 °C): δ δ 1.05-1.35 (m, 5H, CH_2), 1.55-1.87 (m, 3H, CH_2), 2.25 (d, *J*=11.7 Hz, 2H, CH_2), 2.95 (m, 2H, NH_2), 3.27 (m, 1H, CH), 3.90 (s, 3H, N-CH_3), 5.70 (s, 2H, N-CH_2), 6.63 (s, 1H, CH_{im}), 6.85 (s, 1H, CH_{im}), 7.59 (d, *J*=8.1 Hz, 2H, H_{ar}), 7.87 (d, *J*=8.1Hz, 2H, H_{ar}), 10.01 (s, 1H, CHO); ^{13}C NMR ($CDCl_3$, 75 MHz, 20 °C): δ 24.8 (CH_2), 25.3 (CH_2), 35.9 (CH_2), 38.3 (N-CH_3), 53.9 (CH), 54.9 (N-CH_2), 120.0 (CH_{im}), 122.6 (CH_{im}), 129.3 (C_{ar}), 130.1 (C_{ar}), 136.2 (C_{ar}), 141.1 (C-Pt), 142.2 (C_{ar}),191.7 (CHO); MS (positive ESI) [M-I]: calculated for $C_{18}H_{25}I_1N_3O_1Pt_1$ 621.069 found 621.072, [M-I+CH_3CN]: calculated for $C_{18}H_{25}I1N_3O_1Pt_1CH_3CN$ 662.095, found 662.096.

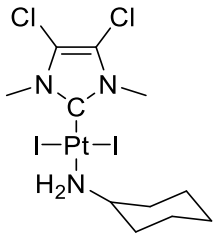

35. *Synthesized according to procedure C.* Yellow solid, 15.3 mg, 84%. ^{1}H NMR ($CDCl_3$, 300 MHz, 20 °C): δ 1.11-1.80 (m, 8H, CH_2), 2.27 (m, 2H, CH_2), 2.96 (m, 2H, NH_2), 3.24 (m, 1H, CH), 3.86 (s, 6H, N-CH_3); ^{13}C NMR ($CDCl_3$, 75 Mz, 20 °C): δ 25.0 (CH_2), 25.4 (CH_2), 36.0 (CH_2), 36.4 (N-CH2), 55.2 (CH_2), 116.1 (C_{im}), 141.3 (C-Pt).

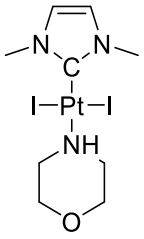

36. *Synthesized according to procedure C.* Yellow solid, 25.4 mg, quant. ^{1}H NMR ($CDCl_3$, 300 MHz, 20 °C): δ 2.88 (d, *J*=11 Hz, 2H, CH), 3.25 (bs, 1H, NH), 3.52-3.57 (m, 4H, CH), 3.81 (s, 6H, N-CH_3), 6.78 (s, 2H, CH_{im}); ^{13}C NMR ($CDCl_3$, 75 MHz, 20 °C): δ 38.1 (N-CH_3), 50.6 (CH_2), 68.8 (CH_2), 121.8 (CH_{im}), 135.8 (C-Pt).

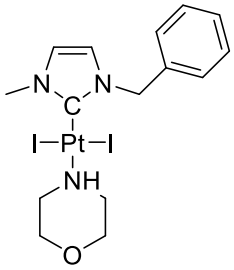

37. *Synthesized according to procedure C.* Yellow solid, 17.6 mg, yield 58%. ^{1}H NMR ($CDCl_3$, 300 MHz, 20 °C): δ 2.92 (d, *J*=11.4 Hz, 2H, CH_2), 3.15-3.45 (m, 1H, NH), 3.46-3.71 (m, 4H, CH), 3.82 (d, *J*=12.3 Hz, 2H, CH_2), 3.86 (s, 3H, N-CH_3), 5.56 (s, 2H, N-CH_2), 6.56 (s, 1H, CH_{im}), 6.77 (s, 1H, CH_{im}), 7.28-7.48 (m, 5H, H_{ar}); ^{13}C NMR ($CDCl_3$, 75 MHz, 20 °C): δ 38.2 (N-CH_3), 50.6 (CH_2), 54.5 (CH_2), 68.7 (CH_2), 120.0 (CH), 122.3 (CH), 128.3 ($CH_{aromatic}$), 128.8 ($CH_{aromatic}$), 129.1 ($CH_{aromatic}$), 135.3 ($C_{aromatic}$), 136.3 (C-Pt). HRMS (positive ESI) [M+Na]: calcd for $C_{15}H_{21}I_2N_3OPt$.Na 730.932, found 730.929.

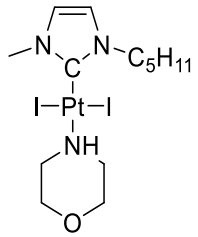

38. *Synthesized according to procedure C.* Yellow solid, 15.1 mg, yield 58%. ^{1}H NMR ($CDCl_3$, 300 MHz, 20 °C): δ 0.92 (t, *J*=6.7 Hz, 3H, CH_3), 1.38 (m, 4H, CH_2), 1.95 (m, 2H, CH_2), 2.87 (d, *J*=12.9 Hz, 2H, CH_2), 3.27 (bs, 1H, NH), 3.49-3.66 (m, 4H, CH_2), 3.80 (s+m, 5H, N-CH_3+CH_2), 4.27 (m, 2H, N-CH_2), 6.79 (s, 2H, CH_{im}); ^{13}C NMR ($CDCl_3$, 75 MHz, 20 °C): δ 14.1 (CH_3), 22.3 (CH_2), 28.9 (CH_2), 29.3 (CH_2), 38.3 (N-CH_3), 50.6 (CH_2), 50.9 (H_2N-CH), 68.9 (N-CH_2), 120.4 (CH_{im}), 121.9 (CH_{im}), 135.0 (C-Pt).

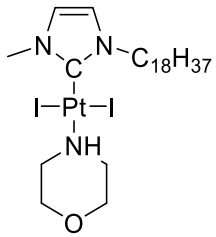

39. *Synthesized according to procedure C.* Yellow solid, 10 mg, yield 58%. ^{1}H NMR ($CDCl_3$, 300 MHz, 20 °C): δ 0.87 (t, *J*=6.6 Hz, 3H, CH_3), 1.25 (m, 30H, CH_2), 1.95 (m, 2H, CH_2), 2.88 (m, 2H, CH_2), 3.30 (bs, 1H, NH), 3.50-3.63 (m, 4H, CH_2), 3.82-4.03 (s+m, 5H, N-CH3 overlap CH_2), 4.27 (m, 2H, N-CH_2), 6.78 (s, 2H, CH_{im}); ^{13}C NMR ($CDCl_3$, 75 MHz, 20 °C): δ 13.1 (CH_3), 21.7 (CH_2), 23.8 (CH_2), 24.3 (CH_2), 25.7 (CH_2), 28.1 (CH_2), 28.2 (CH_2), 28.3 (CH_2), 28.4 (CH_2), 28.5 (CH_2), 28.6 (CH_2), 28.7 (CH_2), 29.9 (CH_2), 30.9 (CH_2), 34.8 (N-CH_3), 37.0 (CH_2), 49.7 (CH_2), 52.4 (HN-CH), 53.8 (N-CH_2), 119.2 (CH_{im}), 120.6 (CH_{im}), C-Pt could not be seen.

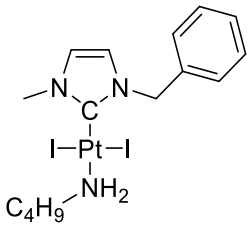

40. *Synthesized according to procedure C.* Yellow solid, 19 mg, yield 65%. ^{1}H NMR ($CDCl_3$, 300 MHz, 20 °C): δ 0.94 (t, 3H, CH_3), 1.25-1.40 (m, 2H, CH_2), 1.60 (m, 2H, CH_2), 2.99 (bs, 4H, CH_2+NH_2), 3.89 (s, 3H, N-CH_3), 5.59 (s, 2H, N-CH_2), 6.56 (d, *J*=2.1 Hz, 1H, CH_{im}), 6.77 (d, *J*=2.1 Hz, 1H, CH_{im}), 7.34-7.46 (m, 5H, H_{ar}); ^{13}C NMR ($CDCl_3$, 75 MHz, 20 °C): δ 13.8 (CH_3), 19.8 (CH_2), 31.1 (CH_2), 34.4 (CH_2), 38.3 (CH_3), 45.3 (CH_2), 54.6 (N-CH_2), 120.0 (CH_{im}), 122.4 (CH_{im}), 128.4 (C_{ar}), 128.9 (C_{ar}), 129.2 (C_{ar}), 135.6 (C_{ar}), 139.7 (C-Pt).

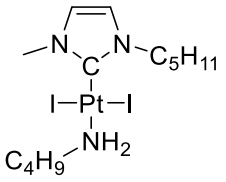

41. *Synthesized according to procedure C.* Yellow solid, 18,1 mg, yield 61%. ^{1}H NMR ($CDCl_3$, 300 MHz, 20 °C): δ 0,90-0,97 (q, 6H, CH_3), 1,36-1,43 (m, 6H, CH_2), 1,56-1,62 (m, 2H, CH_2), 1,96 (m, 2H, CH_2), 2,89-3,04 (m+bs, 4H, H_2N-CH_2), 3,84 (s, 3H, N-CH_3), 4,30 (m, 2H, N-CH_2), 6,79 (s, 2H, CH_{im}); ^{13}C NMR ($CDCl_3$, 75 MHz, 20 °C): δ 14.9 (CH_3), 14.1 (CH_3), 19.8 (CH_2), 22.4 (CH_2), 28.9 (CH_2), 29.5 (CH_2), 34.3 (CH_2), 38.3 (CH_3), 45.3(CH_2), 50.9 (CH_2), 120.4 (s+d, *J*=30.6 Hz, CH_{im}), 121.8 (s+d, *J*=30.6 Hz, CH_{im}), 138.4 (C-Pt).

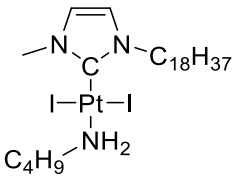

42. *Synthesized according to procedure C.* Yellow solid, 8.5 mg, yield 57%. ^{1}H NMR ($CDCl_3$, 300 MHz, 20 °C): δ 0,88-0,94 (m, 6H, CH_3), 1,30-1,42 (m, 32H, CH_2), 1,64-1,66 (m, 2H, CH_2), 1, 99 (m, 2H, CH_2), 2,91-3,02 (m+bs, 4H, H_2N-CH_2), 3,87 (s, 3H, N-CH_3), 4,33 (m, 2H, N-CH_2), 6,80 (s, 2H, CH_{im}).

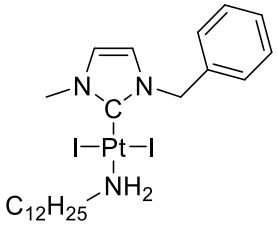

43. *Synthesized according to procedure C.* Yellow solid, 18 mg, yield 52%. ^{1}H NMR ($CDCl_3$, 300 MHz, 20 °C): δ 0.88 (t, 3H, CH_3), 1.25 (m, 20H, CH_2), 2.99 (m, 2H, NH_2), 3.89 (s, 3H, N-CH_3), 5.59 (s, 2H, N-CH_2), 6.56 (d, *J*=2.1 Hz, 1H, CH_{im}), 6.77 (d, *J*=2.1 Hz, 1H, CH_{im}), 7.34-7.46 (m, 5H, H_{ar}); ^{13}C NMR ($CDCl_3$, 75 MHz, 20 °C): δ 14.3 (CH_3), 22.8 (CH_2), 26.6 (CH_2), 29.3-30.2 (CH_2), 31.1 (CH_3), 32.1 (CH_2), 32.3 (CH_2), 38.3 (CH_3), 45.7 (CH_2), 54.6 (N-CH_2), 120.0 (CH_{im}), 122.4 (CH_{im}), 128.4 (C_{ar}), 128.9 (C_{ar}), 129.2 (C_{ar}), 135.6 (C_{ar}), 139.7 (C-Pt).

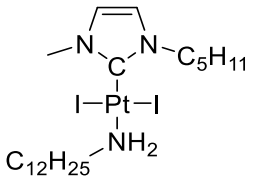

44. *Synthesized according to procedure C.* Yellow solid, 18,7 mg, yield 54%. ^{1}H NMR ($CDCl_3$, 300 MHz, 20 °C): δ 0.85-0.95 (q+q, 6H, CH_3), 1.26-1.39 (m, 22H, CH_2), 1.60-1.65 (m, 2H, CH_2), 1.96 (m, 2H, CH_2), 2.89-3.00 (m+bs, 4H, H_2N-CH_2), 3.85 (s, 3H, N-CH_3), 4.30 (m, 2H, N-CH_2), 6.79 (s, 2H, CH_{im}); ^{13}C NMR ($CDCl_3$, 75 MHz, 20 °C): δ 14.1 (CH_3), 14.3 (CH_3), 22.4 (CH_2), 22.8 (CH_2), 26.6 (CH_2), 28.9 (CH_2), 29.3 (CH_2), 29.5 (CH_2), 29.6 (CH_2), 29.7 (CH_2), 29.8 (CH_2), 32.0 (CH_2), 32.3 (CH_2), 38.3 (CH_2), 45.6 (N-CH_2), 50.9 (N-CH_2), 120.3 (CH_{im}), 121.8 (CH_{im}), 139.3 (C-Pt).

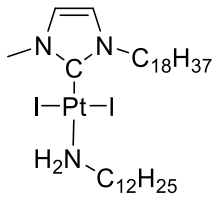

45. *Synthesized according to procedure C.* Yellow solid, 8.7 mg, yield 52%. ^{1}H NMR ($CDCl_3$, 300 MHz, 20 °C): δ 0.88 (t, J=6.7 Hz, 6H, CH_3), 1.26-1.37 (m, 48H, CH_2), 1.60-1.67 (m, 2H, CH_2), 1,.96 (m, 2H, CH_2), 2.92-2.99 (m+bs, 4H, H_2N-CH_2), 3.84 (s, 3H, N-CH_3), 4.30 (m, 2H, N-CH_2), 6.79 (s, 2H, CH_{im}).

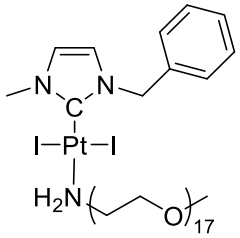

46. *Synthesized according to procedure C.* Yellow oil, 28 mg, yield 47%. ^{1}H NMR ($CDCl_3$, 300 MHz, 20 °C): δ 3.37 (s, 3H, OCH_3), 3.63-3.66 (m, 68H, CH_2 + NH_2), 3.87 (s, 3H, N-CH_3), 5.58 (s, 2H, N-CH_2), 6.55 (d, *J*=2.1 Hz, 1H, CH_{im}), 6.77 (d, *J*=2.1 Hz, 1H, CH_{im}), 7.33-7.42 (m, 5H, CH_{ar}); ^{13}C NMR ($CDCl_3$, 75 MHz, 20 °C): δ 38.3 (CH_2), 45.2 (CH_2), 54.5 (N-CH_3), 59.1 (CH_2), 70.3 (N-CH_2), 70.7 (CH_2), 72.1 (CH_3), 119.9 (CH_{im}), 122.3 (CH_{im}), 128.4 (CH_{ar}), 128.9 (CH_{ar}), 129.1 (CH_{ar}), 135.6 (C_{ar}), 139.7 (C-Pt).

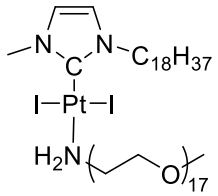

47. *Synthesized according to procedure C.* Yellow oil, 4,9 mg, yield 36%. ^{1}H NMR ($CDCl_3$, 300 MHz, 20 °C): δ 0.89 (t, *J*=6,8Hz, 3H, CH_3), 1.28 (m, 28H, CH_2), 1.95 (m, 2H, CH_2), 3.20 (bs, 2H, NH_2), 3.35 (s, 3H, O-CH_3), 3.62 (m, 70H, CH_2), 3.84 (s, 3H, N-CH_3), 4.31 (m, 2H, N-CH_2), 6.86 (s, 2H, CH_{im}); ^{13}C NMR ($CDCl_3$, 75 MHz, 20 °C): δ 14.3 (CH_3), 23.0 (CH_2), 27.1 (CH_2), 29.6 (CH_2), 29.7 (CH_2), 29.8 (CH_2), 29.9 (CH_2), 30.1 (CH_2), 30.9 (CH_2), 32.3 (CH_2), 38.3 (CH_2), 45.5 (CH_2), 51.0 (N-CH_3), 70.6 (N-CH_2), 72.3 (O-CH_3), 120.6 (CH_{im}), 120.0 (CH_{im}), 138.9 (C-Pt).

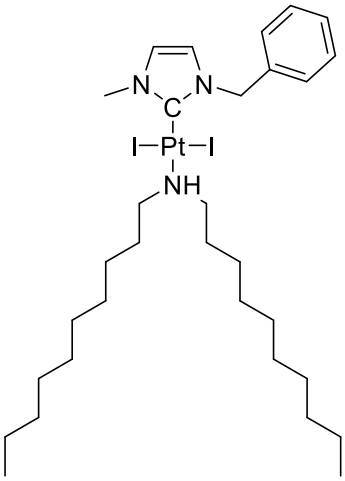

48. *Synthesized according to procedure C.* Yellow oil, 11.3 mg, yield 32%. ^{1}H NMR ($CDCl_3$, 300 MHz, 20 °C): δ 0.87 (t, *J*=6.6 Hz, 6H, CH_3), 1.23-1.43 (m, 28H, CH_2), 1.80 (m, 2H, CH_2), 2.15 (m, 2H, CH_2), 2.81 (m, 2H, CH_2), 3.28 (m, 3H, NH+CH_2), 3.88 (s, 3H, N-CH_3), 5.85 (s, 2H, N-CH_2), 6.55 (d, *J*=2.1 Hz, 1H, CH_{im}), 6.77 (d, *J*=2.1 Hz, 1H, CH_{im}), 7.33-7.49 (m, 5H, CH_{ar}); ^{13}C NMR ($CDCl_3$, 75 MHz, 20 °C): δ 14.1 (CH_3), 22.6 (CH_2), 26.9 (CH_2), 28.9 (CH_2), 29.3 (CH_2), 29.3 (CH_2), 29.4 (CH_2), 29.5 (CH_2), 31.9 (CH_2), 37.9 (N-CH_3), 54.1 (N-CH_2), 55.1 (N-CH_2), 119.7 (CH_{im}), 122.1 (CH_{im}), 128.2 (CH_{ar}), 128.8 (CH_{ar}), 129.1 (CH_{ar}), 135.4 (C_{ar}), 138.7 (C-Pt).

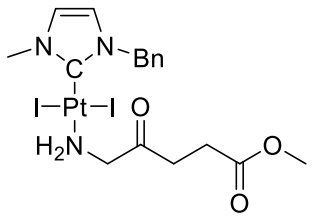

49. *Synthesized according to procedure C.* Yellow oil, 6.8 mg, yield 27%. ^{1}H NMR ($CDCl_3$, 300 MHz, 20 °C): δ 2.68 (m, 4H, CH_2), 3.35 (bs, 2H, NH_2), 3.68 (s, 3H, N-CH_3), 3.88-3.96 (s+m, 5H, CH_3+CH_2), 5.58 (s, 2H, N-CH_2), 6.57 (d, *J*=2.1 Hz, 1H, CH_{im}), 6.78 (d, *J*=2.1 Hz, 1H, CH_{im}), 7.34-7.42 (m, 5H, CH_{ar}); ^{13}C NMR ($CDCl_3$, 75 MHz, 20°C): δ 27.6, 29.8, 34.4, 38.4, 52.2, 53.9, 54.6, 120.1 (CH_{im}), 122.4 (CH_{im}), 128.5 (CH_{ar}), 128.9 (CH_{ar}), 129.1 (CH_{ar}), 135.4 (C_{ar}), 138.1 (C-Pt), 127.7 (CO).

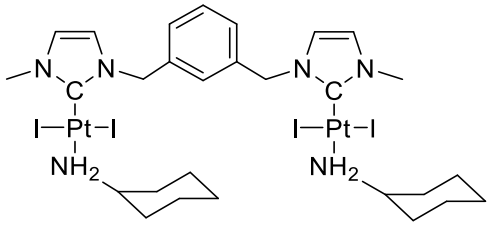

50. *Synthesized according to procedure C.* Yellow oil, 7.8 mg, yield 52%. ^{1}H NMR ($CDCl_3$, 300 MHz, 20°C): δ 3.99 (s, 6H, N-CH_3), 5.72 (s, 4H, N-CH_2), 6.74 (d, *J*=2.1 Hz, 2H, CH_{im}), 6.81 (d, *J*=2.1 Hz, 2H, CH_{im}), 7.32 (m, 4H, H_{pyr}), 7.39 (m, 1H, H_{ar}), 7.50-7.58 (m, 3H, H_{ar}), 7.71 (m, 2H, H_{pyr}), 9.04 (m, 4H, H_{pyr}).

- **Procedure D: Synthesis of Neutral NHC-Platinum-Pnictogen Complexes**

A solution of the corresponding trans [(NHC)PtI_2(pyr)] complex (1 equiv.) and the Pnictogen ligand (1.2 equiv.) in ethanol (1–5 mL) was stirred overnight at 55 °C, under argon atmosphere.[3] The crude mixture was then concentrated under reduced pressure and purified by silica gel chromatography (pentane/CH_2Cl_2, 1:1 to CH_2Cl_2) to afford the desired complex as a yellow solid.

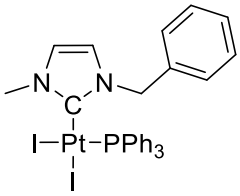

51a. *Synthesized according to procedure D*. Yellow solid, 32.1 mg, yield 51%. ^{1}H NMR ($CDCl_3$, 300 MHz, 20°C): δ 3.53 (s, 3 H, N-CH_3), 4.32 (d, *J*=14.0 Hz, 1 H, N-CH_2), 5.84 (d, *J*=14.0 Hz, 1 H, N-CH_2), 6.25 (d, *J*=2.1 Hz, 1 H, CH_{im}), 6.54 (d, *J*=2.1 Hz, 2 H, 2 H_{Ar}), 7.15–7.64 (m, 20 H, 20 H_{Ar}) ppm; ^{31}P NMR ($CDCl_3$, 121 MHz, 20°C): δ 8.46 (s + d, $J_{P,Pt}$=3684 Hz) ppm; ^{13}C NMR ($CDCl_3$, 75 MHz, 20°C): δ 37.7 (N-CH_3), 53.8 (N-CH_2), 119.8 (CH_{im}), 122.7 (CH_{im}), 128.2, 128.7, 129.6, 130.2, 131.0 (CH_{ar}), 133.8 (C_{ar}), 134.0 (CH_{ar}), 134.5 (C_{ar}), 154.0 (C-Pt) ppm. $C_{29}H_{27}I_2N_2PPt$ (883.42): calcd. C 39.43, H 3.08, N 3.17; found C 38.92, H 3.17, N 3.43.

[3] M. Bouché, G. Dahm, A. Maisse-François, T. Achard, S. Bellemin-Laponnaz *Eur. J. Inorg. Chem.* **2016**, 2828-2836

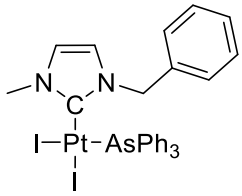

51b. *Synthesized according to procedure D.* Yellow solid, 54.2 mg, yield 82%. ^{1}H NMR ($CDCl_3$, 300 MHz, 20°C): δ 3.56 (s, 3 H, N-CH_3), 4.57 (d, *J*=14.1 Hz, 1 H, N-CH_2), 5.77 (d, *J*=14 Hz, 1 H, N-CH_2), 6.32 (d, *J*=2.1 Hz, 1 H, CH_{im}), 6.51 (d, *J*=2.1 Hz, 1 H, CH_{im}), 7.12–7.55 (m, 20 H, H_{Ar}) ppm; ^{13}C NMR ($CDCl_3$, 75 MHz, 20°C): δ 37.6 (N-CH_3), 54.0 (N-CH_2), 120.1 (CH_{im}), 122.2 (CH_{im}), 128.6, 128.9, 129.5, 130.6 and 131.8 (CH_{ar}), 133.2 (Car), 133.4 (CH_{ar}), 133.9 (C_{ar}), 151.5 (C-Pt) ppm; MS (positive ESI): *m/z* calcd for $C_{29}H_{27}IN_2AsPt$ [M – I] 800.01; found 800.00. MS (positive ESI): *m/z* calcd for $C_{29}H_{27}IN_2AsPtCH_3CN$ [M – I + CH_3CN] 841.03; found 841.03. $C_{29}H_{27}AsI_2N_2Pt$ (927.37): calcd. C 37.56, H 2.93, N 3.02; found C 36.89, H 2.98, N 3.24.

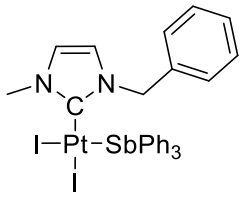

51c. *Synthesized according to procedure D.* Yellow solid, 64.0 mg, yield 92%. ^{1}H NMR ($CDCl_3$, 300 MHz, 20°C): δ 3.58 (s, 3 H, N-CH_3), 5.11 (d, *J*=14.2 Hz, 1 H, N-CH_2), 5.50 (d, *J*=14.2 Hz, 1 H, N-CH_2), 6.52 (d, *J*=2.1 Hz, 1 H, CH_{im}), 6.55 (d, *J*=2.1 Hz, 1 H, CH_{im}), 7.00–7.71 (m, 20 H, H_{Ar}) ppm; ^{13}C NMR ($CDCl_3$, 75 MHz, 20°C): δ 37.8 (N-CH_3), 54.4 (N-CH_2), 120.9 (CH_{im}), 122.8 (CH_{im}), 128.7, 128.8, 129.1, 129.5, 130.8 (CH_{ar}), 134.3 (Car), 135.7 (CH_{ar}), 136.9 (C_{ar}), 150.1 (C-Pt) ppm; MS (positive ESI): m/z calcd for $C_{29}H_{27}SbIN_2Pt$ [M – I] 846.99; found 846.98; *m/z* calcd for $C_{29}H_{27}SbIN_2PtCH_3CN$ [M – I + CH_3CN] 888.02; found 888.00; *m/z* calcd for $C_{29}H_{27}SbI_2N_2PtNa$ [M + Na] 996.88; found 996.9. $C_{29}H_{27}I2N_2PtSb$ (974.19): calcd. C 35.75, H 2.79, N 2.88; found C 35.24, H 2.88, N 2.78.

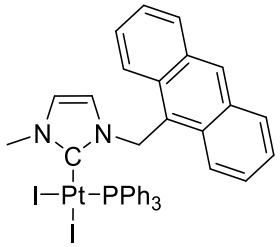

52a. Synthesized according to procedure with a slight modification. At the end of the reaction a pale-yellow precipitate was observed in solution. Ethanol was carefully removed with a syringe, and the yellowish precipitate was washed once with cold ethanol (0.5 mL) and dried under vacuum. Pure compound was obtained after silica gel chromatography (pentane/CH_2Cl_2, 20:80). Yellow solid, 32.1 mg, yield 58%. ^{1}H NMR (300 MHz, CD_2Cl_2, 20°C): δ 3.60 (s, 3 H, N-CH_3), 5.39 (d, *J*=14 Hz, 1 H, N-CH_2), 5.68 (d, *J*=2 Hz, 1 H, CH_{im}), 6.44 (d, *J*=2 Hz, 1 H, CH_{im}), 6.67 (d, *J*=15 Hz, 1 H, N-CH_2), 7.91–7.33 (m, 21 H, CH_{Anth}, CH_{ar}), 8.07 (d, *J*=7.9 Hz, 2 H, CH_{Anth}), 8.59 (s, 1 H, CH_{Anth}) ppm; ^{31}P NMR (CD_2Cl_2, 121 MHz, 20°C): δ 8.18 ($J_{P,Pt}$=3704 Hz) ppm; ^{13}C NMR ($CDCl_3$, 75 MHz, 20°C): δ 30.3 (N-CH_3), overlap by CD_2Cl_2 peak (NCH_2), 120.6 (CH_{im}), 121.92 (CH_{im}), 121.9 (C_{ar}), 124.0 (C_{ar}), 124.8 (C_{ar}), 125.9 (CH_{ar}), 127.8 (CH_{ar}), 128.9 (CH_{ar}), 129.0 (CH_{ar}), 129.7 (CH_{ar}), 130.4 (C_{ar}), 131.6 (C_{ar}), 131.7 (C_{ar}), 131.9 (C_{ar}), 134.6–135.4 (bs) ppm.

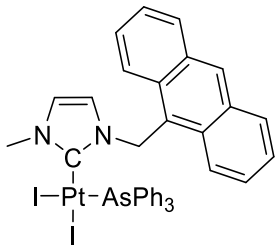

52b. *Synthesized according to procedure D.* Yellow solid, 22.4 mg, yield 35%. ^{1}H NMR ($CDCl_3$, 300 MHz, 20°C): δ 3.64 (s, 3 H, N-CH_3), 5.44 (d, *J*=14.5 Hz, 1 H, N-CH_2), 5.72 (s, 1 H, CH_{im}), 6.39 (s, 1 H, CH_{im}), 6.73 (d, *J*=14.5 Hz, 1 H, N-CH_2), 7.34–7.62 (m, 18 H, H_{Ar}, H_{Anth}), 8.01 (d, 2 H, H_{Ar}), 8.54 (s, 1 H, H_{Ar}) ppm; ^{13}C NMR ($CDCl_3$, 75 MHz, 20°C): δ 38.2 (NCH_3), 47.0 (N-CH_2), 124.3 (CH_{im}), 125.5 (CH_{im}), 127.5 (C_{ar}), 129.2 (C_{ar}), 129.3 (C_{ar}), 130.8 (C_{ar}), 131.3 (C_{ar}), 131.5 (C_{ar}), 132.4 (C_{ar}), 133.7 (C_{ar}) ppm. The signal for the (C-Pt) carbon was not observed. MS (positive ESI): compound decomposed under both low and high resolution.

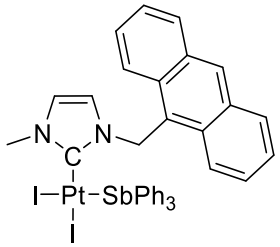

52c. *Synthesized according to procedure D.* Yellow solid, 9.4 mg, yield 28%. ^{1}H NMR ($CDCl_3$, 300 MHz, 20°C): δ 3.63 (s, 3 H, N-CH_3), 5.49 (d, *J*=14.5 Hz, 1 H, N-CH_2), 5.72 (s, 1 H, CH_{im}), 6.39 (s, 1 H, CH_{im}), 6.73 (d, *J*=14.5 Hz, 1 H, N-CH_2), 7.32–7.61 (m, 21 H, HAr, H_{Anth}), 8.01 (d, 2 H, H_{Anth}), 8.54 (s, 1 H, H_{Anth}) ppm; ^{13}C NMR ($CDCl_3$, 75 MHz, 20°C): δ 38.2 (N-CH_3), 53.9 (N-CH_2), 120.8 (CH_{im}), 121.8 (CH_{im}), 123.5 (C_{ar}), 124.2 (C_{ar}), 125.5 (C_{ar}), 125.7 (C_{ar}), 127.6 (C_{ar}), 128.7 (C_{ar}), 129.0 (C_{ar}), 129.3 (C_{ar}), 129.7 (C_{ar}), 130.9 (C_{ar}), 131.2 (C_{ar}), 131.4 (C_{ar}), 135.8 (C_{ar}), 136.4 (C_{ar}), 138.5 (C_{ar}) ppm. The signal for the (C-Pt) carbon was not observed. HRMS (positive ESI): *m*/*z* calcd for $C_{37}H_{31}IN_2SbPt$ [M – I] 947.0218; found 947.0215.

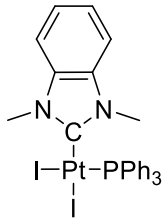

53a. *Synthesized according to procedure D.* Yellow solid, 21.8 mg, yield 69%. ^{1}H NMR ($CDCl_3$, 300 MHz, 20°C): δ 3.75 (s, 6 H, N-CH_3), 7.07–7.32 (m, 13 H, H_{Ar}), 7.57–7.64 (m, 6 H, H_{Ar}) ppm; ^{13}C NMR ($CDCl_3$, 75 MHz, 20°C): δ 34.1 (N-CH_3), 109.8 (CH_{ar}), 123.1, 127.9, 128.1 (CH_{ar}), 129.7 (C_{ar}), 130.5 (C_{ar}), 130.9, 130.9, 134.0, 134.2, 134.3 (CH_{ar}), 166.3 (C-Pt) ppm; ^{31}P NMR ($CDCl_3$, 121 MHz, 20°C): *δ* 8.36 ($J_{P,Pt}$=3664 Hz) ppm. HRMS (positive ESI): *m*/*z* calcd for $C_{27}H_{25}PIN_2Pt$ [M – I] 730.0448; found 730.0388; *m*/*z* calcd for $C_{27}H_{24}PN_2Pt$ [M – I – H] 602.1325; found 602.1341.

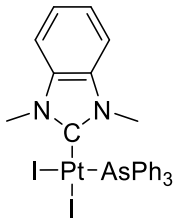

53b. *Synthesized according to procedure D.* Yellow solid, 16.6 mg, yield 50%. ^{1}H NMR ($CDCl_3$, 300 MHz, 20°C): *δ* 3.78 (s, 6 H, N-CH_3), 7.06–7.29 (m, 13 H, H_{Ar}), 7.53 (m, 6 H, H_{Ar}) ppm; ^{13}C NMR ($CDCl_3$, 75 MHz, 20°C): δ 34.1 (NCH_3), 109.8 (CH_{ar}), 123.2, 128.8, 130.8 (CH_{ar}), 131.5 (C_{ar}), 133.3 (CH_{ar}), 134.6 (C_{ar}), 163.9 (C-Pt) ppm. HRMS (positive ESI): *m*/*z* calcd for $C_{27}H_{25}AsI_2N_2PtNa$ [M + Na] 923.8868; found 923.8794; *m*/*z* calcd for $C_{27}H_{25}AsIN_2Pt$ [M – I] 773.9926; found 773.9950.

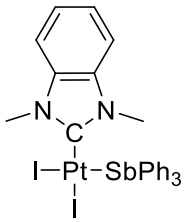

53c. *Synthesized according to procedure D.* Yellow solid, 24.2 mg, yield 69%. ^{1}H NMR ($CDCl_3$, 300 MHz,): δ 3.82 (s, 6 H, N-CH_3), 7.04–7.32 (m, 13 H, H_{Ar}), 7.52 (m, 6 H, H_{Ar}) ppm^{13}C NMR ($CDCl_3$, 75 MHz, 20°C): δ 34.2 (NCH_3), 109.8, 123.2, 128.6, 129.4, 129.7, 130.9, 134.3, 134.9, 135.4 (C_{ar}), 163.2 (C-Pt) ppm; HRMS (positive ESI): *m*/*z* calcd for $C_{27}H_{25}SbI_2N_2PtNa$ [M + Na] 970.8691; found 970.8620; *m*/*z* calcd for $C_{27}H_{25}SbIN_2PtCH_3CN$ [M – I + CH_3CN] 862.0010; found 861.9932.

- **Procedure E: Synthesis of Neutral NHC-Platinum-Pnictogen Complexes**

A solution of the corresponding trans [(NHC)PtI_2(pyr)] complex (1 equiv.), [H-P(*n*Bu)$_3$]·BF_4 (1 equiv.) and DIPEA (1 equiv.) in ethanol (1–5 mL) was stirred overnight at 55 °C, under argon atmosphere. The crude mixture was then concentrated under reduced pressure and purified by silica gel chromatography (pentane/CH_2Cl_2, 1:1 to CH_2Cl_2) to afford the desired complex as a light yellow oil.

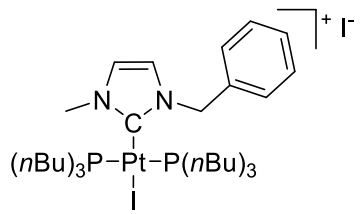

54. *Synthesized according to procedure E.* Yellow solid, 10.4 mg, yield 31%. ^{1}H NMR ($CDCl_3$, 300 MHz, 20°C): δ 1.30–1.87 (m, 54 H, nBu), 3.94 (s, 3 H, N-CH_3), 5.39 (s, 2 H, N-CH_2), 7.12 (s, 1 H,

CH_{im}), 7.15–7.18 (m, 2 H, H_{Ar}), 7.40–7.43 (m, 3 H, H_{Ar}), 7.80 (s, 1 H, CH_{im}) ppm; ^{31}P NMR ($CDCl_3$, 121 MHz, 20°C): δ 4.63 ($1J_{P,Pt}$ = 2196 Hz) ppm; ^{13}C NMR ($CDCl_3$, 75 MHz, 20°C): δ 13.7, 14.2, 19.8, 22.8, 23.6, 23.8, 24.2 (t, *J*=7.1 Hz, P-CH_2), 26.5 (t, *J*=10 Hz, P-CH_2), 29.5 (CH_2), 29.8 (CH_2), 30.1 (CH_2), 32.0 (CH_2), 37.2 (CH_3), 38.2 (N-CH_3), 53.8 (N-CH_2), 122.1 (CH_{im}), 125.7 (CH_{im}), 126.9 (C_{ar}), 129.0 (C_{ar}), 129.6 (C_{ar}), 133.5 (C_{ar}) ppm; the signal for the (CPt) carbon was not observed; HRMS (positive ESI): *m*/*z* calcd for $C_{35}H_{66}IN_2P_2Pt$ [M – I-(C_6H_{14})] 898.3494; found 898.3650.

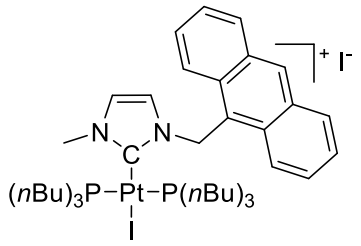

55. *Synthesized according to procedure E.* Yellow solid, 8.3 mg, yield 24%. ^1H NMR ($CDCl_3$, 300 MHz, 20°C): δ 1.20–1.54 (m, 27 H, nBu), 4.07 (s, 3 H, N-CH_3), 5.91 (s, 2 H, N-CH_2), 6.05 (s, 1 H, CH_{im}), 7.52–7.61 (m, 4 H, H_{Ar}), 7.66 (s, 1 H, CH_{im}), 7.85 (d, 2 H, H_{Ar}), 8.16 (d, 2 H, H_{Ar}), 8.71 (s, 1 H, H_{Ar}) ppm; ^{13}C NMR ($CDCl_3$, 75 MHz, 20°C): δ 13.8, 14.3, 22.8, 24.3, 24.4, 24.5, 24.7, 27.0, 29.8, 30.5, 32.1, 39.1 (N-CH_3), 46.4 (N-CH_2), 120.6 (CH_{im}), 121.1 (CH_{im}), 121.9 (C_{ar}), 125.6 (C_{ar}), 127.8 (C_{ar}), 130.3 (C_{ar}), 131.1 (C_{ar}), 131.2 (C_{ar}), 131.5 (C_{ar}) ppm; ^{31}P NMR ($CDCl_3$, 121 MHz): δ 4.60 ($1J_{P,Pt}$ = 2197 Hz) ppm. HRMS (positive ESI): m/z calcd for $C_{43}H_{70}IN_2P_2Pt$ [M – I – H] 998.3707; found 998.3703.

- **Procedure F: Synthesis of Cationic NHC-Platinum-Pnictogen**

A solution of the corresponding *trans* [(NHC)PtI_2(pyr)] (1 equiv.) and the Pnictogen ligand [2.0 equiv. in ethanol (1–5 mL)] was stirred overnight at 55 °C, under argon atmosphere. The crude mixture was then concentrated under reduced pressure and purified by silica gel chromatography (pentane/CH_2Cl_2, 1:1 to CH_2Cl_2 and CH_2Cl_2/MeOH, 20:1) to afford the complex as a white solid.

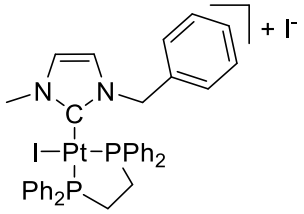

56. General *procedure F* was adapted using the precursor **5** (57 mg, 0.082 mmol) and dppe (1 equiv.). White solid, 62.7 mg, yield 86%. ^{1}H NMR (300 MHz, MeOD, 20°C): δ 2.38–2.86 (m, 4 H, CH_2), 3.37 (s, 3 H, N-CH_3), 4.18 (d, *J*=15 Hz, 1 H, N-CH_2), 5.24 (d, *J*=15 Hz, 1 H, N-CH_2), 6.83 (s, 1 H, CH_{im}), 7.12 (m, 6 H, H_{Ar}), 7.44–7.64 (m, 16 H, H_{Ar}), 7.83–7.94 (m, 4 H, H_{Ar}) ppm; ^{13}C NMR (75 MHz, MeOD, 20°C): δ 26.8 (dd, $J_{C,P}$=37 and 9 Hz, CH_2-P), 29.9 (dd, $J_{C,P}$=40 and 10 Hz, CH_2-P), 38.4 (N-CH_3), 54.5 (N-CH_2), 123.3 (CH_{im}),125.8 (CH_{im}), 127.6, 128.3, 128.3, 129.1, 129.2, 129.5, 129.6, 129.8, 130.0, 130.2, 130.3, 130.6, 130.7, 130.8, 133.1, 133.5, 133.7, 133.8, 134.0, 134.1, 134.9, 135.0, 135.1, 135.2, 135.4, 135.8, 165.5 (dd, $J_{C,P\text{-}cis}$=6.3 Hz, $J_{C,P\text{-}trans}$=137 Hz, C-Pt) ppm; ^{31}P NMR (MeOD, 121 MHz, 20°C): δ 40.0 (dd, $J_{P,P}$=12.9, $J_{P,Pt}$=2221 Hz), 41.0 (dd, $J_{P,P}$=12.9 Hz, $J_{P,Pt}$=3306 Hz) ppm. HRMS (positive ESI): *m*/*z* calcd for $C_{37}H_{36}IN_2P_2Pt$ [M – I] 892.1044; found 892.0957.

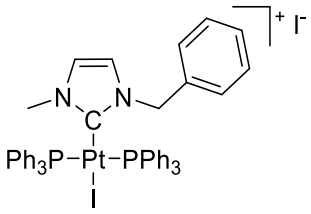

57a. *Synthesized according to procedure F.* Yellow solid, 74.3 mg, yield 98%. ^{1}H NMR ($CDCl_3$, 300 MHz, 20 °C): δ 3.30 (s, 3 H, N-CH_3), 4.70 (s, 2 H, N-CH_2), 6.32 (d, *J*=2 Hz, 1 H, CH_{im}), 6.65 (d, *J*=2 Hz, 2 H, H_{Ar}), 7.08–7.59 (m, 36 H, H_{Ar}, CH_{im}) ppm; ^{31}P NMR ($CDCl_3$, 121 MHz, 20 °C): δ 13.01 (t, *J*=2448 Hz) ppm; ^{13}C NMR ($CDCl_3$, 75 MHz, 20 °C): δ 38.0 (N-CH_3), 54.0 (N-CH_2), 121.0 (CH_{im}), 125.2 (CH_{im}), 128.9, 129.0, 129.1, 129.3, 129.4, 129.6, 131.0, 134.3 (C_{ar}), 150.1 (CPt) ppm. HRMS (positive ESI): *m*/*z* calcd for $C_{47}H_{42}IN_2P_2Pt$ [M – I] 1018.1516; found 1018.1505.

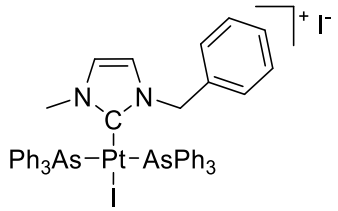

57b. *Synthesized according to procedure F.* Yellow solid, 82.1 mg, quant. ^{1}H NMR ($CDCl_3$, 300 MHz, 20°C): δ 3.47 (s, 3 H, N-CH_3), 4.50 (d, *J*=14 Hz, N-CH_2), 5.70 (d, *J*=14 Hz, N-CH_2), 6.24 (s, 1 H, CH_{im}), 6.45 (s, 1 H, CH_{im}), 7.12–7.43 (m, 35 H, H_{Ar}) ppm; ^{13}C NMR ($CDCl_3$, 75 MHz, 20 °C): δ 37.7 (N-CH_3), 54.1 (N-CH_2), 120.3 (CH_{im}), 122.5 (CH_{im}), 128.3, 128.6, 128.8, 128.8, 129.0, 129.7, 130.7, 132.0, 133.5, 133.8, 134.1, 134.8, 134.9, 139.7 (C_{ar}), 151.6 (C-Pt) ppm. HRMS (positive ESI): *m*/*z* calcd for $C_{47}H_{42}IN_2PtAs_2$ [M – I] 1106.0484; found 1106.0467.

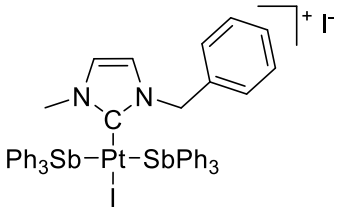

57c. *Synthesized according to procedure F.* Yellow solid, 88.8 mg, quant. ^{1}H NMR ($CDCl_3$, 300 MHz, 20°C): δ 3.58 (s, 3 H, N-CH_3), 5.12 (d, *J*=14 Hz, 1 H, N-CH_2), 5.50 (d, *J*=14 Hz, 1 H, N-CH_2), 6.52 (d, *J*=2.1 Hz, 1 H, CH_{im}), 6.55 (d, *J*=2.1 Hz, 1 H, CH_{im}), 7.04–7.72 (m, 35 H, H_{Ar}) ppm; ^{13}C NMR ($CDCl_3$, 75 MHz, 20 °C): δ 37.8 (N-CH_3), 54.5 (N-CH2), 120.9 (CH_{im}), 122.7 (CH_{im}), 128.7, 129.0, 129.1, 129.5, 130.8 (CH_{ar}), 134.4 (C_{ar}), 135.7, 136.4 (CH_{ar}), 137.0 (Car), 138.5 (Car), 150.7 (C-Pt) ppm. HRMS (positive ESI): *m*/*z* calcd for $C_{47}H_{42}Sb_2IN_2Pt$ [M – I] 1198.0112; found 1198.0082.

3) Synthesis of NHC-Pt(IV) complexes

a. [(NHC)PtBr$_4$L]

- **Procedure G: Direct oxidation with bromine**

In a 10 mL round bottom flask, the precursor [(NHC)PtI_2L][4] (10 mg, 1 equiv.) was dissolved in CH_2Cl_2 (5 mL) and cooled at 0 °C and Br_2 (2 equiv.) was slowly added under nitrogen. After 30 min, pentane (10 mL) was added and the resulting red precipitate [(NHC)$PtBr_4L$] was filtered off, washed and dried.

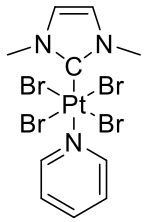

58. *Synthesized according to procedure G.* Red solid, 13.1 mg, yield 99%. ^{1}H NMR ($CDCl_3$, 300 MHz, 20 °C): δ 4.46 (m, 6H, N–CH_3), 7.02 (d, *J*=2.1 Hz, 2H, CH_{im}), 7.45 (m, 2H, H_{pyr}), 7.91 (m, 1H, H_{pyr}), 9.70 (m, 2H, H_{pyr}); ^{13}C NMR ($CDCl_3$, 75 MHz, 20 °C): δ 44.3 (N–CH_3), 53.6 (N–CH_2), 120.7 (C–Pt), 124.9 (s + d, *J*=19.3 Hz, CH_{im}), 125.7 (s + d, *J*=22.1 Hz, CH_{im}), 139.6 (C_{pyr}), 154.6 (s + d, *J*=4.6 Hz, C_{pyr}); HRMS (positive ESI) [2M+Na]: $C_{20}H_{26}Br_8N_6Pt_2Na_1$: 1394.4822, found 1394.5160.

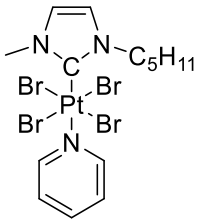

59. *Synthesized according to procedure G.* Red solid, 11.6 mg, yield 99%. ^{1}H NMR ($CDCl_3$, 300 MHz, 20 °C): *δ* 0.93 (t, *J*=7.0 Hz, 3H, CH_3), 1.43 (m, 4H, CH_2), 1.92 (m, 2H, CH_2), 4.44 (s, 3H, N–CH_3), 4.78 (m, 2H, N–CH_2), 7.03 (d, *J*=2.1 Hz, 1H, CH_{im}), 7.12 (d, *J*=2.1 Hz, 1H, CH_{im}), 7.44 (m, 2H, H_{pyr}), 7.89 (m, 1H, H_{pyr}), 9.71 (m, 2H, H_{pyr}); ^{13}C NMR ($CDCl_3$, 75 MHz, 20 °C): δ 14.2 (CH_3), 22.6 (CH_2), 28.8 (CH_2), 44.2 (N–CH_3), 55.4 (N–CH_2), 109.2 (C–Pt), 123.5 (s + d, *J*=11.1 Hz, CH_{im}), 124.7 (s + d, *J*=9.9 Hz, C_{pyr}), 125.8 (s + d, *J*=11.1 Hz, CH_{im}), 139.5 (C_{pyr}), 154.6 (C_{pyr}); HMQC ^{1}H–^{195}Pt NMR ($CDCl_3$, 64.2 MHz, 20 °C): δ −2040 ppm (m); HRMS (positive ESI) [M + Na]:

[4] M. Bouché, G. Dahm, M. Wantz, S. Fournel, T. Achard, S. Bellemin-Laponnaz *Dalton Trans* **2016**, *45*, 11362-11368

$C_{14}H_{21}Br_4N_3Pt_1Na_1$ 764.8010, found 764.8009; elemental anal. calc. for $C_{14}H_{21}Br_4N_3Pt_1$: C 23.54, H 2.84, N 5.63, found: C 23.61, H 2.99, N 5.81.

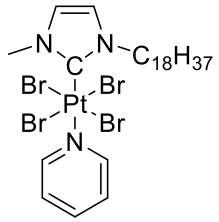

60. *Synthesized according to procedure G.* Red solid, 10,6 mg, yield 99%. ^{1}H NMR ($CDCl_3$, 300 MHz, 20 °C): *δ* 0.88 (t, *J*=7.0 Hz, 3H, CH_3), 1.25 (bs, 30H, CH_2), 1.91 (m, 2H, CH_2), 4.45 (s, 3H, N–CH_3), 4.77 (m, 2H, N–CH_2), 7.02 (d, *J*=2.1 Hz, 1H, CH_{im}), 7.11 (d, *J*=2.1 Hz, 1H, CH_{im}), 7.44 (m, 2H, H_{pyr}), 7.90 (m, 1H, H_{pyr}), 9.70 (m, 2H, H_{pyr}); ^{13}C NMR ($CDCl_3$, 75 MHz, 20 °C): δ 14.2 (CH_3), 22.6 (CH_2), 28.8 (CH_2), 44.2 (N–CH_3), 55.4 (N–CH_2), 109.2 (C–Pt), 123.5 (s + d, *J*=11.1 Hz, CH_{im}), 124.7 (s + d, *J*=9.9 Hz, C_{pyr}), 125.8 (s + d, *J*=11.1 Hz, CH_{im}), 139.5 (C_{pyr}), 154.6 (C_{pyr}); elemental anal. calc. for $C_{27}H_{47}N_3Pt_1Br_4$: C 34.93, H 5.10, N 4.53, found: C34.73, H 5.11, N 4.44.

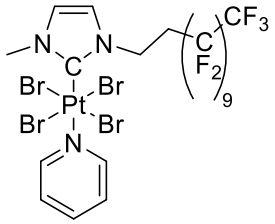

61. *Synthesized according to procedure G.* Red solid, 7.8 mg, yield 99%. ^{1}H NMR ($CDCl_3$, 300 MHz, 20 °C): δ 3.07 (m, 2H, CH_2-CF_2), 3.98 (s, 3H, N-CH_3), 4.81 (dd,2H, N-CH_2), 6.90 (d, 2H, CH_{im}), 7.34 (dd, 2H, H_{pyr}), 7.75 (dd, 1H, H_{pyr}), 8.99 (q, 2H, H_{pyr}); ^{13}C NMR (75 MHz, $CDCl_3$): δ 29.9 (CF_3), 31.1 (CH_2), 33.8 (t, *J*=20.4Hz, CF_2), 44.5 (N-CH_3), 47.4 (N-CH_2), 112.0 (C-Pt), 123.6 (CH_{im}), 125.0 (t, $CH_{o\text{-}pyr}$), 126.7 (CH_{pyr}), 139.8 (CH_{pyr}); ^{13}C NMR (CD_2Cl_2, 75 MHz, 20°C): δ 30.0 (CF_3), 31.0 (CH_2), 33.6-33.9 (CF_2), 44.6 (N-CH_3), 47.5 (N-CH_2), 111.6 (C-Pt), 123.9 (CH_{im}), 125.3 (CH_{im}), 127.2 (t, $CH_{o\text{-}pyr}$), 140.3 (CH_{pyr}), 154.7 (CH_{pyr}); ^{19}F NMR ($CDCl_3$, 75 MHz, 20 °C): δ -126.09 (m, 2F), -123.28 (s, 2F), -122.68 (s,2F), -121.73- -121.49 (m, 10F), -112.95 (m, 2F), -80.73 (dd, 3F)

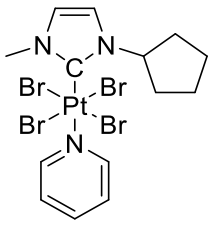

62. *Synthesized according to procedure G.* Red solid, 11.2 mg, yield 96%. ^{1}H NMR ($CDCl_3$, 300 MHz, 20 °C): δ 1.85 (m, 6H, CH_2), 2.57 (m, 2H, CH_2), 4.41 (s, 3H, N–CH_3), 6.17 (m, 1H, N–CH), 7.05 (d, *J*=2.1 Hz, 1H, CH_{im}), 7.07 (d, *J*=2.1 Hz, 1H, CH_{im}), 7.47 (m, 2H, H_{pyr}), 7.92 (m, 1H, H_{pyr}), 9.64 (m, 2H, H_{pyr}); no ^{13}C NMR spectrum could be recorded due to very low solubility; HMQC ^{1}H–^{195}Pt NMR ($CDCl_3$, 64.2 MHz, 20 °C): δ −2032 ppm (m); MS (positive ESI) [M − 2Br]: $C_{14}H_{18}Br_2N_3Pt_1$ 580.95, found 582.95; elemental anal. calc. for $C_{14}H_{19}Br_4N_3Pt$ + Br_2: C 18.60, H 2.12, N 4.65, found: C 18.42, H 2.13, N 4.51.

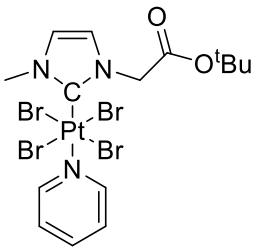

63. *Synthesized according to procedure G.* Red solid, 16.7 mg, yield 99%. ^{1}H NMR ($CDCl_3$, 300 MHz, 20 °C): δ 3.97 (N–CH_3), 5.23 (s, 2H, N–CH_2), 6.87 (d, *J*=2.1 Hz, 1H, CH_{im}), 7.01 (d, *J*=2.1 Hz, 1H, CH_{im}), 7.32 (m, 2H, H_{pyr}), 7.73 (m, 1H, H_{pyr}), 9.03 (m, 2H, H_{pyr}); ^{13}C NMR ($CDCl_3$, 75 MHz, 20 °C): δ 28.0 (C_{tBu}), 44.1 (N–CH_3), 56.7(N–CH_2), 124.7(s + d, *J*=20.2 Hz, CH_{im}), 126.4 (C_{pyr}), 139.4 (C_{pyr}), 154.4 (C_{pyr}), (C-Pt) and (C=O) not seen; HMQC ^{1}H–^{195}Pt NMR ($CDCl_3$, 64.2 MHz, 20 °C): δ −2070(m).

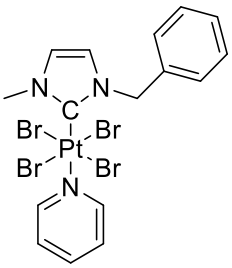

64. *Synthesized according to procedure G.* Red solid, 10.7 mg, yield 98%. ^{1}H NMR (CD_2Cl_2, 500 MHz, 20 °C): δ 4.45 (s, 3H, N–CH_3), 6.09 (s, 2H, N–CH_2), 6.78 (d, *J* = 2.1 Hz, 1H, CH_{im}), 7.01 (d, *J*=2.1 Hz, 1H, CH_{im}), 7.32–7.37 (m, 7H, H_{ar}), 7.46 (m, 2H, H_{pyr}), 7.94 (m, 1H, H_{pyr}), 9.64 (m, 2H, H_{pyr}); ^{13}C NMR (CD_2Cl_2, 125 MHz, 20 °C): δ 44.1 (N–CH_3), 59.1 (N–CH_2), 109.3 (C–Pt), 124.4 (s + d, *J*=10.8 Hz, CH_{im}), 124.8 (CH_{ar}), 125.7 (s + d, *J*=10.8 Hz, CH_{im}), 128.7 (CH_{ar}), 128.8 (CH_{ar}), 136.7 (C_{pyr}), 139.8 (C_{pyr}), 154.3 (C_{pyr}); HMQC ^{1}H–^{195}Pt NMR ($CDCl_3$, 64.2 MHz, 20 °C): δ −2048 (m); MS (positive ESI) [M − 3Br]: $C_{16}H_{16}Br_1N_3Pt_1$: 523.01, found 524.01; elemental anal. calc. for $C_{16}H_{17}Br_4N_3Pt_1$: C 25.09, H 2.24, N 5.49, found: C 24.74, H 2.23, N 5.40.

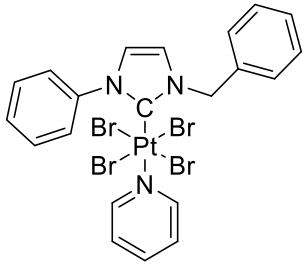

65. *Synthesized according to procedure G.* Red solid, 12.2 mg, yield 99%. ^{1}H NMR ($CDCl_3$, 300 MHz, 20 °C): δ 6.23 (s, 2H, N-CH_2), 6.84 (d, *J*=2.1 Hz, 1H, H_{im}), 6.91 d, *J*=2.1 Hz, 1H, H_{im}), 7.35-7.54 (m, 10H, H_{ar}), 7.75 (m, 2H, H_{pyr}), 7.84 (m, 1H, $H_{pyr)}$, 9.34 (m, 2H, H_{pyr}); ^{1}H NMR (CD_2Cl_2, 300 MHz, 20 °C): δ (s, 2H, N-CH_2), (d, *J*=2.0 Hz, 1H, CH_{im}), (d, *J*=2.0 Hz, 1H, CH_{im}), (m, 11H, CH_{ar}+CH_{pyr}, overlap $CDCl_3$), (m, 2H, H_{pyr}), (m, 2H, H_{pyr}); ^{13}C NMR (CD_2Cl_2, 75 MHz, 20 °C): δ 55.0 (N-CH_2), 114.2 (CH_{im}), 117.2 (CH_{im}), 123.8 (C_{pyr}), 126.1 (C_{pyr}), 127.1 (CH_{ar}), 128.9 (CH_{ar}), 129.3 (CH_{ar}), 130.3 (CH_{ar}), 135.8 (C_{ar}), 140.3 (N-C_{ar}), 141.5 (CH_{ar}), 153.7 (C_{pyr}), (C-Pt) not seen; MS (positive ESI) [M - 2Br]: $C_{21}H_{19}Br_2N_3Pt_1$ 667.963, found 667.952.

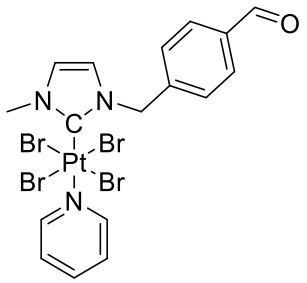

66. *Synthesized according to procedure G.* Red solid, 12.3 mg, yield 99%. ^{1}H NMR ($CDCl_3$, 300 MHz, 20 °C): δ 4.50 (s, 3H, N-CH_3), 6.23 (s, 2H, N-CH_2), 6.74 (q, J_1=4.8 Hz, J_2=2.5 Hz, 1H, CH_{im}), 7.03 (q, J_1=4.8 Hz, J_2=2.5 Hz, 1H, CH_{im}), 7.45 (dd, 2H, H_{ar}), 7.52 (d, 2H, H_{ar}), 7.87-7.94 (m, 3H, H_{pyr}), 9.63-9.72 (m, 2H, H_{pyr}), 10.02 (s, 1H, CHO); ^{13}C NMR ($CDCl_3$, 75 MHz, 20°C): δ 44.3 (N-CH_3), 58.9 (N-CH_2), 110.8 (C-Pt), 124.1 (t, J=10.8Hz, CH_{im}), 124.8 (t, J=18.9Hz, C_{pyr}), 125.8 (t, J=10.8 Hz, CH_{im}), 129.1 (CH_{ar}), 130.1 (CH_{ar}), 136.2 (C_{ar}), 139.5 (C_{pyr}), 143.0 (Car), 154.4 (C_{pyr}), 191.6 (CHO); ^{13}C NMR ($CDCl_3$, 75 MHz, 20°C): δ 31.0, 44.6, 59.1, 110.6 (s+d, J=1034 Hz, C-Pt), 124.8 (CH_{im}), 125.2 (C_{pyr}), 126.6 (CH_{im}), 129.3 (CH_{ar}), 130.2 (CH_{ar}), 136.5 (CH_{ar}), 140.2 (C_{pyr}), 143.7 (C_{pyr}), 191.2 (CHO).

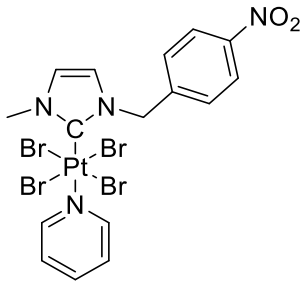

67. *Synthesized according to procedure G.* Red solid, 11.3 mg, yield 99%. ^{1}H NMR ($CDCl_3$, 300 MHz, 20 °C): δ 4.54 (s, 3H, N–CH_3), 6.29 (s, 2H, N–CH_2), 6.74 (d, J=2.1 Hz, 1H, CH_{im}), 7.06 (d, J=2.1 Hz, 1H, CH_{im}), 7.44–7.55 (m, 4H, H_{ar}), 7.93 (m, 1H, H_{pyr}), 8.22 (m, 2H, H_{pyr}), 9.67 (m, 2H, H_{pyr}); ^{13}C NMR ($CDCl_3$, 75 MHz, 20°C): δ 44.3 (s, N–CH_3), 58.4 (s, N–CH_2), 123.9 (CH_{im}), 124.1 (C_{pyr}), 124.8 (CH_{im}), 129.2 (C_{ar}), 139.6 (C_{ar}), 143.5 (C_{ar}), 147.8 (C_{ar}), 147.8 (C_{pyr}), 154.4 (C_{pyr}); the carbene resonance peak was not observed; HMQC ^{1}H–^{195}Pt NMR ($CDCl_3$, 64.2 MHz, 20 °C): δ −2067 ppm (m); HRMS (positive ESI) [M + CH_3CN + Na]: $C_{18}H_{19}Br_4N_5O_1Pt_1Na_1$ 870.7813, found 870.7812.

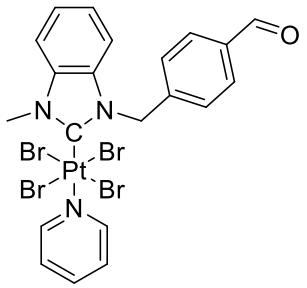

68. *Synthesized according to procedure G.* Red solid, 12.1 mg, yield 99%. ^{1}H NMR ($CDCl_3$, 300 MHz, 20 °C): δ 4.73 (s, 3H, N-CH_3), 6.63 (s, 2H, N-CH_2), 6.94 (d, *J*=8.3 Hz, 1H, H_{ar}), 7.18 (t, *J*=7.8 Hz, 1H, H_{ar}), 7.34 (m, 3H, H_{ar}), 7.46 (t, *J*=7.1 Hz, 2H, H_{pyr}), 7.57 (d, *J*=8.3 Hz, 1H, H_{ar}), 7.80 (d, *J*=8.3 Hz, 2H, H_{ar}), 7.89-7.94 (tt, *J*=7.6 Hz, 1H, H_{pyr}), 9.66-9.75 (q, *J*=16.5 Hz et *J*=10.7 Hz, 2H, H_{pyr}), 9.97 (s, 1H, CHO); ^{13}C NMR ($CDCl_3$, 75 MHz, 20°C): δ 41.3 (N-CH_3), 57.2 (N-CH_2), 111.9 (N-C_{im}), 113.2 (N-C_{im}), 124.7 (t, *J*=9.8 Hz),125.1, 125.3, 127.4, 129.8, 133.9 (C-Pt), 135.6, 139.5, 143.1, 154.5, 191.5 (CHO).

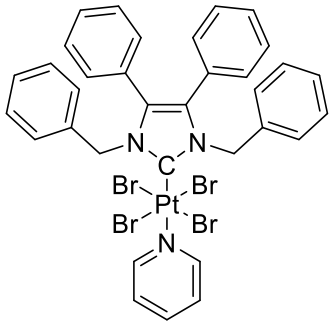

69. *Synthesized according to procedure G.* Red solid, 10.8 mg, yield 99%. ^{1}H NMR ($CDCl_3$, 300 MHz, 20 °C): *δ* 6.25 (bs, 4H, N–CH_2), 6.73-6.75 (m, 4H, H_{ar}), 6.81 (m, 4H, H_{ar}), 6.99 (m, 4H, H_{ar}), 7.10-7.12 (m, 8H, H_{ar}), 7.46 (m, 2H, H_{pyr}), 7.91 (m, 1H, H_{pyr}), 9.75 (m, 2H, H_{pyr}); No ^{13}C NMR could be recorded due to low solubility. ^{1}H-^{13}C HMBC NMR ($CDCl_3$, 500 MHz, 20 °C).

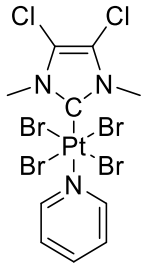

70. *Synthesized according to procedure G.* Red solid, 11.5 mg, yield 99%. ^{1}H NMR ($CDCl_3$, 300 MHz, 20 °C): δ 4.45 (m, 6H, N–CH_3), 7.46 (m, 2H, H_{pyr}), 7.93 (m, 1H, H_{pyr}), 9.65 (m, 2H, H_{pyr}); ^{13}C NMR ($CDCl_3$, 75 MHz, 20°C): δ 29.8 (N–CH_3), 43.1 (N–CH_2), 110.7 (C–Pt), 120.7 (C_{pyr}), 124.9 (s + d, *J*=10.4 Hz, 2C_{im}), 139.8 (C_{pyr}), 154.7 (s + d, *J*=4.6 Hz, C_{pyr}); HMQC ^{1}H–^{195}Pt NMR ($CDCl_3$, 64.2

MHz, 20 °C): δ −2058 ppm (m); MS (positive ESI) [M + Na]: $C_{10}H_{11}Br_4Cl_2N_3Pt_1Na_1$ 776.6609, found 776.6604.

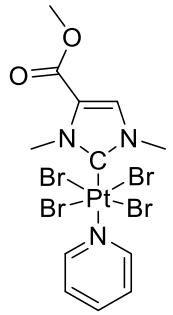

71. *Synthesized according to procedure G.* Red solid, 12.5 mg, yield 99%. ^{1}H NMR (CD_2Cl_2, 300 MHz, 20 °C): δ 3.91 (s, 3H, O-CH_3), 4.53 (s, 3H, N-CH_3), 4.66 (s, 3H, N-CH_3), 7.47 (t, *J*=7.3 Hz, 2H, CH_{pyr}), 7.72 (t, *J*=3.0 Hz, 1H, CH_{im}), 7.93 (t, *J*=14.6 Hz, 1H, CH_{pyr}), 9.66 (m, 2H, CH_{pyr}); ^{13}C NMR ($CDCl_3$, 75 MHz, 20°C): δ 43.1 (N-CH_3), 44.3 (N-CH_3), 51.8 (O-CH_3), 115.4 (t, *J*=1046.8 Hz, C-Pt), 124.2 (s+d, *J*=19.8 Hz, CH_{im}), 125.8 (s+d, *J*=25.0 Hz, C_{im}), 131.3 (s+d, *J*=22.4 Hz, CH_{pyr}), 138.9 (CH_{pyr}), 153.7 (CH_{pyr}), 157.2 (C=O).

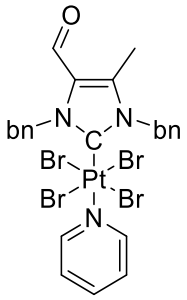

72. *Synthesized according to procedure G.* Red solid, 10.9 mg, yield 99%. ^{1}H NMR ($CDCl_3$, 300 MHz, 20 °C): δ 2.24 (s, 3H, CH_3), 6.37 (s, 2H, N-CH_2), 6.64 (s, 2H, N-CH_2), 7.11-7.18 (m, 4H, CH_{ar}), 7.28-7.46 (m, 8H, CH_{pyr}+CH_{ar}), 7.90 (m, 1H, CH_{pyr}), 9.57 (s, 1H, CHO), 9.66 (m, 2H, CH_{pyr}); No ^{13}C NMR could be recorded due to low solubility; HMQC ^{1}H–^{195}Pt NMR ($CDCl_3$, 64.2 MHz, 20 °C): *δ* −2081 ppm (m); ^{1}H-^{13}C HMBC NMR ($CDCl_3$, 500 MHz, 20 °C).

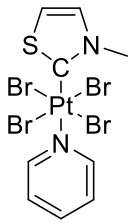

73. *Synthesized according to procedure G.* Red solid, 12.7 mg, yield 99%. ^{1}H NMR ($CDCl_3$, 300 MHz, 20 °C): δ 4.69 (s, 3H, N-CH_3), 7.60 (s, 2H, CH_{im}); HMQC ^{1}H–^{195}Pt NMR ($CDCl_3$, 64.2 MHz, 20 °C): *δ* − 2071(m). Insoluble.

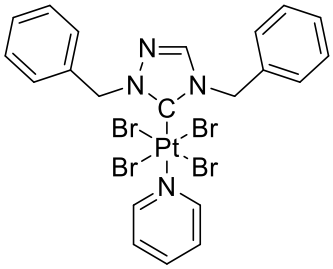

74. *Synthesized according to procedure G.* Red solid, 12.1 mg, yield 99%. ^{1}H NMR ($CDCl_3$, 300 MHz, 20 °C): δ 6.24 (s, 2H, N–CH_2), 6.35 (s, 2H, N–CH_2), 7.34-7.44 (m, 14H, H_{ar}+H_{pyr}), 7.74 (s, 1H, CH_{im}), 7.96 (m, 1H, H_{pyr}), 9.73 (m, 2H, H_{pyr}); ^{13}C NMR (75 MHz, $CDCl_3$, 20 °C): δ 57.5 (N–CH_2), 61.4 (N–CH_2), 119.5 (C-Pt), 125.1 (s + d, *J*=21.1 Hz, CH_{im}), 128.3 (C_{ar}), 128.6 (C_{pyr}), 129.1 (C_{ar}), 129.3 (C_{ar}), 129.5 (C_{ar}), 134.7 (C_{ar}), 135.6 (C_{ar}), 139.9 (C_{ar}), 145.0 (C_{pyr}), 154.7 (C_{pyr}).

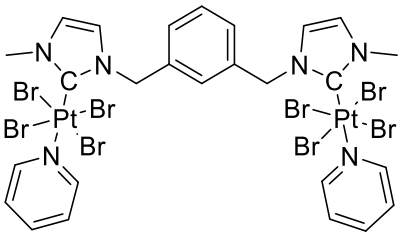

75. *Synthesized according to procedure G.* Red solid, mg, yield 99%. ^{1}H NMR ($CDCl_3$, 300 MHz, 20 °C): *δ* 4.47 (s, 6H, N-CH_3), 6.11 (s, 4H, N-CH_2), 6.85 (s, 4H, CH_{im}), 7.39-7.51 (m, 8H, CH_{ar}+CH_{pyr}), 7.90 (m, 2H, CH_{pyr}), 9.69 (m, 4H, CH_{pyr}).

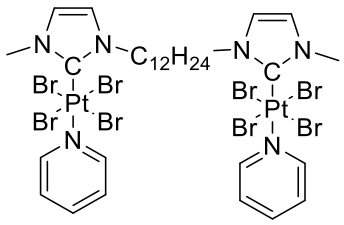

76. *Synthesized according to procedure G.* Red solid, 9.5 mg, yield 76%. ^{1}H NMR (CD_2Cl_2, 300 MHz, 20 °C): δ 1.30-1.89 (m, 22H, CH_2), 4.32 (s, 6H, N-CH_3), 4.67 (m, 4H, N-CH_2), 7.06 (s, 2H, CH_{im}), 7.15 (s, 4H, CH_{im}), 7.54 (m, 4H, H_{pyr}), 7.98 (m, 2H, H_{pyr}), 9.22 (m, 4H, H_{pyr}); ^{13}C NMR ($CDCl_3$, 75 MHz, 20°C): δ 26.8 (CH_2), 29.6 (CH_2), 29.8 (CH_2), 31.0 (CH_2), 32.3 (N-CH_3), 41.6 (N-CH_2), 111.3 (s+d, *J*=1021 Hz, C-Pt), 123.8 (CH_{im}), 125.4 (C_{pyr}), 126.2 (CH_{im}), 130.6 (C_{pyr}), 137.6 (C_{pyr}).

- **Procedure H: Ligand exchange on NHC-Pt(IV) complexes**

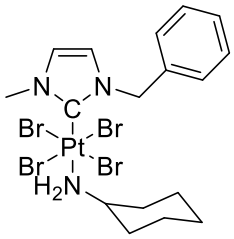

77. *Synthesized according to procedure H.* Red solid, 11.3 mg, yield 99%. ^{1}H NMR ($CDCl_3$, 300 MHz, 20 °C): δ 1.22–1.47 (m, 6H, CH_2), 1.72–1.79 (m, 2H, CH_2), 2.33 (m, 2H, CH_2), 3.59 (m, 1H, N–CH), 3.9–4.2 (bs, 2H, NH_2), 4.36 (s, 3H, N–CH_3), 5.97 (s, 2H, N–CH_2), 6.73 (d, *J*=2.1 Hz, 1H, CH_{im}), 6.94 (d, *J*=2.1 Hz, 1H, CH_{im}), 7.35 (m, 5H, H_{ar}); ^{13}C NMR ($CDCl_3$, 125 MHz, 20 °C): δ 24.4 (CH_2), 25.2 (CH_2), 35.4 (CH_2), 43.6 (CH), 54.6 (N–CH_3), 58.9 (N–CH_2), 115.2 (C–Pt), 124.0 (s + d, *J*=11.1 Hz, CH_{im}), 125.2 (s + d, *J*=11.1 Hz, CH_{im}), 128.3 (C_{ar}), 128.8 (C_{ar}), 136.1 (C_{ar}); HMQC ^{1}H–^{195}Pt NMR ($CDCl_3$, 64.2 MHz, 20 °C): δ −2167 (m); MS (positive ESI) [M − 3Br]: $C_{17}H_{25}N_3Pt_1Br_1$ 546.08, found 546.09; elemental anal. calc. for $C_{17}H_{25}Br_4N_3Pt_1$: C 25.97, H 3.21, N 5.35, found: C 26.00, H 3.28, N 5.27.

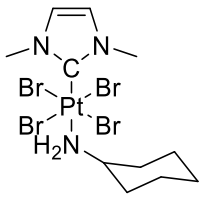

78. *Synthesized according to procedure H.* Red solid, 11.2 mg, yield 99%. ^{1}H NMR ($CDCl_3$, 300 MHz, 20 °C): *δ* 1.19-1.46 (m, 5H, CH_2), 1.65-1.78 (m, 3H, CH_2), 2.30 (m, 2H, CH_2), 3.55 (bs, 1H, C*H*-NH_2), 3.99 (bs, 2H, NH_2), 4.32 (s, 6H, N-CH_3), 6.99 (s, 2H, CH_{im}); ^{13}C NMR ($CDCl_3$, 125 MHz, 20 °C): δ 23.6 (CH_2), 24.4 (CH_2), 34.6 (CH_2), 42.9 (s+d, *J*=144.1 Hz, N-CH_3), 53.8 (CH) , 113.4 (s+d, *J*=1036.4 Hz, C-Pt), 124.6 (s+d, *J*=22.5 Hz, CH_{im}).

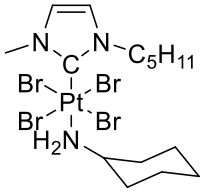

79. *Synthesized according to procedure H.* Red solid, 8.2 mg, yield 99%. ^{1}H NMR ($CDCl_3$, 300 MHz, 20 °C): δ 0.92 (m, 3H, CH_3), 1.29-1.48 (m, 8H, CH_2), 1.71-1.86 (m, 6H, CH_2), 2.33 (m, 2H, CH_2), 3.57 (m, 1H, H_2N-C*H*), 4.01 (bs, 2H, NH_2), 4.31 (s, 3H, N-CH_3), 4.62 (m, 2H, N-CH_2), 6.99 (s, 1H, CH_{im}), 7.08 (s, 1H, CH_{im}); ^{13}C NMR ($CDCl_3$, 75 MHz, 20 °C): δ 14.1 (CH_3), 22.6 (CH_2), 24.5 (CH_2), 25.3 (CH_2), 28.7 (CH_2), 31.8 (CH_2), 35.5 (CH_2), 43.7 (N-CH_3), 54.5 (H_2N-CH), 54.8 (N-CH_2), 114.9 (C-Pt), 123.2 (t, *J*=10.5 Hz, CH_{im}), 125.6 (t, *J*=10.5 Hz, CH_{im}).

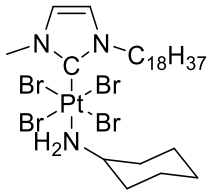

80. *Synthesized according to procedure H.* Red solid, 8.8 mg, yield 99%. ^{1}H NMR ($CDCl_3$, 300 MHz, 20 °C): δ 0.87 (t, 3H, *J*=6.7 Hz, CH_3), 1.35-1.45 (m, 34H, CH_2), 1.62-1.87 (m, 6H, CH_2), 2.32 (m, 2H, CH_2), 3.60 (m, 1H, H_2N-C*H*), 4.03 (bs, 2H, NH_2), 4.32 (s, 3H, N-CH_3), 4.63 (m, 2H, N-CH_2), 6.97 (d, *J*=2.1 Hz, 1H, CH_{im}), 7.06 (d, *J*=2.1 Hz, 1H, CH_{im}); ^{13}C NMR ($CDCl_3$, 75 MHz, 20 °C): δ 14.2 (CH_3), 22.8 (CH_2), 24.5 (CH_2), 25.3 (CH_2), 26.5 (CH_2), 29.3 (CH_2), 29.4 (CH_2), 29.5 (CH_2), 29.6 (CH_2),

29.7 (CH_2), 29.8 (CH_2), 32.0 (CH_2), 32.1 (CH_2), 35.5 (CH_2), 43.6 (N-CH_3), 54.5 (H_2N-CH), 54.9 (N-CH_2), 114.9 (C-Pt), 123.2 (CH_{im}), 125.6 (CH_{im}).

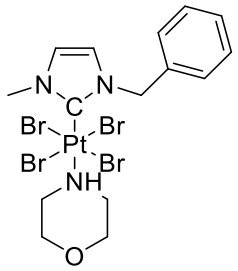

81. *Synthesized according to procedure H.* Red solid, 11.2 mg, yield 97%. ^{1}H NMR ($CDCl_3$, 300 MHz, 20 °C): *δ* 3.46–3.52 (m, 2H, CH_2), 3.65–3.82 (m, 4H, CH_2), 4.01–4.06 (m, 2H, CH_2), 4.36 (s + d, *J*=1.9 Hz, 3H, N–CH_3), 5.98 (s + d, *J* = 2.1 Hz, 2H, N–CH_2), 6.73 (d, *J*=2.1 Hz, 1H, CH_{im}), 6.93 (d, *J*=2.1 Hz, 1H, CH_{im}), 7.34–7.38 (m, 5H, H_{ar}); ^{13}C NMR ($CDCl_3$, 75 MHz, 20°C): δ 44.2 (N–CH_3), 52.0 (O–CH_2), 59.4 (N–CH_2), 69.2 (s + d, *J*=9.8 Hz, N–CH_2), 112.7 (C–Pt), 124.4 (s + d, *J*=11.4 Hz, CH_{im}), 125.6 (s + d, *J*=11.4 Hz, CH_{im}), 128.5 (C_{ar}), 128.9 (C_{ar}); HMQC ^{1}H–^{195}Pt NMR ($CDCl_3$, 64.2 MHz, 20 °C): *δ* −2080 ppm (m); MS (positive ESI) [M − 3Br]: $C_{15}H_{21}N_3O_1Pt_1Br_1$ 534.05, found 534.04; elemental anal. calc. for $C_{15}H_{20}Br_4N_3O_1Pt_1$: C 23.28, H 2.73, N 5.43, found: C 22.92, H 2.82, N 5.43.

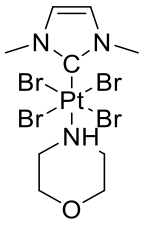

82. *Synthesized according to procedure H.* Red solid, 11.0 mg, yield 97%. ^{1}H NMR ($CDCl_3$, 300 MHz, 20 °C): *δ* 3.42-3.47 (m, 2H, CH_2), 3.65-3.77 (m, 4H, CH_2), 3.87 (bs, 1H, NH), 4.01-4.06 (m, 2H, CH_2), 4.32 (s, 6H, N-CH_3), 7.01 (s, 2H, CH_{im}); ^{13}C NMR ($CDCl_3$, 75 MHz, 20°C): δ 43.0 (N–CH_3), 50.8 (N–CH_2), 69.2 (t, *J*=19.3 Hz, HN–CH_2), 111.0 (t, *J*=526.6 Hz, C–Pt), 124.6 (t, *J*=11.4 Hz, CH_{im}); HMQC ^{1}H–^{195}Pt NMR ($CDCl_3$, 64.2 MHz, 20 °C): δ -2083 ppm.

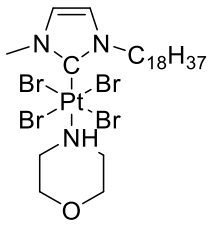

83. *Synthesized according to procedure H.* Red solid, 10.6 mg, yield 99%. 1H NMR ($CDCl_3$, 300 MHz, 20 °C): δ 0.86 (t, *J*=6.8Hz, 3H, CH_3), 1.25 (bs, 30H, CH_2), 1.83 (m, 2H, CH_2), 3.48 (m, 2H, CH_2), 3.64-4.00 (m, 5H, CH_2 + NH), 4.01 (d, *J*=13.0Hz, 2H, CH_2), 4.31 (s, 3H, N-CH_3), 4.62 (m, 2H, N-CH_2), 7.01 (s, 1H, CH_{im}), 7.09 (s, 1H, CH_{im}); ^{13}C NMR ($CDCl_3$, 75 MHz, 20°C): δ 13.1 (CH_3), 21.6 (CH_2), 25.4 (CH_2), 28.2 (CH_2), 28.3 (CH_2), 28.4 (CH_2), 28.5 (CH_2), 28.6 (CH_2), 28.7 (CH_2), 30.9 (CH_2), 42.9 (N-CH_3), 50.8 (CH_2), 54.1 (N-CH_2), 68.1 (HN-CH), 111.0 (C-Pt), 122.4 (CH_{im}), 124.7 (CH_{im}).

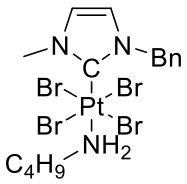

84. *Synthesized according to procedure G.* Red oil, 10.7 mg, yield 99%. ^{1}H NMR ($CDCl_3$, 300 MHz, 20 °C): *δ* 0.96 (t, *J*=7.1 Hz, 3H, CH_3), 1.42 (q, *J*=15.3 Hz, 7,9Hz, 2H, CH_2), 1.62 (q, J_1=15.3 Hz, J_2=7.9 Hz, 2H, CH_2), 3.22 (m, 2H, CH_2), 4.09 (bs, 2H, NH_2), 4.31 (s, 3H, N-CH_3), 5.92 s, 2H, N-CH_2), 6.71 (d, *J*=2.3Hz, 1H, CH_{im}), 6.94 (d, *J*=2.3Hz, 1H, CH_{im}), 7.32 (m, 5H, CH_{ar}); ^{13}C NMR ($CDCl_3$, 75 MHz, 20°C): δ 13.5 (CH_3), 19.6 (CH_2), 33.7 (s+d, *J*=11.1 Hz, N-CH_3), 43.4 (CH_2), 44.9 (CH_2), 58.6 (N-CH_2), 124.1 (s+d, *J*=11.1 Hz, CH_{im}), 125.4 (s+d, *J*=11.1 Hz, CH_{im}), 128.2 (CH_{ar}), 128.6 (CH_{ar}), 128.7 (CH_{ar}), 136.2 (C_{ar}), C-Pt signal could not be seen; HRMS (positive ESI) [2M +Na+H]: $C_{30}H_{47}N_6Pt_2Br_8Na_1$ 1542.6400, found 1542.6361.

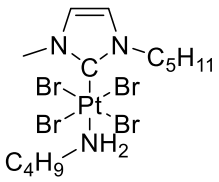

85. *Synthesized according to procedure G.* Red oil, 10.8 mg, yield 99%. ^{1}H NMR ($CDCl_3$, 300 MHz, 20 °C): δ 0.91-1.00 (m, 6H, CH_3), 1.26-1.67 (m, 8H, CH_2), 1.86 (m, 2H, CH_2), 3.27 (m, 2H, CH_2),

4.07 (bs, 2H, NH_2), 4.31 (s, 3H, N-CH_3), 4.63 (m, 2H, N-CH_2), 6.99 (d, *J*=2.1 Hz, CH_{im}), 7.07(d, *J*=2.1 Hz, CH_{im}); ^{13}C NMR ($CDCl_3$, 75 MHz, 20°C): δ 13.8 (CH_3), 14.2 (CH_3), 19.8 (CH_2), 22.6 (CH_2), 28.7 (CH_2), 28.9 (CH_2), 30.2 (CH_2), 31.1 (CH_2), 31.9 (CH_2), 34.0 (s+d, *J*=11.2 Hz, N-CH_3), 43.6 (CH_2), 44.9 (CH_2), 54.8, (s+d, *J*=5.3 Hz, N-CH_2), 115.3 (C-Pt), 123.3 (s+d, *J*=10.6 Hz, CH_{im}), 125.6 (s+d, *J*=10.6 Hz, CH_{im}); HRMS (positive ESI) [2M+Na+2H]: $C_{26}H_{56}N_6Pt_2Br_8Na_1$ 1503.7100, found 1503.2886.

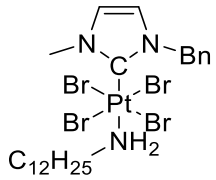

86. *Synthesized according to procedure G.* Red oil, 12.4 mg, yield 99%. ^{1}H NMR ($CDCl_3$, 300 MHz, 20 °C): δ 0.88 (m, 3H, CH_3), 1.27-1.48 (m, 18H, CH_2), 1.69 (m, 2H, CH_2), 3.25 (m, 2H, H_2N-CH_2), 4.09 (bm, 2H, NH_2), 4.34 (s, 3H, N-CH_3), 5.94 (s, 2H, N-CH_2), 6.75 (d, *J*=2.2 Hz, 1H, CH_{im}), 6.96 (d, *J*=2.2 Hz, 1H, CH_{im}), 7.36 m, 5H, CH_{ar}); ^{13}C NMR ($CDCl_3$, 75 MHz, 20°C): δ 14.3 (CH_3), 22.8 (CH_2), 26.6 (CH_2), 29.3 (CH_2), 29.5 (CH_2), 29.6 (CH_2), 29.7 (CH_2), 29.8 (CH_2), 32.0 (CH_2), 43.7 (N-CH_3), 45.3 (H2N-CH_2), 58.9 (N-CH_2), 124.2 (CH_{im}), 125.4 (CH_{im}), 128.5 (CH_{ar}), 128.9 (CH_{ar}), 129.0 (CH_{ar}), 136.3 (CH_{ar}), C-Pt signal could not be seen; HRMS (positive ESI) [2M+Na+H]: $C_{46}H_{79}N_6Pt_2Br_8Na_1$ 1766.89, found 1766.8905; elemental anal. calc. for $C_{23}H_{39}N_3Pt_1Br_4$: C 31.67, H 4.51, N 4.82, found: C 31.14, H 4.53, N 4.57.

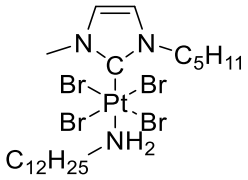

87. *Synthesized according to procedure G.* Red oil, 10.8 mg, yield 99%. ^{1}H NMR ($CDCl_3$, 300 MHz, 20 °C): δ 0.88-1.39 (m, 28H, CH_2+CH_3), 1.63-1.87 (m, 4H, CH_2), 3.26 (m, 2H, H_2N-CH_2), 4.09 (m, 2H, NH_2), 4.32 (s, 3H, N-CH_3), 4.63 (m, 2H, N-CH_2), 6.99 (d, *J*=2.2Hz, 1H, CH_{im}), 7.08 (d, *J*=2.2Hz, 1H, CH_{im}); ^{13}C NMR (75 MHz, $CDCl_3$): *δ* 14.2 (CH_3), 14.3 (CH_3), 22.6 (CH_2), 22.9 (CH_2), 26.6 (CH_2), 28.7 (CH_2), 29.3 (CH_2), 29.5-29.8 (CH_2), 31.1 (CH_2), 31.9 (CH_2), 32.1 (CH_2), 43.6 (N-CH_3), 45.2 (H2N-CH_2), 54.9 (N-CH_2), 104.8 (C-Pt), 123.3 (CH_{im}), 125.6 (CH_{im}).

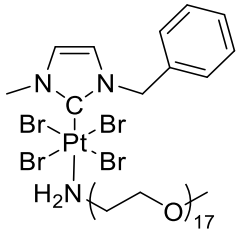

88. *Synthesized according to procedure G.* Red oil, 10.4 mg, yield 99%. ^{1}H NMR ($CDCl_3$, 500 MHz, 20 °C): δ 3.42 (s, 3H, CH_3), 3.73 (m, 71H, CH_2), 4.37 (s, 3H, N-CH_3), 5.97 (s, 2H, N-CH_2), 6.72 (d, *J*=Hz, 1H, CH_{im}), 6.96 (bs, 1H, CH_{im}), 7.36 (s, 5H, CH_{ar}), 7.62 (bs, 2H, NH_2); ^{13}C NMR $CDCl_3$, 125 MHz, 20°C): δ 43.7 (N-CH_3), 44.7 (O-CH_3), 58.9 (N-CH_2), 59.2 (CH_2), 69.9 (t, *J*=10.9 Hz, N-CH), 70.5 (CH_2), 70.7 (CH_2), 70.8 (CH_2), 72.0 (CH_2), 115.7 (t, *J*=520.3 Hz, C-Pt), 124.1 (t, *J*=10.7 Hz, CH_{im}), 125.4 (t, *J*=10.7 Hz, CH_{im}), 128.5 (CH_{ar}), 128.9 (CH_{ar}), 129.0 (CH_{ar}), 136.3 (C_{ar}); HRMS (positive ESI) [M +Na+H]: $C_{46}H_{86}N_3Pt_1Br_4Na_1$ 1490.22, found 1490.8083.

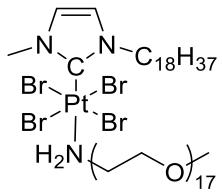

89. *Synthesized according to procedure G.* Red oil, 11.0 mg, yield 99%. ^{1}H NMR ($CDCl_3$, 300 MHz, 20 °C): δ 0.88 (t, *J*=6.9Hz, 3H, CH_3), 1.26 (bs, 30H, CH_2), 1.86 (m, 2H, CH_2), 3.39 (s, 3H, CH_3), 3.66 (bs, 70H, CH_2), 4.32 (s, 3H, N-CH_3), 4.59 (m, 2H, N-CH_2), 7.00 (d, *J*=2.2Hz, 1H, CH_{im}), 7.08 (d, *J*=2.2Hz, 1H, CH_{im}).

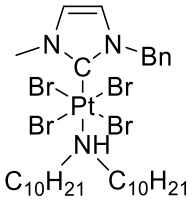

90. *Synthesized according to procedure G.* Red oil, 5.3 mg, yield 99%. ^{1}H NMR ($CDCl_3$, 300 MHz, 20 °C): *δ* 0.87 (t, *J*=7.1 Hz, 6H, CH_3), 1.27-1.35 (m, 28H, CH_2), 1.66 (m, 2H, CH_2), 1.83 (m, 2H, CH_2), 3.09 (m, 2H, CH_2), 3.73 (m, 2H, CH_2), 3.96 (bs, 1H, NH), 4.38 (s, 3H, N-CH_3), 6.00 (s, 2H, N-CH_2), 6.72 (d, *J*=2.1Hz, 1H, CH_{im}), 6.91 (d, *J*=2.1Hz, 1H, CH_{im}), 7.33-7.36 (m, 5H, CH_{ar}); ^{13}C NMR ($CDCl_3$,

75 MHz, 20°C): δ 14.2 (CH_3), 22.8 (CH_2), 26.7 (CH_2), 29.3 (CH_2), 29.4 (CH_2), 29.5 (CH_2), 29.7 (CH_2), 29.8 (CH_2), 32.0 (CH_2), 44.2 (N-CH_3), 53.5 (HN-CH_2), 59.4 (N-CH_2), 112.9 (C-Pt), 124.5 (CH_{im}), 125.5 (CH_{im}), 128.4 (CH_{ar}), 128.9 (CH_{ar}), 128.9 (CH_{ar}), 136.4 C_{ar}).

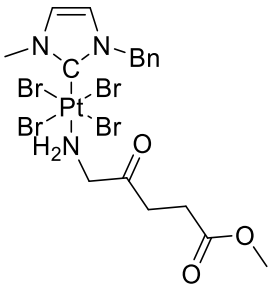

91. *Synthesized according to procedure G.* Red oil, 5.3 mg, yield 99%. ^{1}H NMR ($CDCl_3$, 300 MHz, 20 °C): *δ* 2.72 (m, 2H, C*H*$_2$-C(O)-O), 2.82 (m, 2H, C*H*$_2$-C(O)-CH_2-NH_2), 3.70 (s, 3H, O-CH_3), 4.28 (s+d, *J*= 6.9Hz, C*H*$_2$-NH_2), 4.35 (s, 3H, N-C*H*$_3$), 4.72 (bs, 2H, NH_2), 5.96 (s, 2H, N-CH_2), 6.73 (d, *J*=2.2Hz, CH_{im}), 6.93 (d, *J*=2.2Hz, CH_{im}), 7.36 (s, 5H, CH_{ar}).

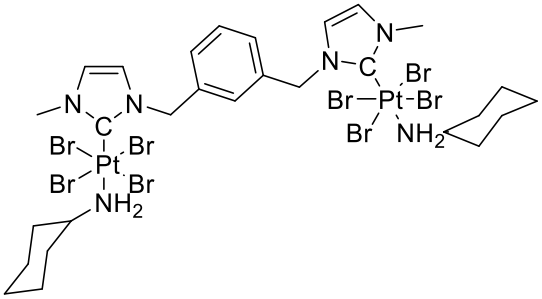

92. *Synthesized according to procedure G.* Red oil, 7.6 mg, yield 99%. ^{1}H NMR ($CDCl_3$, 300 MHz, 20 °C): *δ* 1.29-1.46 (m, 10H, CH_2), 1.73-1.78 (m, 6H, CH_2), 2.28 (m, 4H, CH_2), 3.54 (m, 2H, CH), 3.99 (bs+d, 4H, NH_2), 4.34 (s, 6H, N-CH_3), 5.93 (s, 4H, N-CH_2), 6.75 (m, 2H, CH_{ar}), 7.02 (s, 2H, CH_{im}), 7.30 (m, 2H, CH_{ar}); ^{13}C NMR ($CDCl_3$, 75 MHz, 20°C): *δ* 24.6, 25.3, 35.5, 43.4, 43.9, 54.9, 55.1, 58.4, 59.1, 110.0 (C-Pt), 114.8 (CH_{im}), 115.2 (CH_{im}), 117.0 (CH_{im}), 117.2 (CH_{im}), 124.6-124.8, 125.2, 126.2-126.4, 127.6, 127.9, 128.3-128.6, 129.2, 129.4, 129.6, 136.4, 136.7, 137.3, 137.4; HMQC ^{1}H–^{195}Pt NMR ($CDCl_3$, 64.2 MHz, 20 °C): *δ* -2158 ppm (m).

b. [(NHC)PtCl$_4$L]

- **Procedure I: Direct oxidation with PhICl$_2$**

In a 10 mL round bottom flask, the precursor (10 mg, 1 equiv.) was dissolved in CH_2Cl_2 (5 mL) and cooled at 0 °C and $PhICl_2$ (10 equiv.) was slowly added. After 1 hour at 0 °C, the addition of pentane (10 mL) caused the precipitation of [(NHC)PtCl$_4$L] as a light yellow powder, which was filtered off, washed and dried.

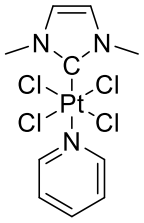

93. *Synthesized according to procedure I.* Light yellow solid, 9.5 mg, yield 99%. ^{1}H NMR ($CDCl_3$, 300 MHz, 20 °C): δ 4.38 (t, 6H, N–CH_3), 7,01 (d, *J*=2.1 Hz, 2H, CH_{im}), 7.54 (m, 2H, H_{pyr}), 7.93 (m, 1H, H_{pyr}), 9.28 (m, 2H, H_{pyr}); ^{13}C NMR ($CDCl_3$, 75 MHz, 20°C): δ 41.6 (N-CH_3), 125.1 (C_{pyr}), 125.5 (CH_{im}), 139.9 (C_{pyr}), 151.1 (C_{pyr}).

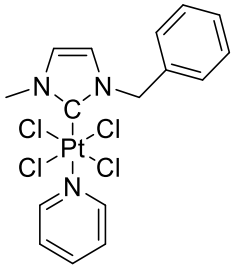

94. *Synthesized according to procedure I.* Light yellow solid, 8.1 mg, yield 97%. ^{1}H NMR ($CDCl_3$, 300 MHz, 20 °C): δ 4.42 (t, 3H, N–CH_3), 6.03 (s, 2H, N–CH_2), 6.77 (d, *J*=2.1 Hz, 1H, CH_{im}), 6.95 (d, *J*=2.1 Hz, 1H, CH_{im}), 7.35–7.41 (m, 5H, H_{ar}), 7.55 (m, 2H, H_{pyr}), 7.96 (m, 1H, H_{pyr}), 9.31 (m, 2H, H_{pyr}); no ^{13}C NMR could be recorded due to very low solubility. HMQC ^{1}H–^{195}Pt NMR ($CDCl_3$, 64.2 MHz, 20 °C): δ −755 ppm (m); HRMS (positive ESI) [M + Na]: $C_{16}H_{17}Cl_4N_3Pt_1Na_1$ 608.9718, found 608.9634; elemental anal. calc. for $C_{16}H_{17}Cl_4N_3Pt_1$: C 32.67, H 2.91, N 7.14, found: C 32.52, H 2.87, N 7.02.

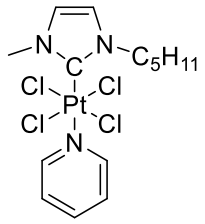

95. *Synthesized according to procedure I.* Light yellow solid, 9.1 mg, yield 94%. ^{1}H NMR ($CDCl_3$, 300 MHz, 20 °C): δ 0.92 (t, *J*=7.0 Hz, 3H, CH_3), 1.41 (m, 4H, CH_2), 1.91 (m, 2H, CH_2), 4.37 (s, 3H, N–CH_3), 4.71 (m, 2H, N–CH_2), 7.01 (d, *J*=2.1 Hz, 1H, CH_{im}), 7.11 (d, *J*=2.1 Hz, 1H, CH_{im}), 7.53 (m, 2H, H_{pyr}), 7.94 (m, 1H, H_{pyr}), 9.30 (m, 2H, H_{pyr}); ^{13}C NMR ($CDCl_3$, 75 MHz, 20°C): δ 13.9 (CH_3), 22.3 (CH_2), 28.7 (CH_2), 41.4 (N–CH_3), 52.9 (N–CH_2), 111.5 (C–Pt), 123.1 (s + d, *J*=11.1 Hz, CH_{im}), 124.8 (C_{pyr}), 125.6 (s + d, *J*=11.1 Hz, CH_{im}), 139.7 (C_{pyr}), 150.9 (C_{pyr}); HMQC ^{1}H–^{195}Pt NMR (CDCl3, 64.2 MHz, 20 °C): δ −810 ppm (m); HRMS (positive ESI) [M + Na]: $C_{14}H_{21}Cl_4N_3Pt_1Na_1$ 589.0031, found 589.0084; elemental anal. calc. for $C_{14}H_{21}Cl_4N_3Pt_1$ + CH_2Cl_2: C 29.59, H 3.73, N 7.40, found: C 29.09, H 3.52, N 7.44.

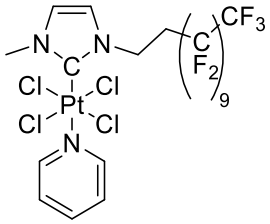

96. *Synthesized according to procedure I.* Light yellow solid, 9.7 mg, yield 99%. ^{1}H NMR ($CDCl_3$, 300 MHz, 20 °C): δ 2.84-2.87 (m, 2H, CH_2), 4.41 (s, 3H, N-CH_3), 5.16 (m, 2H, N- CH_2), 7.11 (m, 2H, CH_{im}), 7.55 (m, 2H, H_{Pyr}), 7.97 (m, 1H, H_{Pyr}), 9.28 (m, 2H, H_{Pyr}); ^{13}C NMR ($CDCl_3$, 75 MHz, 20 °C): δ 33.9 (t, *J*=21.3Hz, CH_2), 41.8 (N-CH_3), 45.2 (N- CH_2), 114.4 (C-Pt), 123.6 (CH_{im}), 125.2 (C_{Pyr}), 126.7 (CH_{im}), 140.1 (C_{Pyr}), 151.2 (C_{Pyr}). CF_2 and CF_3 signals could not be seen.

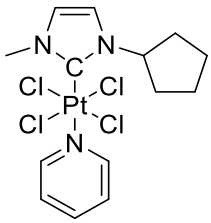

97. *Synthesized according to procedure I.* Light yellow solid, 9.2 mg, yield 96%. ^{1}H NMR ($CDCl_3$, 300 MHz, 20 °C): δ 1.64–1.85 (m, 6H, CH_2), 2.46–2.50 (m, 2H, CH_2), 4.36 (s, 3H, N–CH_3), 6.11 (m, 1H, N–CH), 7.02 (d, *J*=2.1 Hz, 1H, CH_{im}), 7.12 (d, *J*=2.1 Hz, 1H, CH_{im}), 7.53 (m, 2H, H_{pyr}), 7.92 (m, 1H, H_{pyr}), 9.30 (m, 2H, H_{pyr}); ^{13}C NMR ($CDCl_3$, 75 MHz, 20°C): δ 24.6 (CH_2), 30.8 (CH_2), 35.4 (N–CH), 41.3 (N–CH_3), 63.0 (N–CH_2), 120.9 (CH_{im}), 124.9 (C_{pyr}), 125.9 (CH_{im}), 139.7 (C_{pyr}), 151.0 (C_{pyr}), the carbene resonance peak was not observed; HMQC ^{1}H–^{195}Pt NMR ($CDCl_3$, 64.2 MHz, 20 °C): δ −1320 ppm (m); MS (positive ESI) [M + Na]: $C_{14}H_{19}Cl_4N_3Pt_1Na_1$ 586.99, found 586.98.

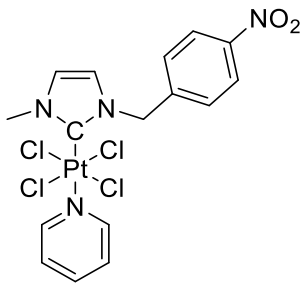

98. *Synthesized according to procedure I.* Light yellow solid, 9.2 mg, yield 96%. ^{1}H NMR ($CDCl_3$, 300 MHz, 20 °C): δ 4.45 (s, 3H, N–CH_3), 6.16 (s, 2H, N–CH_2), 6.76 (d, *J* = 2.1 Hz, 1H, CH_{im}), 7.06 (d, *J* = 2.1 Hz, 1H, CH_{im}), 7.51–7.61 (m, 4H, H_{ar}), 7.97 (m, 1H, H_{pyr}), 8.21 (m, 2H, H_{pyr}), 9.26–9.29 (m, 2H, H_{pyr}); ^{13}C NMR ($CDCl_3$, 75 MHz, 20°C): δ 41.8 (N–CH_3), 56.2 (N–CH_2), 123.9 (CH_{im}), 124.2 (C_{pyr}), 125.2 (CH_{im}), 129.4 (C_{ar}), 137.6 (C_{ar}), 140.1 (C_{ar}), 143.5 (C_{ar}), 148.0 (C_{pyr}), 151.1 (C_{pyr}), the carbene resonance peak was not observed; HMQC ^{1}H–^{195}Pt NMR ($CDCl_3$, 64.2 MHz, 20 °C): δ −834 ppm (m); MS (positive ESI) [2M + Na]: $C_{32}H_{32}Cl_8N_8Pt_2Na_1$ 1284.92, found 1284.89.

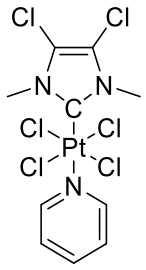

99. *Synthesized according to procedure I.* Light yellow solid, 9.4 mg, yield 98%. ^{1}H NMR ($CDCl_3$, 300 MHz, 20 °C): δ 4.37 (s, 6H, N–CH_3), 7.54 (m, 2H, H_{pyr}), 7.94 (m, 1H, H_{pyr}), 9.25 (m, 2H, H_{pyr}); ^{13}C NMR ($CDCl_3$, 75 MHz, 20°C): δ 31.0 (N–CH_3), 40.1 (N–CH_2), 112.9 (C–Pt), 120.8 (C_{pyr}), 125.2 (s

+ d, *J* = 18.9 Hz, C_{im}), 140.2 (C_{pyr}), 151.2 (s + d, *J* = 4.6 Hz, C_{pyr}); HMQC ^{1}H–^{195}Pt NMR ($CDCl_3$, 64.2 MHz, 20 °C): δ −825 ppm (m); HRMS (positive ESI) [M + Na]: Calculated for $C_{10}H_{11}Cl_6N_3Pt_1Na_1$ 600.8625, found 600.8624.

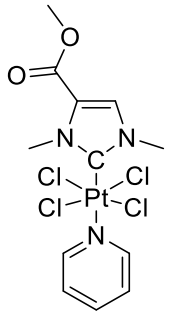

100. *Synthesized according to procedure I.* Light yellow solid, 8.9 mg, yield 93%. ^{1}H NMR ($CDCl_3$, 500 MHz, 20 °C): δ 3.91 (s, 3H, O-CH_3), 4.46 (s, 3H, N-CH_3), 4.61 (s, 3H, N-CH_3), 7.54 (m, 2H, CH_{pyr}), 7.71 (s, 1H, CH_{im}), 7.96 (m, 1H, CH_{pyr}), 9.26 (m, 2H, CH_{pyr}); ^{13}C NMR ($CDCl_3$, 125 MHz, 20°C): δ 39.7 (N-CH_3), 41.4 (N-CH_3), 51.5 (O-CH_3), 117.3 (t, *J*=1035.7 Hz, C-Pt), 124.0 (t, *J*=9.4 Hz, CH_{im}), 125.3 (t, *J*=12.8 Hz, CH_{pyr}), 130.9 (t, *J*=9.4 Hz, C_{im}), 138.9 (C=O); HRMS (positive ESI) [M+Li]: $C_{12}H_{15}N_3O_2Pt_1Cl_4Li_1$ 574.97, found 574.9717.

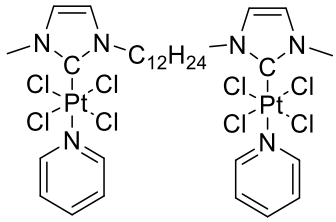

101. *Synthesized according to procedure I.* Light yellow solid, 9.2 mg, yield 96%. ^{1}H NMR ($CDCl_3$, 300 MHz, 20 °C): δ 1.25-1.41 (m, 20H, CH_2), 1.88 (m, 2H, 4H), 4.32 (s, 6H, N-CH_3), 4.66 (m, 4H, N-CH_2), 7.06 (d, *J*= 2.1 Hz, 2H, CH_{im}), 7.15 (d, *J*= 2.1 Hz, 2H, CH_{im}), 7.55 (m, 4H, CH_{pyr}), 7.98 (m, 2H, H_{pyr}), 9.23 (m, 4H, H_{pyr}); ^{13}C NMR ($CDCl_3$, 125 MHz, 20 °C): δ 26.8 (CH_2), 29.6 (CH_2), 29.7 (CH_2), 31.0 (CH_2), 32.3 (CH_2), 41.6 (N-CH_3), 111.3 (C-Pt), 123.7 (CH_{im}), 125.4 (C_{pyr}), 126.2 (CH_{im}), 140.4 (C_{pyr}), 151.1 (Cpyr); HRMS (positive ESI) [M+Li]: $C_{30}H_{44}N_6Pt_2Cl_8Li_1$ 1165.0586, found 1165.0546.

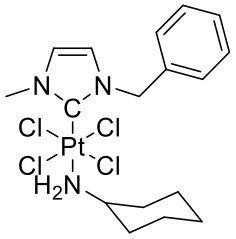

102. *Synthesized according to procedure I.* Light yellow solid, 9.2 mg, yield 96%. ^{1}H NMR ($CDCl_3$, 300 MHz, 20 °C): δ 1.26–1.45 (m, 4H, CH_2), 1.73–1.80 (m, 2H, CH_2), 3.45 (m, 1H, CH), 4.00 (bs, 2H, N–CH_2), 4.30 (s, 3H, N–CH_3), 5.89 (s, 2H, N–CH_2), 6.73 (d, *J*=2.1 Hz, 1H, CH_{im}), 6.90 (d, *J*=2.1 Hz, 1H, CH_{im}), 7.30–7.33 (m, 5H, H_{ar}); ^{13}C NMR ($CDCl_3$, 125 MHz, 20 °C): δ 24.7 (CH_2), 25.3 (CH_2), 35.1 (CH_2), 41.1 (CH), 52.7 (N–CH_3), 56.7 (N–CH_2), 123.7 (CH_{im}), 125.3 (CH_{im}), 128.5 (C_{ar}), 129.0 (C_{ar}), 129.1 (C_{ar}), 136.1 (C_{ar}), the carbene resonance peak was not observed; HMQC ^{1}H–^{195}Pt NMR ($CDCl_3$, 64.2 MHz, 20 °C): δ −885 ppm (m); elemental anal. calc. for $C_{17}H_{25}Cl_4N_3Pt_1$: C 33.57, H 4.14, N 6.91, found: C 33.79, H 4.33, N 6.59.

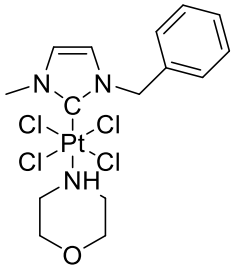

103. *Synthesized according to procedure I.* Light yellow solid, 8.0 mg, yield 96%. ^{1}H NMR ($CDCl_3$, 300 MHz, 20 °C): δ 3.04–3.08 (m, 2H, CH_2), 3.49–3.59 (m, 4H, CH_2), 3.83–3.90 (m, 2H, CH_2), 4.05 (s, 3H, N–CH_3), 5.71 (m, 2H, N–CH_2), 6.64 (d, *J*=2.1 Hz, 1H, CH_{im}), 6.78 (d, *J*=2.1 Hz, 1H, CH_{im}), 7.31–7.43 (m, H_{ar}); ^{13}C NMR ($CDCl_3$, 75 MHz, 20°C): δ 37.6 (N–CH_3), 48.8 (O–CH_2), 54.1 (N–CH_2), 68.1 (HN–*C*H_2), 120.2 (CH_{im}), 122.4 (CH_{im}), 128.7 (C_{ar}), 128.9 (C_{ar}), 136.0 (C_{ar}), the carbene resonance peak was not observed; HMQC ^{1}H–^{195}Pt NMR ($CDCl_3$, 64.2 MHz, 20 °C): δ −850 ppm (m); elemental anal. calc. for $C_{15}H_{21}Cl_4N_3O_1Pt_1$: C 30.22, H 3.55, N 7.05, found: C 30.03, H 3.37, N 7.08.

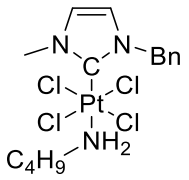

104. *Synthesized according to procedure I.* Light yellow oil, 4.9 mg, yield 52% ^{1}H NMR ($CDCl_3$, 300 MHz, 20 °C): δ 0.99 (t, *J*=7.1 Hz, 3H, CH_3), 1.46 (q, J_1=15.3 Hz, J_2=7.9 Hz, 2H, CH_2), 1.72 (q, *J*=15.3 Hz, 7,9Hz, 2H, CH_2), 3.21 (m, 2H, CH_2), 4.09 (bs, 2H, NH_2), 4.29 (s, 3H, N-CH_3), 5.88 (s, 2H, N-CH_2), 6.74 (d, *J*=2.3Hz, 1H, CH_{im}), 6.92 (d, *J*=2.3Hz, 1H, CH_{im}), 7.27-7.62 (m, 5H, CH_{ar}).

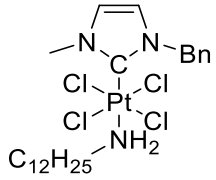

105. *Synthesized according to procedure I.* Light yellow oil, 9.6 mg, yield 47%. ^{1}H NMR ($CDCl_3$, 300 MHz, 20 °C): δ 0.90-0.92 (m, 3H, CH_3), 1.28-1.87 (m, 23H, CH_2), 3.23 (m, 2H, CH_2), 4.08 (bs, 2H, NH_2), 4.27 (m, 3H, N-CH_3), 4.60 (m, 2H, N-CH_2), 6.99 (bs, 1H, CH_{im}), 7.07 (bs, 1H, CH_{im}); ^{13}C NMR ($CDCl_3$, 75 MHz, 20 MHz): δ 14.0 (CH_2), 14.1 (CH_2), 22.4 (CH_2), 22.7 (CH_2), 26.5 (CH_2), 28.6 (CH_2), 29.2-29.6 (CH_2), 31.6 (CH_2), 31.9 (CH_2), 43.1 (m, N-CH_3), 53.0 (m, N-CH_2), 123.0 (CH_{im}), 125.5 (CH_{im}).

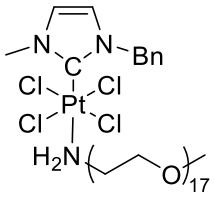

106. *Synthesized according to procedure I.* Light yellow oil, 9.9 mg, yield 35%. ^{1}H NMR ($CDCl_3$, 300 MHz, 20 °C): δ 3.38 (s, 3H, CH_3), 3.64 (bs, 71H, CH_2), 4.30 (s, 3H, N-CH_3), 5.88 (s, 2H, N-CH_2), 6.72 (d, 1H, CH_{im}), 6.91 (bs, 1H, CH_{im}), 7.36 (m, 5H, CH_{ar}).

- **Procedure J: Synthesis of *cis* [(NHC)PtX_2(DMSO)]**

The [(NHC)PtX_2(DMSO)] complexes were synthesized according to reported procedure:[5] A solution of bis(benzyl)imidazol-2-ylidene silver(I) bromide (20 mg, $4.42x10^{-5}$ mol) in DMSO was treated with K_2PtCl_4 (19.3 mg, $4.64x10^{-5}$ mol) and the resulting mixture was stirred at 60 °C for 24 h. After adding CH_2Cl_2 the reaction mixture was filtered and the filtrate was washed with water and then dried over Na_2SO_4. The solvent was removed in vacuum and the remainder recrystallized from CH_2Cl_2/pentane.

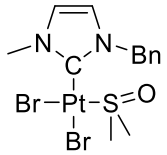

107. The *procedure J* was adapted adding excess of sodium bromide (10 equiv.) White solid, 12.5 mg, yield 47%. 1 H NMR ($CDCl_3$, 300 MHz, 20 °C): δ 3.05 (s+d, *J*=24.8 Hz, 3H, CH_3), 3.47 (s, 3H, CH_3), 3.98 (s, 3H, N-CH_3), 5.33-5.79 (dd, J_1=117.5 Hz, J_2=14.3 Hz, 2H, CH_{im}), 6.85 (d, *J*=2.1 Hz, 1H, CH_{im}), 6.91 (d, *J*=2.1 Hz, 1H, CH_{im}), 7.21-7.36 (m, 5H, CH_{ar}).

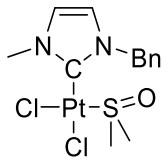

108. *Synthesized according to procedure J.* White solid, 14.8 mg, yield 65%. ^{1}H NMR ($CDCl_3$, 300 MHz, 20 °C): δ 3.03 (s+d, *J*=24.8 Hz, 3H, CH_3), 3.45 (s, 3H, CH_3), 4.01 (s, 3H, N-CH_3), 5.42-5.86 (dd, J_1=117.5 Hz, J_2=14.3 Hz, 2H, CH_{im}), 6.86 (d, *J*=2.1 Hz, 1H, CH_{im}), 6.94 (d, *J*=2.1 Hz, 1H, CH_{im}), 7.29-7.38 (m, 5H, CH_{ar}).

[5] *J*. K. Muenzner, T. Rehm, B. Biersack, A. Casini, I. A. M. de Graaf, P. Worawutputtapong, A. Noor, R. Kempe, V. Brabec, *J*. Kasparkova, R. Schobert *J. Med. Chem.* **2015**, *58*, 6283-6292

4) X-Ray diffraction

- **[(NHC)PtI$_2$(pyr)] complexes**

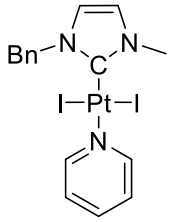

5

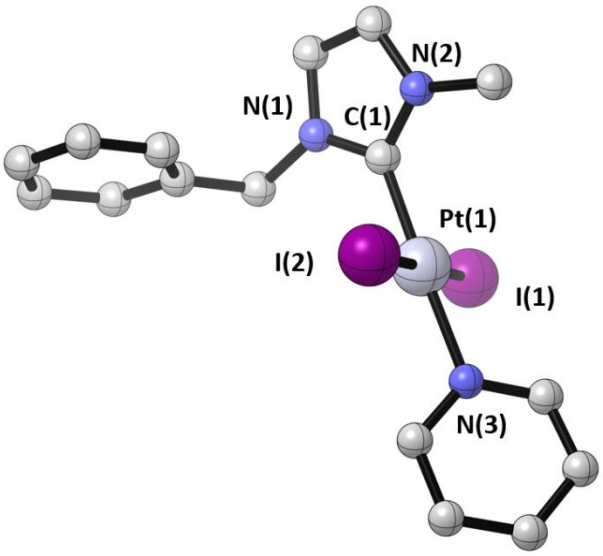

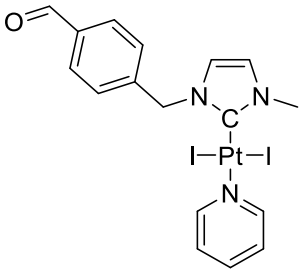

13

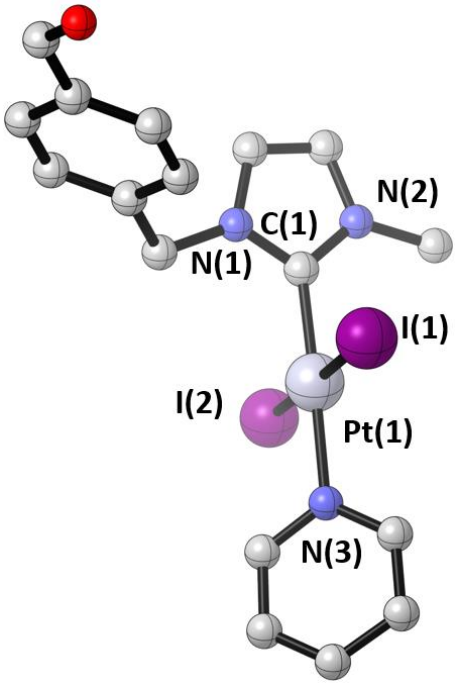

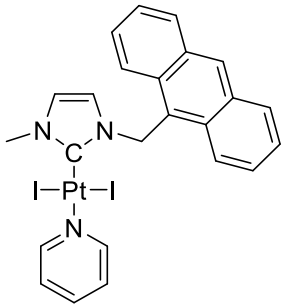

15

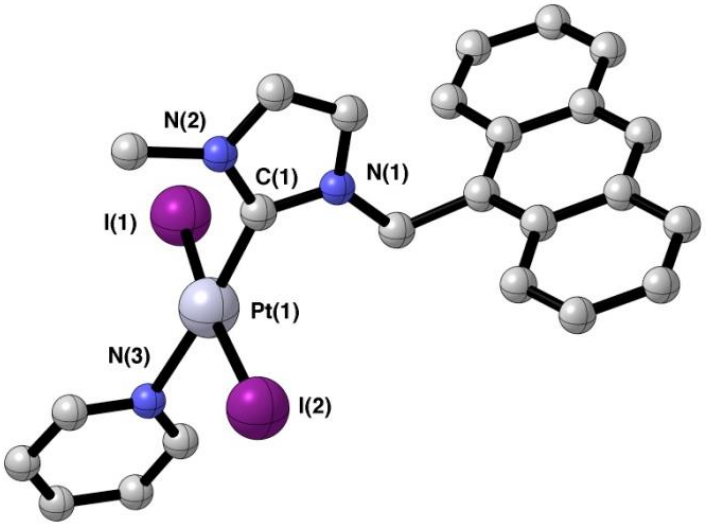

- **[(NHC)PtI$_2$(PnPh$_3$)] complexes**

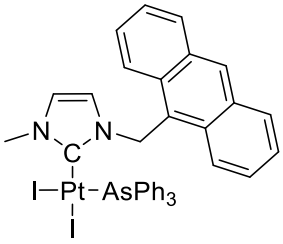

52b

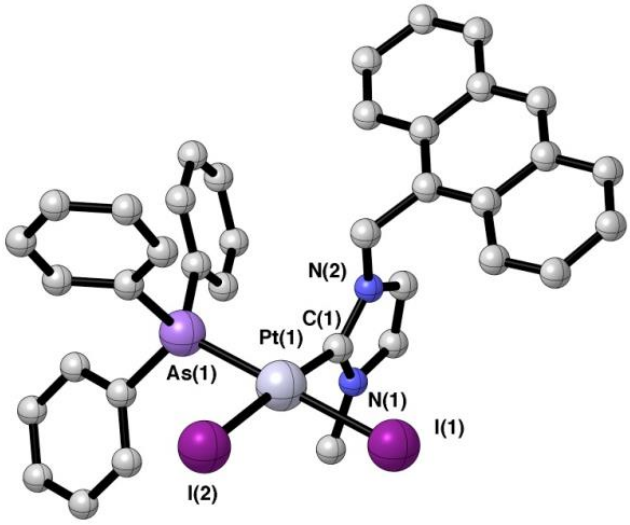

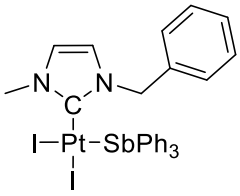

51c

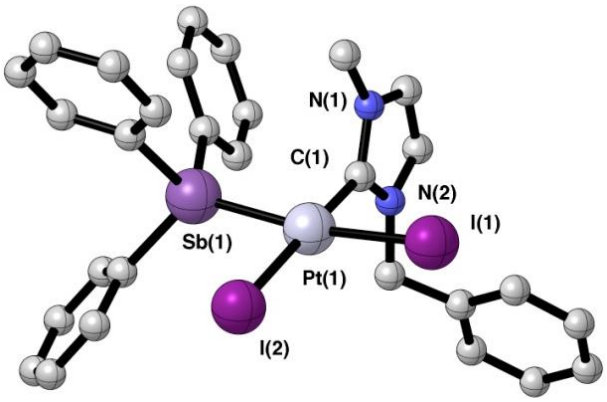

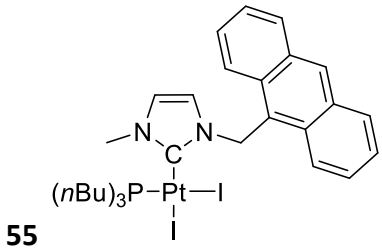

55

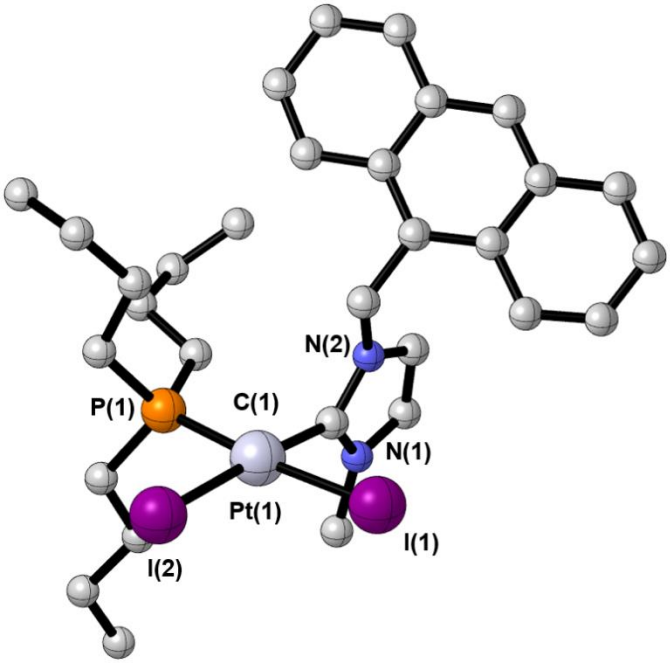

- **[(NHC)PtI ($PnPh_3$)$_2$]$^+$[I]$^-$ complex**

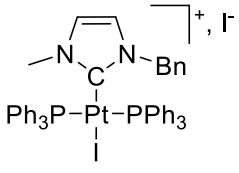

57a

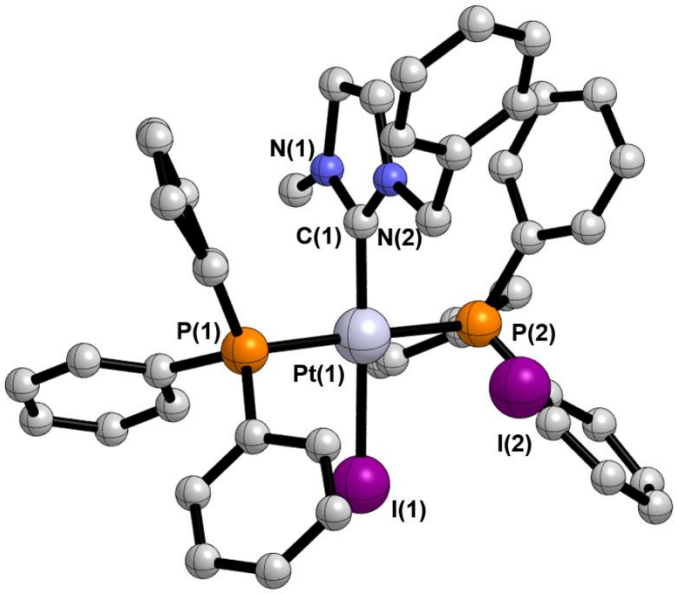

- **[(NHC)PtBr$_4$L] complexes**

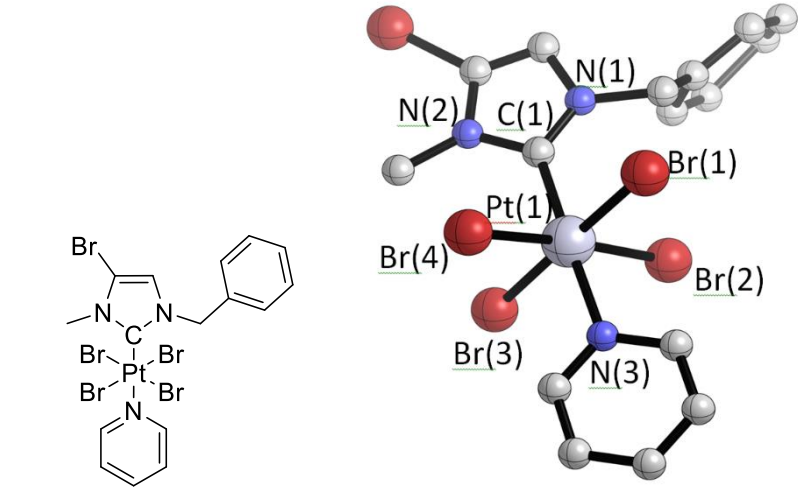

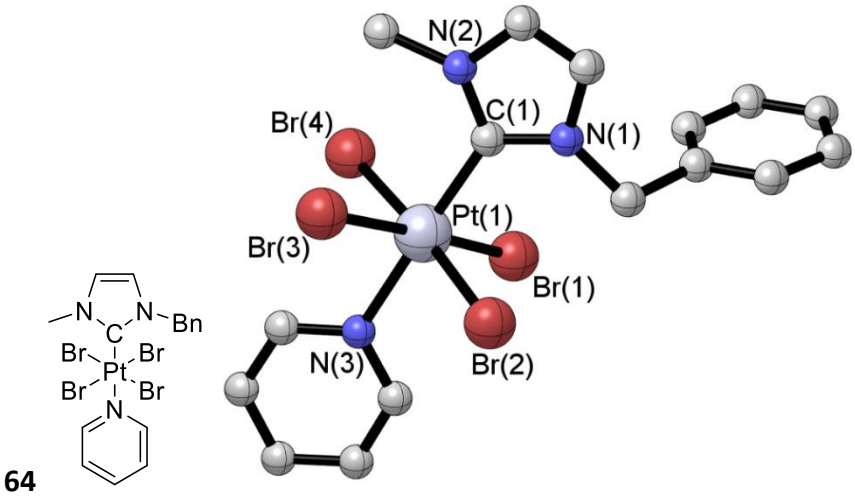

64

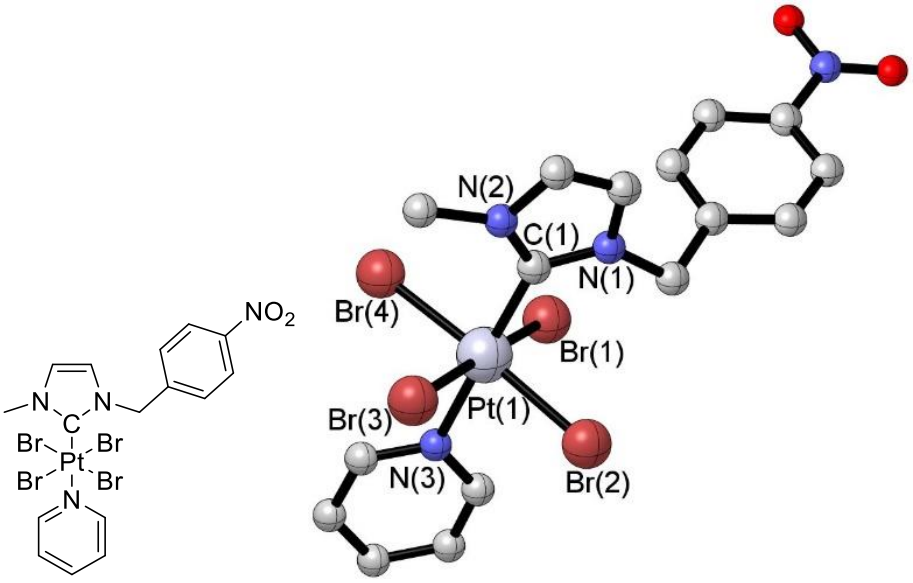

67

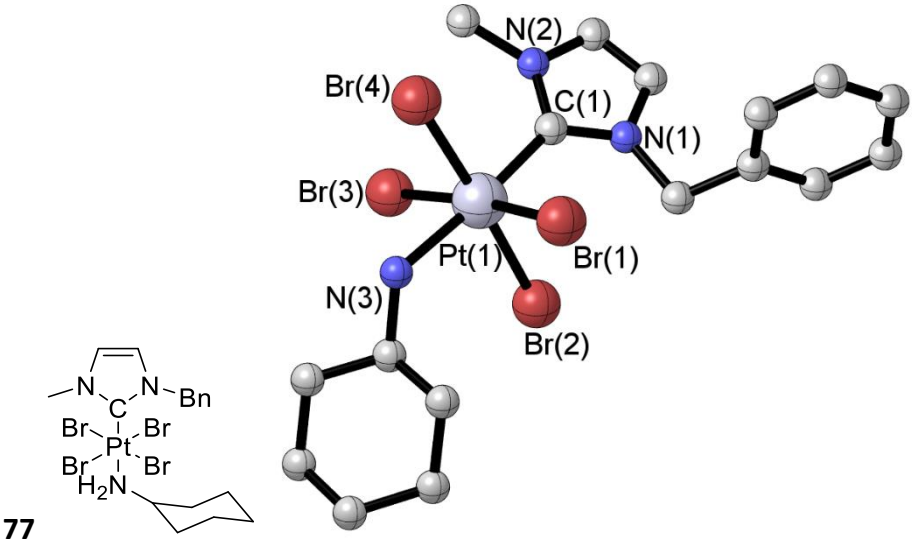

77

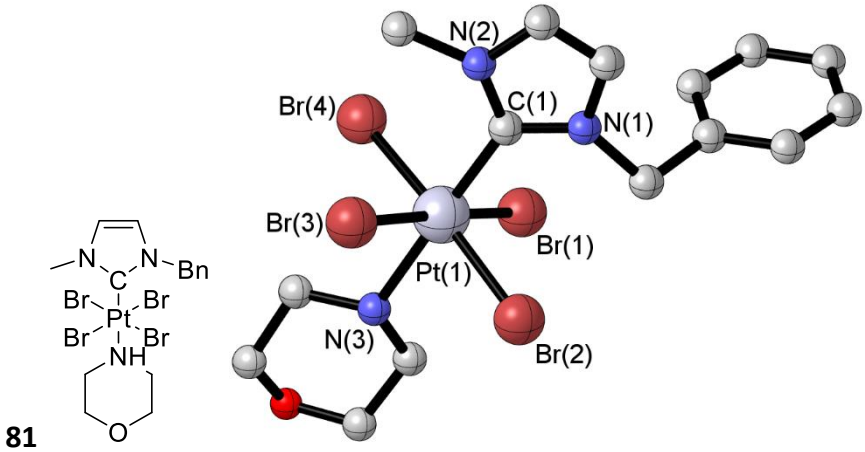

81

- **[(NHC)PtCl$_4$L] complex**

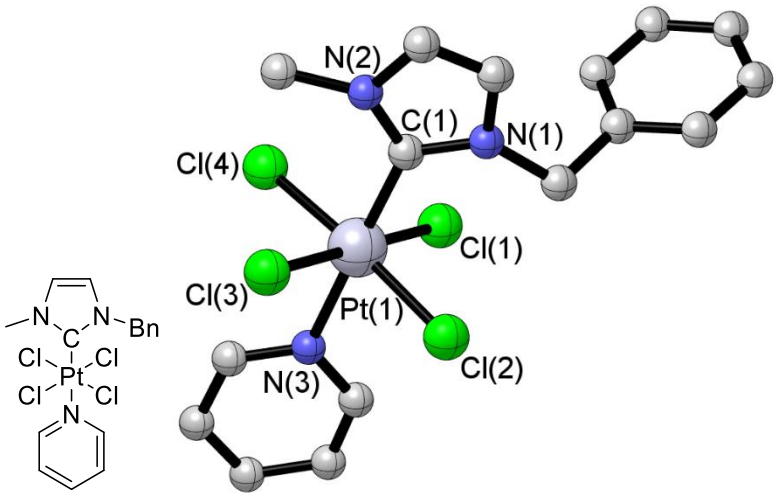

94

5) General procedure for reduction of [(NHC)PtX$_4$(pyridine)] complexes in DMSO

The stability of the complexes was monitored in d_6-DMSO by ^{1}H NMR at 20 °C and at a concentration of 10^{-3} M of platinum. The formation of *cis* [(NHC)PtX$_2$(DMSO)] species was confirmed by comparison with synthetic samples of **107** and **108**. The kinetic of the reaction was monitored via integration of the ^{1}H NMR signals attributed to the ortho-positions in the pyridine moiety in free pyridine (δ=8.8 ppm) versus its platinum-coordinated derivative (δ=9.1 ppm) (in d_6-DMSO, see example Figure A).

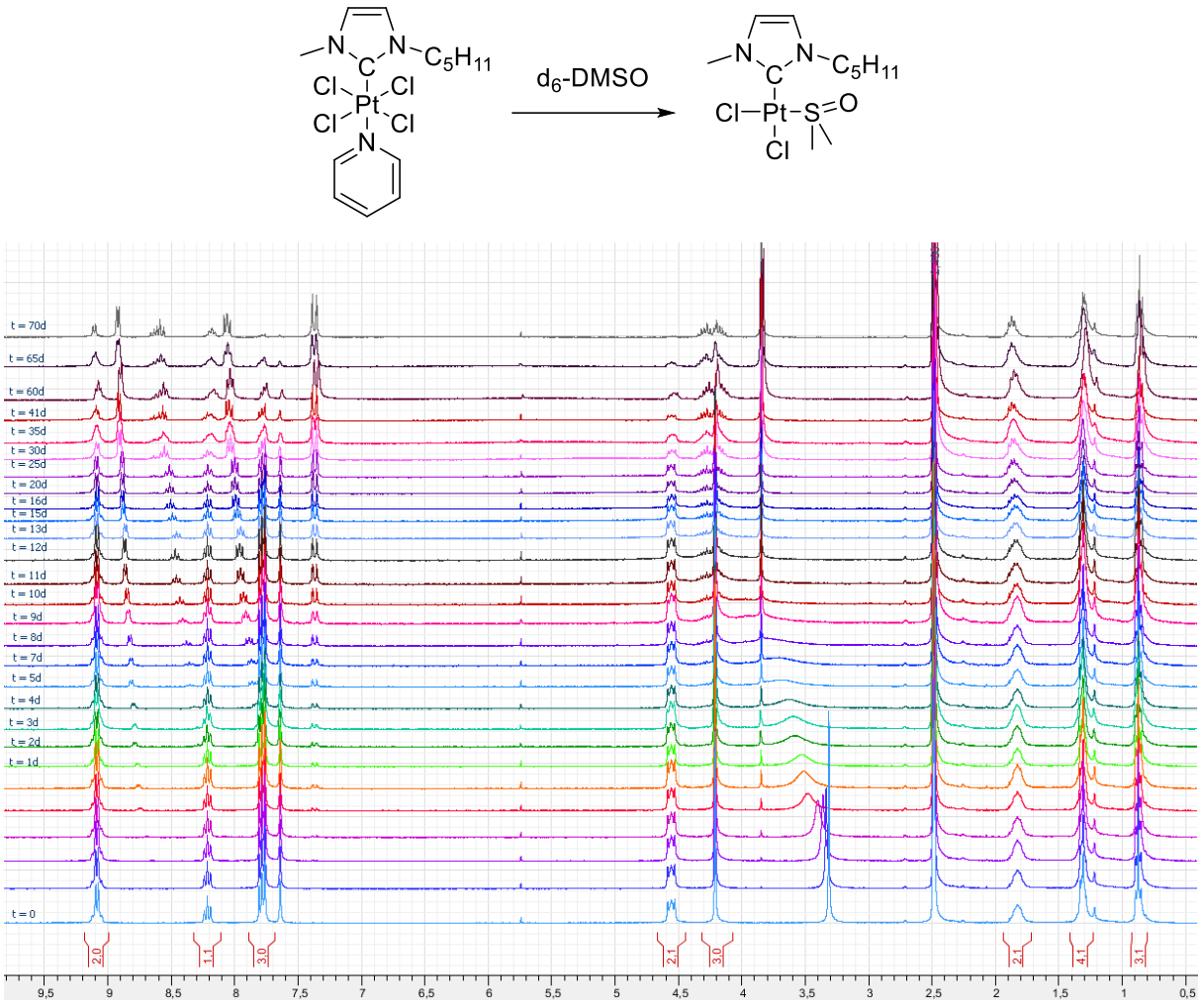

Figure 48: Reaction progress with platinum complex **95** (representative example) at 20 °C in d_6-DMSO.

6) General procedure for reduction of [(NHC)PtX$_4$L] complexes by bioreductants

The reduction of the complexes was monitored in freshly opened DMSO by UV-vis measurement at 25 °C and at a concentration of 10^{-3} M of platinum. The formation of *cis* [(NHC)PtX$_2$L] species was confirmed by comparison with synthetic samples described in chapter 2. The kinetic of the reaction was monitored thanks to the intensity decrease of the absorbance band at λ = 380 nm characteristic of the NHC-Pt(IV) complexes. (in DMSO, see example Figure B).

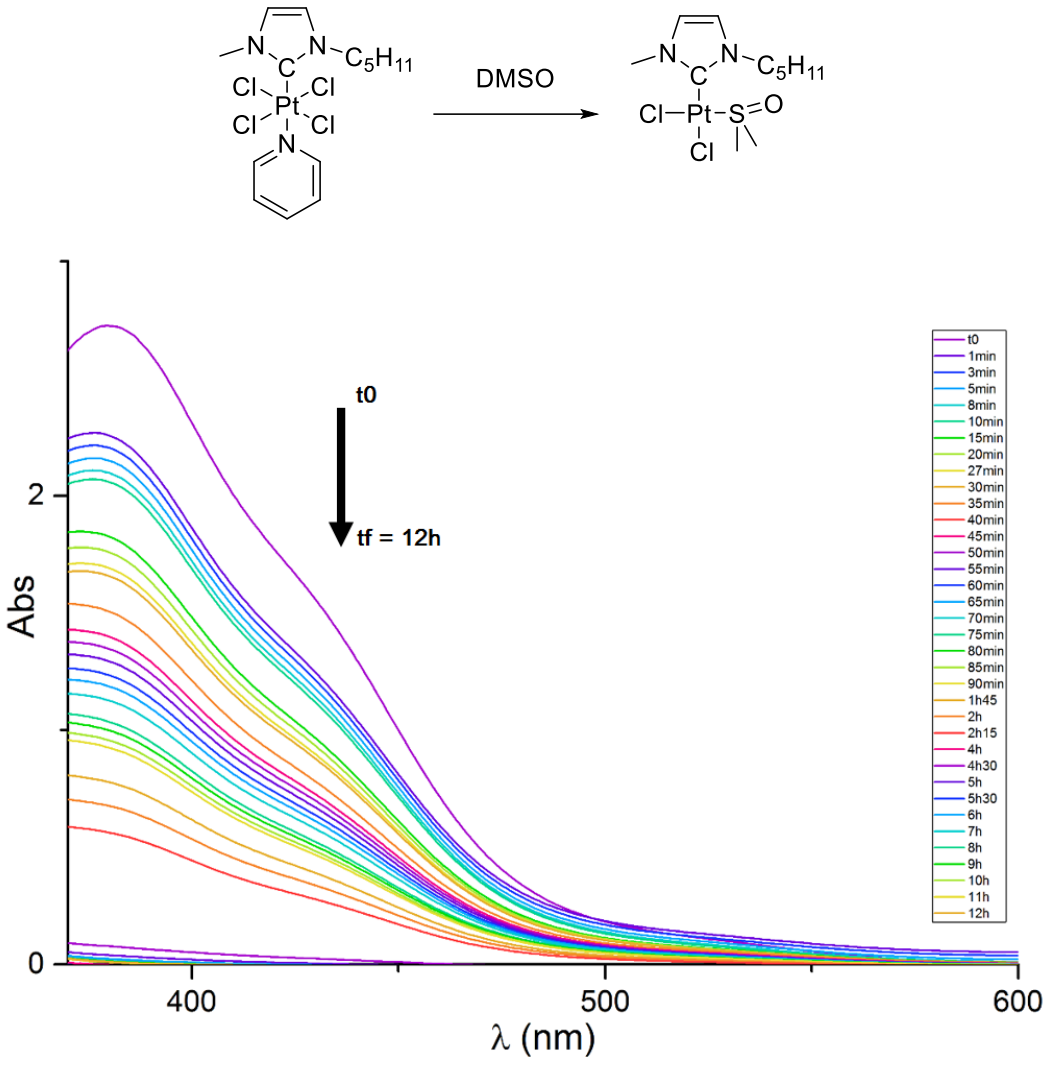

Figure 49: Reaction progress of platinum complex **95** with methionine (representative example) at 20°C in DMSO.

7) Electrochemical investigation by cyclic voltammetry

All the electrochemical measurements were performed in a three-electrode cell using a 3 mm diameter glassy carbon disk working electrode and Pt electrodes as counter electrode and pseudo-reference electrode. To avoid the presence of dissolved oxygen, the solutions were purged with argon before each current-potential curve measurement. The voltammograms discussed in this work were acquired at a scan rate of 100 $mV.s^{-1}$ at room temperature. The current-potential curves displayed in this have been obtained in the presence of a small amount of ferrocene, the origin of the potential axis being referred to the reversible redox waves of the ferrocene.

- **Cyclic voltammetry of NHC-Pt(II) and NHC-Pt(IV) complexes in CH_3CN**

In this case, the platinum complex was added to a 5 mL acetonitrile solution ([Pt]~0.1 mM) containing 0.1 M $TBAPF_6$ as supporting electrolyte. The current-potential curves were first measured in the absence and then in the presence of a small amount of ferrocene added for the potential axis calibration.

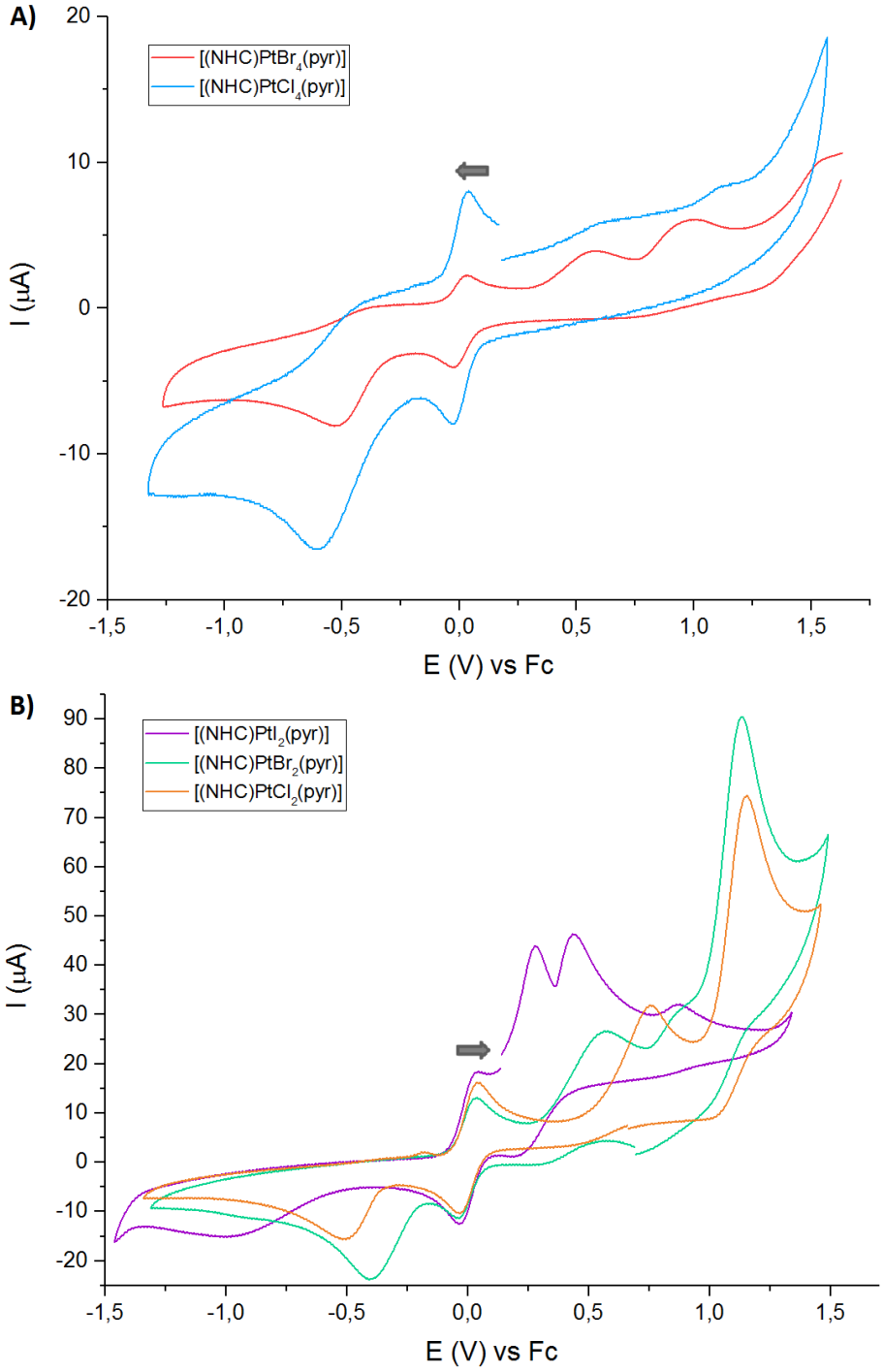

Figure 50: Cyclic voltammetry in 0.1M $TBAPF_6$ and acetonitrile solution at a scan rate of 100 $mV.s^{-1}$ on A) NHC-Pt(IV) complexes **59** and **95**, B) NHC-Pt(II) complexes **2**, **4** and **6**

- **Cyclic voltammetry of NHC-Pt(IV) complexes in DMSO**

In this case, the platinum complex was added to a 5 mL DMSO solution ([Pt]~0.1 mM) containing 0.1 M $TBAPF_6$ as supporting electrolyte. Each voltammograms were acquired at a scan rate of 100 $mV.s^{-1}$ at room temperature after progressive addition of small amounts of water. Small amount of ferrocene was added as a reference for potential calibration.

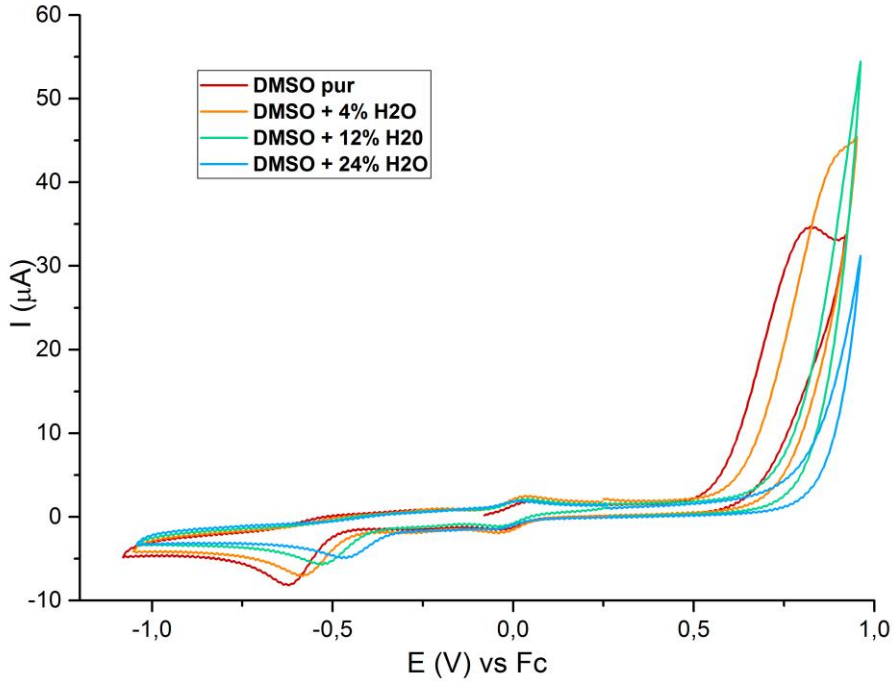

Figure 51: Cyclic voltammetry on bromine NHC-Pt(IV) complex **59** at a scan rate of 100 $mV.s^{-1}$ in a 0.1 M $TBAPF_6$ solution of a) DMSO, b) 95%DMSO/5%H_2O, c) 85%DMSO/15%H_2O, d) 76%DMSO/24%H_2O

- **Cyclic voltammetry of NHC-Pt(IV) complexes in DMSO with glutathione**

In this experiment, the platinum complex was added simultaneously to glutathione to a 5 mL DMSO solution ([Pt]~0.1 mM) containing 0.1 M $TBAPF_6$ as supporting electrolyte. Small amount of ferrocene was added as a reference for potential calibration.

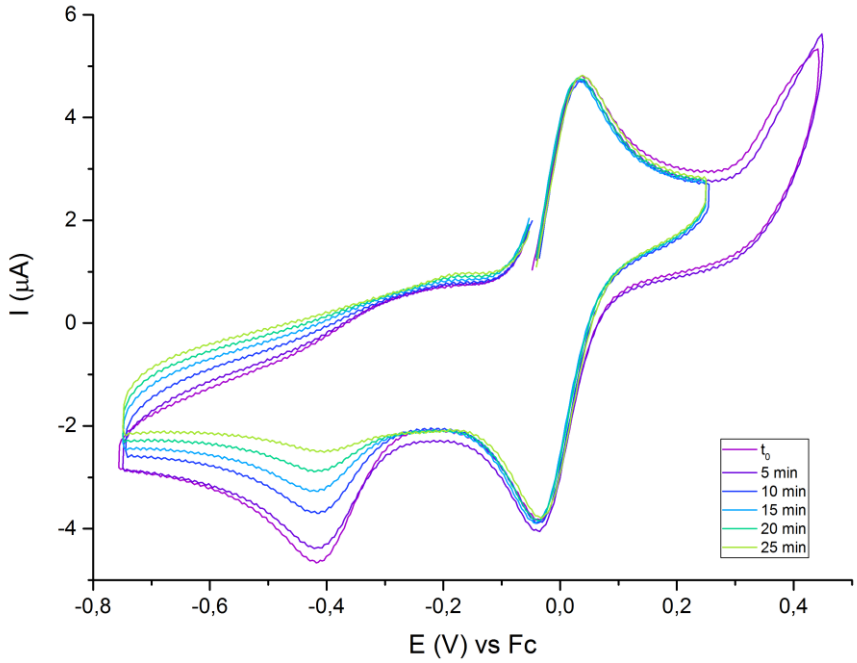

Figure 552: Evolution complex **59** in a DMSO solution with 0.1 M $TBAPF_6$ in the presence of one equivalent of GSH by cyclic voltammetry at 100 $mV.s^{-1}$

8) Apoptosis analysis by Annexin V-Propidium Iodide labelling

The human colon cancer cells HCT116 p53 KO were plated (5*104 cells/well) in 96-well plates. The next day, they were treated either with **95** (0.1, 1, 10 and 100 µM) or with **59** (0.1, 1, 10 and 100 µM) or with oxaliplatin (0.1, 1, 10 and 100 µM), a platinum derivative used as anticancer agent. After 24 h at 37 °C and 5 % CO_2, the cells were dissociated using trypsin-EDTA (Sigma-Aldrich) and incubated with Annexin-V-APC (Becton Dickinson Pharmingen) at 25 °C in the dark for 15 minutes. Cells were then stained with Propidium Iodide (PI) (Sigma Aldrich, 0.01 mg/mL) and analysed by a FacsCalibur (Becton Dickinson) flow cytometer and the CellQuest Pro Software. Between 2000 and 5000 cells were acquired for each experimental condition and the results were processed with Flow*J*o Data Analysis Software. Experiments were performed in triplicate.

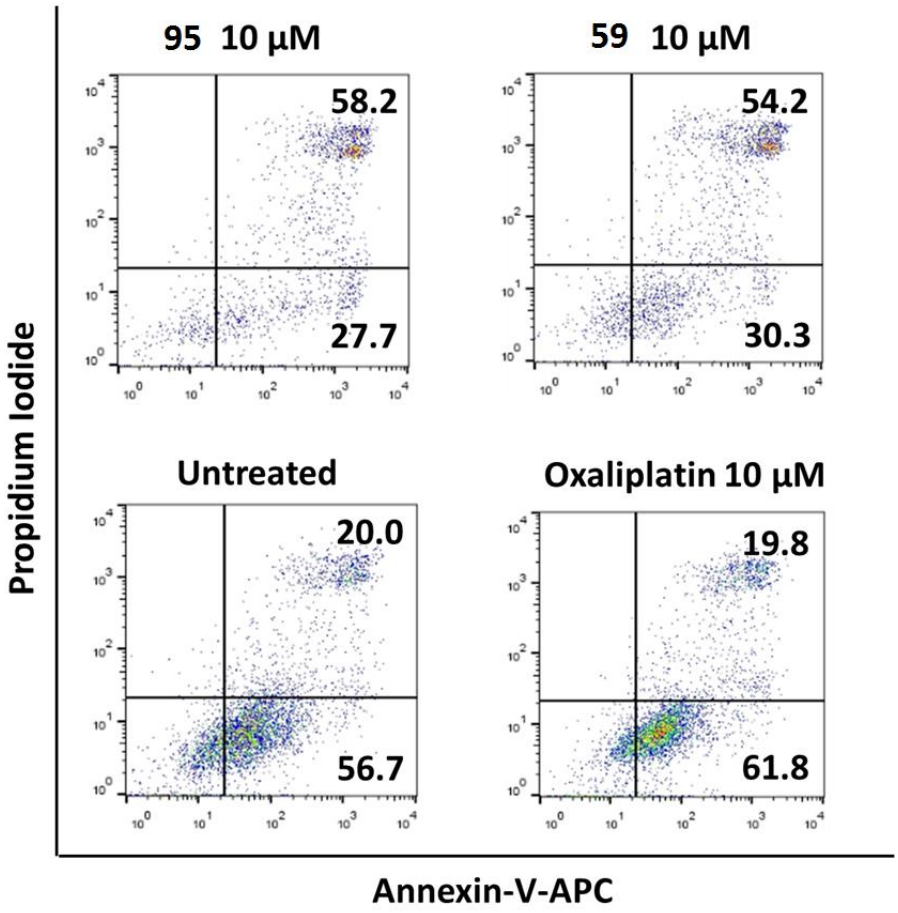

Figure 53: Evaluation of apoptosis on HCT116 p53 KO cell lines after treatment with **95**, **59** or oxaliplatin at indicated concentrations (24 h of incubation). After treatment, cells were labelled Annexin V-APC and Propidium Iodide and analysed by flow cytometry. Significant flow cytometry dot plots showing apoptosis induction are represented. The percentage of early apoptotic cells (Annexin V^+/PI^-) and late apoptotic cells (Annexin V^+/PI^+) are indicated.

9) ROS quantification and mitochondrial respiratory activity (MitoSx and MitoTracker staining)

The human colon cancer cells HCT116 were plated (5*104 cells/well) in 96-well plates and after they had adhered, they were treated either with **95** (0.1, 1, 10 and 100 µM) or **59** (0.1, 1.0, 10 and 100 µM) or with oxaliplatin (0.1, 1, 10 and 100 µM, Sigma-Aldrich), a platinum derivative used as anticancer agent, or with staurosporine (0.1, 1, 10 and 100 µM, Sigma-Aldrich), a

compound known to induce ROS production. After 12 h at 37 °C and 5 % CO_2, the cells were dissociated using trypsin-EDTA (Sigma-Aldrich) and incubated with either MitoSox Red mitochondrial superoxide indicator (1.0 µM, Invitrogen) or with MitoTracker Green FM and MitoTracker Deep Red 633 (0.2 µM, Invitrogen) followed by an incubation at 37 °C in the dark for 30 minutes. Between 2000 and 5000 cells were acquired for each experimental condition using a FacsCalibur (Becton Dickinson) flow cytometer and the CellQuest Pro Software. The results were processed with FlowJo Data Analyis Software. Experiments were performed in triplicate.

10) Synthesis of NHC-Pt-albumin macromolecules

- ***Procedure K: NHC-Pt complex encapsulation into bovin serum albumin***

To a BSA mixture in PBS/DMSO in a 18/1 ratio was slowly added a freshly prepared solution of NHC-Pt complex in DMSO and stirred for 15 minutes at 37 °C. The BSA concentration was maintained constant at 2.5×10^{-6} M for all experiments. The solution was allowed to settle for two complementary hours at 37 °C to ensure complete platinum uptake. Dialyse over one litter of water for 6 hours and subsequent lyophilization of the dialysate afforded the expected macromolecule as a light yellow solid.

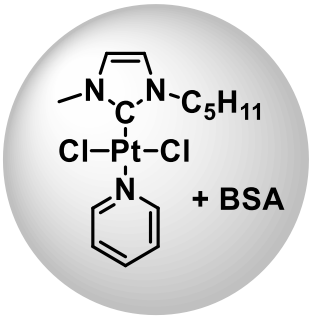

109

109. *Synthesized according to procedure K.* UV-vis (9/1 of H_2O/DMSO) λ_{max} (nm): 239, 270.

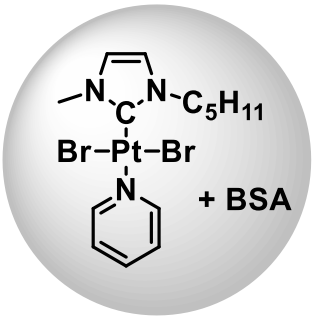

110

110. *Synthesized according to procedure K.* UV-vis (9/1 of H_2O/DMSO) λ_{max} (nm): 239, 275.

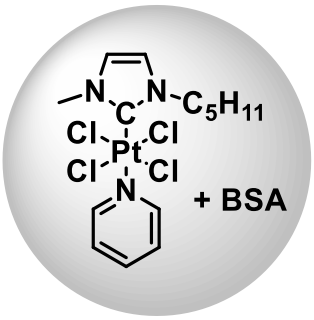

111

111. *Synthesized according to procedure K.* UV-vis (9/1 of H_2O/DMSO) λ_{max} (nm): 238, 269.

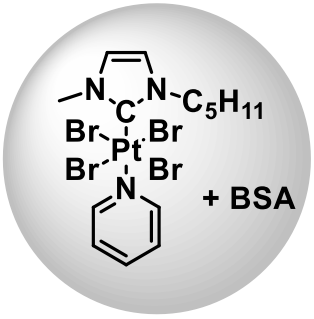

112

112. *Synthesized according to procedure K.* UV-vis (9/1 of H_2O/DMSO) λ_{max} (nm): 238, 278.

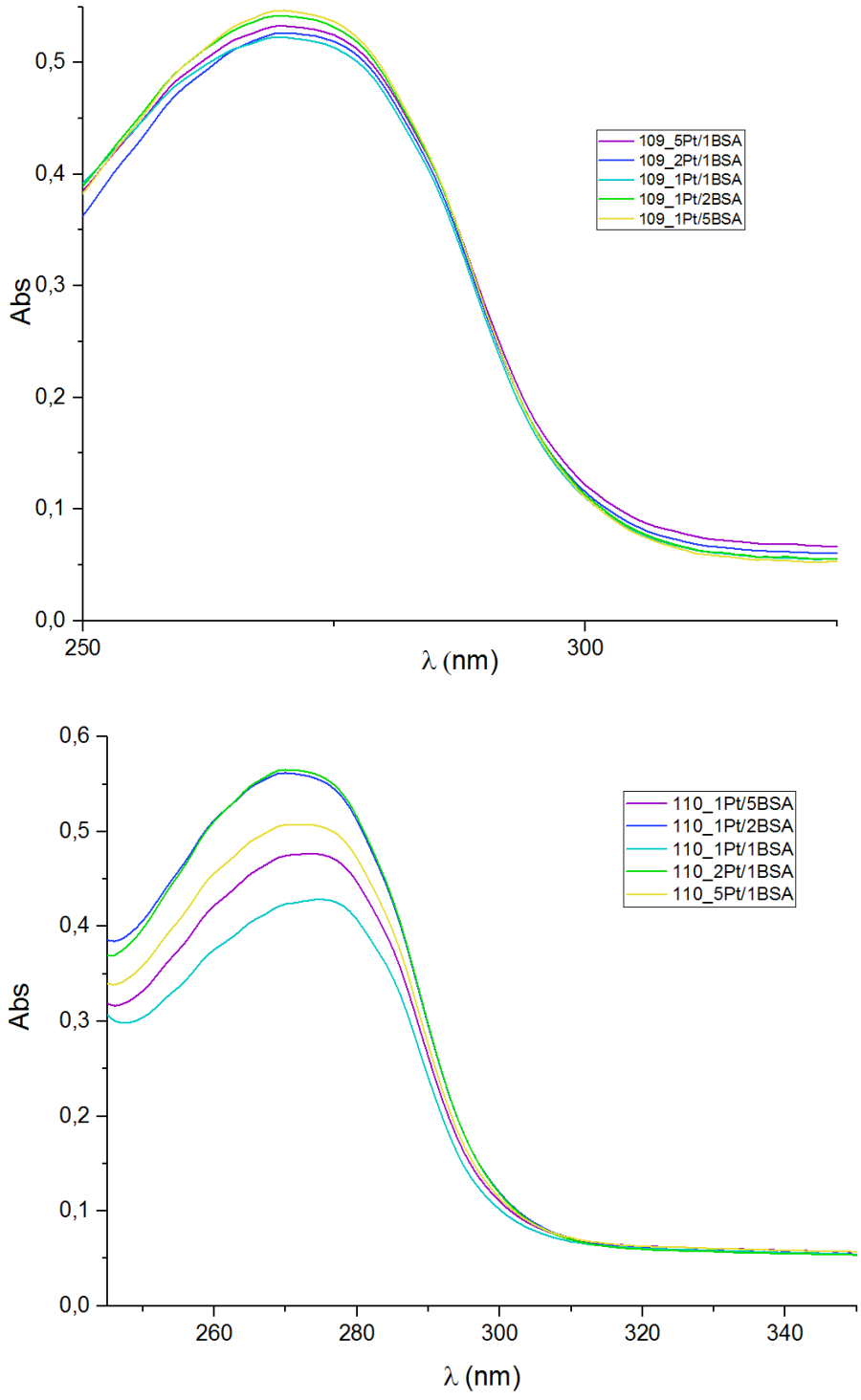

Figure 56: Evaluation of the interaction of NHC-Pt(II) complexes with BSA by UV depending on the Pt/BSA ratio for **109** (*above*) and **110** (*below*)

11) Synthesis of NHC-Pt-PEI complexes

- ***Procedure L: NHC-Pt coordination on PEI***

Under argon, a solution of complex **5** (20 mg, 28.6 µmol) and linear poly(ethyleneimine) of 25k Da (36.9 mg, 1.47 µmol) in ethanol (10 mL) was stirred for two days at 55°C.[6] The resulting solution was then concentrated under reduced pressure, precipitated by addition of excess diethyl ether and further centrifuged for 10 min at 10k rpm to afford the NHC-Pt-PEI conjugate as a white muggy solid.

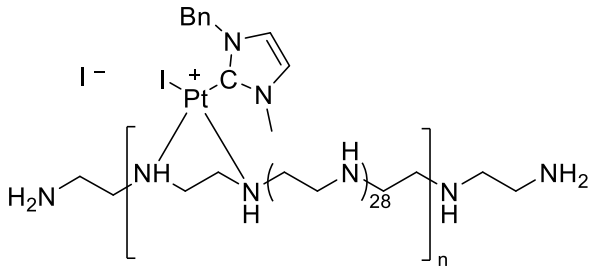

1Pt/30NH

113. *Synthesized according to procedure L.* White muggy solid, quant. 1H NMR (MeOD/CD_3CN, 300 MHz, 20°C): δ 2.2-3.1 (m, $CH_{2,PEI}$), 3.1-3.6 (m, $CH_{2,PEI}$+NH_{PEI} overlap with MeOD), 4.0-4.5 (m, NCH_3), 5.9 (m, NCH_2), 7.1-8.0 (m, CH_{im}+H_{ar}). Elemental Analysis: Calculated for $C_{71}H_{162}I_2N_{32}Pt.25H_2O$: C, 36.08; H, 9.04; N, 18.96; found C, 38.09; H, 7.60; N, 16.24.

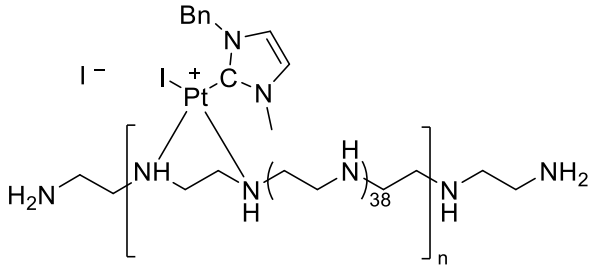

1Pt/40NH

[6] N. Chekkat, G. Dahm, E. Chardon, M. Wantz, J. Sitz, M. Decossas, O. Lambert, B. Frisch, R. Rubbiani, G. Gasser, G. Guichard, S. Fournel, S. Bellemin-Laponnaz *Bioconjugate Chem.* **2016**, *27*, 1942-1948

114. The *procedure L* was adapted using 10.1 mg of complex **5** and 25 mg of PEI to afford **114**. White muggy solid, quant. ^{1}H NMR (MeOD, 500 MHz, 20 °C): δ 0.80-2.11 (m, $CH_{2,PEI}$), 2.36-2.93 (m, $CH_{2,PEI}$), 3.06-4.11 (bs + m, $CH_{2,PEI}$+NH_{PEI} overlap with MeOD), 4.79 (bs, $CH_{2,PEI}$), 5.69 (m, N-CH_2), 6.51 (m, CH_{im}), 6.79 (m, CH_{im}), 7.21-7.62 (m, 94H, CH_{im}+H_{ar}); ^{13}C NMR (MeOD, 125MHz, 20 °C): δ 10.1-10.7, 15.5, 18.4, 23.8, 24.5, 27.4, 29.9-30.8, 32.3, 33.2, 35.3, 38.4-43.0, 45.3-48.1, 50.9-53.3, 55.0-55.7, 56.6-58.1, 58.3, 59.8-60.9, 64.9, 67.0, 77.7, 79.1, 82.4, 119.1 (CH_{im}), 124.2-125.1 (CH_{im}), 129.6-130.8 (CH_{ar}), 131.4 (CH_{ar}), 135.6 (C_{ar}), 138.0 (C_{ar}).

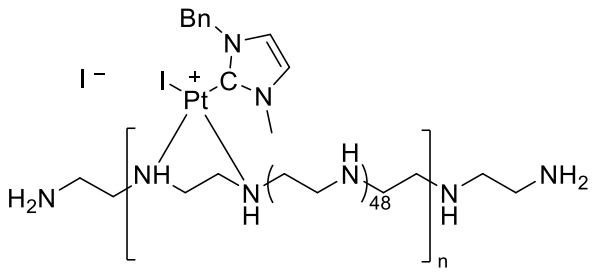

1Pt/50NH

115. The *procedure L* was adapted using 8.1 mg of complex **5** and 25 mg of PEI to afford **115**. White muggy solid, quant. ^{1}H NMR (MeOD, 500 MHz, 20 °C): δ 0.66-2.11 (m, $CH_{2,PEI}$), 2.37-2.91 (m, $CH_{2,PEI}$), 3.06-4.12 (bs + m, NH + NH_{PEI} overlap with MeOD), 4.79 (bs, $CH_{2,PEI}$), 5.24-5.74 (m, N-CH_2), 6.51 (m, CH_{im}), 6.80 (m, CH_{im}), 7.11-8.45 (m, 94H, CH_{im}+H_{ar}); ^{13}C NMR (MeOD, 125 MHz, 20 °C): δ 10.0-10.5,14.5, 19.9, 23.7, 24.3, 27.2, 28.1, 29.9-30.8, 33.1, 35.3, 36.6, 46.3-48.0, 52.5-57.0, 59.9, 79.0-79.6, 119.1 (CH_{im}), 124.3-124.9 (CH_{im}), 129.6-130.6 (CH_{ar}), 131.3 (CH_{ar}), 135.7 (C_{ar}), 138.3 (C_{ar}).

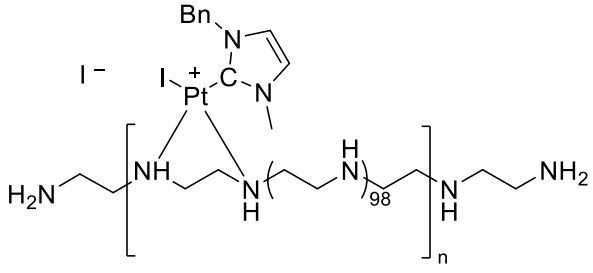

1Pt/100NH

116. The *procedure L* was adapted using 4 mg of complex **5** and 25 mg of PEI to afford **116**. White muggy solid, quant. ^{1}H NMR (MeOD, 500 MHz, 20 °C): δ 0.68-2.11 (m, $CH_{2,PEI}$), 2.34-2.85

(m, $CH_{2,PEI}$), 3.15-4.31 (bs + m, NH + NH_{PEI} overlap with MeOD), 4.80 (bs, $CH_{2,PEI}$), 5.24-5.67 (m, N-CH_2), 6.51 (m, CH_{im}), 6.80 (m, CH_{im}), 6.95-8.45 (m, 94H, CH_{im}+H_{ar});

- ***Procedure M: Condensation of carboxylic acids at the PEI extremities***

  Under argon, a solution of carboxylic acid derivative (2 equiv.) and N-hydroxysuccinimide (3 equiv.) was stirred at 20°C for 10 min. 1.55 mg of N-(3-Dimethylaminopropyl)-N'-ethylcarbodiimide hydrochloride (3 equiv.) was added to the solution and stirred at 20°C for another 30min. Poly(ethyleneimine) of 25k Da (1 equiv. 83 mg, 3.32 µmol) was then added to the solution which was stirred at 50°C for three days. The resulting solution was then concentrated under reduced pressure, precipitated by addition of excess diethyl ether and further centrifuged for 10min at 10k rpm to afford the functionalized PEI as colourless oil.

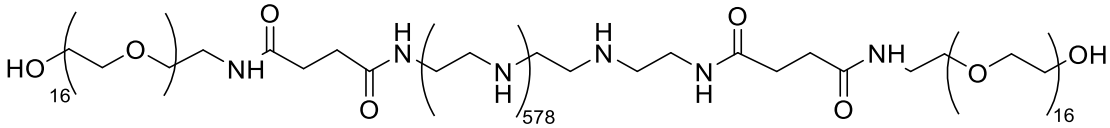

117. *Synthesized according to procedure N.* Colourless oil, quant. ^{1}H NMR (MeOD, 500 MHz, 20 °C): δ 1.08-1.25 (m, $CH_{2,PEI}$), 2.74 (m, $CH_{2,PEI}$), 3.31-3.64 (m, $CH_{2,PEI}$+ $CH_{2,PEG}$), 4.82 (bs, $CH_{2,PEI}$+$CH_{2,PEG}$+NH_{PEI}); ^{13}C NMR (MeOD, 125MHz, 20 °C): δ 10.0 ($CH_{2,PEI}$), 10.4 ($CH_{2,PEI}$), 14.4 ($CH_{2,PEI}$), 14.5 ($CH_{2,PEI}$), 15.8 ($CH_{2,PEI}$), 20.0 ($CH_{2,PEI}$), 23.6 ($CH_{2,PEI}$), 27.0 ($CH_{2,PEI}$), 28.8 ($CH_{2,PEI}$), 29.8-31.1 ($CH_{2,PEI}$), 32.8 ($CH_{2,PEI}$), 33.9 ($CH_{2,PEI}$), 34.6 ($CH_{2,PEI}$), 35.1 ($CH_{2,PEI}$), 35.6 ($CH_{2,PEI}$), 35.7 ($CH_{2,PEI}$), 39.1 ($CH_{2,PEI}$), 40.0 ($CH_{2,PEI}$), 40.1 ($CH_{2,PEI}$), 41.6 ($CH_{2,PEI}$), 45.4 ($CH_{2,PEI}$), 45.8 ($CH_{2,PEI}$), 46.6-49.9 ($CH_{2,PEI}$ + MeOD), 52.4 ($CH_{2,PEG}$), 54.9 ($CH_{2,PEG}$), 57.5 ($CH_{2,PEG}$), 57.9 ($CH_{2,PEG}$), 59.0 ($CH_{2,PEG}$), 60.7 ($CH_{2,PEG}$), 61.4 ($CH_{2,PEG}$), 64.3 ($CH_{2,PEG}$), 70.4 ($CH_{2,PEG}$), 71.1 ($CH_{2,PEG}$), 71.3 ($CH_{2,PEG}$), 73.6 ($CH_{2,PEG}$), 79.1 ($CH_{2,PEG}$), C=O could not be seen.

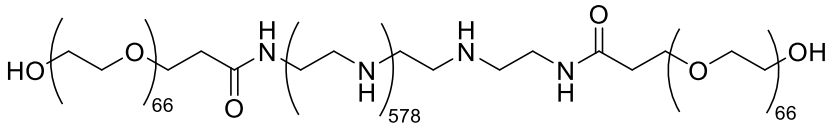

118. *Synthesized according to procedure N.* Colourless oil, quant. ^{1}H NMR (MeOD, 500 MHz, 20 °C): δ 2.73 (m, $CH_{2,PEI}$), 3.28-3.63 (m, $CH_{2,PEI}$+ $CH_{2,PEG}$), 4.86 (bs, $CH_{2,PEI}$+NH_{PEI}); ^{13}C NMR (MeOD,

125 MHz, 20 °C): δ 9.0 ($CH_{2,PEI}$), 13.3 ($CH_{2,PEI}$), 14.6 ($CH_{2,PEI}$), 22.4 ($CH_{2,PEI}$), 25.6 ($CH_{2,PEI}$), 25.7 ($CH_{2,PEI}$), 25.9 ($CH_{2,PEI}$), 26.8 ($CH_{2,PEI}$), 27.6 ($CH_{2,PEI}$), 28.9-29.9 ($CH_{2,PEI}$), 31.7 ($CH_{2,PEI}$), 34.5 ($CH_{2,PEI}$), 36.2 ($CH_{2,PEI}$), 37.9 ($CH_{2,PEI}$), 38.4 ($CH_{2,PEI}$), 42.9-48.4 ($CH_{2,PEI}$+MeOD), 50.1 ($CH_{2,PEG}$), 55.1 ($CH_{2,PEG}$), 56.7 ($CH_{2,PEG}$), 60.9 ($CH_{2,PEG}$), 68.5 ($CH_{2,PEG}$), 69.7-70.2 ($CH_{2,PEG}$), 72.4 ($CH_{2,PEG}$), 159.6 (C=O).

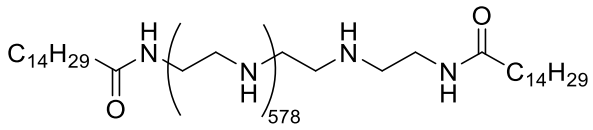

119. *Synthesized according to procedure N.* Colourless oil, quant. ^{1}H NMR (MeOD, 500 MHz, 20 °C): δ 0.87 (t, *J*=6.7 Hz, CH_{3alc}), 1.09 (m, CH_{2PEI} + CH_{2alc}), 1.23 (q, J_1=14.1 Hz, J_2=6.7 Hz, overlap m, CH_{2PEI} + CH_{2alc}), 1.56-1.88 (m, $CH_{2,PEI}$), 2.24-2.57 (m, $CH_{2,PEI}$), 2.75-2.87 (m, $CH_{2,PEI}$), 3.28-3.72 (m, $CH_{2,PEI}$), 4.11 (bs, $CH_{2,PEI}$+NH_{PEI}).

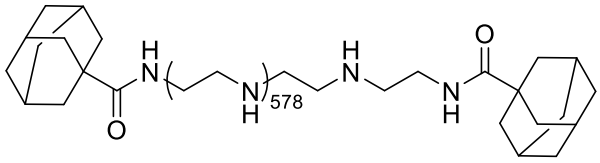

120. *Synthesized according to procedure N.* Colourless oil, quant. ^{1}H NMR (MeOD, 500 MHz, 20 °C): δ 1.11-1.28 (m, $CH_{2,PEI}$+$CH_{2,adamantyl}$), 1.72-1.75 (bs, $CH_{2,PEI}$+$CH_{2,adamantyl}$), 2.25 (m, $CH_{2,PEI}$), 2.38-2.54 (m, $CH_{2,PEI}$), 2.73-2.81 (m, $CH_{2,PEI}$), 3.32-3.75 (m, $CH_{2,PEI}$), 4.11 (m, $CH_{2,PEI}$+NH_{PEI}).

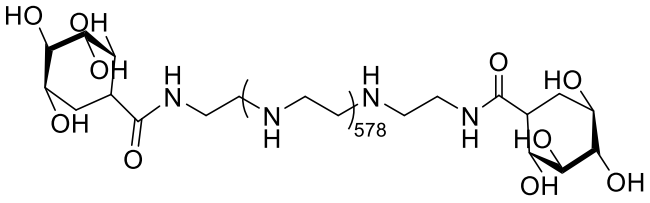

121. *Synthesized according to procedure N.* Colourless oil, quant. ^{1}H NMR (MeOD, 500 MHz, 20 °C): δ 1.10-1.31 (m, $CH_{2,PEI}$+$CH_{2,alc}$), 1.77-2.74 (m, $CH_{2,PEI}$+$CH_{2,alc}$), 3.21-3.71 (m, $CH_{2,PEI}$), 4.13-4.21 (bs, $CH_{2,PEI}$+NH_{PEI}).

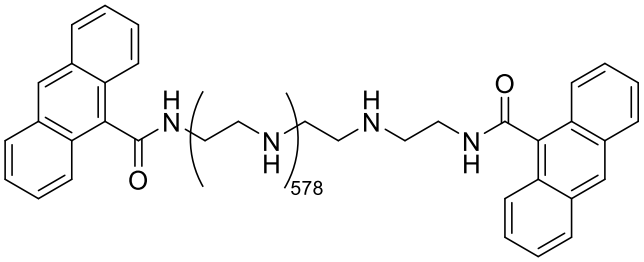

122. *Synthesized according to procedure N.* Light yellow oil, quant. ^{1}H NMR (MeOD, 500 MHz, 20 °C): δ 1.10-1.31 (m, $CH_{2,PEI}$), 1.61-1.87 (m, $CH_{2,PEI}$), 2.23-2.25 (m, $CH_{2,PEI}$), 2.34-2.84 (m, $CH_{2,PEI}$), 3.19-3.70 (m, $CH_{2,PEI}$ + $NH_{2,PEI}$), 3.96-4.10 (bs, $CH_{2,PEI}$+NH_{PEI}), 7.49 (m, $CH_{anthracene}$), 8.05 (m, $CH_{anthracene}$), 8.21-8.23 (m, $CH_{anthracene}$), 8.41 (m, $CH_{anthracene}$); ^{13}C NMR (MeOD, 125 MHz, 20 °C): δ 9.9 ($CH_{2,PEI}$), 10.1 ($CH_{2,PEI}$), 14.4 ($CH_{2,PEI}$), 14.6 ($CH_{2,PEI}$), 15.8 ($CH_{2,PEI}$), 18.1 ($CH_{2,PEI}$), 26.7-27.0 ($CH_{2,PEI}$), 31.2 ($CH_{2,PEI}$), 36.8 ($CH_{2,PEI}$), 37.3 ($CH_{2,PEI}$), 40.6 ($CH_{2,PEI}$), 44.1 ($CH_{2,PEI}$), 44.8 ($CH_{2,PEI}$), 45.6 ($CH_{2,PEI}$), 45.8 ($CH_{2,PEI}$), 45.9 ($CH_{2,PEI}$), 46.8 ($CH_{2,PEI}$), 47.2 ($CH_{2,PEI}$), 47.8 ($CH_{2,PEI}$), 48.8-49.1 ($CH_{2,PEI}$), 56.1-56.8 ($CH_{2,PEI}$), 58.1 ($CH_{2,PEI}$), 160.7 ($CH_{anthracene}$), 163.2.6-163.1 ($C_{anthracene}$), 163.3 ($CH_{anthracene}$), 164.1 ($CH_{anthracene}$), 176.1 (C=O); UV-vis (EtOH) λ_{max} (nm): 256; Fluorescence: λ_{ex}=390 nm, λ_{em}=359 nm.

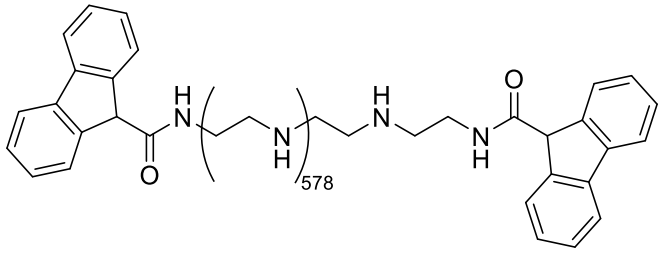

123. *Synthesized according to procedure N.* Light yellow oil, quant. ^{1}H NMR (MeOD, 500 MHz, 20 °C): δ 1.1-1.23 (m, $CH_{2,PEI}$), 1.74 (m, $CH_{2,PEI}$), 2.23 (s, $CH_{2,PEI}$), 2.37-2.43 (m, $CH_{2,PEI}$), 2.50-2.54 (m, $CH_{2,PEI}$), 3.20-3.38 (m, $CH_{2,PEI}$+MeOD), 4.10-4.22 (bs, $CH_{2,PEI}$+NH_{PEI}), 6.93 (m, $CH_{fluorene}$), 7.35-7.52 (m, $CH_{fluorene}$), 7.85 (m, $CH_{fluorene}$); ^{13}C NMR (MeOD, 125MHz, 20 °C): δ 14.6 ($CH_{2,PEI}$), 18.5 ($CH_{2,PEI}$), 26.8 ($CH_{2,PEI}$), 26.9 ($CH_{2,PEI}$), 35.7 ($CH_{2,PEI}$), 37.3 ($CH_{2,PEI}$), 37.4-37.6 ($CH_{2,PEI}$), 40.9 ($CH_{2,PEI}$), 44.1 ($CH_{2,PEI}$), 44.7-44.9 ($CH_{2,PEI}$), 47.8-49.8 ($CH_{2,PEI}$ + MeOD), 56.2 ($CH_{2,PEI}$), 58.1 ($CH_{2,PEI}$), 61.2 ($CH_{2,PEI}$), 61.3 ($CH_{2,PEI}$), 158.2 ($CH_{fluorene}$), 157.0 ($CH_{fluorene}$), 159.9-160.7 ($CH_{fluorene}$), 162.9-163.3 ($CH_{fluorene}$), 164.4 ($CH_{fluorene}$), 173.3 ($C_{fluorene}$), 173.4 ($C_{fluorene}$), 176.1 (C=O); UV-vis (EtOH) λ_{max} (nm): 205; Fluorescence: λ_{ex}= 390nm, λ_{em}=357 nm.

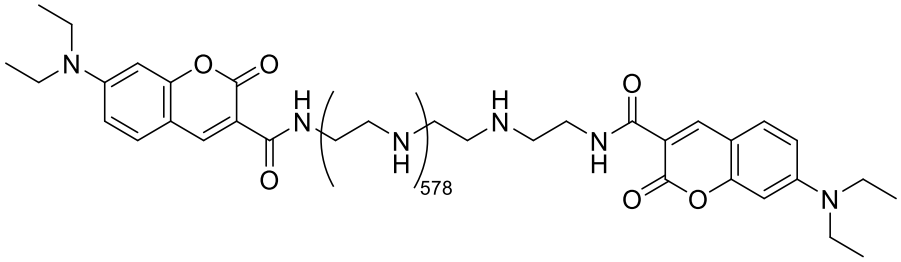

124. *Synthesized according to procedure N.* Yellow oil, quant. ^{1}H NMR (MeOD, 500 MHz, 20 °C): δ 1.90-3.04 (m, $CH_{2,PEI}$), 3.43-4.14 (m, $CH_{2,PEI}$ overlap MeOD), 4.89 (bs, $CH_{2,PEI}$+NH_{PEI}), 5.80-5.89 (m, N-CH_2), 7.40-7.78 (m, H_{ar}+$H_{coumarin}$); ^{13}C NMR (MeOD, 125 MHz, 20 °C): δ 10.1 (CH_3), 13.0 (CH_3), 17.2 ($CH_{2,PEI}$), 18.6 ($CH_{2,PEI}$), 30.5 ($CH_{2,PEI}$), 30.7 ($CH_{2,PEI}$), 41.8 ($CH_{2,PEI}$), 42.8 ($CH_{2,PEI}$), 45.4-47.9 ($CH_{2,PEI}$), 49.8 (CH_2-N), 51.6-52.8 ($CH_{2,PEI}$), 55.6 ($CH_{2,PEI}$), 76.1-76.4 ($CH_{2,PEI}$), 112.1 ($CH_{coumarin}$), 118.9 ($CH_{coumarin}$), 125.6 ($CH_{coumarin}$), 125.9 ($CH_{coumarin}$), 128.7 ($CH_{coumarin}$), 144.1 ($CH_{coumarin}$), 1632.9-163.4 ($C_{coumarin}$), 171.0-171.5 (C=O); UV-vis (EtOH) λ_{max} (nm): 204, 250, 417 ; Fluorescence: λ_{ex}=390 nm, λ_{em}=361 nm.

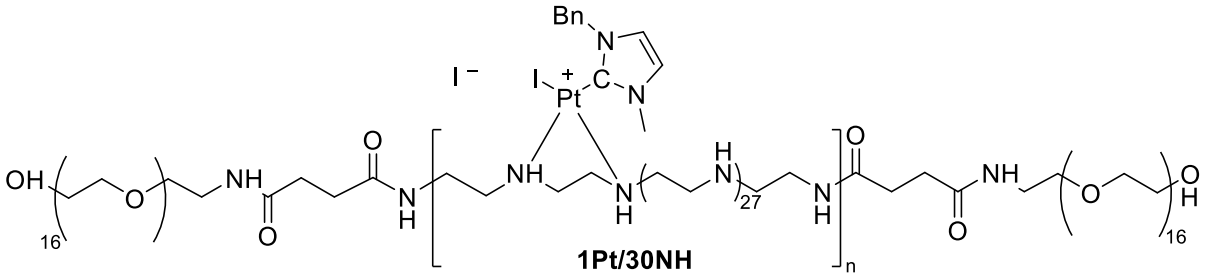

125. *Synthesized according to procedure L.* Light yellow oil, quant. ^{1}H NMR (MeOD, 500 MHz, 20 °C): δ 0.98-2.16 (m, $CH_{2,PEI}$), 2.27-2.65 (m, $CH_{2,PEI}$), 2.96-4.03 (bs + m, $CH_{2,PEI}$+N-CH_3 overlap with MeOD), 4.76 (bs, $CH_{2,PEI}$+NH_{PEI}), 5.50 (m, N-CH_2), 6.72 (m, CH_{im}), 7.02 (m, CH_{im}), 7.22-7.41 (m, 94H, CH_{im}+H_{ar}); DEPT NMR (MeOD, 125 MHz, 20 °C): δ 18.3 (CH_2), 18.5, 19.6, 20.1, 31.1, 31.3, 31.4, 32.9, 33.3, 34.6, 37.0, 38.0, 38.8, 39.7, 41.4, 41.5, 43.1, 43.2, 44.9, 48.9-53.4 (N-CH_3), 60.6 (N-CH_2), 62.0, 62.4, 66.6, 75.4 , 132.9-134.0 (CH), 176.2 (C=O), 183.7 (C=O).

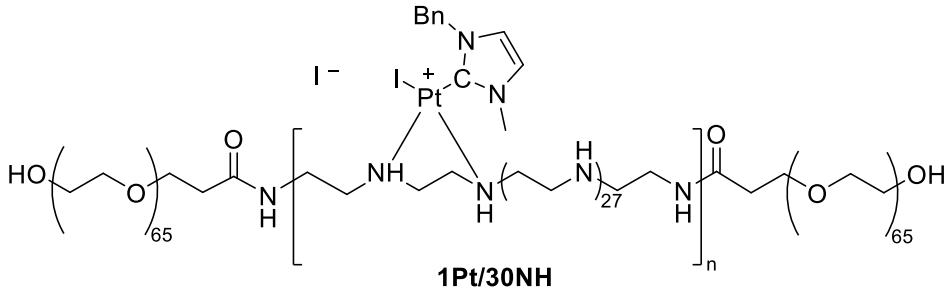

126. *Synthesized according to procedure L.* Light yellow oil, quant. ^{1}H NMR (MeOD, 500 MHz, 20 °C): δ 1.79-2.20 (m, $CH_{2,PEI}$), 2.31-2.95 (m, $CH_{2,PEI}$), 3.07-4.04 (bs + m, $CH_{2,PEI}$+N-CH_3 overlap with MeOD), 4.10-4.49, 4.55 (bs, $CH_{2,PEI}$+NH_{PEI}), 6.22-6.92 (m, N-CH_2), 7.52-7.81 (m, CH_{im}), 7.95-8.46 (m, CH_{im}+H_{ar}).

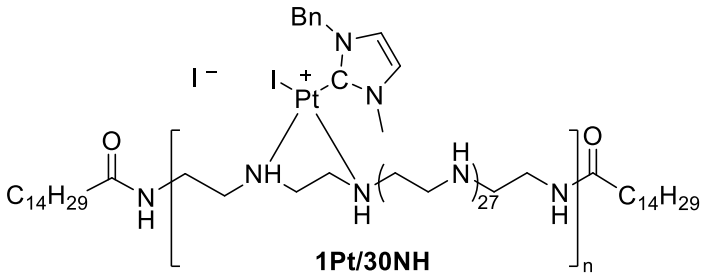

127. *Synthesized according to procedure L.* Colourless oil, quant. ^{1}H NMR (MeOD, 500 MHz, 20 °C): δ 0.80 (t, *J*=6.7Hz, $CH_{2,PEI}$), 1.00 (m, $CH_{2,PEI}$+ $CH_{2,alc}$), 1.07 (t, *J*=6.7Hz, $CH_{2,PEI}$), 1.13-1.24 (m, $CH_{2,PEI}$+ $CH_{2,alc}$), 1.49-1.92 (m, $CH_{2,PEI}$), 2.05 (bs, $CH_{2,PEI}$), 2.13-2.65 (m, $CH_{2,PEI}$), 3.24 (bs, $CH_{2,PEI}$), 3.32-4.03 (m, $CH_{2,PEI}$+N-CH_3), 4.75 (bs, $CH_{2,PEI}$+NH_{PEI}), 5.22 5.89 (m, N-CH_2), 6.66-7.15 (m, CH_{im}), 7.17-7.49 (m, H_{ar}).

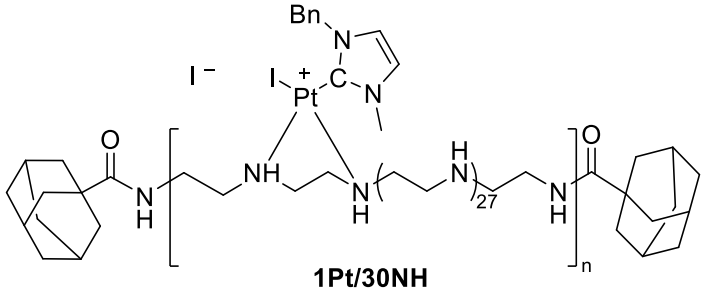

128. *Synthesized according to procedure L.* Colourless oil, quant. ^{1}H NMR (MeOD, 500 MHz, 20 °C): δ 0.88-2.04 (m, $CH_{2,PEI}$+$CH_{2,adamantyl}$), 2.13-2.99 (m, $CH_{2,PEI}$+$CH_{2,adamantyl}$), 3.23-4.20 (bs + m,

$CH_{2,PEI}$+N-CH_3 overlap with MeOD), 4.90 (bs, $CH_{2,PEI}$+ NH_{PEI}), 5.33-6.00 (m, N-CH_2), 6.61 (m, CH_{im}), 6.89 (m, CH_{im}), 7.05-7.59 (m, 94H, CH_{im}+H_{ar}); ^{13}C NMR (MeOD, 125 MHz, 20 °C): δ 14.4, 14.6, 19.9, 23.7, 26.9, 27.3, 28.1, 29.9-30.8 ($CH_{2,PEI}$+N-CH_3), 33.1 (N-CH_3), 35.2 ($CH_{2,adamantyl}$+$CH_{2,PEI}$), 35.7 ($CH_{2,adamantyl}$+$CH_{2,PEI}$), 37.4 ($CH_{2,adamantyl}$+$CH_{2,PEI}$), 42.7-47.0 ($CH_{2,adamantyl}$+$CH_{2,PEI}$), 53.5-55.3 (N-CH_2), 58.2, 61.4, 119.0-124.9 (CH_{im}), 129.1-131.3 (CH_{ar}), 135.6 (CH_{ar}), 138.1-138.2 (CH_{ar}), 175.3 (C=O).

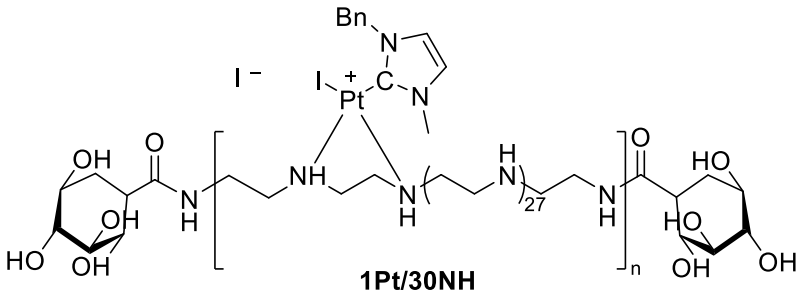

1Pt/30NH

129. *Synthesized according to procedure L.* Colourless oil, quant. ^{1}H NMR (MeOD, 500 MHz, 20 °C): δ 1.05-1.30 (m, $CH_{2,PEI}$+$CH_{2,alc}$), 2.24-2.72 (m, $CH_{2,PEI}$+ $CH_{2,alc}$), 3.27-4.09 (m, $CH_{2,PEI}$+N-CH_3), 4.84 (bs, $CH_{2,PEI}$+ NH_{PEI}), 5.25-5.58 (m, N-CH_2), 6.78-6.80 (m, CH_{im}), 7.01-7.55 (m, H_{ar}).

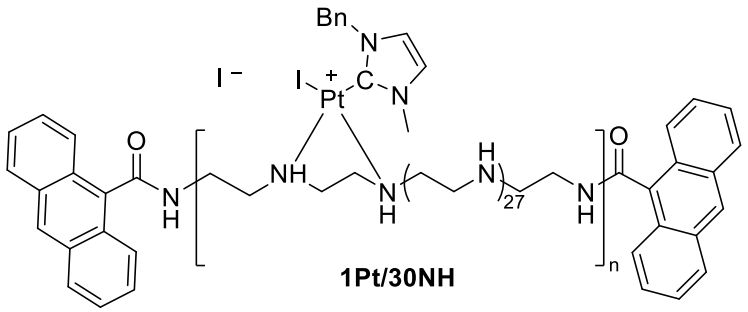

1Pt/30NH

130. *Synthesized according to procedure L.* Light yellow oil, quant. ^{1}H NMR (MeOD, 500 MHz, 20 °C): δ 2.02-3.01 (m, $CH_{2,PEI}$), 3.31-4.14 (m, $CH_{2,PEI}$), 3.96 (bs, $CH_{2,PEI}$+NH_{PEI}), 5.70-6.11 (m, N-CH_2), 7.27-7.78 (m, H_{ar}+$H_{anthracene}$); ^{13}C NMR (MeOD, 125MHz, 20 °C): δ 10.1-61.2 ($CH_{2,PEI}$+N-CH_2+N-CH_3), 124.2-130.6 (CH_{ar}), 161.4-164.5 (CH_{ar}+C-Pt), 173.6-177.3 (C=O).

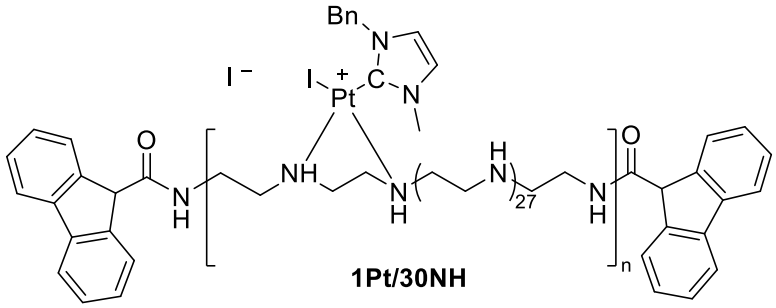

131. *Synthesized according to procedure L.* Light yellow oil, quant. ^{1}H NMR (MeOD, 500 MHz, 20 °C): δ2.27-3.03 (m, $CH_{2,PEI}$), 3.49-4.23 (m, $CH_{2,PEI}$+NH_{PEI}), 5.80-5.92 (m, N-CH_2), 7.40-7.61 (m, CH_{im} + H_{ar}); ^{13}C NMR (MeOD, 125 MHz, 20 °C): δ 10.1-61.6 (CH_2+N-CH_2+N-CH_3), 124.3-125.0 (CH_{im}), 129.7-130.6 (CH_{ar}), 137.1-138.3 (CH_{ar}), 161.4-164.5 (CH_{ar}+C-Pt), 171.4-177.2 (C=O).

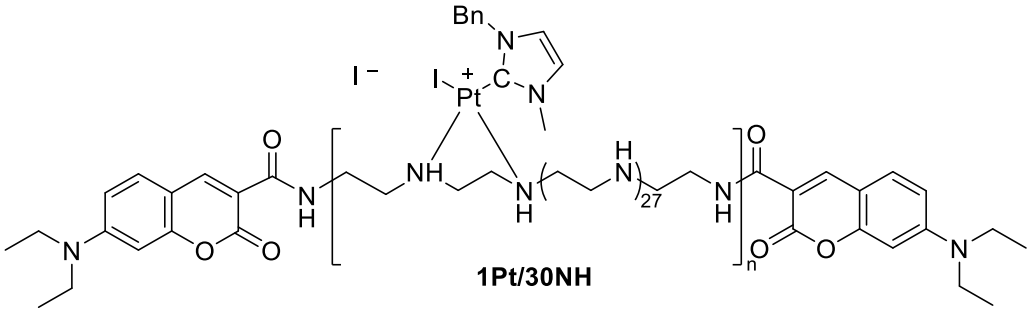

132. *Synthesized according to procedure L.* Yellow oil, quant. ^{1}H NMR (MeOD, 500 MHz, 20 °C): δ 1.13-1.31 (m, $CH_{2,PEI}$), 2.14-3.07 (m, $CH_{2,PEI}$), 3.33-3.66 (m, $CH_{2,PEI}$ overlap MeOD), 4.02-4.24 (bs, $CH_{2,PEI}$+ $CH_{2,PEI}$+NH_{PEI}+N-CH_3), 5.82-5.90 (m, N-CH_2), 7.29-7.77 (m, Har+$H_{coumarin}$); ^{13}C NMR (MeOD, 125MHz, 20 °C): δ 10.1 (CH_3), 13.0 (CH_3), 17.2 ($CH_{2,PEI}$), 18.6 ($CH_{2,PEI}$), 30.5 ($CH_{2,PEI}$), 30.7 ($CH_{2,PEI}$), 41.8 ($CH_{2,PEI}$), 42.8 ($CH_{2,PEI}$), 45.4-47.9 ($CH_{2,PEI}$), 49.8 (CH_2-N), 51.6-52.8 ($CH_{2,PEI}$), 55.6 ($CH_{2,PEI}$), 76.1-76.4 ($CH_{2,PEI}$), 112.1 ($CH_{coumarin}$), 118.9 ($CH_{coumarin}$), 125.6 ($CH_{coumarin}$), 125.9 ($CH_{coumarin}$), 128.7 ($CH_{coumarin}$), 144.1 ($CH_{coumarin}$), 1632.9-163.4 ($C_{coumarin}$), 171.0-171.5 (C=O).

- ***Procedure N: Fluorescein thioisocyanate condensation at the NHC-Pt-PEI conJugate 113***

To a solution of **113** (20 mg, 0.54 µmol) in DMSO (1 mL) and PBS 7.4 (2 mL) was added a solution of fluorescein isothiocyanate (0.026 mg, 0.054 µmol) in DMSO (100 µL) and stirred in the dark at 20°C, for 3 h. The solution was concentrated under reduced pressure, diluted in ethanol (0.3

mL) and subsequently dialysed toward PBS 7.4 (500 mL) at 20°C for 24h. The **133** solution was then recovered and lyophilized under reduced pressure to afford deep orange muggy solid.

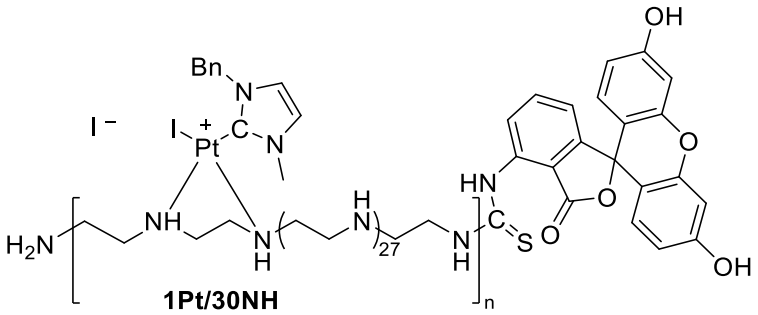

1Pt/30NH

133. *Synthesized according to procedure N.* Orange oil, quant. ^{1}H NMR (MeOD, 500 MHz, 20 °C): δ 0.81-1.19 (m, $CH_{2,PEI}$), 2.87 (bs, $CH_{2,PEI}$), 3.22 (bs, $CH_{2,PEI}$), 3.25-3.55 (m, $CH_{2,PEI}$), 3.87-4.12 (m, $CH_{2,PEI}$+N-CH_3), 4.75 (bs, $CH_{2,PEI}$+ NH_{PEI}), 5.41-5.90 (m, N-CH_2), 6.41-6.42 (m, H), 7.01-8.46 (m, H_{ar}); UV-vis (EtOH) λ_{max} (nm): 508; Fluorescence: λ_{ex}=508 nm, λ_{em}=525 nm.

- ***Procedure O: Condensation by intermolecular ring opening***

(Z)-3-(1-hydroxy-3-(naphthalen-2-yl)-3-oxoprop-1-en-1-yl)-6,6,9a-trimethyl-5,6-dihydro-2H-furo[3,2-g]isochromene-2,9(9aH)-dione (0.12 mg, 0.27 µmol) was solubilized in 4mL of H_2O/HCl (pH 2.5). A solution of **113** (10 mg, 0.27 µmol) in ethanol (1 mL) was then added and further stirred in the dark at 20°C for 24 h. The resulting solution was lyophilized under reduced pressure to afford a deep red muggy solid.

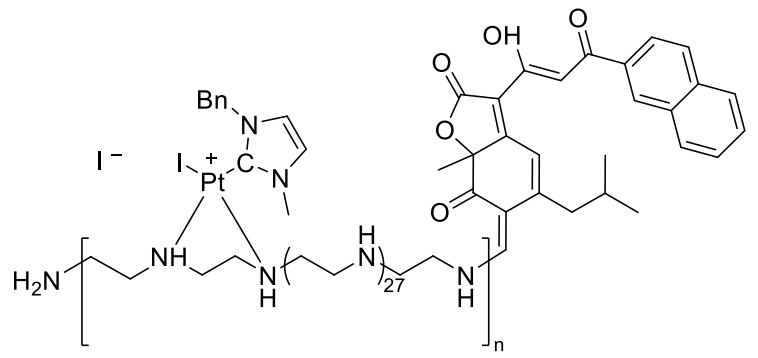

1Pt/30NH

134. *Synthesized according to procedure O.* Red muggy solid, quant. ^{1}H NMR (MeOD, 500 MHz, 20 °C): δ 1.12 (t, *J*=6.7 Hz, $CH_{2,PEI}$), 1.25 (m, $CH_{2,PEI}$+ H_{epico}), 1.30 (t, *J*=6.7 Hz, $CH_{2,PEI}$), 2.45-2.69 (m, $CH_{2,PEI}$), 2.77 (bs, $CH_{2,PEI}$), 3.34 (bs, $CH_{2,PEI}$), 3.44-3.51 (m, $CH_{2,PEI}$), 3.93-4.23 (m, $CH_{2,PEI}$+N-CH_3), 4.85 (bs, $CH_{2,PEI}$+ NH_{PEI}), 5.34-5.91 (m, N-CH_2), 7.30-7.73 (m, H_{ar}+CH_{im}+H_{epico}); UV-vis (EtOH) λ_{max} (nm): 231, 418.

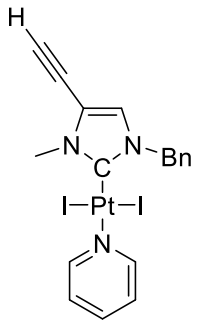

135. *Synthesized according to procedure B starting from a TMS-protected imidazolium and subsequent TMS deprotection by 6h stirring on a methanol suspension at room temperature.*

- ***Procedure P: Click reaction***

By adaptation of a reported synthesis,[7] a solution of alkyne derivative (3 mg, 0.042 mmol) in THF (1.5 mL) and a solution of benzyl azide (3 mg, 0.014 mmol) in THF (1 mL) were added to a solution of [RuClCp*(PPh_3)$_2$] (0.6 mg, 7.45x10^{-7} mol) in THF (1 mL). The mixture was then heated overnight at 75°C. The solvent was then removed under vacuum. The residue was purified by means of silica gel chromatography using a mixture of CH_2Cl_2/pentane 3:1 followed by CH_2Cl_2 and then ethyl acetate to afford the compound as a yellow-brown oil.

[7] E. Chardon, G. L. Puleo, G. Dahm, S. Fournel, G. Guichard, S. Bellemin-Laponnaz *Chem. Plus Chem.* **2012**, *77*, 1028-1038

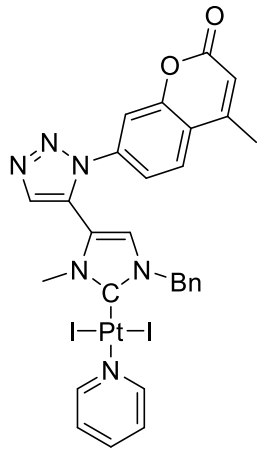

136. *Synthesized according to procedure P and further reacted without further purification.*

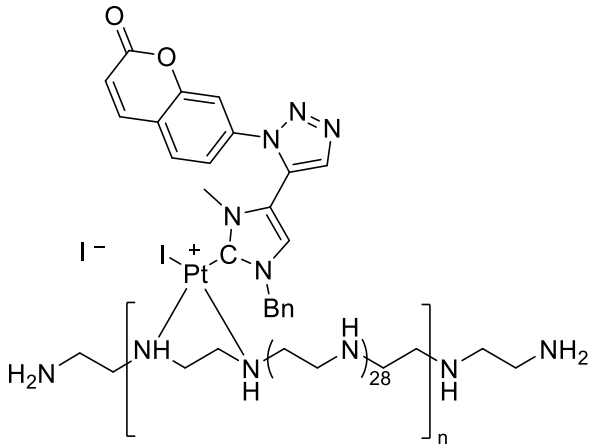

1Pt/30NH

137. *Synthesized according to procedure L.* Colourless oil, quant. ^{1}H NMR (MeOD, 500 MHz, 20 °C): δ 0.91 (t, *J*=6.7 Hz, $CH_{2,PEI}$), 1.12 (t, *J*=6.7 Hz, $CH_{2,PEI}$), 1.26-1.41 (m, $CH_{2,PEI}$), 1.61-2.47 (m, $CH_{2,PEI}$), 2.77 (m, $CH_{2,PEI}$), 3.42-3.65 (m, $CH_{2,PEI}$), 5.08-5.37 (m, $CH_{2,PEI}$+N-CH_3), 5.50 (bs, $CH_{2,PEI}$+ NH_{PEI}), 5.95 (m, N-CH_2), 6.51 (m, CH_{im}), 6.62 (m, H_{ar}), 6.91 (m, H_{ar}), 6.93-7.47 (m, H_{ar}), 8.07 (m, H_{ar}), 8.56 (s, H_{ar}).

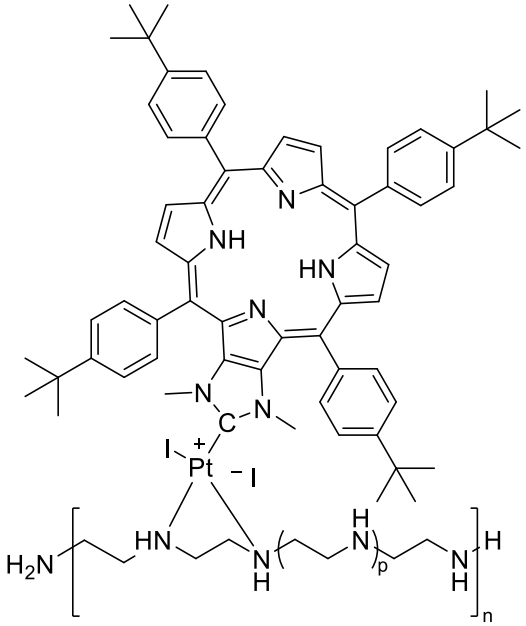

138. *Synthesized according to procedure L adapted to react for 7 d.* Red oil, quant. ^{1}H NMR (MeOD, 500 MHz, 20 °C): δ -0.34 (bs, $NH_{pyrrole}$), 0.87 (t, *J*=6.6 Hz, $CH_{2,PEI}$), 1.07 (t, *J*=6.6 Hz, $CH_{2,PEI}$), 1.19-1.57 (m, $CH_{2,PEI}$), 2.05 (bs, $CH_{2,PEI}$), 2.58-3.90 (bs, $CH_{2,PEI}$+N-CH_3 overlap MeOD), 4.75 (bs, $CH_{2,PEI}$+NH_{PEI}), 6.51 (s, NHC), 6.80 (m, NHC), 7.24 (m, NHC), 7.78-8.07 (m, NHC), 8.44 (m, NHC), 8.61 (m, NHC), 8.86 (m, NHC); UV-vis (EtOH) λ_{max} (nm): 205, 421, 540.

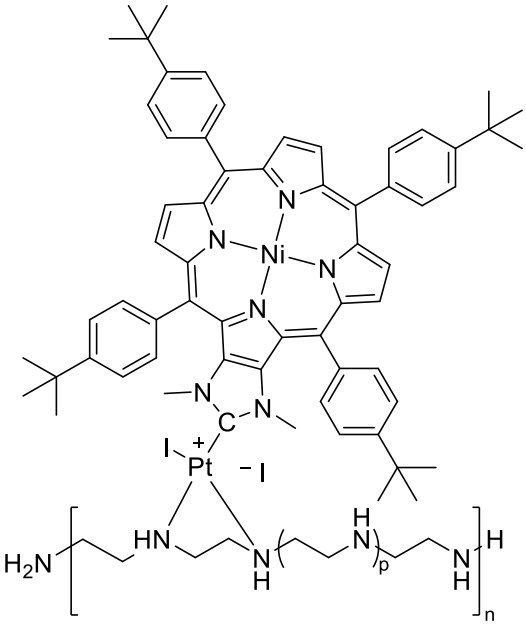

139. *Synthesized according to procedure L adapted to react for 7 d.* Red oil, quant. ^{1}H NMR (MeOD, 500 MHz, 20 °C): δ 1.01-1.56 (m, $CH_{2,PEI}$), 2.05 (s, $CH_{2,PEI}$), 2.67 (bs, $CH_{2,PEI}$), 3.06-3.83 (bs $CH_{2,PEI}$+N-CH_3 overlap MeOD), 4.75 (bs, $CH_{2,PEI}$+NH_{PEI}), 7.22 (m, NHC), 7.39-7.43 (dd, J_1=14.4 Hz, J_2=2.1Hz, NHC), 7.61-7.86 (m, NHC), 8.44 (s, NHC), 8.55-8.70 (m, NHC); UV-vis (EtOH) λ_{max} (nm): 203, 426, 536.

- ***Procedure Q: Condensation of SPDP moiety***

Under argon, a succinimidyl 3-(2-pyridyldithio)propionate solution (1.3 mg, 4.4 µmol) in DMSO (1 mL) was added to a solution of linear poly(ethyleneimine) of 25kDa (50 mg, 2 nmol) in ethanol (4 mL) and stirred for 3 h at 20°C. The solution was then concentrated under reduced pressure, precipitated by addition of excess diethyl ether and further centrifuged for 10 min at 10k rpm to afford the compound as light yellow oil.

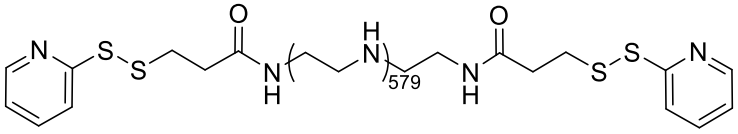

140. *Synthesized according to procedure Q.* Colourless oil, quant. ^{1}H NMR (MeOD, 500 MHz, 20 °C): δ 2.43-2.74 (m, $CH_{2,PEI}$), 3.32-3.47 (m, $CH_{2,PEI}$+C(O)CH_2+CH_2-S overlap MeOD), 4.86 (bs, $CH_{2,PEI}$+NH_{PEI}), 6.99 (s, CH_{SPDP}), 7.44 (m, CH_{SPDP}), 7.82-7.84 (m, CH_{SPDP}), 8.05-8.07 (m, CH_{SPDP}), 8.44 (m, CH_{SPDP}); ^{13}C NMR (MeOD, 125 MHz, 20 °C): δ 9.9-10.4 ($CH_{2,PEI}$), 14.4 ($CH_{2,PEI}$), 18.2 ($CH_{2,PEI}$), 23.6 ($CH_{2,PEI}$), 26.8 (CH_2-CH_2-S), 27.0 ($CH_{2,PEI}$), 30.0-30.7 (CH_2-CH_2-S), 32.8 ($CH_{2,PEI}$), 35.3-36.3 ($CH_{2,PEI}$), 39.7-39.8 ($CH_{2,PEI}$), 41.5 ($CH_{2,PEI}$), 42.8 ($CH_{2,PEI}$), 46.6-54.6 ($CH_{2,PEI}$ + MeOD), 57.4 ($CH_{2,PEI}$), 60.7 ($CH_{2,PEI}$), 64.3 ($CH_{2,PEI}$), 120.8 (CH_{pyr}), 122.3 (CH_{pyr}), 126.3 (CH_{pyr}), 138.9 (CH_{pyr}), 150.5 (C_{pyr}), 160.8 (CH), 165.1 (C=O), 176.3 (CH).

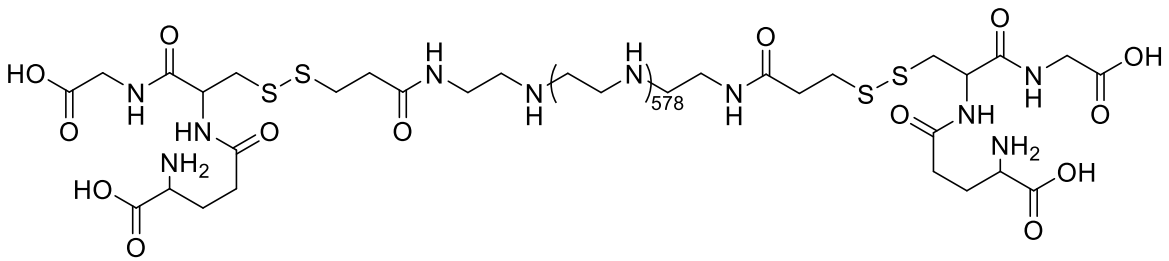

141. *Synthesized according to procedure O.* Colourless oil, quant. ^{1}H NMR (MeOD, 500 MHz, 20 °C): δ 0.87-1.41 (m, $CH_{2,PEI}$), 2.15-2.54 (m, $CH_{2,PEI}$), 2.73 (bs, $CH_{2,PEI}$), 3.46-3.64 (m, $CH_{2,PEI}$), 4.85 (bs, $CH_{2,PEI}$+NH_{PEI}), 5.33 (m, $CH_{2,GSH}$), 6.61 (s, CH_{GSH}), 6.90 (s, CH_{GSH}), 6.92 (s, CH_{GSH}), 7.18-7.33 (m, CH_{GSH}), 8.08 (m, CH_{GSH}).

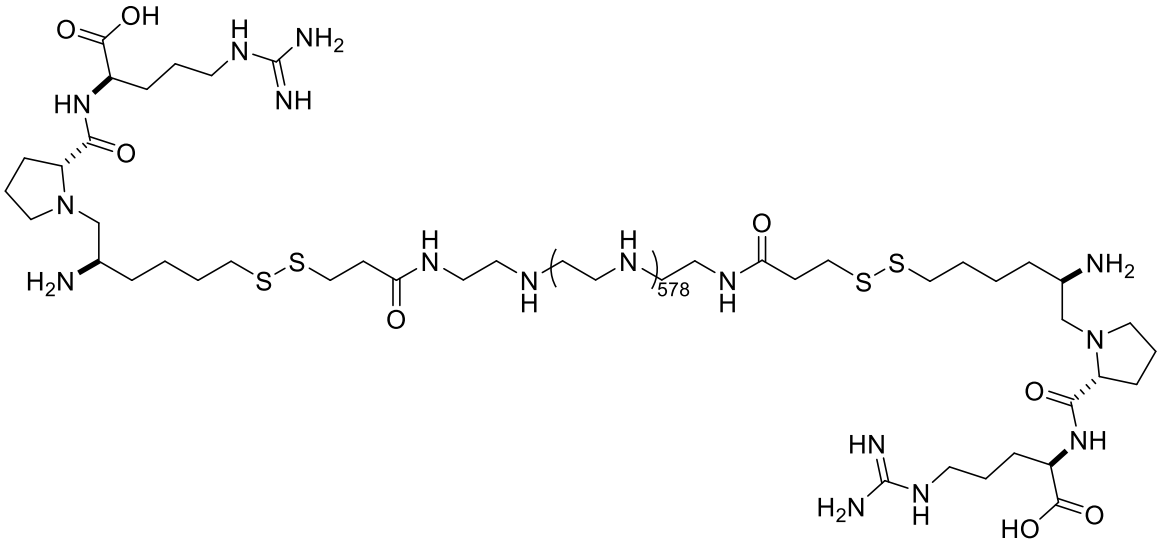

142. *Synthesized according to procedure O.* Colourless oil, quant. ^{1}H NMR (MeOD, 500 MHz, 20 °C): δ 1.09-1.82 (m, $CH_{2,PEI}$), 1.89 (bs, $CH_{2,PEI}$), 2.03-2.57 (m, $CH_{2,PEI}$), 2.76 (bs, $CH_{2,PEI}$), 3.44-4.43 (m, $CH_{2,PEI}$), 4.86 (bs, $CH_{2,PEI}$+NH_{PEI}), 7.35 (m, HB19), 8.09 (m, HB19), 8.55 (m, HB19).

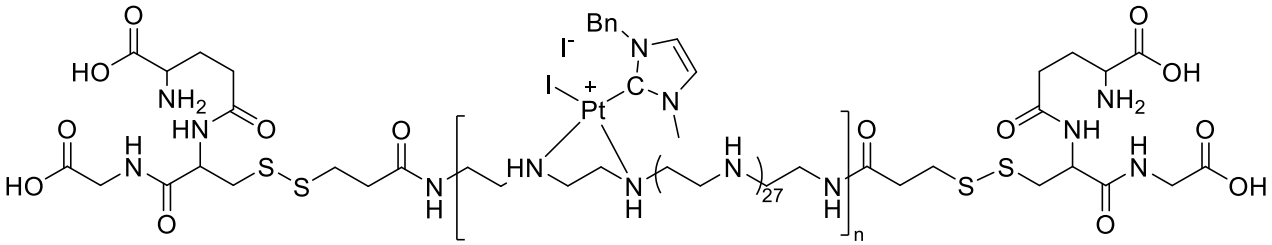

1Pt/30NH

143. *Synthesized according to procedure L.* Light yellow oil, quant. ^{1}H NMR (MeOD): δ 1.12 (t, *J*=7.2 Hz, $CH_{2,PEI}$), 1.29 (m, $CH_{2,PEI}$), 1.69-2.15 (m, $CH_{2,PEI}$+$CH_{2,GSH}$), 2.79 (bs, $CH_{2,PEI}$+$CH_{2,GSH}$), 3.46-3.62 (m, $CH_{2,PEI}$), 3.94-4.22 (m, $CH_{2,PEI}$), 4.85 (m, $CH_{2,PEI}$+NH_{PEI}+N-CH_3), 5.82 (m, N-CH_2), 7.42-7.74 (m, H_{ar}+CH_{im}), 8.10 (m, $CH_{2,GSH}$), 8.58 (s, $CH_{2,GSH}$).

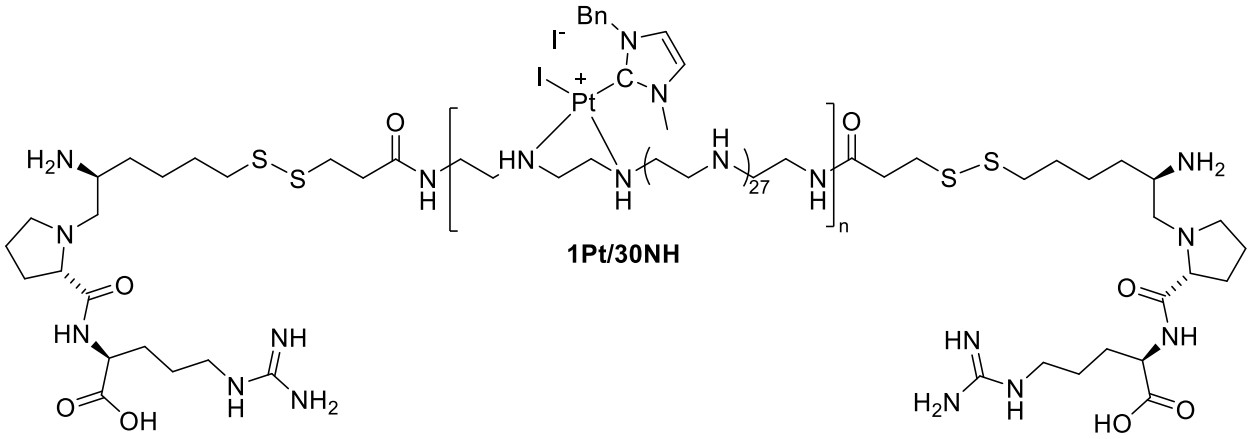

144 *Synthesized according to procedure L.* Light yellow oil, quant. ^{1}H NMR (MeOD): δ 0.92 (t, *J*=7.3 Hz, $CH_{2,PEI}$), 1.14 (m, $CH_{2,PEI}$), 1.19 (t, *J*=7.3 Hz, $CH_{2,PEI}$), 1.27-1.36 (m, $CH_{2,PEI}$+$CH_{2,HB19}$), 1.91 (s, $CH_{2,PEI}$), 2.18 (s, $CH_{2,PEI}$), 2.21 (t, *J*=7.3 Hz, $CH_{2,PEI}$), 2.37 (t, *J*=3.7Hz, $CH_{2,PEI}$), 2.77-2.98 (m, $CH_{2,PEI}$+$CH_{2,HB19}$), 3.36 (bs, $CH_{2,PEI}$), 3.50-3.67 (m, $CH_{2,PEI}$), 3.97-4.25 (m, $CH_{2,PEI}$+NH_{PEI}+N-CH_3), 5.85-5.87 (m, N-CH_2), 7.41-7.77 (m, H_{ar}+CH_{im}), 8.58 (s, HB19).

12) Characterization of PEI-AuNPs

- **Synthesis of 10 nm PEI-AuNPs**

To a solution of $HAuCl_4.6H_20$ (25 mg, 0.73 mmol, C_{Au} = 6.4 mM) in water is added 0.02 equivalents of PEI and stirred for 30 minutes at 20°C. Then, a solution of TBAB (0.01 equivalents) in water is slowly added to the mixture and vigorously stirred for one hour at 50°C until appearance of the characteristic dark red colour. The reaction mixture is then purified by dialysis over 500 mL of water using a 10 kDa cut-off membrane for 24 h and obtained as a stable dark red solution in water.

- **Synthesis of 30 nm PEI-AuNPs**

To a solution of $HAuCl_4.6H_20$ (25 mg, 0.73 mmol, C_{Au} = 6.4 mM) in water is added 0.02 equivalents of PEI and stirred for 30 minutes at 20°C. Then, a solution of TBAB (0.1 equivalents) in water is slowly added to the mixture and vigorously stirred for 20 minutes at 20°C until appearance of the characteristic dark red colour. The reaction mixture is then purified by

dialysis over 500 mL of water using a 10 kDa cut-off membrane for 24 h and obtained as a stable dark red solution in water.

- **UV-vis analysis of selected batch**

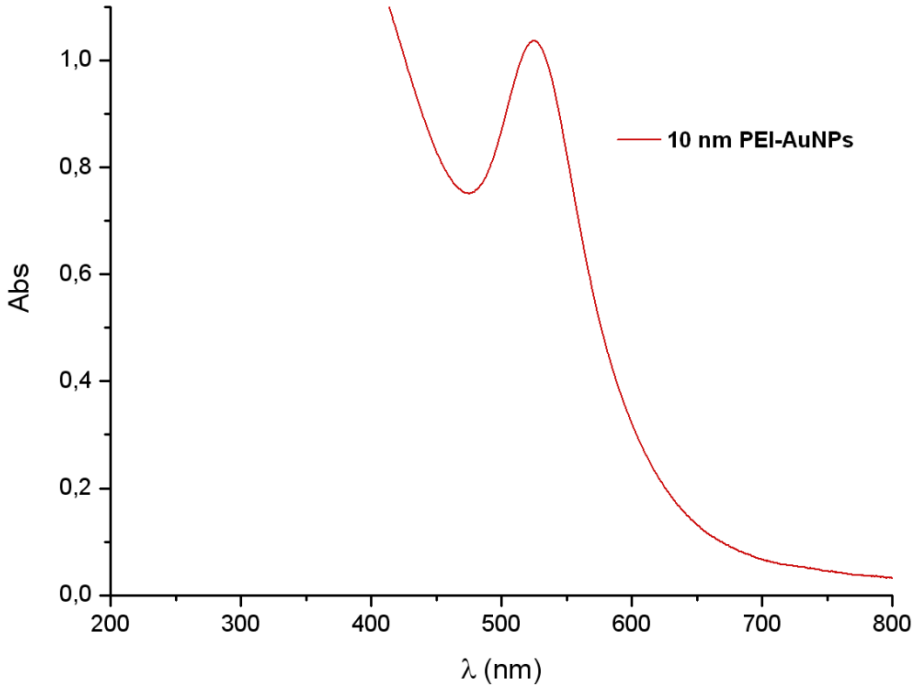

Figure 54: UV-vis spectra of ~10 nm PEI-AuNPs

- **DLS measurement of PEI-AuNPs**

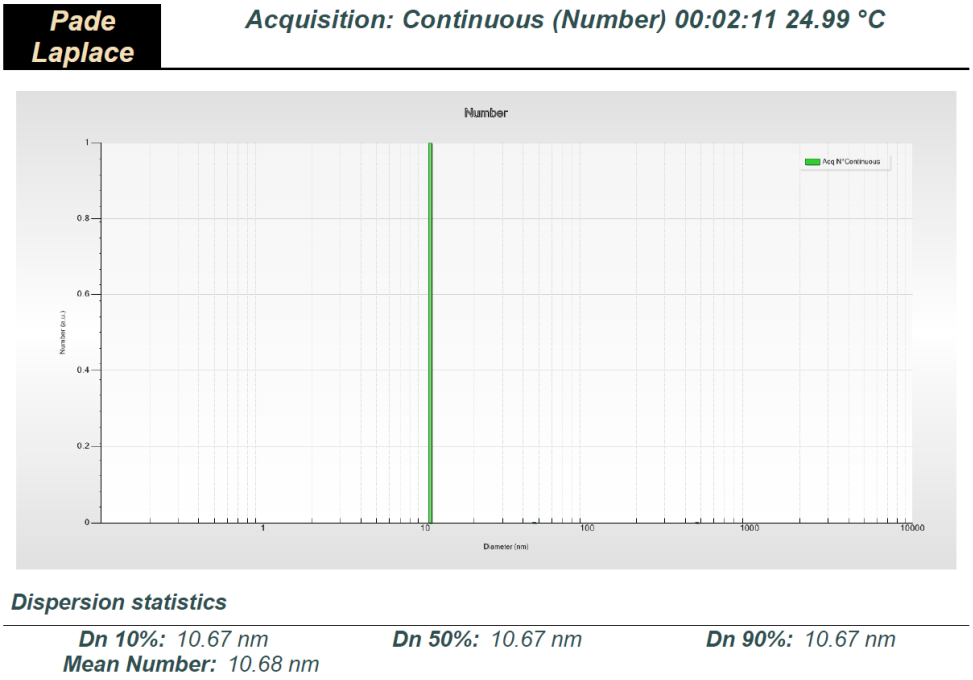

Figure 55: DLS measurement on ~10 nm PEI-AuNPs

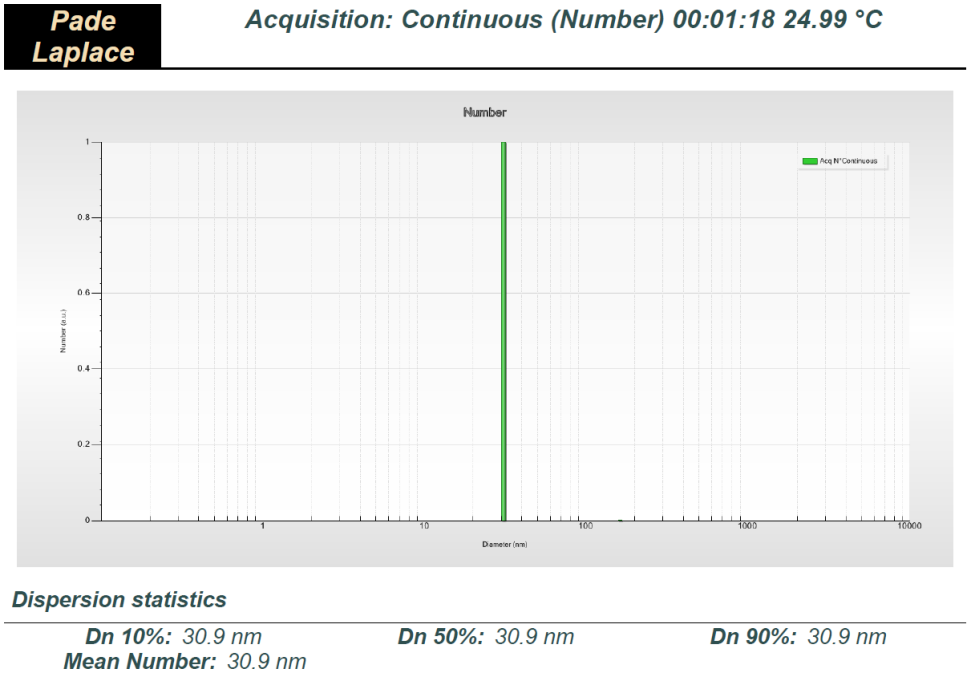

Figure 56: DLS measurement on ~30 nm PEI-AuNPs

- **TEM images of PEI-AuNPs**

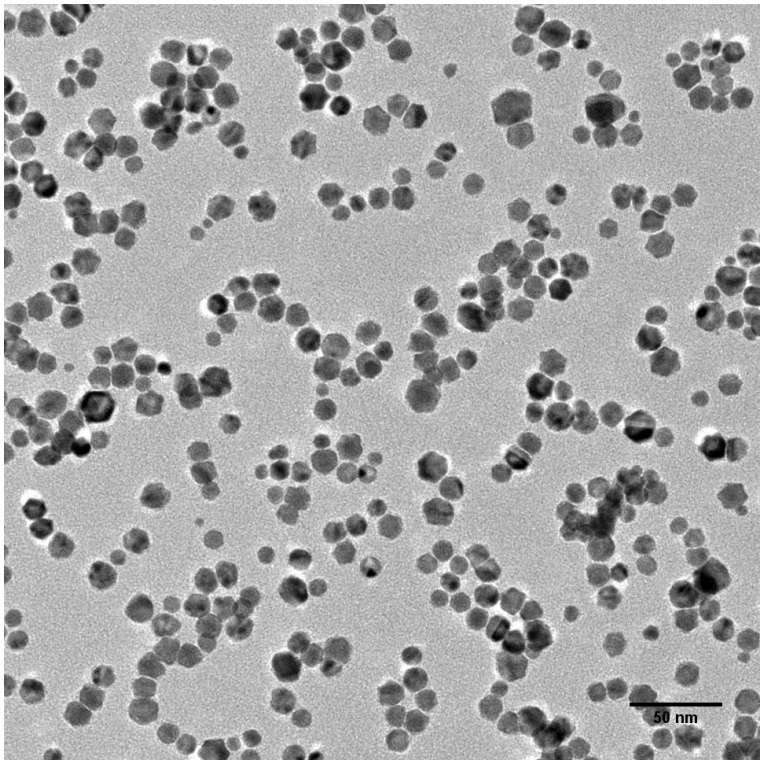

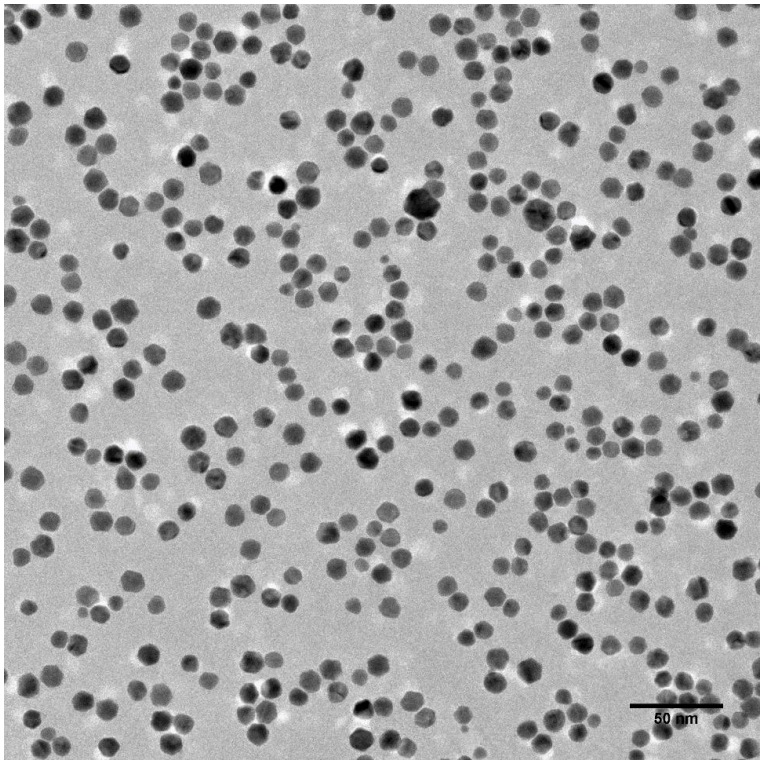

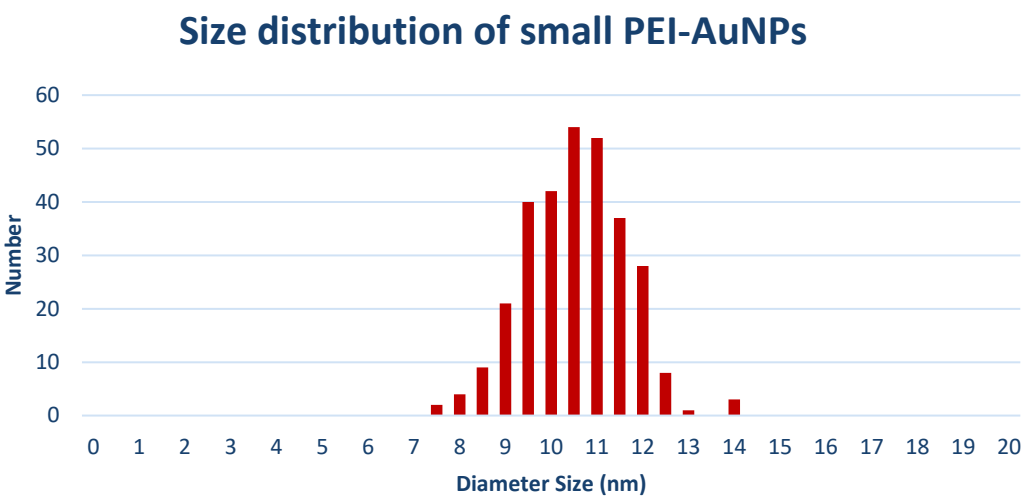

Figure 57: TEM images and size distribution of ~10 nm PEI-AuNPs

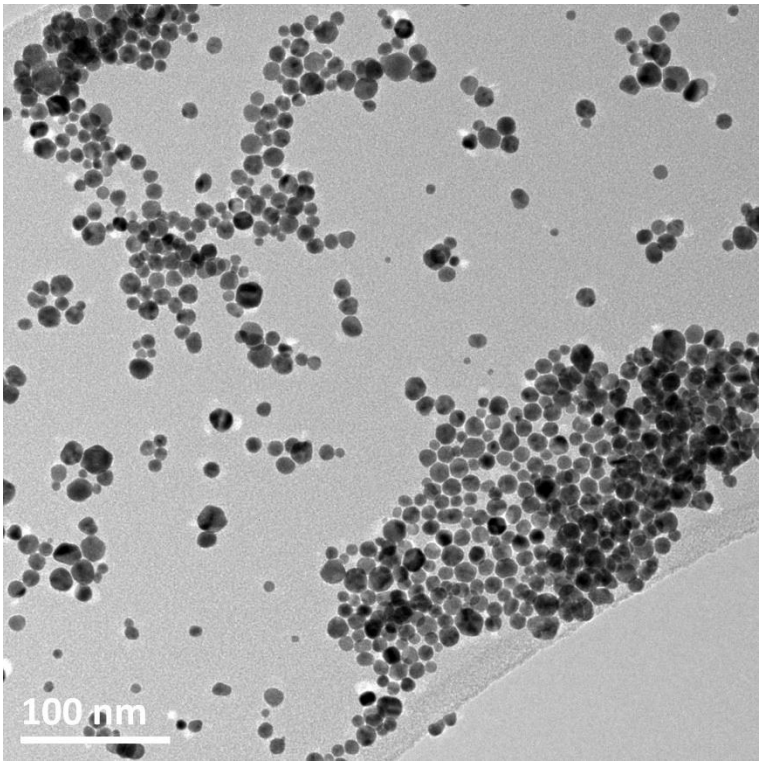

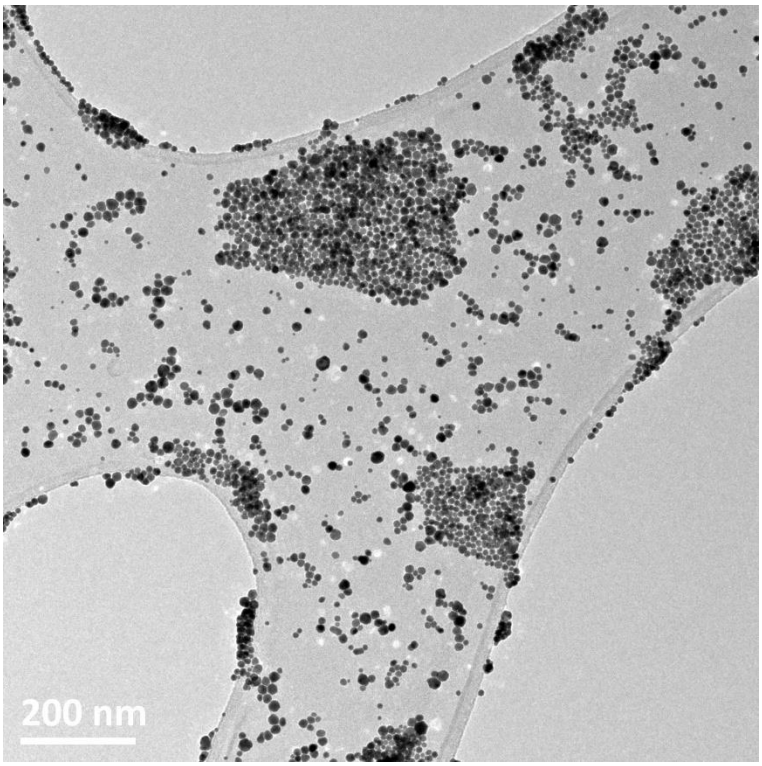

Figure 58: TEM images of ~30 nm PEI-AuNPs

- **Stability studies**

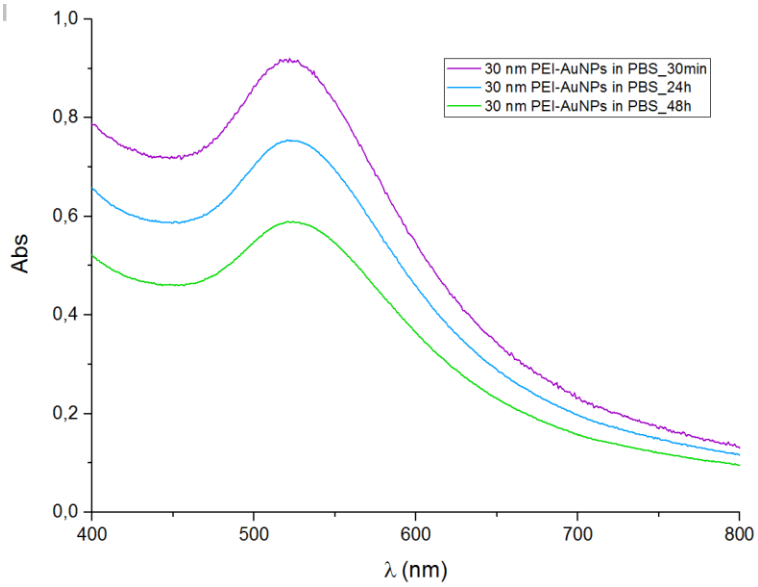

Figure 57: Stability of 30nm PEI-AuNPs in PBS

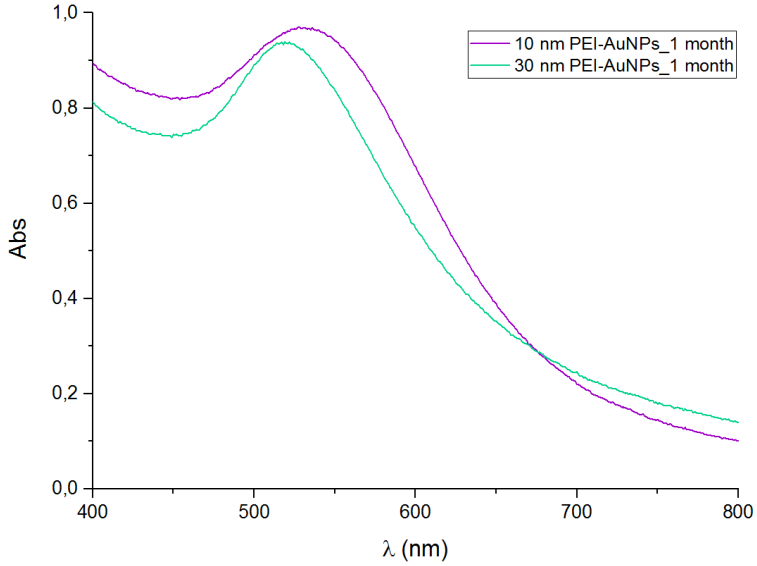

Figure 58: Stability of PEI-AuNPs over 1 month

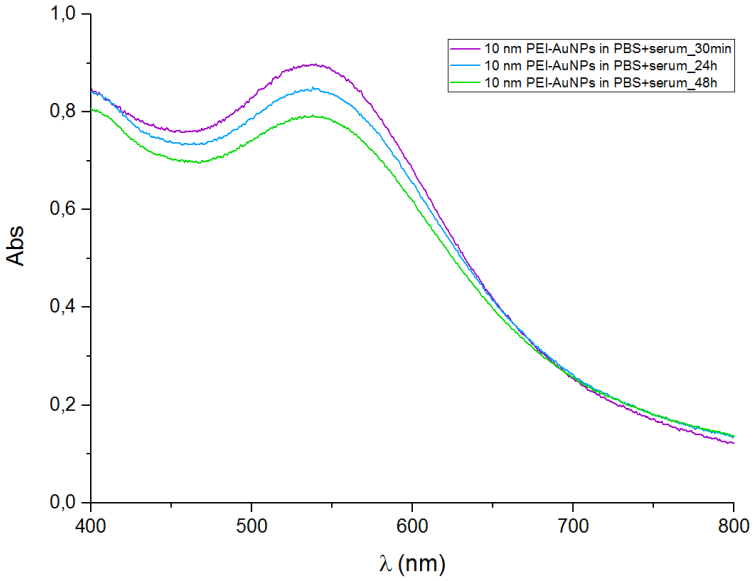

Figure 59: Stability of 10nm PEI-AuNPs with serum

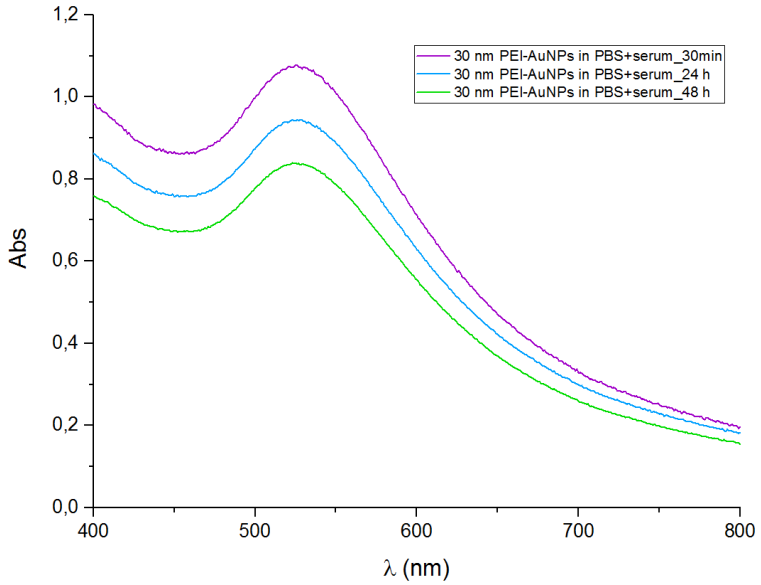

Figure 60: Stability of 30nm PEI-AuNPs with serum

Bibliography

[1] N. Farrell *Coord. Chem. Rev.* **2002**, *232*, 1-4

[2] G. Gasser, I. Ott, N. Metzler-Nolte *J. Med. Chem.* **2011**, *54*, 3-25

[3] M. Patra, G. Gasser *ChemBioChem* **2012**, *13*, 1232-1251

[4] G. Sava, R. Gagliardi, M. Cocchietto, K. Clerici, I. Capozzi, M. Marrella, E. Alessio, G. Mestroni, R. Milanino *Pathology Oncology Research* **1998**, *4*, 30-36

[5] A. E. Finkelstein, D. T. Walz, V. Batista, M. Mizraji, F. Roisman, A. Misher *Ann. Rheum. Dis.* **1976**, *35*, 251-257

[6] B. K. Keppler, D. Schmahl *Drug Research* **1986**, *36-2*, 1822-1828

[7] Cisplatin represents up to 40% overall anticancer drug prescription

[8] B. Rosenberg, L. VanCamp, J. E. Trosko, V. H. Mansour *Nature* **1969**, *222*, 385-386

[9] G. J. Bosl, D. F. Bajorin, J. Sheinfeld, R. Motzer, R.S. K. Chaganti *Cancer: Principles & Practice of Oncology*, ed. V. T. DeVita Jr, S. Hellman and S. A. Rosenberg, Lippincott Williams & Wilkins, Philadelphia, 6th Ed., **2001**, 1491-1518

[10] R. A. Alderden, M. D. Hall, T. W. Hambley *J. Chem. Educ.* **2006**, *83*, 728-734

[11] D. P. Gately, S. B. Howell *Br. J. Cancer* **1993**, *67*, 1171-1176

[12] P. A. Andrews, S. B. Howell *Cancer Cell-Mon Rev.* **1990**, *2*, 35-43

[13] S. W. Johnson, K. V. Ferry, T. C. Hamilton *Drug Resist. Update* **1998**, *1*, 243-254

[14] A. Yonezawa, K. Inui *Biochem. Pharmacol.* **2011**, *81*, 563-568

[15] R. Safaei, S. B. Howell *Crit. Rev. Oncol. Hemat.* **2005**, *53*, 13-23

[16] Z. D. Liang, D. Stockton, N. Savaraj, M. Tien Kuo *Mol. Pharmacol.* **2009**, *76*, 843-853

[17] A. K. Wernimont, D. L. Huffman, A. L. Lamb, T. V. O'Halloran, A. C. Rosenzweig *Nat. Struct. Biol.* **2000**, *7*, 766-771

[18] S. Ishida, J. Lee, D. J. Thiele, I. Herskowitz *Proc. Natl. Acad. Sci. U.S.A.* **2002**, *99*, 14298-14302

[19] A. K. Holzer, G. Samimi, K. Katano, W. Naerdemann, X. Lin, R. Safaei, S. B. Howell *Mol. Pharmacol.* **2004**, *66*, 817-823

[20] M. D. Hall, M. Okabe, D.-W. Shen, X.-J. Liang, M. M. Gottesman *Annu. Rev. Pharmacol. Toxicol.* **2008**, *48*, 495-535

[21] Y. Jung, S. J. Lippard *Chem. Rev.* **2007**, *107*, 1387–1407

[22] S. Z. Zhang, K. S. Lovejoy, J. E. Shima, L. L. Lagpacan, Y. Shu, A. Lapuk, Y. Chen, T. Komori, J. W. Gray, X. Chen, S. J. Lippard, K. M. Giacomini *Cancer Res.* **2006**, *66*, 8847-8857

[23] A. Yonezawa *J. Pharm. Soc. Japan* **2012**, *132*, 1281-1285

[24] J. Reedijk *Proc. Natl. Acad. Sci. U.S.A.* **2003**, *100*, 3611-3616

[25] D. P. Bancroft, C. A. Lepre, S. J. Lippard *J. Am. Chem. Soc.* **1990**, *112*, 6860-6871

[26] S. J. Lippard, J. D. Hoeschele *Proc. Natl. Acad. Sci. U.S.A.* **1979**, *76*, 6091-6095

[27] F. R. Luo, T. Y. Yen, S. D. Wyrick, S. G. Chaney *J. Chromatogr. B: Biomed. Sci. Appl.* **1999**, *724*, 345-356
[28] C. Deutsch, J. S. Taylor, D. F. Wilson *Proc. Natl. Acad. Sci. U.S.A.* **1982**, *79,* 7944-7948
[29] A. L. Pinto, S. J. Lippard *Biochim. Biophys. Acta* **1985**, *780*, 167-180
[30] R. Faggiani, B. Lippert, C. J. L. Lock, B. Rosenberg *J. Am. Chem. Soc.* **1977**, *99*, 777-781
[31] E. R. Jamieson, S. J. Lippard *Chem. Rev.* **1999**, *99*, 2467-2498
[32] J. S. Saad, G. Natile, L. G. Marzilli *J. Am. Chem. Soc.* **2009**, *131*, 12314-12324
[33] J. S. Saad, M. Benedetti, G. Natile, L. G. Marzilli *Inorg. Chem.* **2011**, *50*, 4559-4571
[34] M. Kartalou, J. M. Essigmann *Mutat. Res.* **2001**, *478*, 23-43
[35] M. S. Davies, S. J. Berners-Price, T. W. Hambley *Inorg. Chem.* **2000**, *39*, 5603-5613
[36] M. A. Fuertes, J. Castilla, C. Alonso, J. M. Pérez *Curr. Med. Chem. Anticancer Agents* **2002**, *2*, 539-551
[37] D. B. Zamble, D. Mu, J. T. Reardon, A. Sancar, S. J. Lippard *Biochemistry* **1996**, *35*, 10004-10013
[38] R. B. Ciccarelli, M. J. Solomon, A. Varshavsky, S. J. Lippard *Biochemistry* **1985**, *24*, 7533-7540
[39] S. C. Popoff, D. J. Beck, W. D. Rupp *Mutat*. *Res*. **1987**, *183*, 129-137
[40] E. Bernal-Méndez, M. Boudvillain, F. González-Vílchez, M. Leng *Biochemistry* **1997**, *36*, 7281-7287
[41] K. E. Sandman, S. J. Lippard *Cisplatin*, Zurich: Verlag Helvetica Chimica Acta, **1999**
[42] L. Galluzzi, L. Senovilla, I. Vitale, J. Michels, I. Martins, O. Kepp, M. Castedo, G. Kroemer *Oncogene* **2012**, *31*, 1869-1883
[43] K. M. Comess, J. N. Burstyn, J. M. Essigmann, S. J. Lippard *Biochemistry* **1992**, *31*, 3975-3990
[44] J. Q. Svejstrup *Nat. Rev. Mol. Cell Biol.* **2002**, *3*, 21-29
[45] J. Q. Svejstrup *J. Cell Sci.* **2003**, *116*, 447-451
[46] W. Dong, S. J. Lippard *Nat. Rev. Drug Discov. 4* **2005**, *4*, 307-320
[47] B. Köberle, M. T. Tomicic, S. Usanova, B. Kaina *Biochim. Biophys. Acta* **2010**, *1806*, 172-182
[48] S. M. Patrick, J. J. Turchi *J*. *Biol*. *Chem*. **1999**, *274*, 14972-14978
[49] S.G. Chaney, A. J. Sancar *Natl. Cancer Inst.* **1996**, *88*, 1346-1360
[50] T. Furuta, T. Ueda, G. Aune, A. Sarasin, K. H. Kraemer, Y. Pommier *Cancer Res.* **2002**, *62*, 4899-4902
[51] C. Welsh, R. Day, C. McGurk, J. R. W. Masters, R. D. Wood, B. Köberle *Int. J. Cancer* **2004**, *110*, 352-361
[52] G. Strathdee, M. J. MacKean, M. Illand, R. Brown *Oncogene* **1999**, *18*, 2335-2341
[53] J. E. Clodfelter, M. B. Gentry, K. Drotschmann *Nucleic Acids Res.* **2005**, *33*, 3323-3330
[54] B. A. Teicher, T. S. Herman, S. A. Holden, Y. Wang, M. R. Pfeffer, J. W. Crawford, E. Frei, III *Science* **1990**, *247*, 1457-1461
[55] P. A. Andrews, M. P. Murphy, S. B. Howell *Eur*. *J. Cancer Clin*. *Oncol*. **1989**, *25*, 619-625

[56] V. M. Richon, N. Schulte, A. Eastman *Cancer Res*. **1987**, *47*, 2056-2061
[57] W. R. Waud *Cancer Res*. **1987**, *47*, 6549-6555
[58] M. Foka, J. Belehradek, J. Paoletti *Biochem*. *Pharmacol*. **1988**, *37*, 3467-3472
[59] R. A. Hromas, P. A. Andrews, M. P. Murphy, C. P. Burns *Cancer Lett*. **1987**, *34*, 9-13
[60] D.E. Fisher *Cell* **1994**, *78*, 539-542
[61] K. Hientz, A. Mohr, D. Bhakta-Guha, T. Efferth *Oncotarget.* **2017**, *5*, 8921-8946
[62] F. Muggia *Gynecol. Oncol*. **2009**, *112*, 275-281
[63] R. Schierl, B. Rohrer, J. Hohnloser *Cancer Chemother. Pharmacol.* **1995**, *36*, 75-78
[64] R. Cetin, E. Devrim, B. Kilicoglu, A. Avci, O. Candir, I. Durak *J. Appl. Toxicol.* **2006**, *26*, 42-46
[65] A. A. Al-Majed, M. M. Sayed-Ahmed, A. A. Al-Yahya, A. M. Aleisa, S. S. Al-Rejaie, O. A. Al-Shabanah *Pharmacol. Res.* **2006**, *53*, 278-286
[66] G. J. Dugbartey, L. J. Peppone, I. A. de Graaf *Toxicology* **2016**, *371*, 58-66
[67] I. Arany, R. L. Safirstein *Semin. Nephrol.* **2003**, *23*, 460-464
[68] D. M. Cheff, M. D. Hall *J. Med. Chem.* **2017**, *60*, 4517-4532
[69] V. M. Gonzalez, M. A. Fuertes, C. Alonso, J. M. Perez *Mol. Pharmacol.* **2001**, *59*, 657–663
[70] L. Messori, A. Merlino *Coord. Chem. Rev.* **2016**, *315*, 67-89
[71] C. Bischin, A. Lupan, V. Taciuc, R. Silaghi-Dumitrescu *Mini-Rev Med. Chem.* **2011**, *11*, 214-224
[72] J. Will, W. S. Sheldrick, D. Wolters *J. Biol. Inorg. Chem.* **2008**, *13*, 421-434
[73] M. Kato, H. Yamamoto, T. Okamura, N. Maoka, R. Masui, S. Kuramitsu, N. Ueyama *Dalton Trans.* **2005**, *6*, 1023-1026
[74] L. H. Damelin, R. Jivan, R. B. Veale, A. L. Rousseau, D. Mavri-Damelin *BMC Cancer* **2014**, *14*, 314-325
[75] R. C. Todd, S. J. Lippard *Metallomics* **2009**, *1*, 280-291
[76] C. A. Rabik, M. E. Dolan *Cancer Treat. Rev.* **2007**, *33*, 9-23
[77] G. Santabarbara, P. Maione, A. Rossi, C. Gridelli *Expert Opin. Pharmacother.* **2016**, *17*, 561-570
[78] N. J. Wheate, S. Walker, G. E. Craig, R. Oun *Dalton Trans.* **2010**, *39*, 8113-8127
[79] S. Dilruba, G. V. Kalayda *Chemother. Pharmacol.* **2016**, *77*, 1103-1024
[80] A. J. Di Pasqua, J. Goodisman, J. C. Dabrowiak *Inorganica Chimica Acta* **2012**, *389*, 29-35
[81] J. Graham, M. Muhsin, P. Kirkpatrick *Nat. Rev. Drug Discovery* **2004**, *3*, 11-12
[82] M. Shimada, H. Itamochi, J. Kigawa *Cancer Manage. Res.* **2013**, *5*, 67-76
[83] D. K. Kim, J. S. Ahn, G. Ryu, K. H. Kim, C. W. Park, M. S. Kim, M. H. Chung, S. G. Shin, Y. H. Suh, Y. S. Kim *Drug Res. (Stuttgart, Ger.)* **1994**, *44*, 1080-1088
[84] M. J. McKeage *Expert. Opin. Investig. Drugs* **2001**, *10*, 119-128
[85] Adis R&D Profile *Drugs R&D* **2003,** *4*, 369-372
[86] T. W. Hambley *Coord. Chem. Rev.* **1997,** *166*, 181-223
[87] S. Bellemin-Laponnaz, S. Dagorne *N-Heterocyclic Carbenes: Effective Tools for Organometallic Synthesis*, Weinheim: Wiley-VCH Verlag GmbH & Co, **2014**.

[88] V. César, S. Bellemin-Laponnaz, L. Gade *Chem. Soc. Rev.* **2004**, *9*, 619-636
[89] M. Poyatos, J. A. Mata, E. Peris *Coord. Chem. Rev.* **2009**, *109*, 3677-3707
[90] R. Visbal, M. C. Gimeno *Chem. Soc. Rev.* **2014**, *43*, 3551-3574
[91] K. M. Hindi, M. J. Panzner, C. A. Tessier, C. L. Cannon, W. J. Youngs *Chem. Rev.* **2009**, *109*, 3859-3884
[92] V. Lavallo, Y. Canac, C. Präsang, B. Donnadieu, G. Bertrand *Angew. Chem. Int. Ed.* **2005**, *44*, 5705-5709
[93] H. W. Wanzlick, H. J. Schönherr *Angew. Chem. Int. Ed Engl.* **1968**, *7*, 141-142
[94] K. J. Öefele *J. Organomet. Chem.* **1968**, *12*, 42-43
[95] A. Igau, H. Grutzmacher, A. Baceiredo, G. Bertrand *J. Am. Chem. Soc.* **1988**, *110*, 6463-6466
[96] A. Igau, A. Baceiredo, G. Trinquier, G. Bertrand *Angew. Chem. Int. Ed. Engl.* **1989**, *28*, 621-622
[97] A. J. Arduengo, III, R. L. Harlow, M. Kline *J. Am. Chem. Soc.* **1991**, *113*, 361-363
[98] A. J. Arduengo, III, H. Bock, H. Chen, M. Denk, D. A. Dixon, J. C. Green, W. A. Herrmann, N. L. Jones, M. Wagner, R. West *J. Am. Chem. Soc.* **1994**, *116*, 6641-6649
[99] E. Baba, T. R. Cundari, I. Firkin *Inorg. Chim. Acta* **2005**, *358*, 2867-2875
[100] M.-T. Lee, C.-H. Hu *Organometallics* **2004**, *23*, 976-983
[101] D. J. Nelson, S. P. Nolan *Chem. Soc. Rev.* **2013**, *42*, 6723-6753
[102] L. Falivene, L. Cavallo *Coord. Chem. Rev.* **2016**, *344*, 101-114
[103] Q. Teng, H. V. Huynh *Dalton Trans* **2017**, *46*, 614-627
[104] B. Cetinkaya, E. Cetinkaya, H. Kucubay, R. Durmaz *Arzneim.-Forsch/Drug Res.* **1996**, *46*, 821-823
[105] R. Durmaz, H. Kucubay, E. Cetinkaya, B. Cetinkaya *Turk. J. Med. Sci.* **1997**, *27*, 59-61
[106] W. Liu, R. Gust *Coord. Chem. Rev.* **2016**, *329*, 191-213
[107] W. Liu, R. Gust *Chem. Soc. Rev.* **2013**, *42*, 755-773
[108] L. Oehninger, R. Rubbiani, I. Ott *Dalton Trans.* **2013**, *42*, 3269-3284
[109] B. Bertrand, A. Casini *Dalton Trans*. **2014**, *43*, 4209-4219
[110] M. Baron, S. Bellemin-Laponnaz, C. Tubaro, M. Basato, S. Bogialli, A. Dolmella *J. Inorg. Biochem*. **2014**, *141*, 94-102
[111] T. J. Siciliano, M. C. Deblock, K. M. Hindi, S. Durmus, M. J. Panzner, C. A. Tessier, W. J. Youngs *J. Organomet. Chem*. **2011**, *696*, 1066-1071
[112] A. Citta, E. Schuh, F. Mohr, A. Folda, M. L. Massimino, A. Bindoli, A. Casini, M. P. Rigobello *Metallomics* **2013**, *5*, 1006-1015
[113] M.-L. Teyssot, A.-S. Jarrousse, A. Chevry, H. A. De, C. Beaudoin, M. Manin, S. P. Nolan, S. Diez-Gonzalez, L. Morel, A. Gautier *Chem. Eur. J.* **2009**, *15*, 314-318
[114] J. Lemke, N. Metzler-Nolte *J. Organomet. Chem.* **2011**, *696*, 1018-1022
[115] S. Ray, R. Mohan, J. K. Singh, M. K. Samantaray, M. M. Shaikh, D. Panda, P. Ghosh *J. Am. Chem. Soc.* **2007**, *129*, 15042-15053

[116] A. W. Salman, R. A. Haque *Eur. J. Chem.* **2016**, *7*, 115-120

[117] E. Chardon, G. Dahm, G. Guichard, S. Bellemin-Laponnaz *Chem. Asian J.* **2013**, *8*, 1232-1242

[118] E. Chardon, G. L. Puleo, G. Dahm, G. Guichard, S. Bellemin-Laponnaz *Chem. Comm.* **2011**, *47*, 5864-5866

[119] M. Skander, P. Retailleau, B. Bourrié, L. Schio, P. Maillet, A. Marinetti *J. Med. Chem.* **2010**, *53*, 2146-2154

[120] A. Gautier, F. Cisnetti *Metallomics* **2012**, 1, 23-32

[121] E. A. Baquero, J. C. Flores, J. Perles, P. Gómez-Sal, E. de Jesús *Organometallics* **2014**, *33*, 5470-5482

[122] D. Brissy, M. Skander, P. Retailleau, G. Frison, A. Marinetti *Organometallics* **2009**, *28*, 140-151

[123] P. Mailliet, A. Marinetti, M. Skander WO2009/118475

[124] M. Chtchigrovsky, L. Eloy, H. Jullien, L. Saker, E. Ségal-Bendirdjian, J. Poupon, S. Bombard, T. Cresteil, P. Retailleau, A. Marinetti *J. Med. Chem.* **2013**, *56*, 2074-2086

[125] E. Chardon *PhD Thesis* **2011**, University of Strasbourg

[126] G. Dahm *PhD Thesis* **2014**, University of Strasbourg

[127] E. Chardon, G. Dahm, G. Guichard, S. Bellemin-Laponnaz *Organometallics* **2012**, *31*, 7618-7621

[128] E. Chardon, G. L. Puleo, G. Dahm, S. Fournel, G. Guichard, S. Bellemin-Laponnaz *Chem. Plus Chem.* **2012**, *77*, 1028-1038

[129] E. Borré, G. Dahm, G. Guichard, S. Bellemin-Laponnaz *New J. Chem.* **2016**, *40*, 3164-3171

[130] G. Dahm, E. Borré, G. Guichard, S. Bellemin-Laponnaz *Eur. J. Inorg. Chem.* **2015**, *10*, 1665-1668

[131] L. Tabrizi, H. Chiniforoshan *J. Organomet. Chem.* **2016**, *818*, 98-105

[132] J. Dinda, S. Das Adhikary, G. Roymahapatra, K. K. Nakka, M. K. Santra *Inorg. Chim. Acta* **2014**, *413*, 23-31

[133] R. W.-Y. Sun, A. L.-F. Chow, X.-H. Li, J. J. Yan, S. S.-Y. Chui, C.-M. Che *Chem. Sci.* **2011**, *2*, 728-736

[134] T. Zou, C. N. Lok, Y. M. Fung, C. M. Che *Chem. Commun.* **2013**, *49*, 5423-5425

[135] J.-F. Betzer, F. Nuter, M. Chtchigrovsky, F. Hamon, G. Kellermann, S. Ali, M.-A. Calméjane, S. Roque, J. Poupon, T. Cresteil, M.-P. Teulade-Fichou, A. Marinetti, S. Bombard *Bioconjugate Chem.* **2016**, *27*, 1456-1470

[136] M. D. Hall, T. W. Hambley *Coord. Chem. Rev.* **2002**, *232*, 49-67

[137] D. Gibson *Dalton Trans.* **2009**, *48*, 10681-10689

[138] N. Graf, S. J. Lippard *Adv. Drug Deliv. Rev.* **2012**, *64*, 993-1004

[139] M. D. Hall, H. L. Daly, J. Z. Zhang, M. Zhang, R. A. Alderden, D. Pursche, G. J. Foran, T. W. Hambley *Metallomics* **2012**, *4*, 568-575

[140] M. D. Hall, C. T. Dillon, M. Zhang, P. Beale, Z. Cai, B. Lai, A. P. K. Stampfl, T. W. Hambley *J. Biol. Inorg. Chem.* **2003**, *8*, 726-732

[141] M. D. Hall, G. J. Foran, M. Zhang, P. J. Beale, T. W. Hambley *J. Am. Chem. Soc.* **2003**, *125*, 7524-7525

[142] M. D. Hall, R. A. Alderden, M. Zhang, P. J Beale, Z. Cai, B. Lai, A. P. Stampfl, T. W. Hambley *J. Struct. Biol.* **2006**, *155*, 38-44

[143] E. J. New, R. Duan, J. Z. Zhang, T. W. Hambley *Dalton Trans.* **2008**, *16*, 3092-3101

[144] T. J. O'Rourke, G. R. Weiss, P. New, H. A. III Burris, G. Rodriguez, J. Eckhardt, J. Hardy, J. G. Kuhn, S. Fields, G. M. Clark *Anticancer Drugs* **1994**, *5*, 520-526

[145] E. S. Casper, T. C. Smart, T. B. Hakes, M. Ochoa, R. J. Kaufman *Inves. New Drugs* **1988**, *6*, 87-91

[146] B. O. Vondálová, I. Jelínková, A. H. Vaculová, P. Sova, J. Hofmanová, A. Kozubík *Cell Prolif.* **2013**, *46*, 665-676

[147] C. F. O'Neill, B. Koberle, J. R. W. Masters, L. R. Kelland *Br. J. Cancer*, **1999**, *81*, 1294-1303

[148] L. R. Kelland, G. Abel, M. J. McKeage, M. Jones, P. M. Goddard, M. Valenti, B. A. Murrer, K. R. Harrap *Cancer Res.* **1993**, 53, 2581-2586.

[149] F. I. Raynaud, P. Mistry, A. Donaghue, G. K. Poon, L. R. Kelland, C. F. Barnard, B. A. Murrer, K. R. Harrap *Cancer Chemother. and Pharmacol.* **1996**, *38*, 155-162

[150] X. Han, J. Sun, Y. Wang, Z. He *Med. Res. Rev.* **2015**, *35*, 1268-1299

[151] I. F. Tannock, R. de Wit, W. R. Berry, J. Horti, A. Pluzanska, K. N. Chi, S. Oudard, C. Théodore, N. D. James, I. Turesson, M. A. Rosenthal, M. A. Eisenberger *N. Engl. J. Med.* **2004**, *351*, 1502-1512

[152] M. Á. Medrano, A. Álvarez-Valdés, J. Perles, J. Lloret-Fillol, S. Muñoz-Galván, A. Carnero, C. Navarro-Ranninger, A. G. Quiroga *Chem. Commun.* **2013**, *49*, 4806-4808

[153] L. Cubo, T. W. Hambley, P. J. Sanz Miguel, A. Carnero, C. Navarro-Ranninger, A. G. Quiroga *Dalton Trans.* **2011**, *40*, 344-347

[154] J. Reedijk, P. H. M. Lohman *Pharmaceutisch Weekblad 7*, **1985**, *7*, 173-180

[155] S. Diez-Gonzalez *N-Heterocyclic Carbenes; From Laboratory Curiosities to Efficient Synthetic Tools*, Cambridge: Royal Society of Chemistry, **2016**

[156] J. J. Wilson, S. J. Lippard *Chem. Rev.* **2014**, *114*, 4470-4495

[157] L. Tschugajeff, W. Chlopin, E. Z. Fritzmann *Z. Anorg. Allg. Chem.* **1926**, *151*, 253

[158] R. A. Taylor, D. J. Law, G. J. Sunley, A. J. P. White *Chem. Comm.* **2008**, *24*, 2800-2802

[159] J. Lorenzo, Á. M. Montaña *J. Mol. Graph. Model.* **2016**, *69*, 39-60

[160] T. C. Johnstone, K. Suntharalingam, S. J. Lippard *Chem. Rev.* **2016**, *116*, 3436-3486

[161] S. Q. Yap, C. F. Chin, A. H. H. Thng, Y. Y. Pang, H. K. Ho, W. H. Ang *Chem. Med. Chem.* **2017**, *4*, 300-311

[162] I. Zanellato, I. Bonarrigo, D. Colangelo, E. Gabano, M. Ravera, M. Alessio, D. Osella *J. Inorg. Biochem.* **2014**, *140*, 219-227

[163] Y. Song, K. Suntharalingam, J. Yeung, M. Royzen, S. J. Lippard *Bioconjugate Chem.* **2013**, *24*, 1733-1740

[164] N. Graf, T. E. Mokhtari, I. A. Papayannopoulos, S. J. Lippard *J. Inorg. Biochem.* **2012**, *110*, 58-63

[165] Z. Wang, Z. Xu, G. Zhu *Angew. Chem. Int. Ed.* **2016**, *55*, 1-6

[166] S. Savino, N. Denora, R. M. Iacobazzi, L. Porcelli, A. Azzariti, G. Natile, N. Margiotta *Int. J. Mol. Sci.* **2016**, *17*, 1010

[167] X. Xue, S. You, Q. Zhang, Y. Wu, G. Z. Zou, P. C. Wang, Y. L. Zhao, Y. Xu, L. Jia, X. Zhang, X. J. Liang *Mol. Pharmaceutics* **2012**, *9*, 634–644

[168] L. Ma, R. Ma, Y. Wang, X. Zhu, J. Zhang, H. C. Chan, X. Chen, W. Zhang, S.-K. Chiu, G. Zhu *Chem. Commun.* **2015**, *51*, 6301-6304

[169] W. Neuman, B. C. Crews, L. J. Marnett, E. Hey-Hawkins *Chem. Med. Chem.* **2014**, *9*, 1150-1153

[170] W. Neuman, B. C. Crews, M. B. Sárosi, C. M. Daniel, K. Ghebreselasie, M. S. Scholz, L. J. Marnett, E. Hey-Hawkins *Chem. Med. Chem.* **2015**, *10*, 183-192

[171] D. Gibson *Dalton Trans.* **2016**, *45*, 12983-12991

[172] K. R. Barnes, A. Kutikov, S. J. Lippard *Chem. Biol.* **2004**, *11*, 557-564

[173] S. Mukhopadhyay, C. M. Barnés, A. Haskel, S. M. Short, K. R. Barnes, S. J. Lippard *Bioconjugate Chem.* **2008**, *19*, 39-49

[174] O. C. Farokhzad, R. Langer *ACS Nano* **2009**, *3*, 16-20

[175] B. Devasier, K. Sanghyo *Application of Nanotechnology in Drug Delivery*, DOI: 10.5772/58422

[176] M. Ravera, E. Perin, E. Gabano, I. Zanellato, G. Panzarasa, K. Sparnacci, M. Laus, D. Osella *J. Inorg. Biochem.* **2015**, *151*, 132-142

[177] S. L. Yoong, B. S. Wong, Q. L. Zhou, C. F. Chin, J. Li, T. Venkatesan, H. K. Ho, V. Yu, W. H. Ang, G. Pastorin *Biomaterials* **2014**, *35*, 748-759

[178] J. Li, A. Pant, C. F. Chin, W. H. Ang, C. Ménard-Moyon, T. R. Nayak, D. Gibson, S. Ramaprabhu, T. Panczyk, A. Bianco, G. Pastorin *Nanomedicine: NBM* **2014**, *10*, 1465-1475

[179] T. C. Johnstone, S. J. Lippard *Inorg. Chem.* **2013**, *52*, 9915-9920

[180] N. Margiotta, S. Savino, N. Denora, C. Marzano, V. Laquintana, A. Cutrignelli, J. D. Hoeschele, V. Gandin, G. Natile *Dalton Trans.* **2016**, *45*, 13070-13081

[181] V. D. Demidov, Y. N. Kukushkin, L. N. Deveneeva, A. N. Belayev *Zh. Obshch. Khim.* **1988**, *58*, 738-741

[182] E. M. Prokopchuk, R. J. Puddephatt *Organometallics* **2003**, *22*, 563-566

[183] N. Tsoureas, A. A. Danopoulos *J. Organomet. Chem.* **2015**, *775*, 178-187

[184] R. Lindner, C. Wagner, D. Steinborn *J. Am. Chem. Soc.* **2009**, *131*, 8861-8874

[185] O. Rivada-Wheelaghan, M. Roselló-Merino, J. Díez, C. Maya, J. López-Serrano, S. Conejero *Organometallics* **2014**, *33*, 5944-5947

[186] D. Serra, P. Cao, J. Cabrera, R. Padila, F. Rominger, M. Limbach *Organometallics* **2011**, *30*, 1885-1895

[187] A. Biffis, M. Cipani, E. Bressan, C. Tubaro, C. Graiff, A. Venzo *Organometallics* **2014**, *33*, 2182-2188

[188] D. Meyer, S. Ahrens, T. Strassner *Organometallics* **2010**, *29*, 3392-3396

[189] L. Benhamou, E. Chardon, G. Lavigne, S. Bellemin-Laponnaz, V. César *Chem. Rev.* **2011**, *111*, 2705-2733

[190] Log P value for cisplatin determined in: J. J. Wilson, S. J. Lippard *J. Med. Chem.* **2012**, *55*, 5326-5336

[191] H. Jullien, D. Brissy, R. Sylvain, P. Retailleau, J.-V. Naubron, S. Gladiali, A. Marinetti *Adv. Synth. Catal.* **2011***, 353*, 1109-1124

[192] C. P. Newman, R. J. Deeth, G. J. Clarkson, J. P. Rourke *Organometallics* **2007**, *26*, 6225-6233

[193] D. Brissy, M. Skander, P. Retailleau, A. Marinetti *Organometallics* **2007**, *26*, 5782-5785

[194] J. K. Muenzner, T. Rehm, B. Biersack, A. Casini, I. A. M. de Graaf, P. Worawutputtapong, A. Noor, R. Kempe, V. Brabec, J. Kasparkova, R. J. Schobert *J. Med. Chem.* **2015**, *58*, 6283-6292

[195] D. J. Cardin, B. Çetinkaya, M. F. Lappert *J. Organomet. Chem.* **1974**, *1*, 139-143

[196] G. Jaouen, N. Metzler-Nolte *Medicinal Organometallic Chemistry* Heidelberg Springer-Verlag Berlin, **2010**

[197] M. Bouché, G. Dahm, A. Maisse-François, T. Achard, S. Bellemin-Laponnaz *Eur. J. Inorg. Chem.* **2016**, *17*, 2828-2836

[198] K. R. Dixon, M. Fakley, A. Pidcock *Can. J. Chem.* **1976**, *54*, 2733-2738

[199] R. Favez, R. Roulet, A. A. Pinkerton, D. Schwarenbach *Inorg. Chem.* **1980***, 19*, 1356-1365

[200] IC_{50} value for cisplatin was not evaluated toward MRC5, human foetus cell lung.

[201] Same procedure can be applied to either (NHC)$PtBr_2$(pyr) or (NHC)$PtCl_2$(pyr) precursors without any yield drop.

[202] S.-X. Guo, D. N. Mason, S. A. Turland, E. T. Lawrenz, L. C. Kelly, G. D. Fallon, B. M. Gatehouse, A. M. Bond, G. B. Deacon, A. R. Battle, T. W. Hambley, S. Rainone, L. K. Webster, C. Cullinane *J. Inorg. Biochem.* **2012**, *115*, 226-239

[203] $PhICl_2$ synthesized following previously reported pathway: T. C. Johnstone, S. M. Alexander, J. J. Wilson, S. J. Lippard *Dalton Trans.* **2014**, *44*, 119-129

[204] D. F. Banks, E. F. Huyeser, J. J. Kleinberg *Org. Chem.* **1964**, *29*, 3692-3693

[205] D. Meyer, S. Ahrens, T. Strassner *Organometallics* **2010**, *15*, 3392-3396

[206] T. A. Perera, M. Masjedi, P. R. Sharp *Inorg. Chem.* **2014**, *53*, 7608-7621

[207] T. C. Johnstone, K. Suntharalingam, S. J. Lippard *Chem. Rev.* **2016**, *116*, 3436-3486

[208] For similar trend in *bis* NHC-palladium complexes, see: A. S. McCall, S. Kraft *Organometallics* **2012**, *31*, 3527-3538

[209] R. A. Taylor, D. J. Law, G. J. Sunley, A. J. P. White, G. J. P. Britovsek *Chem. Commun.* **2008**, *24*, 2800-2802

[210] J. J. Wilson, S. J. Lippard *Polyhedron* **2013**, *58*, 71-78

[211] D. Paschoal, C. Fonseca Guerra, M. A. L. de Oliveira, T. C. Ramalho, H. F. Dos Santos *J. Comp. Chem.* **2016**, *26*, 2360-2373

[212] A. C. Tsipis, I. N. Karapetsas *Dalton Trans.* **2014**, *43*, 5409-5426

[213] H. V. Huynh *The organometallic chemistry of N-heterocyclic carbenes*. Berlin: Wiley Verlag, **2017**

[214] S. J. Fischer, L. M. Benson, A. Fauq, S. Naylor, A. J. Windebank *Neurotoxicology* **2008**, *29*, 444-452

[215] M. D. Hall, K. A. Telma, K.-E. Chang, T. T. Lee, J. P. Madigan, J. R. Lloyd, I. S. Goldlust, J. D. Hoeschele, M. M Gottesman *Cancer Res.* **2014**, *14*, 3913-3922

[216] C. Massart, C. Le Tellier, J. Gibassier, G. Leclech, M. Nicol *Toxicol. In Vitro* **1993**, *7*, 87-94

[217] H. Y. Huang, N. Humbert, V. Bizet, M. Patra, H. Chao, C. Mazet, G. Gasser *J. Organomet. Chem.* **2017**, *839*, 15-18

[218] H. P. Varbanov, D. Ortiz, D. Höfer, L. Menin, M. Galanski, B. K. Keppler, P. J. Dyson *Dalton Trans.* **2017**, *46*, 8929-8932

[219] S. Choi, C. Filotto, M. Bisanzo, S. Delaney, D. Lagasee, J. L. Whitworth, A. Jusko, C. Li, N. A. Wood, J. Willingham, A. Schwenker, K. Saulding *Inorg. Chem.* **1998**, *37*, 2500-2504

[220] E. Petruzzella, N. Margiotta, M. Ravera, G. Natile *Inorg. Chem.* **2013**, *52*, 2393-2403

[221] B. Erdlenbruch, M. Nier, W. Kern, W. Hiddemann, A. Pekrun, M. Lakomek *Eur. J. Clin. Pharmacol.* **2001**, *57*, 393-402

[222] J. L. Carr, M. D. Tingle, M. J. McKeage *Cancer Chemother. Pharmacol.* **2002**, *50*, 9-15

[223] J. F. Neault, H. A. Tajmir-Riahi *Biochim. Biophys. Acta* **1998**, *1384*, 153-159

[224] N. A. Kratochwil, A. I. Ivanov, M. Patriarca, J. A. Parkinson, A. M. Gouldsworthy, P. del Socorro Murdoch, P. J. Sadler *J. Am. Chem. Soc.* **1999**, *121*, 8193-8203

[225] R. Xie, W. Johnson, L. Rodriguez, M. Gounder, G. S. Hall, B. Buckley *Anal. Bioanal. Chem.* **2007**, *387*, 2815-2822

[226] Binding of Ru complex to HSA evidenced by ICP-MS and X-ray: A. Bijelic, S. Theiner, B. K. Keppler, A. Rompel *J. Med. Chem.* **2016**, *59*, 5894-5903

[227] V. Pichler, S. Göschl, E. Schreiber-Brynzak, M. A. Jakupec, M. Galanski, B. K. Keppler *Metallomics* **2015**, *7*, 1078-1090

[228] M. D. Hall, R. A. Alderden, M. Zhang, P. J. Beale, Z. Cai, B. Lai, A. P. J. Stampfl, T. W. Hambley *J. Struct. Biol.* **2006**, *155*, 38-44

[229] M. Galanski, B. K. Keppler *Anti-Cancer Agents Med. Chem.* **2007**, *7*, 55-73

[230] F. Michelet, R. Gueguen, P. Leroy, M. Wellman, A. Nicolas, G. Siest *Clin. Chem.* **1995**, 41, 1509-1517

[231] J. P. Richie, L. Skowronski, P. Abraham, Y. Leutzinger *Clin. Chem.* **1996**, *42*, 64-70

[232] V. Pichler, S. Göschl, S. M. Meier, A. Roller, M. A. Jakupec, M. Galanski, B. K. Keppler *Inorg. Chem.* **2013**, *52*, 8151-8162

[233] H. P. Varbanov, S. M. Valiahdi, C. R. Kowol, M. A. Jakupec, M. Galanski, B. K. Keppler *Dalton Trans.* **2012**, *41*, 14404-14415

[234] C. K. J. Chen, J. Z. Zhang, J. B. Aitken, T. W. Hambley *J. Med. Chem.* **2013**, *56*, 8757-8764

[235] S. Goto, T. Iida, S. Cho, M. Oka, S. Kohno, T. Kondo *Free Radic. Res.* **1999**, *6*, 549-558

[236] M. Kato, H. Yamamoto, T. Okamura, N. Maoka, R. Masui, S. Kuramitsu, N. Ueyama *Dalton Trans.* **2005**, *0*, 1023-1026

[237] E. S. J. Arnér, H. Nakamura, T. Sasada, J. Yodoi, A. Holmgren, G. Spyrou *Free Radic. Biol. Med.* **2001**, *31*, 1170-1178

[238] M. J. McKeage *Expert Opin. Investig. Drugs* **2001**, *10*, 119-128

[239] P. W. Ayers, R. G. Parr, R. G. Pearson *J. Chem. Phys.* **2006**, *124*, 194107-194115

[240] M. Sinisi, F. P. Intini, G. Natile *Inorg. Chem.* **2012**, *51*, 9694-9704

[241] S. Jovanovic, B. Petrovic, Z. D. Bugarcic, R. van Eldik *Dalton Trans.* **2013**, *42*, 8890-8896

[242] S. Karmakar, S. Chatterjee, K. Purkait, A. Mukherfee *Dalton Trans.* **2016**, *45*, 11710-11722

[243] J. Z. Zhang, E. Wexselblatt, T. W. Hambley, D. Gibson *Chem. Commun.* **2012**, *48*, 847-849

[244] S. Göschl, E. Schreiber-Brynzak, V. Pichler, K. Cseh, P. Heffeter, U. Jungwirth, M. A. Jakupec, W. Berger, B. K. Keppler *Metallomics* **2017**, *9*, 309-322

[245] R. Song, K. Mook Kim, Y. Soo Sohn *Bull. Korean Chem. Soc.* **2000**, *21*, 1000-1004

[246] IC_{50} data for cisplatin toward A2780 and A2780R were taken from: A. O. S. Altoum, J. Vanco, R. Krikavova, Z. Travnicek, Z. Dvofak, M. Altaf, S. Ahmad, A. A. A. Sulaiman, A. A. Isab *Polyhedron* **2017**, *128*, 2-8

[247] M. Schuler, E. Bossy-Wetzel, J. C. Goldstein, P. Fitzgerald, D. R. Green *J. Biol. Chem.* **2000**, *275*, 7337-7342

[248] K. M. Henkels, J. J. Turchi *Canc. Res.* **1999**, *59*, 3077-3083

[249] D. K. Hattangadi, G. A. DeMasters, T. D. Walker, K. R. Jones, X. Di, I. F. Newsham, D. A. Gewirtz *Biochem. Pharmacol.* **2004**, *68*, 1699-1708

[250] D.E. Fisher, *Cell* **1994**, *78*, 539-542

[251] L. Galluzz, L. Senovilla, I. Vitale, J. Michels, I. Martins, O. Kepp, M. Castedo, G. Kroemer *Oncogene* **2011**, *31*, 1869-1883

[252] O. Novakova, O. Vrana, V. I. Kiseleva, V. Brabec *Eur. J. Biochem*. **1995**, *228*, 616-624

[253] R. M. Roat, J. Reedijk *J. Inorg. Biochem*. **1993**, *52*, 263- 274

[254] E. G. Talman, Y. Kidani, L. Mohrmann, J. Reedijk *Inorg. Chim. Acta* **1998**, *283*, 251-255

[255] S. Karmakar, S. Chatterjee, K. Purkait, A. Mukherjee *Dalton Trans.* **2016**, *45*, 11710-11722
[256] T. Li, H. Lin, T. Li, W. He, Y. Li, Y. Zhang, Y. Zhu, Z. Guo *Inorg. Chim. Acta* **2009**, *362*, 967-974
[257] A. Ariafard, N. M. Ghohe, K. K. Abbasi, A. J. Canty, B. F. Yates *Inorg. Chem.* **2013**, *52*, 707-717
[258] I. Kipouros, S. M. Fica-Contreras, G. J. K. Bowe, S. Choi *J. Biol. Inorg. Chem.* **2015**, *20*, 1327-1341
[259] S. Choi, B. R. Cooley, A. Voutchkova, C. H. Leung, L. Vastag, D. E. Knowles *J. Am. Chem. Soc.* **2005**, *127*, 1773-1781
[260] R. Kohen, A. Nyska *Toxicol. Pathol.* **2002**, *30*, 620-650
[261] M. Valko, K. Jomova, C. J. Rhodes, K. Kuca, K. Musilek *Arch. Toxicol.* **2016**, *90*, 1-37
[262] H. Pelicano, D. Carney, P. Huang *Drug Resist. Updat.* **2004**, *7*, 97-110
[263] J. Zajac, H. Kostrhunova, V. Novohradsky, O. Vrana, R. Raveendran, D. Gibson, J. Kasparkova, V. Brabec *J. Inorg. Biochem.* **2016**, *156*, 89-97
[264] X. Xue, S. You, Q. Zhang, Y. Wu, G. Z. Zou, P. C. Wang, Y. L. Zhao, Y. Xu, X. N. Zhang, X. J. Liang *Mol. Pharm.* **2012**, *3*, 634-644
[265] H. Q. Song, H. H. Xiao, Y. Zhang, H. D. Cai, R. Wang, Y. H. Zheng, Y. B. Huang, Y. X. Li, Z. G. Xie, T. J. Liu, X. B. Jing *J. Mater. Chem. B.* **2013**, *6*, 762-772
[266] G. N. Kaluđerović, S. A. Mijatović, B. B. Zmejkovski, M. Z. Bulatović, S. Gómez-Ruiz, M. K. Mojić, D. Steinborn, D. M. Milijković, H. Schmidt, S. D. Stošić-Grujičić, T. J. Sabo, D. D. Maksimović-Ivanić *Metallomics* **2012**, *4*, 979-987
[267] K. Suntharalingam, Y. Song, S. J. Lippard *Chem. Commun.* **2014**, *19*, 2465-2468
[268] U. Jungwirth, C. R. Kowol, B. K. Keppler, C. G. Hartinger, W. Berger, P. Heffeter *Antioxid. Redox. Signal.* **2011**, *15*, 1085-1127
[269] M. L. Circu, T. Y. Aw *Free Radic. Res.* **2008**, *42*, 689-706
[270] J. Gil, S. Almeida, C. R. Oliveira, A. C. Rogez *Free Radic. Biol. Med.* **2003**, *35*, 1500-1514
[271] B. Chazotte *Cold Spring Harb. Protoc.* **2011**, *8*, 990-992
[272] J. S. Butler, P. J. Sadler *Cur. Opin. Chem. Biol.* **2013**, *17*, 175-188
[273] X. Wang, Z. Guo *Chem. Soc. Rev.* **2013**, *42*, 202-224
[274] E. C. Dreaden, M. A. Mackey, X. Huang, B. Kang, M. A. El-Sayed *Chem. Soc. Rev.* **2011**, *40*, 3391-3404
[275] A. Farrugia *Transfus. Med. Rev.* **2010**, *24*, 53-63
[276] L. Turell, R. Radi, B. Alvarez *Free Radic. Biol. Med.* **2013**, *65*, 244-253
[277] O. Pinato, C. Musetti, C. Sissi *Metallomics* **2014**, *6*, 380-395
[278] F. Kratz *J. Control. Release* **2008**, *132*, 171-183
[279] K. Park *J. Control. Release* **2012**, *157*, 3
[280] A. O. Elzoghby, W. M. Samy, N. A. Elgindy *J. Controlled Release* **2012**, *157*, 168-182
[281] R. C. Dolman, G. B. Deacon, T. W. Hambley *J. Inorg. Biochem.* **2002**, *88*, 260-267
[282] G. Ferraro, L. Massai, L. Messori, A. Merlino *Chem. Commun.* **2015**, *51*, 9436-9439

[283] A. Farrugia *Transus. Med. Rev.* **2010**, *24*, 53-63

[284] X. M. He, D. C. Carter *Nature* **1992**, *358*, 209-215

[285] G. Sudlow, D. J. Birkett, D. N. Whade *Molec. Pharmacol.* **1975**, *11*, 824-832

[286] G. Sudlow, D. J. Birkett, D. N. Whade *Molec. Pharmacol.* **1976**, *12*, 1052-1061

[287] Y.-R. Zheng, K. Suntharalingam, T. C. Johnstone, H. Yoo, W. Lin, J. G. Brooks, S. J. Lippard *J. Am. Chem. Soc.* **2014**, *136*, 8790-8798

[288] A. O. Elzoghby, W. M. Samy, N. A. Elgindy *J. Control. Release* **2012**, *157*, 168-182

[289] M. T. Larsen, M. Kuhlmann, M. L. Hvam, K. A. Howard *Mol. Cell Ther.* **2016**, *4*, 3

[290] Y. Gou, F. Yang, H. Liang *Curr. Top. Med. Chem.* **2016**, *16*, 996-1008

[291] S. Jacobs, C. L. Mccully, R. F. Murphy, J. Bacher, F. M. Balis, E. Fox *Cancer Chemother. Pharmacol.* **2010**, *65*, 817-824

[292] V. Pichler, J. Mayr, P. Heffeter, O. Dömötör, É. A. Enyedy, G. Hermann, D. Groza, G. Köllensperger, M. Galanski, W. Berger, B. K. Keppler, C. R. Kowol *Chem. Commun.* **2013**, *49*, 2249-2251

[293] J. Mayr, P. Heffeter, D. Groza, L. Galvez, G. Köllensperger, A. Roller, B. Alte, M. Haider, W. Berger, C. R. Kowol, B. K. Keppler *Chem. Sci.* **2017**, *8*, 2241-2250

[294] N. A. Kratochwil, A. I. Ivanov, M. Patriarca, J. A. Parkinson, A. M. Gouldsworthy, P. D. S. Murdoch, P. J. Sadler *J. Am. Chem. Soc.* **1999**, *121*, 8193-8203

[295] Keppler *et al.* recognized that no cytotoxicity could be observed in *in vitro* experiments

[296] M. B. Shahsavani, S. Ahmadi, M. D. Aseman, S. M. Nabavizadeh, M. M. Alavianmehr, R. Yousefi *J. Photochem. Photobiol.* **2016**, *164*, 323-334

[297] Q. M. Wang, L. Yang, J. H. Wu, H. Wang, J. L. Song, X. H. Tang *Biometals* **2017**, *30*, 17-26

[298] S.B. Thourson, C.A. Marsh, B.J. Doyle, S.J. Timpe *Colloids Surf. B: Biointerfaces* **2013**, *111*, 707-712

[299] C. Icsel, V. T. Yilmaz, Y. Kaya, S. Durmus, M. Sarimahmut, O. Buyukgungor, E. Ulukaya *J. Inorg. Biochem.* **2015**, *152*, 38-52

[300] D. S. Raja, N. S. P. Bhuvanesh, K. Natarajan *Eur. J. Med. Chem.* **2011**, *46*, 4584-4594

[301] Y. Reza, M. Jamshidi, M. B. Shahsavani, S. M. Nabavizadeh, M. G. Haghighi, M. Rashidi, A. Taheri-Kafrani, A. Niazi, F. Keshavarz, M. M. Alavinamehr *J. Iran. Chem. Soc.* **2016**, *4*, 617-630

[302] A. Akbarzadeh, R. Rezaei-Sadabady, S. Davaran, S. W. Joo, N. Zarghami, Y. Hanifehpour, M. Samiei, M. Kouhi, K. Nejati-Koshki *Nanoscale Res. Lett.* **2013**, *8*, 102-110

[303] H. Maeda *Adv. Drug Deliv. Rev.* **2015**, *91*, 3-6

[304] P. Neuberg, A. Kichler *Adv. Genet.* **2014**, *88*, 263-288

[305] O. Boussif, F. Lezoualc'h, M. A. Zanta, M. D. Mergny, D. Scherman, B. Demeneix, J.-P. Behr *Proc. Natl. Acad. Sci. USA* **1995**, *92*, 7297-7301

[306] A. P. Pandey, K. K. Sawant *Mater. Sci. Eng. C. Mater. Biol. Appl.* **2016**, *68*, 904-918

[307] C. K. Choudhury, S. Roy *Soft Matter* **2013**, *9*, 2269-2281

[308] N. D. Sonawane, F. C. Szoka, A. S. Verkman *J. Biol. Chem.* **2003**, *278*, 44826-44831

[309] N. Chekkat, G. Dahm, E. Chardon, M. Wantz, J. Sitz, M. Decossas, O. Lambert, B. Frisch, R. Rubbiani, G. Gasser, G. Guichard, S. Fournel, S. Bellemin-Laponnaz *Bioconjugate Chem.* **2016**, *27*, 1942-1948

[310] Q.-D. Hu, G.-P. Tang, P. K. Chu *Acc. Chem. Res.* **2014**, *47*, 2017-2025

[311] A. Harada, Y. Takashima, M. Nakahata *Acc. Chem. Res.* **2014**, *47*, 2128-2140

[312] A. Kasprzak, M. Poplawska, H. Krawczyk, S. Molchaniv, M. Kozlowski, M. Bystrzejewski *J. Incl. Phenom. Macrocycl. Chem.* **2017**, *87*, 53-65

[313] I. Bohm, H. Ritter, *Macromol. Chem. Phys.* **2011**, *212*, 1080-1085

[314] J. A. Mackintosh, H.-Y. Choi, S. H. Bae, D. A. Veal, P. J. Bell, B. C. Ferrari, D. D. Van Dyk, N. M. Verrills, Y. K. Paik, P. Karuso *Proteomics* **2003**, *3*, 2273-2288

[315] G. B. Smejkal, M. H. Robinson, A. Lazarev *Electrophoresis* **2004**, *25*, 2511-2519

[316] T. H. Steinberg, L. J. Jones, R. P. Haugland, V. L. Singer *Anal. Biochem.* **1996**, *239*, 223-237

[317] G. Dahm, E. Borré, G. Guichard, S. Bellemin-Laponnaz *Eur. J. Inorg. Chem.* **2015**, *10*, 1665-1668.

[318] G. Dahm, C. Bailly, L. Karmazin, S. Bellemin-Laponnaz *J. Organomet. Chem.* **2015**, *794*, 115-124

[319] C. Callebaut, E. Jacotot, G. Guichard, B. Krust, M.-A. Rey-Cuille, D. Cointe, N. Benkirane, J. Blanco, S. Muller, J.-P. Briand, A. G. Hovanessian *Virology* **1996**, *218*, 181-192

[320] B. Krust, R. Vienet, A. Cardona, C. Rougeot, E. Jacotot, C. Callebaut, G. Guichard, J.-P. Briand, J. M. Grognet, A. G. Hovanessian, L. Edelman *PNAS* **2001**, *24*, 14090-14095

[321] S. Nisole, E. A. Said, C. Mische, M.-C. Prevost, B. Krust, P. Bouvet, A. Bianco, J.-P. Briand, A. G. Hovenassian *J. Biol. Chem.* **2002**, *277*, 20877-20886

[322] C. Birmpas, J.-P. Briand, J. Courty, P. Katsoris *Vasc. Cell* **2012**, *4*, 21-32

[323] K. Kunath, T. Merdan, O. Hegener, H. Häberlein, T. Kissel *J. Gene Med.* **2003**, *5*, 588-599

[324] www.nist.gov.

[325] M. A. Dobrovolskaia, S. E. McNeil *Nat. Nanotechnol.* **2007**, *2*, 469-478

[326] P. C. Chen, S. C. Mwakwari, A. K. Oyelere *Nanotechnol. Sci. Appl.* **2008**, *1*, 45-66

[327] G. G. Lazarus, M. Singh *Colloids Surf. B Biointerfaces* **2016**, *145*, 906-911

[328] M. Ortega-Muñoz, D. Giron-Gonzalez, R. Salto-Gonzalez, A. B. Jodar-Reyes, S. E. De Jesus, F. J. Lopez-Jaramillo, F. Hernandez-Mateo, F. Santoyo-Gonzalez *Chem. Asian J.* **2016**, *23*, 3365-3375

[329] T. Tencomnao, A. Apijaraskul, V. Rakkhithawatthana, S. Chaleawlret-umpon, N. Pimpa, W. Sajomsang, N. Saengkrit *Carbohydrate Polymers* **2011**, *84*, 216-222

[330] Y. Zhang, S. Wen, L. Zhao, D. Li, C. Liu, W. Jiang, X. Gao, W. Gu, N. Ma, J. Zhao, X. Shi, Q. Zhao *Nanoscale* **2016**, *10*, 5567-5577

[331] B. Zhou, J. Yang, C. Peng, J. Zhu, Y. Tang, X. Zhu, M. Shen, G. Zhang, X. Shi *Colloids and Surfaces B: Biointerfaces* **2016**, *140*, 489-496

[332] R. Shahbazi, I. Ozcicek, G. Ozturk, K. Ulubayram *Nanotechnology* **2017**, *28*

[333] J. Turkevich, P. C. Stevenson, J. Hillier *Discuss. Farady Soc.* **1951**, *11*, 55-75

[334] X. Wang, D. C. Niu, C. Hu, P. Li *Curr. Pharm. Des.* **2015**, *42*, 6140-6156

[335] S. Prabha, G. Arya, R. Chandra, B. Ahmed, S. Nimesh *Artif. Cells Nanomed. Biotechnol.* **2016**, *44*, 83-91

[336] D. A. Gilijohann, D. S. Seferos, A. E. Prigodich, P. C. Patel, C. A. Mirkin *J. Am. Chem. Soc.* **2009**, *131*, 2072-2073

Mathilde BOUCHÉ

Carbène-Platine conjugués: de nouveaux outils thérapeutiques dans la lutte antitumorale

Résumé

Bien que les agents anticancéreux à base de platine soient bien établis en clinique, plusieurs paramètres restent à optimiser, notamment leur toxicité et les phénomènes de résistances.

La combinaison platine-carbènes N-hétérocycliques (NHCs) a montré des résultats prometteurs dans la lutte antitumorale. Ainsi, afin de développer des agents anticancéreux innovants, ce travail résume les modifications structurales étudiées dans le but d'augmenter la cytotoxicité tout en réduisant les effets secondaires des complexes.

Une stratégie développée ici porte sur l'introduction de pnictogènes par échange de ligand pour observer un effet synergétique. Autrement, les efforts se sont concentrés sur les complexes de NHC-platine(IV) de leur synthèse à l'étude de leur stabilité, activité anticancéreuse et mécanisme d'action. Finalement, la combinaison des NHC-Pt à des nanotransporteurs a été étudiée afin d'améliorer leur biocompatibilité et sélectivité.

Mots clés : Carbène N-hétérocyclique, Platine, Anticancer, Médecine Inorganique, Nanotransport

Résumé en anglais

Although platinum-based anticancer drugs are well established, several shortcomings have raised concerns, namely their toxicity and resistance mechanisms. Therefore, improved anticancer drugs are strongly awaited to substitute drugs currently used in clinics.

Remarkably, the combination of *N*-Heterocyclic Carbenes (NHCs) to platinum has recently demonstrated very promising results as anticancer agents. In the aim to access novel drugs, this work emphasizes several structural modifications to improve the cytotoxicity and lower side effects.

One strategy developed herein focus on the introduction of pnictogens by ligand exchange to access a synergistic effect. Otherwise, efforts mainly focused on NHC-platinum(IV) complexes from their synthesis to stability investigation and anticancer activities and mechanism of action. Finally, the combination of NHC-Pt drugs to nanodelivery devices has been investigated in order to improve both their biocompatibility and selectivity toward cancer cells.

Keywords : N-Heterocyclic Carbene, Platinum, Anticancer, Inorganic Medicine, Nanodelivery